A Smart Wheelchair System using a Combination of Stereoscopic and Spherical Vision Cameras

By

Jordan Son Nguyen

Submitted to the Faculty of Engineering and Information Technology

in partial fulfilment of the requirements for the degree of

Doctor of Philosophy

at the University of Technology, Sydney

UNIVERSITY OF TECHNOLOGY SYDNEY

November 2012

Certificate of Authorship / Originality

I, Jordan Son Nguyen, certify that the work in this thesis has not previously been submitted for a degree, nor has it been submitted as part of the requirements of a degree, except as fully acknowledged within the text.

I also certify that this thesis has been written by me. Any help that I have received in my research work and in the preparation of the thesis itself has been acknowledged. In addition, I certify that all information sources and literature used are indicated in the thesis.

Signature of Candidate

November 2012

Acknowledgements

To the lovely people in MCU marketing and FEIT marketing, you have all made my time during this thesis an unforgettable experience. You have contributed greatly to my many media appearances with the TIM smart wheelchair, but most important of all you have all been great friends to me.

To all of my friends who have kept me sane and contributed largely to the fun I have had over these past years in uni, I thank you all. Work is always better when I know I have people who are always there to support me the way I am for them.

And last but not least, I would like to thank my amazing family. The greatest credit of all goes to you because none of this would have ever been possible without having you wonderful people in my life. My dad Hung has been my lifelong inspiration and mentor, and my mum Lesley has always been the light that guides me, she means everything to me. My sister and brothers Zohara, Alexander and Tristan are much more than siblings, we support and look out for one another and nothing will ever come between us. My grandparents Shirley and Rob are always there for me and I only hope to make you proud. I love you all more than words can describe and your constant love, support, and guidance over the years have allowed me to become the person I am today.

To all who have helped

Table of Contents

List of Figures

List of Tables

Nomenclature

1D	1-Dimensional
2D	2-Dimensional
3D	3-Dimensional
AB	Able-Bodied
ADC	Analog-Digital Converter
AWF	Automatic Wall Following
BCI	Brain-Computer Interface
CAN	Controller Area Network
CCD	Charge-Couple Device
CCW	Counter-Clockwise
CNS	Central Nervous System
CPU	Central Processing Unit
CW	Clockwise
CWA	Collaborative Wheelchair Assistant
DAQ	Data Acquisition
DLL	Dynamic Link Library
DOS	Disk Operating System
DP	Door Passing
EEG	Electroencephalograph
FM	Fundamental Matrix
FN	False-Negative
FOV	Field Of View
FP	False-Positive
FPS	Frames Per Second
GOA	General Obstacle Avoidance
GPIO	General-Purpose Input/Output
GPS	Global Positioning System
GUI	Graphical User Interface
HMC	Head-Movement Controller
HIS	Hue/Saturation/Intensity
HFOV	Horizontal Field Of View
IEEE	Institute of Electrical and Electronic Engineers
IR	Infrared
LED	Light-Emitting Diode
LIS	Locked-In Syndrome
NI	National Instruments
NSW	New South Wales
PC	Personal Computer
PCB	Printed Circuit Board
PFM	Potential Field Method
PGR	Point Grey Research
POC	Proof Of Concept
QUEST	Quebec User Evaluation of Satisfaction with Assistive Technology
RGB	Red/Green/Blue
RRCS	Royal Rehabilitation Centre, Sydney
RSU	Rehabilitation Studies Unit
SAD	Sum of Absolute Differences
SCI	Spinal Cord Injury

SD	Standard Deviation
SLAM	Simultaneous Localisation And Mapping
TFT	Thin-Film Transistor
TIM	Thought-controlled Intelligent Machine
TIM-VPH	Thought-controlled Intelligent Machine – Vector Polar Histogram
TN	True-Negative
TOF	Time-Of-Flight
TP	True-Positive
USB	Universal Serial Bus
UTS	University of Technology, Sydney
VFF	Vector Force Field
VFH	Vector Field Histogram
VPH	Vector Polar Histogram
WCCP	Wheelchair Centre Point

Abstract

Reports have shown growing numbers of people who fall into the categories of the elderly or those living with some form of disability. Physical and functional impairments are broad-ranging across these groups and the causes are numerous, including strokes, spinal cord injury, spina bifida, multiple sclerosis, muscular dystrophy, and various degenerative disorders. Rehabilitation technologies are a solution to many of these impairments and aim to improve the quality of life for the people who require them. Smart wheelchair developments, in particular, have the purpose of assisting those with mobility disabilities. Providing independence in mobility can have many significant benefits to the users in their daily lives, including improved physical, cognitive, confidence, communication, and social skills.

Unfortunately for many, particularly those with tetraplegia (partial or total loss of functionality through illness or injury to all four limbs and torso), there is a serious lack of options available for adequately and safely controlling mobility devices such as wheelchairs. There are few options for hands-free controlling wheelchairs, and furthermore, there are no accessible options for intelligent assistance from the wheelchair to make hands-free control easy and safe. This is a serious issue since the limited hands-free control options available can be difficult to use, resulting in many accidents. There are also new control technology devices emerging in research, such as brain-computer interfaces (BCIs), which could potentially provide an adequate means of control for many people who cannot use currently commercial options, but require intelligent assistance from the wheelchair to make use of such a system safe.

In this thesis, the design and development of a new smart wheelchair, named TIM, is introduced to address these issues. The TIM smart wheelchair was created with the intention of providing intelligent assistance during navigation for any hands-free control technology, both currently commercial and new devices produced in research. This aims to vastly improve the options available to the people who are in need of such smart wheelchair developments.

A method of utilising stereoscopic cameras for adaptive, real-time vision mapping is presented in this thesis, as cameras are increasingly becoming a more accessible and inexpensive form of artificial sensor. The mapping process in this method involves acquisition from the left and right stereo pair of cameras, which then undergo a range of image pre-processing techniques before being stereo-processed, which includes matching and correlation algorithms, to produce a disparity image. This disparity image contains depth information about the scene, which is then converted into a 3-dimensional (3D) point map, placing all mapped pixels of the environment, and features within, into a 3D plane. Unnecessary information, such as the floor and everything above the maximum height of the TIM smart wheelchair, is removed and the remaining data extracted into a 2-dimensional (2D) bird‟s eye view environment map. This mapping representation assists the wheelchair in the later steps of making intelligent navigational decisions based on the relative placement of objects in the environment.

Wheel encoders on the drive wheels are also acquired during operation, and odometry change calculations are performed to facilitate the ability of the system to „remember‟ mapped object points that have passed outside the vision range. This is performed frequently to construct a real-time environment map, and to remember the placement of objects that have moved out of the range of vision, in order to further avoid collisions. This is particularly useful for static environments and creating maps of the static object placements within. A wheel parameter correction process was also employed to increase the accuracy of this mapping process and successfully reduce the errors associated with drive wheel specifications, which in turn can affect the mapping process based on the wheel encoder information. Correction of these parameters helped optimise the „memory mapping‟ process and reduce skewing and accumulative errors in the maps.

A process for intelligent stereo processing parameter selection was designed, as the quality of disparity images, and hence the quality of environmental-mapping, is heavily dependent on the stereo processing parameters, which may work well when set for one environment but produce problems in another. The differences that affected performance between

environments were found to mostly be the lighting conditions which resulted from the varying types of environments. As such, this proposed method involves classifying environmental categories in real-time, based on image data available, and adapting the parameters accordingly. The environment types were separated into four categories to account for most encountered environmental situations, being 1) „General Illumination Contrast", 2) „Extreme Illumination Contrast", 3) „Consistent Dark", and 4) „Consistent Bright". The proposed method successfully allowed classification in real-time of the environment categories and adaptation of the stereo processing parameters in accordance, producing a system that can change its settings „on the fly" to suit the environment the wheelchair is navigating through.

Limited vision and trouble with dynamic objects were found to be downfalls with the stereoscopic vision, so to address these, methods of utilising a spherical vision camera system were introduced for obstacle detection over a wide vision range. Spherical vision is an extension of monoscopic cameras, producing 360º of panoramic vision. A strategy to utilise these panoramic images is presented, in which the images are separated into segments and „Traffic Light" zones. The segments display different areas of the image representing the allocated areas around the wheelchair. The „Traffic Light" zones within the segments are separated into three categories: 1) Red, meaning an obstruction is present around the wheelchair, 2) Yellow, indicating to take caution as an object is nearby, and 3) Green, meaning there are no objects close to the wheelchair in this segment. Image processing techniques have been assembled as a pre-processing strategy, and neural networks are used for intelligent classification of the segmented images into the zone categories. This method provides a wider range of vision than the stereoscopic cameras alone, and also takes into account the issue of detecting dynamic obstacles, such as people moving around.

A unique combination of the stereoscopic cameras and the spherical vision cameras is then introduced. This combination and system configuration is biologically inspired by the equine vision system. Horses inherently have a large vision range, which includes a wide monocular vision range around and a binocular vision overlap ahead of the horse. In accordance with this effective vision system, the camera configuration on the TIM smart wheelchair was modelled similarly and advanced software integration strategies then followed.

A method for advanced real-time obstacle avoidance is presented, which utilises algorithms in research, such as Vector Field Histogram (VFH) and Vector Polar Histogram (VPH) methods, and adapts them for use with the specified camera configuration. Further improvement upon the algorithms for this application provides safer obstacle avoidance during navigation in

unknown environments, with an added emphasis on making automated navigational decisions towards areas with more available free space. Speed and manner of obstacle avoidance is dependent upon the placement spread of objects in an environment and how close they are to the wheelchair during navigation.

Finally, the combination and integration of the automated guidance and obstacle avoidance capabilities of the wheelchair with hands-free control technologies are introduced. The aim of the TIM smart wheelchair system was to effectively provide safe navigation with automated obstacle avoidance in a manner that ultimately executes the user's intentions for travel. As such, a head-movement control (HMC) device and a brain-computer interface (BCI) device are both separately integrated with the TIM smart wheelchair, providing a display of two new options for hands-free control.

Experimental studies were conducted using these two control devices separately, to assess the performance of the TIM smart wheelchair, as well as its ability to carry out user's navigational intentions safely and effectively. Eight able-bodied participants trialled the system, including four male and four female, with ages ranging from 21 to 56 years old. All of these able-bodied participants have not previously had any experience operating a wheelchair. In addition, two male tetraplegic (C-6 to C-7) participants also completed the experimental study, aged 20 and 33. Both tetraplegic participants are wheelchair users, so these experiments were of great importance. The same tasks applied to all, and included navigating obstacle courses with the use of the head-movement control system and the brain-computer interface for control. Experiment runs were conducted for each control system with automated navigational guidance assistance from TIM, and repeated for some capable participants without the assistance from TIM. This process was also conducted in two types of obstacle courses, being 1) a „Static Course" and 2) a „Dynamic Course", requiring different types of challenges in obstacle avoidance. This provided results to assess the performance and safety of the TIM smart wheelchair in a range of environments and situations.

Evaluation of the results displayed the feasibility and effectiveness of the developed TIM smart wheelchair system. This system, once equipped with a unique camera configuration and reliable obstacle avoidance strategies, was able to successfully allow users to control the wheelchair with research-produced hands-free interface devices and effectively navigate safely through challenging environments. The TIM smart wheelchair system is able to adapt to people with various types and levels of physical impairment, and ultimately provide ease-of-use as well as safety during navigation.

Chapter 1

Introduction

"Human beings must have action; and they will make it if they cannot find it."

- Albert Einstein

1.1 Problem Statement

The motivation of this research comes from the unsolved issues surrounding severe physical disability, which affects the lives of a significant proportion of Australia's population, and furthermore, the world's population. There is a concerning lack of safe mobility options being made available to people who experience physical paralysis beyond what is classified as „paraplegia". For these people the options for independent control over such mobility-assisting devices as wheelchairs do not have adequate safety mechanisms in place. Consequently, harm can be caused to either the user or those in proximity when operated. These issues are addressed by the research done in this thesis.

Due to conditions such as spinal cord injury (SCI) or muscular dystrophy, physical mobility impairment can result in fewer socialising and leisure opportunities, decreased pursuit of goals, loss of physical independence, and heightened risk of depression in sufferers. Mobility aids, such as electric-powered wheelchairs, can provide significant improvements to the quality of life for many people living with physical disability. Independent mobility can enhance early learning and enrich the lives of children, and raise self-esteem for adults (Simpson 2005). Additionally, independent mobility significantly increases vocational and educational opportunities.

For these reasons and many more, a standard power wheelchair provides many opportunities beyond mobility independence. However, if the level of disability restricts the person"s capability to control such a system, then the safety of operation is compromised. These restrictions in control over joysticks, or other standard wheelchair input, can be caused by the individual"s potential lack of physical or perceptual ability, visual field reduction, spasticity, tremors, or cognitive defects.

Severe disability in many cases results in the complete inability to use conventional power wheelchair control methods such as a joystick. This has increased the demand for hands-free power wheelchairs and other assistive devices, which are essential developments toward mobility independence for many people living with such conditions as C1-4 tetraplegia, cerebral palsy, multiple sclerosis, spina bifida, muscular dystrophy, strokes, head trauma, SCI, and locked-in syndrome (LIS). In recent years a number of techniques have been developed for hands-free control over power wheelchairs and other assistive devices. These include voice control, chin-movement joysticks, eye-gaze tracking and eye-wink control, inhaling and exhaling through a tube, head-movement units, and brain-machine interfaces. The hands-free control option used by an individual is generally based on their level of disability, usually in which the higher the level of physical disability, the fewer the number of control options is available.

This is where intelligent assistive technology, such as smart wheelchairs, can contribute to increasing the safety of operation. Smart wheelchairs, being an important area of research since the early 1980s, typically involve a processing unit, such as a computer, along with a range of sensors being equipped to a power wheelchair. The combination of these with appropriate real-time software facilitates designs that can provide autonomous navigational

assistance through artificial sensory perception and analysis of the local environment. Particularly important here is when navigating through doors, corridors, and in places where people and other objects become potential obstacles. Collision-avoidance is a must in these situations and can be a challenge of significant complexity for many people operating conventional power wheelchairs.

Although the availability of hands-free controls is crucial for the large number of people who cannot adequately use conventional methods, they are nevertheless difficult to use in many cases. So the need for smart wheelchairs to be combined with hands-free control is important, allowing the user to communicate their intent for movement and the wheelchair to assist in the safe execution of those intentions. Uniting the hands-free control with autonomous navigational assistance also requires adequate shared-control strategies for overall semi-autonomous capabilities. Relying only on the user's control abilities can cause physical and mental stress to the user as well as potentially being dangerous. On the other hand, relying solely on an autonomous system can be frustrating to the user and is not feasible when navigating in unknown environments.

It is extremely likely for any given wheelchair user to require navigation in unknown environments, whereby the environment is dynamic and changes, has not previously been seen and therefore does not contain known landmarks, or has not been accurately analysed and mapped by artificial sensors. Semi-autonomous smart wheelchairs for this reason can be very useful for carrying out the user's commands whilst providing assistive features such as automated obstacle detection, mapping, speed variation, and collision avoidance. This significantly increases the safety of operation and reduces the risk of potentially harmful accidents.

With the increasing range of developments in state-of-the-art hands-free wheelchair control technology, there is evidently an increasing need for accompanying semi-autonomous smart wheelchair capabilities. In addition, the costs associated with smart wheelchairs can be far too expensive for many people living with the conditions that require such technologies, and as a result only a fraction of the target market may benefit. This gives rise to the need for affordable, accessible, and useful smart wheelchair technology, which is a major drawback of current smart wheelchair designs. Cameras, being a type of sensor not often used in smart wheelchairs, are affordable, easily-accessible, and provide a wealth of useful environmental information. With ideas for future potential commercialisation of these developments, the

focus of this thesis is on the development of a semi-autonomous wheelchair system with the use of cameras as the primary sensor type.

1.2 Aims

This thesis presents the design and development of a smart semi-autonomous wheelchair system which uses cameras as the primary sensor type, as well as the strategies developed to utilise camera data and allow the wheelchair to assist users with automated navigational guidance. The aim is to not only produce a new smart wheelchair system, but to also adopt the advantages in other smart wheelchair designs, reduce the disadvantages, and produce an advanced system with many superior qualities. The hardware system, and physical configuration thereof, are developed and advanced alongside the software developments, which encompass both algorithm and methodological strategy designs. There are two different camera system types utilised in this project to provide vision to the wheelchair, being a stereoscopic camera system and a spherical vision camera system.

These camera systems are combined to work together as the wheelchair's two primary sensory systems, allowing it to perceive its environment and make real-time decisions during navigation. The idea of this smart wheelchair is to accompany any control system, hands-free in particular, for use by any person who requires semi-autonomous assistance capabilities due to a lack of safe control or an inability to utilise current commercialised control methods.

As such, the research in this project has the following aims:

1. Develop a smart wheelchair system through the use of a commercial power wheelchair with added sensors and motor control devices, computing unit, custom frames, and generally effective hardware configurations.

2. Implement stereoscopic cameras and image processing strategies for real-time, environmental mapping that can adapt to different environments and lighting conditions, and integrate with wheel encoder data from the drive wheels to provide effective memory mapping capabilities.

3. Implement a spherical vision camera system and develop image processing strategies for real-time, obstacle detection capabilities over a wide vision range, addressing the issue of uncontrollable dynamic environments where obstacles move.

4. Determine effective methods of combining the sensors, particularly the camera systems, in useful configurations.

5. Perform an entire system integration to produce a smart, semi-autonomous wheelchair system that can be controlled from any hands-free control device.

6. Investigate the feasibility of controlling the system separately with recently-developed, non-commercial, hands-free control devices.

7. Conduct experimental studies with ten human participants, collect and process data to assess the performance, safety, ease-of-use, effectiveness, and comfort of the developed smart wheelchair prototype.

8. Assess the feasibility of the designed smart wheelchair system for use by the target demographic and determine the further developments, improvements, and modifications necessary to advance the prototype designs toward potential commercialisation.

The overall design and development of the TIM smart wheelchair in this project takes into account a number of design factors which will contribute towards potential commercialisation in later designs following those presented in this thesis. The factors being taken into consideration are individually addressed as follows:

- **Cost:** The fundamental difference in the TIM smart wheelchair design to other reviewed smart wheelchairs in research will be the use of cameras as the primary sensor for mapping, obstacle detection, user interface and control assistance, classification of environmental types and conditions, and general information gathering about the environment within which the wheelchair will be navigating. Costs associated with camera sensors in recent years are drastically decreasing while accessibility is increasing due to the large number of applications they are being used for, including smart phones, portable photography, surveillance systems, and mobile

robotics. The cameras initially selected in this project may be expensive for the sake of functionality and use in the process of prototyping, with the intention of adapting the design outcomes to use inexpensive cameras in future developments. The other sensor selections for this project are reasonably standard to smart wheelchairs and mobile robotic systems, so these are not particularly expensive.

- **Reliability:** The algorithms designed will aim to provide a high level of reliability in safety, which is here considered a feature of utmost importance in a smart wheelchair design. The reliability factor takes into account repeatability, meaning that assistive operations of the smart wheelchair should be consistently safe and experiments able to be repeated with similar displays of high performance levels.

- **Effectiveness:** Despite the fact that cameras are not a sensor commonly used for mapping in such applications as smart wheelchairs, these designs will aim to exhibit a level of effectiveness. The wheelchair is required to assist the user in a way that does not just stay safe when avoiding obstacles, but also executes given tasks in a smooth, comfortable, and desirable manner.

- **Level of System Autonomy and Intelligence:** The level of autonomy will be reasonably adaptable to suit the user's level of control over the wheelchair using hands-free technology. If the user has a higher level of control the wheelchair will reduce the amount of autonomy, and if the user has a lower level of control the wheelchair will perform more of the navigational guidance and obstacle-avoiding manoeuvres. This level of shared control between user and smart wheelchair will be easily adjusted based on the user's desires and control skills. Forward-planning of this concept also takes into account the fact that over time a user will become more accustomed to the smart wheelchair, and as such their coordination will develop and skills of control will improve, in a manner which can be likened to learning to drive a car. As the user's skill levels increase, the level of system autonomy can accordingly decrease, ultimately giving the amount of control to the user that their coordination and abilities command.

- **Ease-of-use:** An important concept to take into account is ease-of-use for the end user. If the system is too complex, it is likely the user (particularly those who are not technologically savvy) will struggle to learn the abilities to control the smart

wheelchair. Alternatively, if the system is too simple it may lack the control options sufficient to adequately control the wheelchair and provide real-time operational commands. A good balance is, therefore, necessary in the designs of user interface and control options. It must be easy to use and contain an appropriate level of understandable control options to the average potential user.

- **Durability:** A durable design is required mainly for the sake of maintenance. There is no point creating the system that needs complete repairs in events such as accidental bumps and knocks to the wheelchair when moving a user in or out of it. As such, durability will be kept in mind when designing frames, which will consist of metal parts, and when considering placement of parts and sensors on the wheelchair. Despite the prototype not being able to take into account all future designs, this is good practice, especially when considering the inevitable bumps and accidental collisions during earlier stages of prototype testing and modification.

- **Comfort:** The wheelchair designs will aim to retain adequate comfort levels for potential users. Frames for additional hardware will be built and various extra components placed on the wheelchair during its transformation, but these must be done in a manner that takes into account the basic fact that a user will be sitting in this smart wheelchair during operation, possibly for extended periods of time. This is especially the case during experimental studies on human participants in this project, because if the user is uncomfortable it will most likely result in a lack of concentration, poor results, or even early termination of experimental testing. Therefore, appropriate levels of comfort will be considered during designs.

- **Adaptability:** As previously mentioned, the wheelchair will require a reasonably high level of adaptability in various areas. It will need to adapt to such variables as differing environmental lighting conditions, physical navigational space changes, and user controllability skills and coordination. System design will facilitate adaptability of the smart wheelchair to a range of these types of important variables.

- **Control Methods:** The aim of this smart wheelchair design is for it to effectively interface with any commercial or research control devices, especially hands-free technology. In the case of testing designs in this project, the main hands-free devices used will be proof-of-concept technology, being a head-movement system and a

brain-computer interface. These will be used separately for control and comparisons made between no assistance from the wheelchair and when navigational assistance is activated during real-time operation, displaying the wheelchair‟s interfacing abilities to such non-commercial research technologies.

1.3 Thesis Contributions

This thesis presents the design, development, implementation, and testing of the TIM smart wheelchair, which uses a combination of both stereoscopic cameras and spherical vision cameras as its primary sensors. The contributions of this thesis are presented as follows:

- Firstly, a method for constructing an adaptive real-time map of the local environment is introduced, as a result of combining data from stereoscopic cameras and wheel encoders attached to the drive wheel shafts. During navigation, the wheelchair constructs the environment map within the range of stereoscopic vision, and updates the position of map features, once they move outside the vision range, with odometry change calculations that use the wheel encoder data.

    This updating procedure allows the stereo processing parameters to change based on the environmental and lighting conditions, so it adapts to the current conditions in an effort to optimise the image processing and map construction reliability. This also enables the ability for the wheelchair to carry out this map building process during navigation in unknown environments. A wheel correction method is also applied to overcome downfalls in the use of wheel encoders, which also improves the accuracies in the construction of environmental maps.

- Secondly, a strategy is proposed and validated for using panoramic images from spherical vision cameras to detect in real-time both static and dynamic obstacles surrounding the wheelchair. This provides 360º of vision to overcome the limited vision range of the stereoscopic cameras. The strategy involves image segmentation of the panoramic representation into five different segments, image pre-processing including an effective obstacle edge-detection method, before neural network classification of the segments into safety radius zones, referred to here as „Traffic Light‟ Zones.

During each update, a neural network will classify each segment image into one of up to three different classifications of the „Traffic Light" Zone categories, the options being 1) Red: Stop, obstacles too close to move in that direction, 2) Yellow: Caution, obstacles near so move slowly if moving in that direction, or 3) Green: Go, no obstacles near so clear to move in that direction. This unique approach provides a method for instantaneous obstacle detection from any angle surrounding the smart wheelchair and, in particular, helps detect dynamic obstacles not previously detected by the stereoscopic environment mapping process.

- Thirdly, a method for effectively integrating and combining the stereoscopic camera system and the spherical vision camera system is presented. This uses the biological inspiration of equine vision in the way that horses have a very wide horizontal vision range that consists of a binocular overlap in front as well as monocular vision of most of the surrounding space at any one time. The unique combination of stereoscopic cameras and spherical cameras were configured on the smart wheelchair in a manner that mimics the binocular and monocular vision of horses, whilst further improving on it by removing the blind spots inherent in the equine vision system.

- Fourthly, the system implementations of this smart wheelchair provide a means of integrating the assistive guidance system with any type of hands-free control device, including newly-developed methods that have not yet become commercially available, such as head-movement controllers and brain-computer interfaces.

  This allows the user to provide hands-free controls, no matter how few or basic, to command the wheelchair through a unique interface that utilises the spherical vision panoramic feed. Whenever the smart wheelchair receives a new directional command it can instantly adjust the directions of travel and continue to make safe automated decisions which take into account both user"s intentions and acquired environmental information.

- Fifthly, an advanced obstacle avoidance strategy for the smart wheelchair to navigate unknown environments using the camera-produced maps and environmental information is presented. Concepts were utilised from two common obstacle avoidance methods which were created for use with laser rangefinders and

sonar/ultrasonic sensors, combined, improved, and adapted for use with the type of mapping information the camera systems could produce.

This method, referred to as TIM-VPH, takes into account at any instant in time the latest input data from the user as well as the environment map data from the combined camera configuration and the wheel encoder data. It can then make safe navigational decisions on how to automatically avoid obstacles whilst navigating towards the user-defined goal directions. The system does not require any prior knowledge about the environment to assist automatically with guidance during navigation, and so has been designed for real-time, unknown environment navigation.

- Lastly, a set of experimental studies on the TIM smart wheelchair system were conducted with 10 participants, consisting of 8 able-bodied and 2 non-able-bodied participants. These were conducted for each participant using two separate options for hands-free wheelchair control, being a head-movement controller and a brain-computer interface. Through two separate obstacle courses, referred to as a „Static Course‟ and a „Dynamic Course‟ tests, the performance of the assistive system of TIM was evaluated. Results and feedback from these experiments provided useful information about the TIM smart wheelchair system, validating the methods designed, and helping to determine the necessary future work following this project.

1.4 Publications

- J.S Nguyen, T.N. Nguyen, Y. Tran, S.W. Su, A. Craig, H.T. Nguyen, "Real-time Performance of a Hands-free Semi-autonomous Wheelchair System using a Combination of Stereoscopic and Spherical Vision', 34th Annual International Conference of the IEEE Engineering in Medicine and Biology Society, San Diego, California, USA, August 28 - September 1, 2012, pp. 2069-2072
- J.S Nguyen, Y. Tran, S.W. Su, H.T. Nguyen, 'Semi-autonomous Wheelchair Developed using a Unique Camera System Configuration Biologically Inspired by Equine Vision', 33rd Annual International Conference of the IEEE Engineering in Medicine and Biology Society, Boston, USA, August 30 - September 3, 2011, pp. 5762-5765.

- V. Kitoko, T.N. Nguyen, J.S Nguyen, Y. Tran, H.T. Nguyen, "Performance of Dry Electrode with Bristle in Recording EEG Rhythms Across Brain State Changes", 33rd Annual International Conference of the IEEE Engineering in Medicine and Biology Society, Boston, USA, August 30 - September 3, 2011, pp. 59-62.

- J.S. Nguyen, S.W. Su, H.T. Nguyen, "Spherical Vision Cameras in a Semi-autonomous Wheelchair System", 32nd Annual International Conference of the IEEE Engineering in Medicine and Biology Society, Buenos Aires, Argentina, August 31 - September 4, 2010, pp. 4064-4067.

- J.S. Nguyen, T.H. Nguyen, H.T. Nguyen, "Semi-autonomous Wheelchair System using Stereoscopic Cameras", 31st Annual International Conference of the IEEE Engineering in Medicine and Biology Society, Minneapolis, Minnesota, USA, September 2-6, 2009, pp. 5068-5071.

- T.H. Nguyen, J.S. Nguyen, H.T. Nguyen, "Bayesian Recursive Algorithm for Width Estimation of Freespace for a Power Wheelchair using Stereoscopic Cameras", 30th Annual International Conference of the IEEE Engineering in Medicine and Biology Society, Vancouver, Canada, August 20-24, 2008, pp. 4234-4237.

- T.H. Nguyen, J.S. Nguyen, D.M. Pham, H.T. Nguyen, "Real-time Obstacle Detection for an Autonomous Wheelchair using Stereoscopic Cameras", 29th Annual International Conference of the IEEE Engineering in Medicine and Biology Society, Lyon, France, August 23-26, 2007, pp. 4775-4778.

1.5 Structure of Thesis

This thesis consists of six chapters, a bibliography and appendices. The following chapters of this thesis are organised as follows:

- *Chapter 2* is a review of literature. This chapter is a review of the key literature associated with this research. Australian and, furthermore, worldwide figures on disability are presented here, and these illustrate the important need for such mobility-assisting devices as smart wheelchairs. Autonomous mobile robotic systems, along with associated design techniques, play a very influential role in the development of smart wheelchair systems, particularly when taking into careful consideration the choice of artificial sensors for environment perception, and algorithms for automated assistance methods during navigation. Presented here are commercial and research

user control interface designs, as well as smart wheelchair developments in literature. This leads to the determination of a market gap, which exposes: 1) the target disability markets which have not adequately been accounted for in previous smart wheelchair designs, 2) where improvements can be made on existing technologies, and 3) what potential system constituents, namely, sensor types, have not previously been investigated for such purposes in detail. A brief background is provided to the camera sensor types of the proposed smart wheelchair system design in this research, followed by a chapter discussion.

- *Chapter 3* presents an adaptive real-time vision mapping system utilising stereoscopic cameras. The smart wheelchair prototype instrumentation and real-time vision mapping strategies, including the process and designed map construction methods, are introduced. Advanced methods for optimising the performance of intelligent vision mapping are then presented, which detail the correction of wheel measurement parameter errors as well as a strategy for automatically adapting stereo processing parameters to various environmental lighting conditions. Experiments were conducted to assess the performance of these designs and the results provided, followed by a discussion and chapter conclusion.

- *Chapter 4* proposes the utilisation of a spherical vision camera system for real-time obstacle detection over a wide vision range. With the aims of expanding the range of vision to the TIM smart wheelchair, new strategies for detecting obstacles surrounding the wheelchair were proposed and implemented. These involve panoramic image feed representations, image segmentation and processing, and neural network classification of obstacles into „Traffic Light" Zone categories to determine what actions can be taken to safely avoid detected obstacles. Following these design details, the results and implementations are discussed.

- *Chapter 5* presents the real-time operation of the TIM hands-free smart wheelchair using a unique camera system configuration, biologically inspired by equine vision. Here the final hardware and software designs, integration, and implementation are presented, along with advanced real-time obstacle avoidance strategies. The interfacing of hands-free control technology devices allow the entire system to be tested and performance evaluated through experimental studies with a total of 10

participants. The results of the designs, experimental studies, and user feedback are discussed at the end of this chapter.

- *Chapter 6* provides a discussion and project conclusion to this thesis, followed by the directions for future work.

- *Bibliography* and *Appendices* are provided at the end of this thesis.

Chapter 2

Review of Literature

"I refuse to allow a disability to determine how I live my life. I don't mean to be reckless, but setting a goal that seems a bit daunting actually is very helpful toward recovery."
- Christopher Reeve

2.1 Introduction

Intelligent wheelchairs with assistive capabilities, known as smart wheelchairs, are developed with the intention of accommodating people with severe disabilities who require more mobility assistance than conventional manual or power wheelchairs can provide. Smart wheelchairs typically consist of an electric-powered wheelchair which has been upgraded with the addition of sensors, computer processing units, and sometimes an advanced user

control interface. The general overall design architecture of a smart wheelchair is displayed in Figure 2-1.
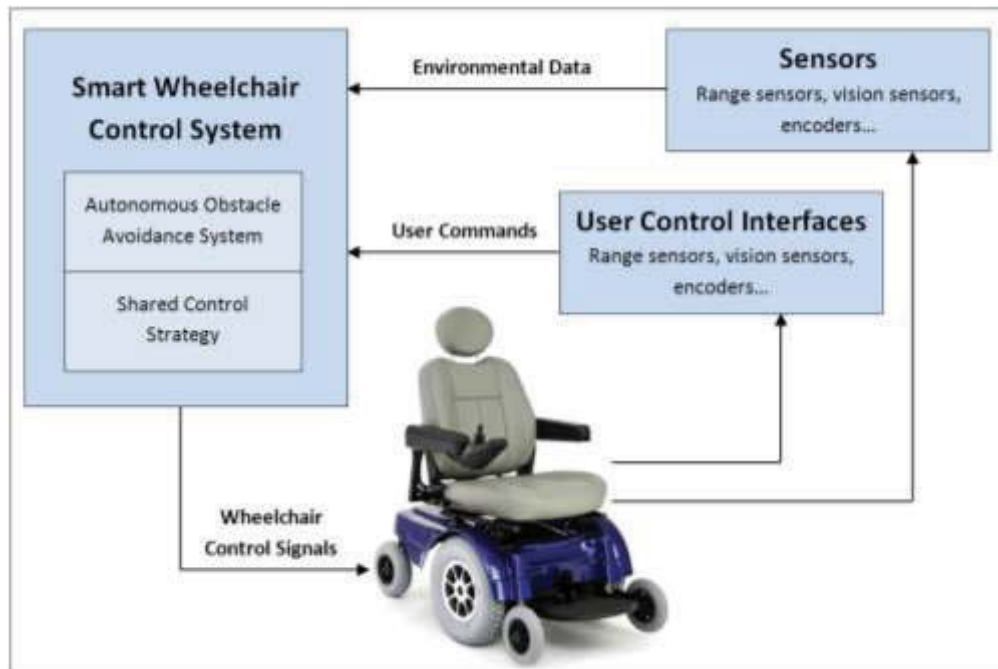
Figure 2-1: General Overall Design Architecture of a Smart Wheelchair System

An intelligent wheelchair software control system can be separated into two sub-systems: 1) an autonomous obstacle avoidance control system, and 2) a shared control strategy. The autonomous obstacles avoidance control system has the purpose of assisting the user by providing increased safety and manoeuvrability during operation. For this, there are two main approaches in obstacle avoidance strategies, the first being to utilise a pre-constructed environmental map of the area as reference, and the other strategy is to base obstacle avoidance on real-time environmental information acquired from onboard sensors. The first method has many downfalls including problems arising with environmental changes and poor performance when dynamic obstacles are present, such as moving people. The latter strategy can, however, deal with environmental changes and dynamic obstacles through the real-time use of onboard sensors, making it a more reliable method in the majority of applications.

A range of user control interfaces is possible for users to drive a smart wheelchair, whereby their intentions are usually combined with inputs acquired from the onboard sensors about the environment, allowing the shared control strategy to make suitable navigation decisions. These shared control strategies are crucial in smart wheelchair design to allow appropriate assistance from the wheelchair with the importance of carrying out the user's intentions. The

idea of shared control between user and smart wheelchair is to complement the capabilities and assist the weaknesses of each other.

The need for certain levels of autonomy in a smart wheelchair is usually dependent on the user‟s capabilities. The types of shared control design can be separated into three categories. The first is closer to the manual end of the scale which relies upon a significant level of control by the user, placing them more towards the capable end of the disability scale. In this case, the user can usually plan a path to a destination and control the wheelchair via such a control interface as a joystick. They would display an adequate level of manoeuvrability skill, perhaps requiring small levels of help from the smart wheelchair to help avoid collisions. The second category is closer to the completely autonomous end of the scale whereby the user would select a destination and the smart wheelchair will do both the path planning and navigational execution. This usually is aimed at the severe forms of disability based on the current commercial control interface technologies, such as joystick, „Chin Stick‟, and „Sip N Puff‟ control methods. These can be difficult for severely disabled users to control with adequate manoeuvres, which is why a high level of autonomy from the smart wheelchair is required. The third category falls in between the first and second, relying on both the autonomous control system and the user‟s capabilities, resulting in *semi-autonomous* operation. In recent years this category has increased in popularity based on the new emerging control interface technologies in research, such as head-movement controllers and brain-computer interfaces. As these technologies develop and improve, along with their ease of control for users, semi-autonomous shared control strategies become more appealing. This is because they allow commercial control technologies to be used with increased ease and safety as well as helping facilitate the emergence of new control technologies for the severely disable, providing higher levels of control along with increased safety during operation. The advantages and disadvantages of these category methods will be discussed further in the following sections.

This chapter has been structured into the following four main sections: Section 2.2 provides an introduction to physical disability and background statistics on relevant areas of disability, which ultimately provide the motivation for this research; Section 2.3 discusses autonomous mobile robotics systems, focussing on common sensory hardware and obstacle avoidance software technique; Section 2.4 reviews smart wheelchairs and shared control strategies, focussing on the types of user control interfaces and popular smart wheelchair designs found in literature; Section 2.5 exposes the market gap which creates the motivation for the

proposed smart wheelchair system in this research. A discussion section is also presented at the end of this chapter.

2.2 Disability

2.2.1 Physiological Information on Spinal Cord Injury

The central nervous system (CNS) comprises of the brain and spinal cord, and controls every function of both the body and the mind. Our brain provides all of our thoughts, interprets all the information from our sensors about the external environment, and is the origin of control over all bodily movements. Similar in nature to a central computing system, it is constantly interpreting a phenomenal range of information from our sensors, mainly sight from the eyes, sound from the ears, smell from the nose, taste from the tongue, and touch from the skin. It controls all voluntary movement, such as speech and walking, and involuntary movement, such as blinking and breathing. It is the core of our thoughts, perceptions and emotions. Motor and sensory nerves outside the CNS constitute the Peripheral Nervous System, and other diffuse systems of nerves, the Sympathetic and Parasympathetic Nervous Systems, control involuntary functions such as blood pressure and temperature regulation.

The spinal cord, surrounded by rings of bone called vertebra, is the communication highway between our brain and body, and different vertebral levels along the spinal cord allow communication with specific parts of the body (Figure 2-2). This is made possible via the entering and exiting of spinal nerves, which carry messages back and forth between the brain and the specific parts of the body. There are four main divisions of the spinal cord, being the Cervical, Thoracic, Lumbar, and Sacral divisions.

Cells called neurons connect with one another to send and receive messages into the brain and spinal cord. The collaboration of many neurons working together facilitates every decision made, every emotion and sensation felt, and every action taken. As many as 10,000 different subtypes of neurons have been identified, each specialised to send and receive certain types of information (SCI Research Advancement 2007).
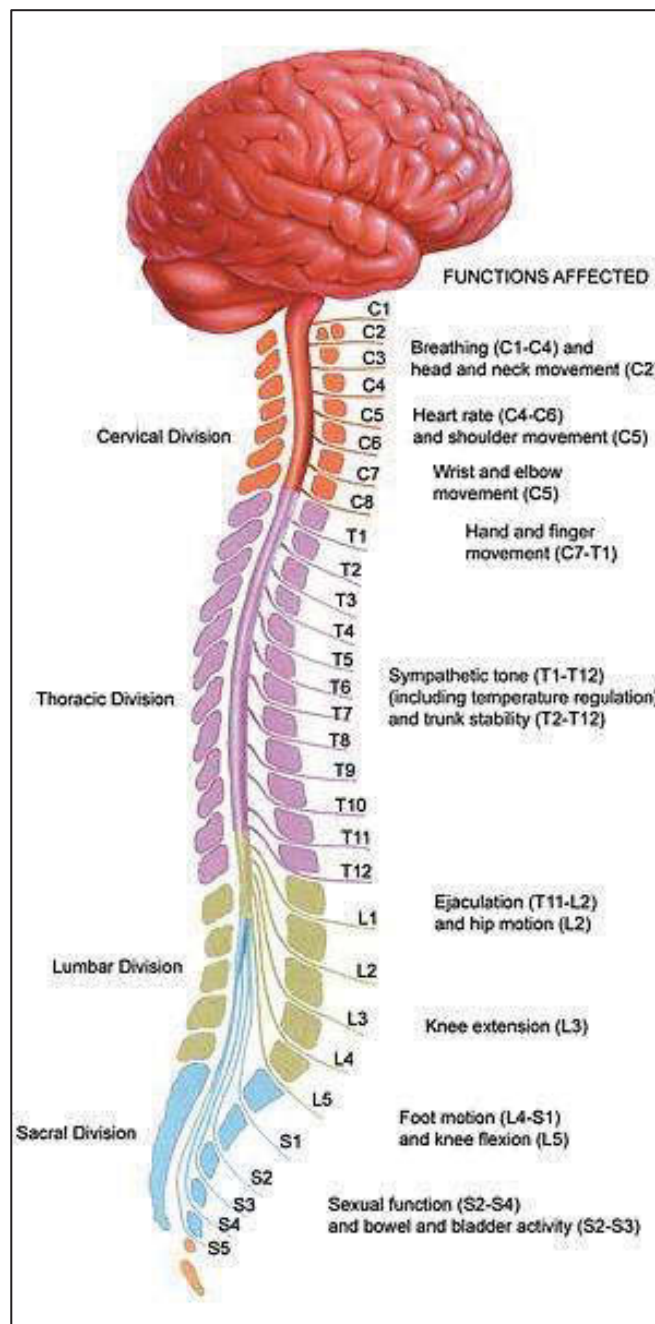
Figure 2-2: Spinal Cord Divisions, Vertebral Levels, and General Functions Affected (Thomas 2012)

The vertebrae are named in accordance with their location (Figure 2-2). The eight vertebrae in the neck are called the Cervical vertebra, the top being C-1, the next being C-2, and so on to the bottom of the Cervical division, being C-8. The twelve vertebrae in the chest are called the Thoracic vertebrae, the top being T-1 and going down to T-12. The five vertebrae in the lower back between the Thoracic vertebrae, where the ribs attach, and the pelvis are called the Lumbar vertebrae (L-1 to L-5). The five vertebrae from the pelvis to the end of the spinal column are called the Sacral vertebrae (S-1 to S-5).
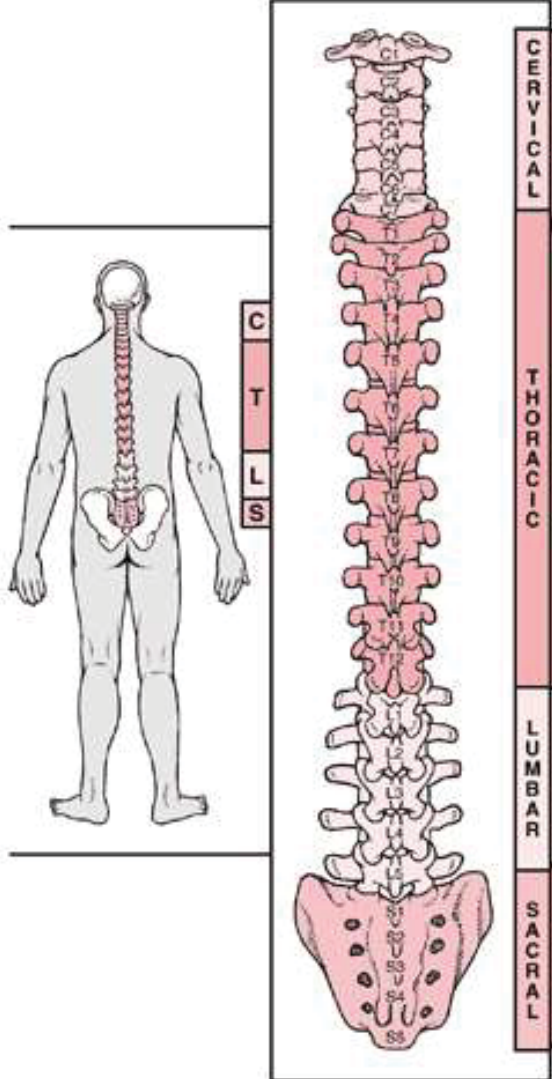
Effects of Spinal Injury

Level of Injury	Effect*
C1 to C5	Paralysis of muscles used for breathing and of all arm and leg muscles; usually fatal.
C5 to C6	Legs paralyzed; slight ability to flex arms
C6 to C7	Paralysis of legs and part of wrists and hands; shoulder movement and elbow bending relatively preserved
C8 to T1	Legs and trunk paralyzed; eyelids droop; loss of sweating on the forehead (Horner's syndrome); arms relatively normal; hands paralyzed
T2 to T4	Legs and trunk paralyzed; loss of feeling below the nipples
T5 to T8	Legs and lower trunk paralyzed; loss of feeling below the rib cage
T9 to T11	Legs paralyzed; loss of feeling below the umbilicus
T12 to L1	Paralysis and loss of feeling below the groin
L2 to L5	Different patterns of leg weakness and numbness
S1 to S2	Different patterns of leg weakness and numbness
S3 to S5	Loss of bladder and bowel control; numbness in the perineum

*Loss of bladder and bowel control can occur with severe injury anywhere along the spinal column

Figure 2-3: Effects of Spinal Injury (Rubin 2007)

When the spinal cord is injured (this cause of physical disability focussed on here for discussion), it disrupts the exchange of information between the brain and specific parts of the body. Many organs and tissues in the body do not require intervention to recover from injury, however, some cells of the central nervous system are so specialised that they cannot divide and create new cells. Therefore, it is extremely difficult to recover from a brain or spinal cord injury. In general, the higher an injury occurs in the spinal cord, the more dysfunction will result in the person.

The effects and severity of dysfunction depend on the type and level of injury to the spinal cord (Figure 2-3), being divided into two types of injury, complete and incomplete. Complete injury results in no function, sensation, or voluntary movement below the level of injury, equally affecting both sides of the body. Incomplete injury results in limited functioning below the primary level of injury, not necessarily equally affecting both sides of the body. This could possibly be the ability to move one limb more than another, retaining sensation of a part that cannot be voluntarily moved, or maybe functioning more on one side of the body than the other.

Cervical (neck) injuries usually result in tetraplegia (a term which replaces quadriplegia), associated with loss of muscle strength in all four limbs. Injuries above the C-4 level can result in loss of many involuntary functions, including the ability to breathe, making necessary the need for mechanical ventilators or diaphragmatic pacemakers. C-5 injuries mostly leave control of shoulder and biceps, but no control of the hands or wrists. C-6 injuries generally retain wrist control with no hand function. C-7 and T-1 injuries allow arms to be controlled but may have problems with dexterity in their hands and fingers. Injuries at the thoracic level and below result in paraplegia, associated with loss of muscle strength in the legs and torso, but not affecting control of the hands. T-1 to T-8 injuries mostly leave hands unaffected, however, poor trunk control can result from lack of abdominal muscle control. Lower Thoracic injuries (T-9 to T-12) retain adequate trunk and abdominal muscle control. Lumbar and Sacral injuries decrease control of hip flexors and legs (Spinal Cord Injury Resource Centre 2012).

In addition to physical mobility and control over various parts of the body, bodily processes and general activities of daily living are also affected. This can involve independence in some tasks all the way to total dependence in others, based on the level of spinal injury and resulting physical disability. An overview of the effect on activities of daily living are displayed in Table 2-1 for injury levels C-1 to C-6, and in Table 2-2 for injury levels C-7 to S-5 (Liverman 2005).

Activities of Daily Living	Level of Injury			
	Cervical 1-3	Cervical 4	Cervical 5	Cervical 6
Respiratory Control	- Ventilator dependent - Inability to clear secretions	May be able to breathe without ventilator	- Low endurance - May require assist to clear secretions	- Low endurance - May require assist to clear secretions
Bowel Control	Total dependence	Total dependence	Total dependence	Independent to total dependence
Bladder Control	Total dependence	Total dependence	Total dependence	Some to total dependence
Bed Mobility	Total dependence	Total dependence	Some dependence	Independent to total dependence
Bed and Wheelchair Transfer	Total dependence	Total dependence	Total dependence	Independent to total dependence
Pressure Relief and Positioning	Total dependence; May be independent with equipment	Total dependence; May be independent with equipment	Independent with equipment	Independent with equipment
Eating	Total dependence	Total dependence	Total dependence for setup; independent eating with equipment	Independent
Dressing	Total dependence	Total dependence	- Lower extremity: total dependence - Upper extremity: some dependence	- Lower extremity: some to total dependence - Upper extremity: independent
Grooming	Total dependence	Total dependence	Some to total dependence	Some dependence to independent
Bathing	Total dependence	Total dependence	Total dependence	- Lower body: some to total dependence - Upper extremity: independent
Wheelchair Propulsion	- Manual: total dependence - Power: possible independence with equipment	- Manual: total dependence - Power: independent	- Manual: independent to some dependence - Power: independent	- Manual: independent to total dependence - Power: independent
Standing and Ambulation	Total dependence	Total dependence	Total dependence	Total dependence
Communication	Total dependence to independent	Total dependence to independent	independent to some dependence	Independent
Transportation	Total dependence	Total dependence	Total dependence to independent	Independent
Amount of Assistance Required	24-hour care	24-hour care	- Home care: 6 hours/day - Personal care: 10 hours/day	- Home care: 4 hours/day - Personal care: 6 hours/day

Table 2-1: Activities of Daily Living in Relation to Level of Spinal Injury (C-1 to C-6)

Activities of Daily Living	Level of Injury			
	Cervical 7-8	Thoracic 1-9	Thoracic 10 - Lumbar 1	Lumbar 2 – Sacral 5
Respiratory Control	- Low endurance - May require assist to clear secretions	Low endurance	Intact function	Intact function
Bowel Control	Some to total dependence	Independent	Independent	Independent
Bladder Control	Independent to some dependence	Independent	Independent	Independent
Bed Mobility	Independent to some dependence	Independent	Independent	Independent
Bed and Wheelchair Transfer	Independent to some dependence	Independent	Independent	Independent
Pressure Relief and Positioning	Independent	Independent	Independent	Independent
Eating	Independent	Independent	Independent	Independent
Dressing	- Lower extremity: some dependence to independent - Upper extremity: independent	Independent	Independent	Independent
Grooming	Independent	Independent	Independent	Independent
Bathing	- Lower body: some dependence to independent - Upper body: independent	Independent	Independent	Independent
Wheelchair Propulsion	Independent to some dependence	Independent	Independent	Independent
Standing and Ambulation	Independent to some dependence	Independent	Independent	Independent
Communication	Independent	Independent	Independent	Independent
Transportation	Independent	Independent	Independent	Independent
Amount of Assistance Required	Home care: 2 hours/day Personal care: 6 hours/day	Homemaking: 3 hours/day	Homemaking: 2 hours/day	Homemaking: 0-1 hour/day

Table 2-2: Activities of Daily Living in Relation to Level of Spinal Injury (C-7 to S-5)

2.2.2 Disability Statistics

Current figures show around 10% of the total world‟s population, or roughly 650 million people, live with a disability (Disabled World 2011). Disability results from long-term physical or mental health conditions that contribute towards restricting one‟s abilities to carry out everyday tasks, such as communication, mobility, and self-care. These issues will be of even greater concern in the years ahead as a result of its rising prevalence. This is mostly due to ageing populations, with the higher risk of disability in older people, as well as global increases in chronic health conditions (World Health Organization 2011).

According to the World Health Organization's Global Burden of Disease Study (World Health Organization 2008), tetraplegia falls into the most severe of the 7 separated categories of disability, and about 185 million people (or 2.9% of the world's population) were severely disabled in 2004. Tetraplegia, also known as quadriplegia, is a condition of paralysis involving the partial or total loss of use of all four limbs and torso, usually as a result of illness or injury. A common cause of this is spinal cord injury (SCI), which often leads to such dysfunction and disability. As emergency and acute healthcare services improve, the number of SCI patients is expected to increase, along with the corresponding requirement for comprehensive medical rehabilitation services (Lim & Tow 2007).

Recent Australian statistics have shown that just under one in five (18.5%) Australians had a disability in 2009, representing approximately 4 million people. Furthermore, 5.8% of Australians, or approximately 1.3 million people, have profound or severe disability which limits core activities in communication, mobility, and self-care (Australian Bureau of Statistics 2011). Of these, the current Australian SCI population is estimated at 11,900 people, and about 300 to 400 new cases of SCI from traumatic or non-traumatic aetiology occur each year (Norton 2010). The ongoing costs for attendant care and equipment associated with the long-term care of the prevalent SCI population in Australia are estimated at A$500 million annually (Walsh et al. 2005).

On the most severe end of the disability scale is the diagnosis of locked-in syndrome (LIS), most commonly resulting from strokes (Hobson 2007). Individuals with LIS experience tetraplegia, in complete paralysis of nearly all voluntary muscles in the body, and anarthia, being the neurological inability to speak (Doble et al. 2003), but maintain preserved consciousness (Haig et al. 1987). Because individuals with LIS remain conscious, "linguistic ability, memory, intellectual, cognitive and emotional functions remain intact….but the inabilities for self-expression are lacking" (Soderholm et al. 2001).

With all these statistics, hospital and homecare wheelchair technology is constantly evolving to provide increased mobility to people with disabilities. Markets are poised to impact the healthcare industry by encouraging mobility and exercise for people who were previously bed-ridden. Wheelchairs impact care delivery, providing more control over the care delivery to patients and family, permitting the movement from bed and facilitating exercise, and allowing the care to be delivered in familiar settings (WinterGreen Research Inc. 2007).

There are still, however, many people living with severe or profound disability, such as those living with LIS, who are unable to use the current commercial wheelchair solutions. Hence, further developments in this field will have an even greater impact on the healthcare industry. This leads to developments such as „smart wheelchairs", which are based on mobile robotic applications, whereby additional equipment such as sensors and processing units are added to a conventional power wheelchair as well as software intelligence built into the wheelchair to allow it to assist the user in a range of ways, throughout navigational operations.

2.3 Autonomous Mobile Robotic Systems

2.3.1 Common Artificial Sensors Introduction

Artificial sensors have an important role in mobile robot applications for providing information to the control system about the surrounding environment. The mobile robot then uses this information for a range of reasons including obstacle detection and collision avoidance in both static and dynamic environments. The most popular artificial sensors used in autonomous systems are range sensors, particularly sonar, ultrasonic, infrared, and laser rangefinders. Features of each sensor will vary and every sensor has its advantages and limitations, but the careful choice of sensor will generally be determined by the type of autonomous system, the application, and the associated budgets. This section briefly reviews the commonly-used range sensors and their limitations.

Ultrasonic/Sonar Sensors

Sonar and ultrasonic sensors are some of the most popular sensors in mobile robotic applications, being widely used in obstacle detection and map building (Levine et al. 1999, Simpson et al. 2002, Lankenau & Rofer 2001). These sensors are used mainly because they are compact, light-weight, and inexpensive (Wickramasooriya et al. 2008).

Figure 2-4: Typical Sonar Sensor (SRF05)   Figure 2-5: Typical Sonar Sensor Operation
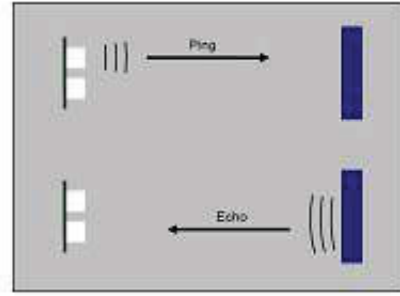
Sonar and ultrasonic sensors operate using electrical energy and a ceramic transducer to emit and receive mechanical energy in the form of sound waves (Banner Engineering Corp. 2006). They determine distance range by emitting a short burst of sound, known as a "ping", and then listening for the echo returning from the sound reflecting off the nearest object (Figure. 2-5). Sonar usually operates at around a 40Hz frequency whilst ultrasonic typically operate around 20kHz frequency range. By accurately measuring the time from when the ping is emitted to when the echo returns back to the sensor, the distance to the nearest sensor can be simply calculated as:

$$d_o = \frac{t_v c_s}{2}$$
(2.1)

where: d_o = distance to object (m)

t_v = time elapsed (s)

c_s = speed of sound in air (m/s)

This type of sensor can detect all types of solid objects, from clear, transparent, and reflective targets, to dark and opaque materials. They have definite advantages over many other sensor types in the ability to easily sense both clear objects and highly reflective objects. However, sonar and ultrasonic sensors have a number of limitations. Firstly, if there is any other acoustic noise at similar frequencies present, this will cause interference in the readings. Likewise, temperature fluctuations and air currents can also affect the signal and cause incorrect readings. As the sound waves are emitted in a cone shape outwards from the transducer, the uncertainty of an object's spatial location increases rapidly with distance. Poor directionality limits the accuracy in the determination of spatial position on an edge, depending on the distance to the object, and the angle between the object surface and acoustic beam. Specular reflections can also occur when the angle is too large between the acoustic

beam and the normal to a smooth surface, again causing range data corruption (Fonseca et al. 2001).

Multiple sonar or ultrasonic sensor arrays are commonly used in an effort to overcome many of these issues and increase accuracy, however, this also presents another problem known as cross-talk phenomenon. This is when a sensor is unable to determine whether the received echo signal was emitted from itself or from a neighbouring sensor. This results in incorrect distance measurements, usually misreading as a shorter distance to the nearest object. To reduce the cross-talk effect, Thomas Rofer introduced a transducer firing technique for the Bremen Rolland wheelchair (Rofer & Lankenau 1999). Although this improved the problems associated with using multiple sonar sensors it adversely slowed down the update rate and limited the maximum speed of the wheelchair.

Infrared Sensors

Infrared (IR) sensors usually used in mobile robotics applications are a simple, light, and inexpensive alternative to other range sensors, mostly being applicable in smaller robotics scenarios. These do not follow the same principle as sonar sensors due to the time-of-flight of a photon being too short for such a simple sensor arrangement to measure. Alternatively, these systems use a pulsed infrared light-emitting diode (LED) operating at about 40kHz, along with a detection array (Figure 2-6).
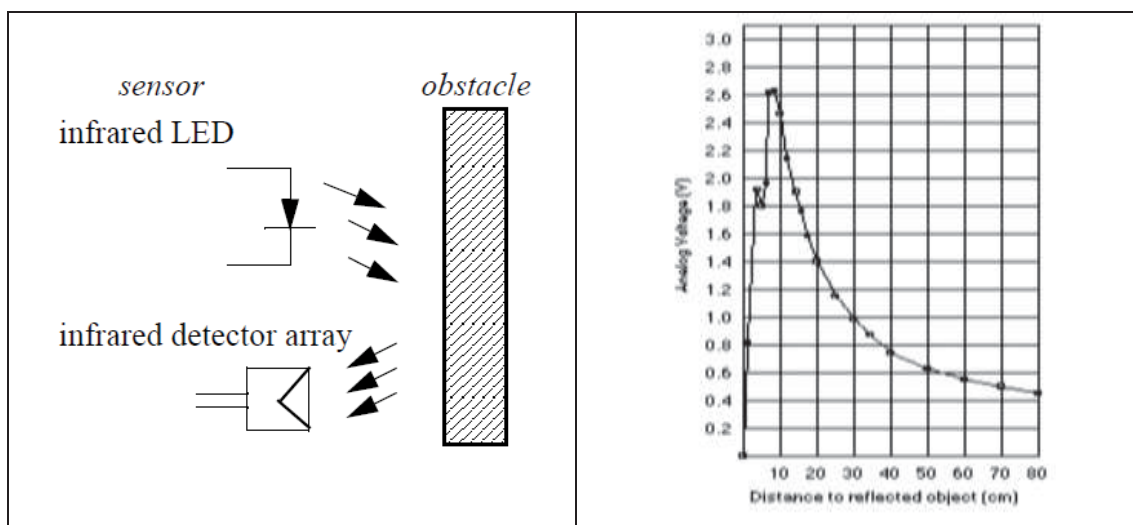
Figure 2-6: Infrared Sensor System   Figure 2-7: Sensor Diagram for a Sharp GP2D12 IR Sensor (Sharp 2012)

The angle under which the detector array receives the reflected beam changes according to the distance to the object reflecting it, resulting in a direct measure of distance. The IR light is invisible to the human eye, typically with a wavelength of 880nm. As can be seen in Figure 2-7, however, these simple and cheap sensors are used for relatively close object detection. In this case of the Sharp GP2D12 IR sensor, the sensing range is between 10 and 80cm.

Laser Rangefinders

Laser rangefinders have the ability to provide accurate range data, with high resolution and high speed streaming of the data. They consist of a laser transmitter and a receiver and operate on a very similar principle to that of ultrasonic sensors. A low power narrow laser beam is emitted, reflects off objects, and is received via the same path it was sent. The time-of-flight (TOF) of the laser signal is recorded and is used to calculate the distance to the object based on the known speed of the laser light. Laser rangefinders are a popular choice in many high-end mobile robotics developments, for such applications as localisation (Diamantas & Crowder 2009), dynamic map building (Cole & Newman 2006), and collision avoidance (An & Wang 2004).

Figure 2-8: Laser Rangefinder Examples: SICK LMS 291 and Hokuyo URG 04 LX (Rockey 2012)

These sensors use a rotating mirror to allow measurements on different angles to be obtained as opposed to an array of sensors such as those used in ultrasonic setups. The advantages of this sensor, over many other sensor types, are the very fast response, the high accuracy of distance measurements, and the operation is not disrupted by external noise or lighting conditions. The disadvantages of this type of sensor are that they typically only send out a beam on a 2D plane, usually having difficulty perceiving glass as the laser tends to go straight through, as well as the fact they are more expensive than all other sensor types mentioned in this chapter.

Camera Systems

Cameras as vision sensors are another common sensor type used in mobile robotic applications. These typically consist of at least one Charge-Couple Device (CCD) camera that can capture images of the environment, containing a lot of useful information such as size, shape, and colour features of obstacles and landmarks. Recent improvements in camera technology have seen this type of sensor reduced in weight, size, and cost, consequently making them a more attractive choice for mobile robotic applications. An example of a camera sensor is shown below (Point Grey Research Inc. 2012)

Figure 2-9: Example of Camera Sensor: Point Grey Research (PGR) Flea 3 Compact Camera

Usually utilised in relatively small-scale mobile robotic applications, camera vision systems have the disadvantages of narrow active vision ranges and are dependent upon lighting conditions, resulting in poor performance in very dark environments. Stereoscopic camera systems are a recent development to extend the capabilities of cameras, utilising two slightly offset cameras to allow instantaneous 3D depth image creation, providing the options of obstacle detection and environmental depth mapping. Spherical vision camera systems are another recent development to overcome the narrow vision range of cameras, utilising a number of cameras in synchronisation to create a very wide vision range, in many cases allowing 360º of horizontal vision range. With the advantages and recent improvements of camera technology, it is increasingly becoming a popular sensor in many mobile robotic developments, even branching out into larger-scale applications.

2.3.2 Obstacle Avoidance Techniques

General obstacle avoidance strategies are amongst the most necessary tasks in any autonomous mobile robotic system. These facilitate safe automated navigation, avoiding collisions, in unknown and unstructured environments. These strategies can be separated into two categories, being techniques used with prior environmental information, and techniques for navigation in unknown and unstructured environments. As such, some researchers rely on prior information about the environment, such as floor maps of buildings in a small-scale Global Positioning System (GPS) fashion, to provide the vehicle with safe navigational guidance (generally used in static environments). Others instead rely on online data acquired in real-time from onboard sensors, allowing obstacle detection and safe navigational guidance in various environments, including dynamic environments such as those where people are walking around. This section reviews most of the popular obstacle avoidance techniques, in each of these categories, which have been made applicable in autonomous mobile robotic systems in literature.

2.3.2.1 Obstacle Avoidance Techniques with Prior Environmental Information

This obstacle avoidance technique requires complete models of the mobile robot's environment, in such forms as environmental maps, floor plans, road-maps, or topology maps. One or more of these types of static maps, otherwise known as global maps, are available to the mobile robot, along with a pre-defined set of navigational path possibilities (Murphy 2000). This technique has the advantage of simplifying computation during real-time navigation, since the options for traversable paths from start to finish have previously been designed offline.

However, this approach is nevertheless impractical for fast obstacle avoidance, as its strength lies in global path planning, mostly suited to static and invariant environments. These methods have proven problematic when the global world model is either inaccurate or unavailable, as is typically the case in most populated indoor environments (Fox et al. 1997). This is particularly the case when the underlying world model is dynamic and can change on the fly, resulting in the need for adjustments of the global plan, which is usually too expensive to be performed repeatedly.

To overcome this, an update procedure was introduced for position corrections, based on sensor data and probabilistic representations (Hu & Brady 1994; Moravec 1998). This technique employs environmental modifications and maintenance, such as introducing known beacons or landmarks, which are commonly used for assisting in localisation correction. These modifications can be expensive depending on the size of the known environment.

Due to the inherent complexities involved in the motion planning of mobile robots in wide and complex environments, this method also limits the maximum speed that is considered safe (Schwartz et al. 1987). With an increase in the size of global maps and/or the number of optional traversable paths, the computational load is significantly increased for this obstacle avoidance technique, which can seriously affect real-time performance.

A method of speeding up the computation for this technique, referred to as a Voronoi diagram, was introduced by Takahashi and Schilling (1989). This method of path planning was demonstrated to be a faster algorithm in cluttered environments, producing a Voronoi diagram of many possible paths quickly, and obtaining the shortest path to the target out of the possible paths. This is still impractical in many situations, and again requires modifications and maintenance to a dynamic environment type.

2.3.2.2 Obstacle Avoidance Techniques in Unknown Environments

Other obstacle avoidance techniques have been designed for unknown environments, in which online sensor data providing knowledge about the environment in real-time is required. These techniques can mostly be performed without requiring any prior knowledge of the environment, and can be used to determine safe navigational paths whilst operating. The main advantages of these associated techniques are 1) the low computational requirement necessary for real-time navigation, and 2) the capabilities to operate in many types of environments, irrespective of whether or not they are dynamic and change.

Many obstacle avoidance algorithms commonly use the concepts of occupancy grids or certainty grids, as a sensor-based representation for a world model of the environment surrounding a given mobile robot. Borenstein and Koren (1989) introduced a real-time obstacle avoidance algorithm called the Virtual Force Field (VFF) method, in which obstacles applied virtual repulsive forces to the mobile robot, whilst the target location applied a virtual attractive force, in an effort to allow the robot to be pulled towards a target and steer as far

clear of objects as possible. This VFF method, however, had several severe limitations, including the inability to pass through narrow passages such as doorways, and instability of motion when travelling in narrow corridors.

This led to a very well-known adaptation in mobile robotics research, called the Vector Field Histogram (VFH) method (Borenstein & Koren 1990) using a 2-dimensional (2D) Cartesian histogram grid concept (Figure 2-10), which was a breakthrough for obstacle avoidance algorithms and involved disposing of vector values. This method updates the world model continuously and in real-time with range data from such sensors as ultrasonic sensors. The accumulated environmental data is then converted, through computation in the VFH method, into a 1-dimensional (1D) polar histogram (Figure 2-11) that is constructed around the mobile robot"s momentary location. Each sector in this 1D polar histogram contains the polar obstacle density in the direction of that sector. Finally, an algorithm is used to determine the most suitable direction for travel from all the candidate polar histogram sectors featuring low obstacle density, and the steering of the robot is then aligned with the selected direction.
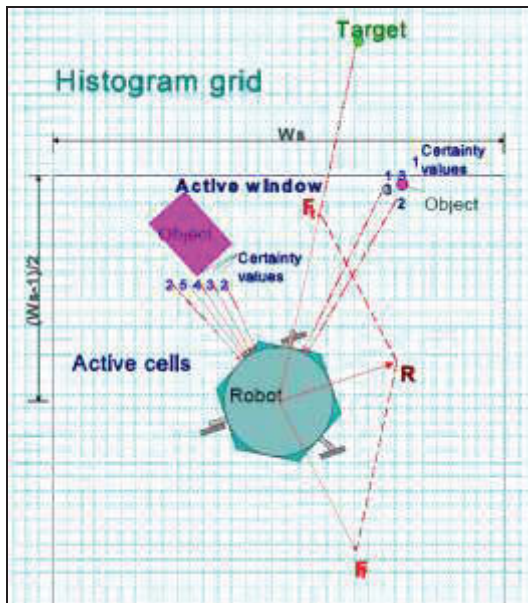
Figure 2-10: 2D Cartesian Histogram Grid   Figure 2-11: Converted 1D Polar Histogram
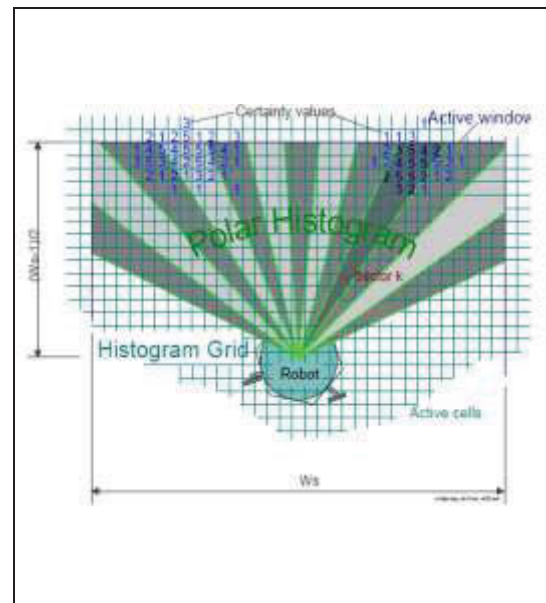
An improved method of VFH was later introduced, referred to as VFH+ (Ulrich and Borenstein 1998). VFH+ was developed to overcome some of the downfalls of VFH, and involves a four-stage data reduction process to compute the new direction of motion. These four stages are 1) mapping the active region of the map grid onto a primary polar histogram, 2) building of a binary polar histogram giving either free or blocked segments, based on the

primary polar histogram and two threshold values, 3) creation of a masked polar histogram to show which directions of motion are possible at the current speed, and 4) selection of a steering direction with the use of a cost function.

The four-stage process of VFH+ provides three main improvements over the two-stage process of VFH. These are 1) VFH+ takes into account the width of the mobile robot by using an implicit configuration space approach, 2) it can commit to a direction due to an improved selection process, which is based on a multivariable cost function, and 3) the candidate direction selection also takes into consideration the robot"s current trajectory at any given time, and places a cost proportional to the deviation away from that trajectory, aiding in the mobile robot being less oscillatory when choosing which free space direction to navigate around an obstacle.

An and Wang (2004) introduced another approach called the Vector Potential Histogram (VPH) method, which combined and further adapted the algorithms used in VFF and VFH+ to remove the certainty grids which are necessary for ultrasonic arrays, but not needed for laser rangefinders. This is due to the low-error and high-resolution nature of laser range data. VPH also takes into account both the real-time velocity of the robot and the vehicle"s maximum deceleration rate for improved safety during variable-speed navigation. The threshold used to facilitate the formation of a binary histogram in VFH+ is a pre-determined and invariable line across all angles, whereas VPH considers the different influences caused by the distribution of angles.

Using VPH, the response of a mobile robot is based on the obstacle distribution reflected on the vector polar histogram. A threshold function is then applied to the polar histogram to produce a binary histogram, and then a set of candidate directions are analysed by a cost function, so a steering direction can be selected and a speed decided upon.

Gong et al. (2007) attempted to improve upon the VPH method, called the enhanced Vector Polar Histogram (VPH+), to allow obstacles to be avoided more efficiently in complicated environments. VPH+ claims a few improvements on both VFH+ and VPH methods. Firstly, VPH+ groups isolated obstacle points detected by laser radar into obstacle blocks, enabling obstacles to be avoided in advance and a more desirable trajectory to be obtained. The second is a time-oriented cost function, in which the speed and heading deviation, between the

current heading and the target direction, are combined. This aims to reduce the time taken for the mobile robot to reach its target goal.

These methods have not varied too much, even in more recent years. Larger vehicles like cars in the simulator described in a paper by Noto et al. (2012), still use potential field algorithms for obstacle avoidance, with attractive potential from goal, repulsive potential from walls, and repulsive potential from obstacles. This shows that adaptation even into mobile robotic applications on a larger scale will still benefit from these styles of obstacle avoidance strategies.

Overall, each of these obstacle avoidance techniques for unknown environments has advantages and disadvantages. They all work well under given situations and applications, however, no single method solves every mobile robot problem. As a result, ideas should be analysed, combinations of algorithms created, and adaptations should be made when considering unique mobile robot applications to best solve the problem at hand, since all these techniques have strong methods across a range of situations.

2.3.3 Computational Intelligence

Computational intelligence consists of methods used to enhance the abilities of a smart wheelchair to actually introduce intelligence into the system as opposed to simply carrying out tasks and responses completely set out by the designer. Artificial intelligence comes in many forms, of which the main type utilised in this research is artificial neural networks, used for enhanced classification systems.

An artificial neuron is a mathematical function modelled on a biological neuron. McCulloch and Pitts (1943) introduced the first formal model of computing neuron, based on the way in which the human brain stores and processes information. The dynamics of the network were fundamentally determined by the connections between the neurons, which is the reason why the field known as „Neural Networks" today was originally referred to as „Connectionism".

Rosenblatt (1958) presented a new model which extended on McCulloch and Pitts" threshold neuron. This model used a continuous function which made training a network of perceptrons easier than a network of threshold neurons. Further advantages were that perceptrons did not require precise connections and timing, as well as producing an analogue output as opposed to

the threshold neuron''s purely binary output. This model could, however, only learn and classify linear categories, being incapable of learning classes of non-linear patterns.

Rumelhart, Hinton, and Williams (1986) solved this problem with the development of a back-propagation training algorithm. This form of neural network has significantly contributed to various applications since its development, through the ability of learning to approximate any complex non-linear function.

A standard feed-forward neural network used in many modern applications is constructed by a set of perceptrons arranged into several perceptron layers, as displayed in Figure 2-12 (Nguyen 2012). Training data is fed into the input layer, then transmitted to the following neural layers, and classified output values are generated at the output layer. This type of neural network has the ability to learn any complicated linear or non-linear process.
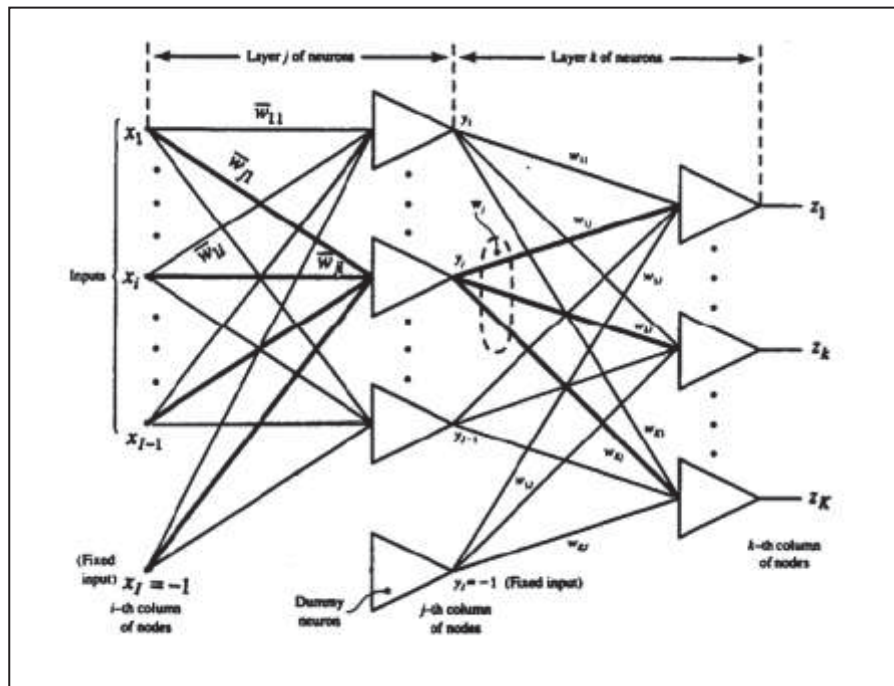
Figure 2-12: Structure of a Two Perceptron-layered Feed-forward Neural Network

This neural network relies on a commonly-used back-propagation training algorithm to minimise the error function that results from differences between the designed and actual network outputs. This algorithm is based on the first derivative descent technique, which is, however, an ineffective and slow method for training. This is particularly noticeable in large-scale problems with several thousand training parameters.

For this reason, there have been many faster algorithm developments, such as the conjugate first derivative (Gill et al. 1980; Moller 1993), quasi-Newton, and Levenberg-Marquardt (Hagan & Menhaj 1994) algorithms. These algorithms estimate the second directional derivative of the error function, instead of relying on the first derivative, in order to convert the training process directly to a local minimum. This provides faster and more consistent standard neural network training.

Although these algorithms increase the speed of training, they still do not solve other shortcomings inherent in standard neural network training, such as the over-fitting phenomenon or the determination of a suitable network structure. As the learning process of a standard neural network involves the minimisation of the error function, it only builds statistical models of the provided training data, rather than an exact representation of the process that generates the data. Hence, the more meticulously a training set of data is learnt, the worse the classification performance of the network will be, due to there being no room for adaptation to variances in the data. This is known as the over-fitting phenomenon.

In order to prevent this occurring, an early stopping technique is employed. The idea of this technique is to stop the training process just before the neural network can learn the noises from the training set and to avoid over-fitting. However, this still does not completely solve the problem as determination of an effective early stopping point is mainly based on the designer‟s experience, along with trial and error.

A more advanced technique overcomes this problem and assists with determination of an effective early stopping point. This technique, known as cross-validation (Ripley 1996), requires an additional data, known as a validation set, to supervise the training process. The network, as it learns the training set, is simultaneously applied to the validation set, along with monitoring of both network output errors, being the training error and the validation error. The training process is stopped as the validation error begins increasing, which is a sign that the network has begun to learn the noises from the training data set. This does require the availability of more data to allow training, validation, and testing of the network with different data sets, and will also vary for different network structures. However, it overcomes many problems with standard neural networks and can assist with optimising a neural network solution for learning complicated linear and non-linear data.

2.4 Smart Wheelchairs and Shared Control Strategies

2.4.1 User Interfaces for Wheelchair Control

Analog and digital are the two types of drive interfaces for controlling wheelchairs. The most common controllers and easiest to use, for those who have the capability, are the analog interfaces. Analog controls provide a continuous type of control within the bounds of speed and steering limits, whereas digital controls provide a discrete type of control, usually with limited speed and steering control, removing the ability for fine adjustments. Various user interfaces for wheelchair control, whether analog or digital, have been produced to target different levels of user abilities. Generally, it is more desirable to have a control option which utilises the best of the user's physical abilities, however, in cases of severe disability, analog controls are simply not feasible, giving rise to the need for more digital control interfaces to be developed.

The main user control interfaces currently on the market are the joystick control, finger drive, touch pad, chin drive controllers, head-actuated control systems, and the Sip'n'Puff drive control system (Wheelchair.ca 2012). The most simple and commonly used interface is the conventional analog joystick control (Figure 2-13). These can easily be mounted on wheelchairs for either right or left hand use. The joystick is manually moved by the user to direct the wheelchair, with the amount of movement determining the speed of operation in that direction. Joystick control units typically feature an on/off switch, battery gauge, maximum speed control, and in some cases, a button or switch for selecting the drive mode.

Figure 2-13. Analog Joystick Controller

If the user has control of their fingers but not enough hand control to use a joystick, two alternatives that use the movement of fingers for control are the finger drive control, shown in

Figure 2-14, and touch pad control system shown in Figure 2-15 (MobilityBasics 2012). The finger control drive system consists of a small square box with a hole in the top. To control the wheelchair, the user places one finger through the hole and moves their finger in the direction for which they want the wheelchair to navigate. The touch pad uses a very similar concept by touching the pad with a finger and moving it in a direction, whereby more movement translates to a higher speed in that direction.

Figure 2-14: Finger Drive Controller   Figure 2-15: Touch Pad Controller

For the many people who cannot use their hands or fingers enough to control the above methods, hands-free control interfaces must be used. As such, the next device here is a chin drive controller (Figure 2-16). This basically works the same as the conventional joystick except it is modified for being moved by a user's chin, and as such is positioned slightly below and in front of the chin. Varying end pieces are available, for example, some are more like the joystick and others in a cup shape, to meet different user needs.

Figure 2-16: Chin Drive Controller (MobilityBasics 2012)

If the user does not have the capacity to move this chin controller option, an alternative is head actuated controllers. One version of this product is called a RIM controller (Figure 2-17), which is an analog device mounted behind the head and attached to the headrest. The user pushes with the back of their head left and right for turning and pushes back to go forward. A drawback of this is that the user cannot use the headrest actuator as an actual headrest, unless the power is switched off. Furthermore, if the user wants to reverse the wheelchair they must activate a switch to change the forward control to a reverse control, and vice-versa. This is not a great concern, however, when more manoeuvres are required it can be frustrating for the user to constantly need to switch between the forward/reverse function.

Figure 2-17: Analog RIM Head Actuated Controller (MobiltiyBasics 2012)

Another version of head actuated control is a digital head control system, which has a larger headrest spanning around to the side of the head (Figure 2-18) and contains switches in each part of the headrest. These switches are activated by physical movements of the head back into the rear headpiece to move forward, and against the left and right headpieces to move in those directions. The advantage of the digital head control system over the RIM analog controller is the user does not need to apply constant pressure throughout the movement, but instead only needs press a direction for that movement to start. The disadvantage of this system to the analog, however, is that there is no speed adjustment due to the digital switching of direction selections. Other similar drawbacks to the analog system include the headrest not being able to be used as a headrest, and again a switch must be activated to change between forward and reverse operations.

Figure 2-18: Digital Head Control System (MobilityBasics 2012)

Moving on from head actuated controllers, if the user is not able to control a wheelchair through any physical movements, another commercial option is the Sip'n'Puff drive controller (Figure 2-19). This type of controller mainly consists of a tube placed in front of the user's mouth. These systems are non-proportional drive controllers that require much practice before the user can adequately and safely control the wheelchair. It operates by the user either sucking from the tube or blowing into it, using soft pressure or hard pressure for each to supply a total of four controls to the wheelchair.

Figure 2-19: Sip'n'Puff Hands-free Drive Controller (MobilityBasics 2012)

2.4.2 Smart Wheelchair Review

Literature has shown a range of different „smart wheelchair" designs, particularly over the past two decades. The majority of smart wheelchairs developed have been tightly integrated with the underlying power wheelchair and require significant modifications to function in an intelligent fashion. The differences have been in their target users, forms of control over the wheelchair, types of assistive sensory technologies used, operational specifications, and algorithms for intelligent assistance. The majority of smart wheelchairs represent the outgrowths of mobile robotics research. One distinct way to classify smart wheelchairs is where along the manual-autonomous scale they belong, or, in other words, how they share the control between the user and the wheelchair's intelligence system.

Some smart wheelchairs operate in a similar manner to autonomous robots, whereby the user provides a final destination and the wheelchair completely plans and executes a path to the desired location. In order for these systems to reach their destinations they typically require either a completed map of the area through which they are navigating, or modifications to the environment such as distinct tracks (e.g. tape or paint) on the floors or distinct markers on the walls. In many cases these are then unable to compensate for disruption by unplanned obstacles or travel in unknown environments. Smart wheelchairs in this category are most appropriate for users who 1) lack the ability to plan and/or execute a path to a destination and 2) spend the majority of their time within the same known and controlled environment.

Other smart wheelchairs are further towards the manual end of the scale (semi-autonomous) and allow the user to do the majority of the planning and navigation whilst providing obstacle detection and collision avoidance strategies. These systems typically do not require prior knowledge of the environment nor specific markers or modifications. They do, however, require more concentration, planning, and control on the part of the wheelchair user, making them most appropriate for users who 1) have the ability to plan paths to destinations, 2) require the freedom of control in between specific destinations, and 3) do not spend the majority of their time in the same environment and like to navigate in „unknown" environments.

Reviewed here are some examples of smart wheelchair prototypes in literature falling into the two categories, being those that rely on prior environmental information or those designed to navigate in unknown environments.

2.4.2.1 Smart Wheelchairs Requiring Prior Environmental Information

Many smart wheelchairs in research have been developed to operate as a large autonomous mobile robot. They operate in a manner such that the user selects a destination from a predefined set of destinations in a known environment, and the wheelchair will navigate along a known or calculated route to get there. Obstacle avoidance is carried out along the way if necessary. These smart wheelchairs require prior knowledge of the environment, and use such obstacle avoidance techniques as those discussed in §2.3.2.1. In many cases these also require modifications to the environment or landmarks to be setup for localisation and other necessary mobile robotic navigation processes.

An example of this application is the *RobChair* (Figure 2-20), being a smart wheelchair prototype developed at the University of Coimbra, Portugal (Pires et al. 1998, Lopez et al. 2007). This prototype has the ability to navigate in known indoor and outdoor environments. In addition to the control interfaces, being the conventional joystick and a voice control interface, it is also equipped with ultrasonic sensors, laser sensors, and a magnetic ruler. These all communicate with an onboard industrial computer, which also drives the motors via the CAN (Controller Area Network) bus.

Figure 2-20: *RobChair* Smart Wheelchair Prototype (Lopez et al. 2007)

The RobChair makes use of prior environmental maps and magnetic markers or tape on the ground to allow paths to known destinations to be calculated and followed. The magnetic ruler at the front of the prototype is used to detect magnetic markers and stay on track. If there are any obstacles in the path the RobChair can utilise the laser and ultrasonic sensors to temporarily divert, avoid the obstacles, and move back to the path being followed. This allows users to select known destinations and the wheelchair to transport them there safely in an autonomous fashion.

Another smart wheelchair prototype which uses this category of control approach is the Collaborative Wheelchair Assistant (*CWA*) (Figure 2-21) from the National University of Singapore (Qiang et al. 2007, Qiang et al. 2008). A conventional joystick was initially used to control the early stages of this prototype, but this was later replaced with a BCI for control by users not able to drive the wheelchair via the joystick. A laptop is used as the main processing and control unit, and a front proximity sensor, a barcode scanner, and two optical encoders are the sensors chosen to allow the wheelchair to stay on-route when navigating along pre-determined paths.

The CWA prototype utilises pre-planned virtual paths stored in the memory of the laptop''s hard drive, as opposed to physically marked or magnetic tape tracks in the known environment. The paths are generated via a walk-through technique, where the wheelchair is driven along potential paths of travel and the sensor data recorded for future reference and repetition when required.

An elastic path strategy was designed and employed here for obstacle avoidance. The virtual path can be modified on the fly to deviate away from the pre-determined path in the event of an obstacle being detected, allowing the wheelchair to move around the obstacle and back to the planned path of navigation. To aid in localisation, artificial landmarks in the form of barcodes are located on doors and walls, allowing the barcode scanner to detect the barcode and send location information to the wheelchair as it navigates the known environment. As such, the user can select known destinations and the wheelchair will autonomously transport them there in a safe manner.
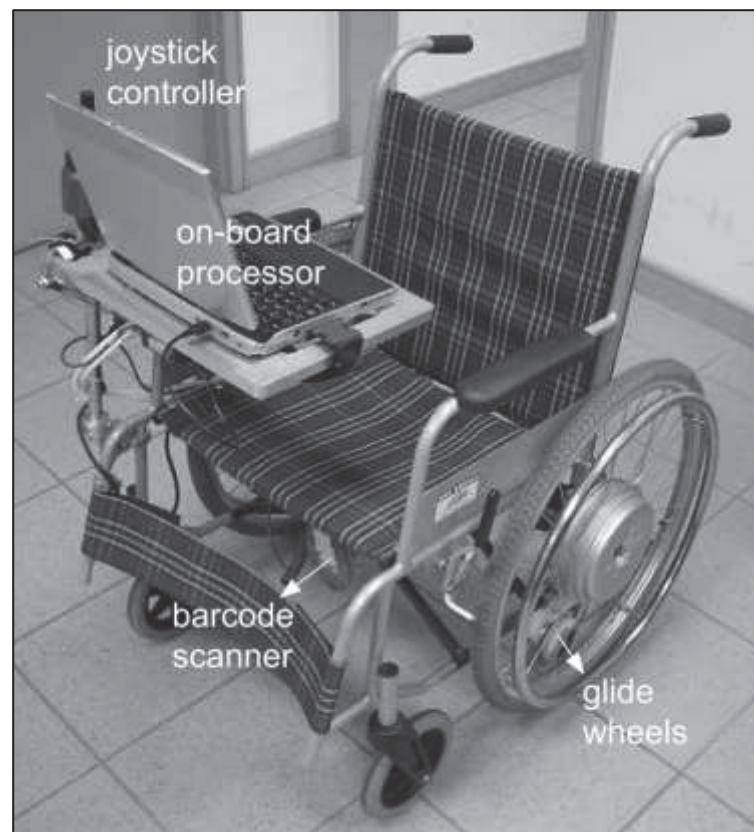
Figure 2-21: Collaborative Wheelchair Assistant (*CWA*) Prototype (Qiang et al. 2008)

The *SENA* robotic wheelchair (Figure 2-22) prototype involves extension of the control approach in this category, by also adding in a human-robot integration idea. This wheelchair is intended to facilitate mobility to impaired and elderly people, exhibiting a high degree of autonomy. SENA is based on a commercial electric wheelchair with the addition of a laptop for processing and several sensor types, including 13 infrared sensors, a laser system, 2 ultrasonic sensors, wheel encoders, and a CCD camera (Gilando et al. 2006, Gonzalez et al. 2006). Considered in this development was the particular case of assistant robots, where the user can physically help the robot with such actions as opening a door, as well as improving the robot abilities such as performing a robust and reliable navigation by manually guiding the wheelchair. The user can participate at several abstraction levels of the system, ranging from a high level (advising a route to a destination) to a low level (reporting information as an extra sensor, such as personally detecting close obstacles).

Figure 2-22: SENA Robotic Wheelchair (Gonzalez et al. 2006)

The aim of this was in the design and implementation of the human-robot integration idea into the SENA robotic wheelchair, allowing the user to improve the autonomy of the whole system by participating at all levels of the robot operation, from deliberating a plan to executing and controlling it. The user is integrated as a constituent part of the system, with the following goals: 1) The system must consider the human physical abilities and allow the user to perform tasks they are capable of, including opening doors or pressing buttons for lifts; 2) Take into account the human perceptual abilities, basically meaning that the user will be doing a lot of the obstacle detection themselves; 3) Detection of execution failures, such as if there is a navigational error, in which case the user will have to manoeuvre the wheelchair with the joystick; 4) High-level communication, such as voice simulation allowing simple communication between user and SENA.

The idea is to give the user the majority of the ability but to assist with alerting the user when obstacles are detected, but mostly the system concentrates on the interaction concepts between SENA and the user. In a known environment SENA can learn paths between locations and give path planning guidance to the user through its verbal communication

abilities, in a small-scale GPS fashion. The laser rangefinder and infrared sensors are used for obstacle detection which in turn alerts the user to potential collisions, allowing them to take these alerts into account when controlling the wheelchair via joystick input. The CCD camera is an additional sensor to help aid SENA in localisation.

This system seems to have put in most types of sensors related to mobile robotics without really making the best use out of each individual system. The human-robot interactions were a good design idea for the fact that forms of communication and the overall cooperative process, improving the system, between SENA and the user is very beneficial for such an application. This is, however, restricted to joystick control and relies quite heavily on the user''s abilities, placing this wheelchair design closer to the manual end of the scale than the autonomous end. It focuses on the interactive and communicative intelligence of the wheelchair instead of physical assistance during navigation, but these ideas of the system and user working together are very important in the process of developing a truly intelligent ,,smart wheelchair'' system.

Overall, these prototypes can work well in known environments that remain reasonably consistent in terms of object placement and structure. However, maintenance and readjustment of the maps and information available to the wheelchair may be necessary if the environment changes. Dense and dynamic environments will also present major problems to these strategies as associated obstacle avoidance techniques, such as the elastic path strategy used in the CWA wheelchair, will only allow avoidance of static obstacles. The modifications to the environments and the setting up of tape tracks and artificial landmarks can be very time consuming, require regular maintenance, and is generally inconvenient.

2.4.2.2 Smart Wheelchairs for Navigation in Unknown Environments

To overcome the disadvantages involved in setting up known environments with all necessary features for autonomous navigation, many researchers focused their efforts on smart wheelchair navigation in unknown environments. This involves providing the smart wheelchair systems with a range of autonomous navigational tasks to assist the user in several different situations. The idea here is that the user sends navigational commands to the wheelchair through a control interface and the wheelchair then attempts to carry out these commands whilst utilising on-board sensor information to assist in the navigational process, such as automatically avoiding obstacles or moving through doorways.

Since end destinations are generally not known or pre-defined in this category of control approach, these smart wheelchair system designs are usually semi-autonomous and include a specific level of shared control. This means that the user has a level of control over the directions of navigation and the smart wheelchair also has a level of control over such tasks as finer manoeuvres during obstacle avoidance. The level of control given to each in the form of shared control will depend on the abilities of the user to adequately control the wheelchair system through the connected control interface. A greater level of user control ability will result in less control being necessary from the smart wheelchair system, whereas a lower level of control ability will require increased assistance from the system.

An example of this application is the *NavChair* prototype (Figure 2-23), which is an assistive wheelchair navigation system based on a commercial power wheelchair system, with the addition of a DOS-based computer system, 12 sonar sensors, and an interface module interposed between the joystick and power module of the wheelchair (Levine et al. 1999). The obstacle avoidance routines used by the NavChair, in conjunction with the ultrasonic sensors for object detection, are modifications of methods originally used in mobile robotics research.

Figure 2-23: NavChair Assistive Wheelchair Navigation System Prototype (Levine et al. 1999)

The NavChair is aimed at assisting individuals who would otherwise find it difficult or impossible to use a powered wheelchair due to motor, sensory, perceptual, or cognitive impairments. The objectives were to share vehicle control decisions with the user in relation to obstacle avoidance, safe object approach, maintenance of a straight path, and other navigational issues, to reduce the motor and cognitive requirements for the user operating it.

It is designed to function semi-autonomously with a shared control system to allow the user a level of control via the joystick input, along with varying forms of assistance from the wheelchair''s software system. It incorporates a mechanism for selecting between three modes of operation, which each have varying abilities to operate the wheelchair in different environment layouts. These three modes are general obstacle avoidance (GOA), door passing (DP), and automatic wall following (AWF).
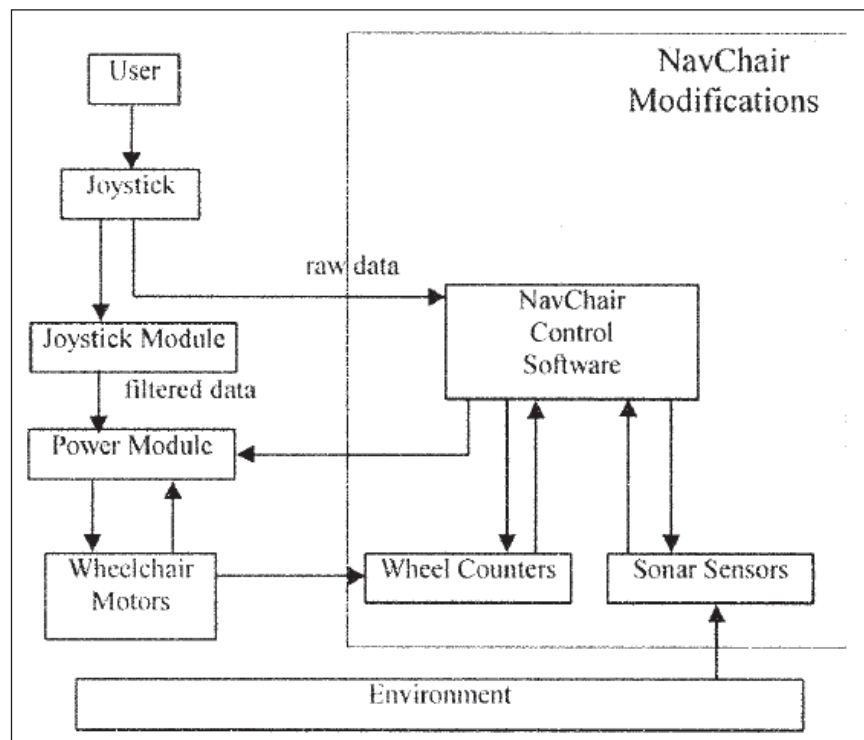
Figure 2-24: Functional diagram of the NavChair prototype''s hardware components

The Lancer''s controller is divided into two components, the joystick module and the power module. The joystick module receives input from the user via the manual movement of the joystick and converts it into a signal representing desired direction. The power module converts the output of the joystick module to a control signal for the left and right wheel motors. During operation, the NavChair system interrupts the connection between the joystick

and the power module. The joystick position and the sonar sensors (reflecting the wheelchair's immediate environment) are used by the control software to determine the control signals that are sent to the power module and hence the wheelchair motors.

Sonar sensors are utilised in an array in this application for their simplicity and low cost. These are used to create a small map of the NavChair's immediate surroundings. The accuracy of the map is also enhanced by keeping track of the wheelchair's motion via wheel rotation sensors built into the Lancer's wheel motors. The combination of the sonar sensor array and the wheel rotation sensors allows the NavChair to locate obstacles nearby within five degrees of angular resolution relative to the centre of the wheelchair, even though the resolution of each individual sonar sensor exceeds 15 degrees.

The control input of the conventional joystick and the sensors being ultrasonic allow for the potential of a relatively inexpensive implementation when considering smart wheelchair designs. This could be an assistive device for people who have a reasonable level of control to utilise such controls as the joystick, but perhaps require extra navigational assistance for obstacle avoidance and the more difficult situations such as door passing. The use of ultrasonic sensors in this situation is a good choice because it is a reactive approach to the immediate and reasonably close obstacles in the environment.

Another example of this application is the *Bremen Autonomous Wheelchair "Rolland"* (Figure 2-25), which was developed as a support tool to help handicapped and elderly people control a wheelchair (Lankenau & Rofer 2001). It implements an obstacle avoidance system with the use of 27 ultrasonic sensors in an array around the wheelchair, wheel encoders, and features two modes of assisting operation for certain actions or manoeuvres the user cannot perform independently any longer. These two modes are a driving assistance mode and a routing assistance mode, implemented in a shared control system.

Figure 2-25: The Bremen Autonomous Wheelchair "Rolland" (Lankenau & Rofer 2001)

This wheelchair operates semi-autonomously with the objective that if the human operator issues a command that could potentially lead to a collision with an obstacle, the wheelchair will activate a change from the dangerous command into a similar yet safe one. To achieve this it features a shared control system between the user, who sends commands via the joystick control, and the Rolland wheelchair, primarily for the obstacle avoidance skills. The basic aim of the proposed obstacle avoidance method is to detour obstacles in a way that is most likely to be acceptable for the operator. Depending on the specific type of user, two different operational modes, so-called "assistants", can be activated. These are called the „Driving Assistant" and the „Route Assistant".

The „Driving Assistant" mode helps the user when they are navigating the wheelchair under normal conditions. In this mode the user can concentrate on the global navigation task by commanding rough directions with the joystick and the driving assistant mode of Rolland is then responsible for the local manoeuvres. This allows the user to control the wheelchair as desired and the control system takes care of local obstacle detections and collision avoidance. In comparison to the driving assistant mode, the responsibilities for the global and local navigation tasks are exchanged in the route assistant mode.

The „Route Assistant" mode allows for known local environments, such as rehabilitation centres, to have set routes remembered for providing assistance to destinations within the place, in a small-scale Global Positioning System (GPS) fashion. This mode is aimed at assisting people like amnesic patients who are very good at carrying out procedural tasks but fail when they should find the way to another place, even if it is somewhere they spend much of their time. Similar to the GPS-based navigation system, the large-scale navigation is done by the route assistant, providing instructions where to go at decision points, and enabling the user to travel around on his or her own, including independently avoiding obstacles. This approach does not use any additional sensors such as cameras to detect landmarks, and instead only requires the wheelchair's odometry data.

A major part of the software design was spent on overcoming issues with the ultrasonic sensors in regards to data accuracy and synchronicity, since only two sensors could fire simultaneously. This affects how quickly Rolland can receive a complete reading from all 27 ultrasonic sensors. When carrying out shared control navigation with the user, Rolland bases its speed on how close obstacles are to it, in that the closer they are, the slower Rolland will move.

This wheelchair is not too different a design to the NavChair physically, but is more suited to the users who do not require a great level of navigational intelligence from the wheelchair. This shifts the shared control system closer to the manual end of the control scale than the autonomous end. It takes two specific target user types into account with the two available operational modes.

Although the approach does not remember maps, Rolland uses the ultrasonic sensor array to produce very local probability maps in the driving assistant mode, allowing the wheelchair to aid in obstacle avoidance whilst the user is controlling via the joystick. This mode is set on assisting users who know where they want to navigate to but struggle in the finer manoeuvres when controlling the wheelchair, resulting in the need for semi-autonomous obstacle avoidance strategy, which is done in a reactive manner in this case.

These modes could ideally be combined in the route assistant mode, allowing assistive obstacle avoidance from Rolland to be active instead of keeping the modes in their individually different states. Furthermore, the route assistant mode can potentially encounter problems in the way it only uses odometry data, which exhibits error increases over time,

instead of using landmark recognition or other such methods for localisation. This, however, is understandably difficult given the sensor limitations and type of data they can produce. The Rolland system is also limited to users who are capable of control over a joystick, not being a very adaptable system to control methods for users with higher levels of disability.

The *Hephaestus Smart Wheelchair System* (Figure 2-26) is another prototype made for navigation in unknown environments, and was envisaged as a series of components that clinicians and wheelchair manufacturers would be able to attach to standard power wheelchairs to convert them into ‚smart wheelchairs" (Simpson et al. 2002). The prototype, mounted on an Everest and Jennings Lancer2000 power wheelchair, bases its navigational assistance on the behaviour developed for the NavChair, but the additional hardware and software was designed with the intent to facilitate commercialisation. The Hephaestus provides shared control navigation assistance to the user, using the conventional joystick for control input, and for perceiving the local environment, 16 sonar sensors and 2 bump sensors were mounted to the wheelchair.

Figure 2-26: The Hephaestus Smart Wheelchair System prototype (Simpson et al. 2002)

As shown in Figure 2-27, 13 sonar sensors are mounted on the lap tray facing forward or to the side of the wheelchair and 3 sonar sensors are on the battery box facing backward. During operation, 2 sonar sensors are fired simultaneously, and coordinated in the configuration shown to reduce erroneous readings from sensor crosstalk. Due to the limited number of sonar

sensors, several „blind spots" were present, creating the possibility of collision even with the navigational assistance from the wheelchair. Any obstacles located a few inches above or below the lap tray or battery tray are unlikely to be detected by the sonar sensors, especially in the areas where there are no sensors around the battery tray.
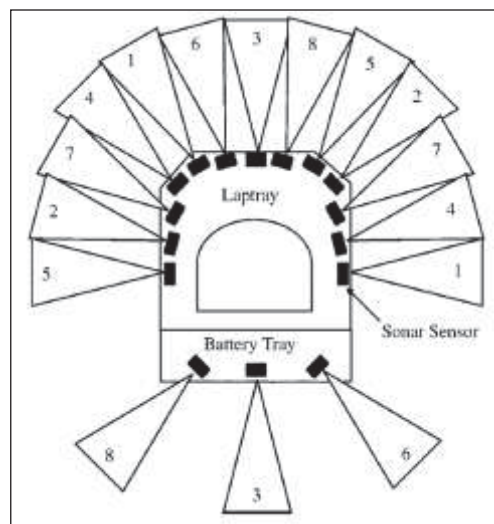
Figure 2-27: Hephaestus Smart Wheelchair Sensor Hardware System

The navigational assistance algorithms of the Hephaestus system are based on the NavChair"s algorithms, with the claimed differences in that the Hephaestus wheelchair:

- does not require the physical modifications to the wheelchairs motors or joystick required by the NavChair;
- has navigation assistance routines that model the shape and trajectory of a wheelchair more closely than those of the NavChair;
- makes use of bump sensors in addition to the sonar sensors.

Apart from these differences the control software has been based very closely on the obstacle avoidance mode from the NavChair"s control software system. Despite the differences claimed about the Hephaestus wheelchair in comparison to the NavChair, they are very similar systems. The NavChair has the three-mode control system developed for improving semi-autonomous control systems for such systems as smart wheelchairs, and the Hephaestus system has the advantages of attempting a stand-alone system that can attach to any power wheelchair which takes into account potential commercialisation. Aside from these the Hephaestus wheelchair still only targets users who can utilise the joystick and has a number of limitations with the sensory layout system, including blind spots and limited detection ranges.

A newer design in smart wheelchairs from research is called the FRIEND system (Fotoohi & Gaser 2011). Made in Switzerland this is constructed as a safe, care-providing robot. It features a robotic arm and multiple sensors for helping with such tasks as pouring drinks or picking up objects.

Figure 2-28: FRIEND System (Fotoohi & Gaser 2011)

This wheelchair uses a number of sensors, however these are limited in the purposes of obstacle detection and collision avoidance. A stereoscopic camera is used for obstacle detection directly ahead of the wheelchair, however, this has a very limited vision range, both horizontally and vertically. Furthermore, algorithms for obstacle detection are not specified and the focus appears to be on the robotic arm and its interactions with the user and environment. This robotic arm is a good idea, but should be applied as an improvement upon smart wheelchair operation, and the main focus of importance should be on reliable guidance assistance in varying environments.

The wheelchairs discussed in this control category have a significant level of applicability for integration into the real world. The ability to travel in unknown environments is important to allow users to venture out to places and areas that are not modified and controlled for autonomous navigation, which in turn increases the user"s independence. In order to adapt to a large range of physical disability levels, the wheelchairs discussed here have ideas that can

be utilised, however, significant factors that must be taken into consideration in designing applicable smart wheelchairs are cost, reliability, effectiveness, level of system autonomy and intelligence, ease-of-use, durability, comfort, adaptability, and the control methods used. These must all be able to take the actual user into account, and this has led to the TIM smart wheelchair designs and strategies developed in this project.

2.5 Proposed Smart Wheelchair System

2.5.1 Research Gap

The research gap facilitating development of the TIM smart wheelchair in this project is quite clear. There are many people with high levels of physical disability resulting from such causes as spinal cord injury (SCI), degenerative muscular dystrophy, and strokes, to name a few. These people can be left with little or no independence in physical mobility, especially in the cases of those with locked-in syndrome (LIS). Access to sources of financial assistance can be difficult and the chances of employment in various fields are no longer feasible. So this gives rise to the need for affordable, accessible, and useful smart wheelchair technology, which is a major drawback of many current smart wheelchair designs.

As discussed in §2.4.2, some smart wheelchairs to-date utilise expensive sensors, such as 3D laser rangefinders, for environmental data gathering, interpretation, and mapping. Others utilise inexpensive sensors, such as sonar or ultrasonic array, which in many cases do not provide adequate information for navigational assistance. Furthermore, some approaches only operate in known environments and require them to be manipulated with various floor tracks, artificial landmarks, and beacons for autonomous localisation and navigation.

Cameras are increasingly becoming an accessible and inexpensive sensor, and provide a wealth of information, but have not been commonly utilised for mapping in smart wheelchair designs. This is likely due to the associated machine processing costs, which are now much more feasible for real-time operation than in past years. Even the recent FRIEND system wheelchair (Fotoohi & Gaser 2012) utilised a stereoscopic camera system, however, have not yet focussed enough on the obstacle detection and collision avoidance strategies, nor the downfalls of the limited vision range it supplies. Taking into consideration the reviews conducted on associated literature, cameras are currently an attractive sensor choice for this

project. Furthermore they are to be used with algorithm designs for allowing the TIM wheelchair in real-time to create maps, obtain information about the surrounding local environment, perform obstacle avoidance of both static and dynamic obstacles, interface with any hands-free control technology, and generally assist the user autonomously during navigation in unknown environments.

So the research gap is found as a combination of factors being integrated into a single intelligent system. Cameras have not previously been efficiently utilised for smart wheelchairs, and it is believed here that they can be extremely effective as a primary sensor for the TIM smart wheelchair. Stereoscopic cameras are commonly used in mobile robotic applications and are suitable to be adapted for mapping in this project. Spherical vision cameras are an extended application of monoscopic vision, which is not commonly used in such applications as smart wheelchairs, but is believed to be an effective addition to the stereoscopic cameras here for obstacle detection and user assistance due to the inherent large vision range.

The focus will be on users who are not able to adequately operate commercial hands-free controls and power wheelchairs. Currently available as well as not yet commercialised hands-free controls should be able to be used to control the TIM smart wheelchair and the intelligent assistance is required to adequately aid in navigation through unknown environments. As with the Hephaestus smart wheelchair, the designs are made with the intention of later adaptation towards commercialisation.

2.5.2 Stereoscopic Vision

Stereoscopic vision technology allows range measurements to be produced as a result of triangulation between the acquired images of two offset cameras. As slightly offset left and right images are acquired from each camera, discrepancies between these images, along with knowledge of the camera geometry, can be used to perform three overall steps for range measurement processing (Point Grey Research Inc. 2003):

- Establish correspondence between image features in the different views of the scene.
- Calculate the relative displacement between feature coordinates in each image.

- Determine, using the knowledge of camera geometry, the 3D location of the feature relative to the cameras.

An example is shown in Figure 2-29 (Point Grey Research Inc. 2003), where an image pair, obtained from horizontally-displaced cameras, is displayed. Points A and B can be identified in both images, whereby point A_{left} corresponds to point A_{right}, and similarly, point B_{left} corresponds to point B_{right}.
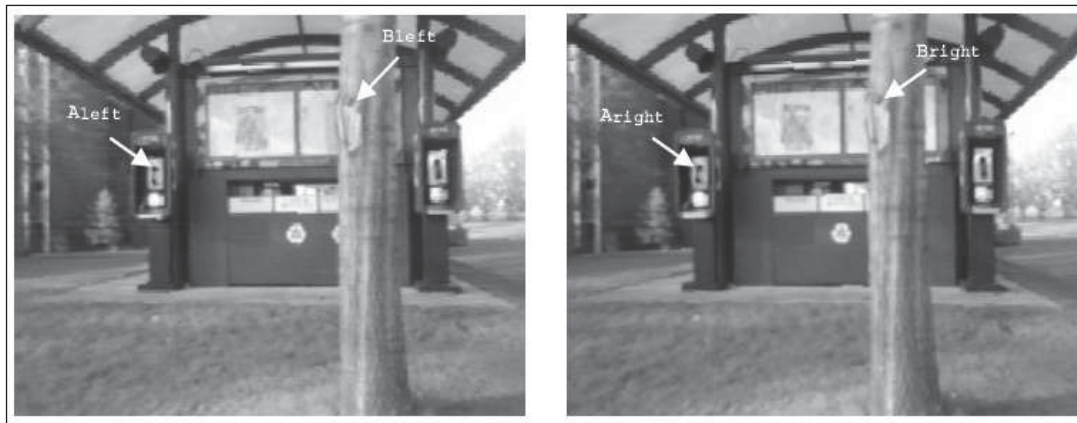
Figure 2-29: Matching Points between Stereoscopic Left and Right Images

If the horizontal distance between the left edge of each image and the points within each image are measured, the distances in the left image are greater than the distances in the right image. For example, the distance to the phone handle (point A) from the left edge of the left image is greater than the distance to the phone handle from the left edge of the right image. The difference between these distances is called disparity and can be used to determine the distance to the phone handle from the stereoscopic camera module.

So disparity will be defined in this project as the horizontal difference between the coordinates of the same feature in the left and right images. Horizontal alignment of the camera results in only horizontal displacements being relevant, as well as producing no discrepancy between the vertical coordinates of the same feature.

Let disparity of the phone handle feature point A be defined as $D(A) = x(A_{left}) - x(A_{right})$ and let disparity of the tree branch node feature point B be $D(B) = x(B_{left}) - x(B_{right})$, where $x(P)$ is the x coordinate of the point P. For the example shown in Figure 2-29, $D(B) > D(A)$, indicating that the tree branch node (point B) in the scene is closer to the cameras than the phone handle (point A).

One of the most recent applications of stereoscopic vision is that of the Microsoft Xbox Kinect (Microsoft 2012), which utilises the abilities of 3D vision for gaming and entertainment system control applications. The sensor is able to detect people and their pose, allowing them to play games through physical movement in front of the sensory device.

Figure 2-30: Microsoft Xbox Kinect (Microsoft 2012)

This has various entertainment applications in the home environment and can be setup to face a scene in a room, so the person is required to be positioned within a reasonably small area to best be detected by the Kinect (Figure 2-31). This is nevertheless a recent and interesting display of stereo the applications for stereo vision.

Although the Kinect sensor was not available when this TIM smart wheelchair project was started, a very similar style of stereoscopic camera was selected at the time. Furthermore, the selected stereoscopic camera is actually a more robust system and more adequate for mounting to a wheelchair than the Kinect sensor.
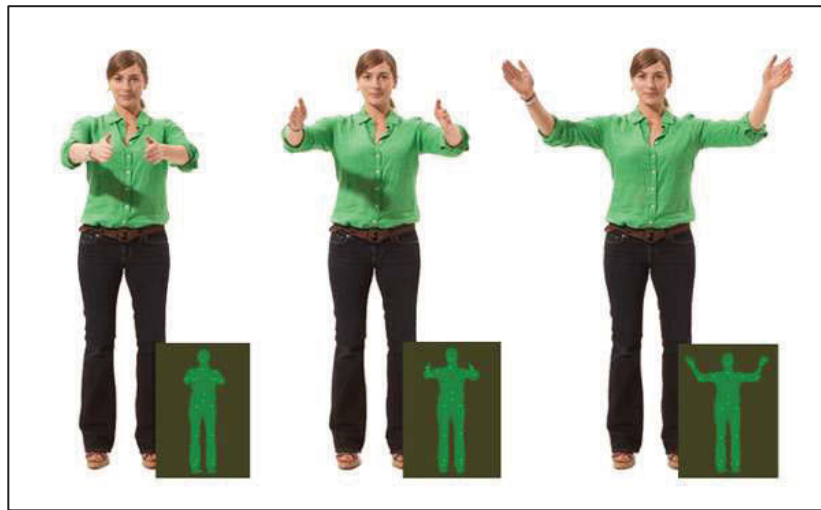
Figure 2-31: Kinect Person Pose Recognition (Microsoft 2012)

2.5.3 Spherical Vision

Spherical vision is an advanced application of monocular camera vision, basically overcoming the short falls in visual field-of-view range by extending the horizontal vision range, typically to the full 360º. Monocular cameras are not often utilised in a dynamic fashion for such applications as autonomous wheelchairs, but rather used more in stationary product assembly or smaller-scale mobile robotic applications with well-defined objects or landmarks being searched for by the cameras used. Zhang et al. (2011) utilised cameras for 2D vision-guided robotic assembly of electronic equipment, providing the assembly robot with enough vision to accurately align itself with appropriate assembly features such as microchips on a printed circuit board (PCB), grasp them, move, and assemble. However, product assembly such as this tend to use stationary cameras and have reasonably well-defined features to extract from the acquired images. When the camera becomes a dynamic sensor in an application such as a mobile robot, the problem complexity is increased.

Common forms of mobile robots that utilise vision are various soccer-playing robots. Wahab et al. (2011) describe a monocular camera being used for vision in a soccer robot, whereby the mobile robot is searching for the soccer ball and making judgements about its position and movement. This problem again involves well-defined features, where the ball, its size, and its colour are known, allowing estimations of position based on the perceptions resulting from the camera images acquired. Object detection and location estimation problems are reasonably easy to define when there is prior information about the objects being detected.

Autonomous navigation using monocular cameras in unknown environments is a more complex and computationally time-intensive task than those of mobile robots following a specific pre-defined object such as the soccer robots. Zhan et al. (2008) presented a mobile robot which utilises monocular vision for autonomous navigation in unknown environments, which is a challenge when attempting a real-time application. This used a method that transformed RGB (Red/Green/Blue) colour space into HSI (Hue/Saturation/Intensity) colour space, extracted histograms of the hue and saturation components of two consecutive time-step acquired images as the robot moved, and then compared the histograms of each to determine if obstacles were present. They faced errors, such as false or missed obstacle detection, in the data when the environment was not controlled and lighting disturbances (such as illumination, reflection, and shadows) were encountered, resulting in controlled experiments that did not reflect „real" environmental situations. Furthermore, the image processing in the controlled environment took anywhere from a few seconds up to 18 seconds based on the image resolutions, how many objects were within the lines of sight, and where they were placed relative to the robot. This is a very relevant display of how real-time dynamic monocular vision has its challenges in both accuracy of obstacle detection and adequate processing time.

Acquisition of information about a local environment for a mobile robot is an important issue, for without appropriate data an autonomous robot is not equipped to make adequate navigational decisions. There are many environmental object features that can be gained based on the type of sensor and data acquisition methods, providing such information as object outlines, placement, size, colour, and material. The usefulness of these types of information depends on the application. However, when it comes to mobile robotics such as the smart wheelchair in this project, placement of objects is the most relevant type of information. It allows the wheelchair to determine where its obstacles to avoid are located and hence where it can find the free-space that will accommodate navigation without collision.

Research for smart wheelchairs that have included cameras have shown cameras, particularly monoscopic or single-view cameras, are not often used as environmental detection sensors. They have usually appeared in applications where the person in the wheelchair is the subject of the camera images, for such reasons as facial gesture and expression recognition (Yoda et al. 2006; Faria et al. 2007). Kim and Hasegawa (2011) did, however, utilise a monoscopic camera for simple unevenness detection of the ground in close proximity regions around an

electric wheelchair as it travelled. It detects significant „bumps" and „dents", resulting from such „bumps" as inclining stairs and „dents" such as the drop of a gutter or curb. It aims to classify the input images into the categories of 0º flat ground, 45º inclination or 45º descent, and 90º rise or 90º fall. The performance of this is reasonable and provides an appropriate add-on application of monoscopic cameras for smart wheelchair designs.

Spherical cameras have been a relatively recent form of monoscopic vision. It is associated with camera configurations that allow 360º of vision around the system, presented in such view forms as fish-eye circular images or panoramic images. Google Earth uses this type of vision for their static panoramic images (Panoramic Earth 2012) on the street views to allow users to see what different places look like from the street and rotate the image around to view every angle if necessary. Despite the popularity of such applications as the Google Earth street view, publications on this type of vision being used in mobile robotic applications are very rare.

Li (2006) proposed a method for using spherical image sensors for visual monitoring around a motor vehicle by dividing the spherical field-of-view into two hemispherical views and displaying them directly to the driver through a monitor. This, at first, did not help detect obstacles or have any automated assistance, it was purely a method for easily displaying the full-view image surrounding the vehicle to the driver. Li and Isago (2007) later used this spherical image sensor to localise the vehicle in a known environment. As the full-view spherical images are independent of the camera rotation, the vehicle could travel through an environment and acquire spherical images surrounding the vehicle. Localisation was then possible as the vehicle could match a current spherical image at any given time with the stored spherical images. This was matched in terms of similarity of the feature vectors computed through histograms of those images. All possibilities are compared and the highest feature vector matches are used to assume location.

Figure 2-32: Spherical camera; images captured; panoramic conversion (Li & Isago 2007)

This method provided high localisation accuracy for a reasonably small „memorised‟ environment. However, due to the nature of the matching algorithm, a large number of spherical images acquired for localisation creates a larger matching set and hence increases processing time. This method may also be let down if there are a large number of occlusions such as other vehicles or objects surrounding the vehicle featured in this research.

Spherical vision, given its inherent large field-of-view, is an attractive addition to the sensors in this project for the reasons of providing real-time video streams to the user, allowing them to view what is happening around the wheelchair, and for 360º obstacle detection purposes. Laser rangefinders, sonar sensors, ultrasonic sensors, and infrared sensors are the conventional type of sensor used for detecting objects in close proximity surrounding a mobile robot in a dynamic environment. However, since vision can provide a wealth of information, including the direct video stream to the user operating the wheelchair, it is a very appropriate sensor choice for the TIM smart wheelchair developments in this research.

2.6 Discussion

The eye-opening disability statistics presented in this chapter provide significant motivation towards the necessity for a project like this to be undertaken. In particular, the statistic that 5.8% of Australians, or approximately 1.3 million people, live with profound or severe disability which limits core activities in communication, mobility, and self-care (Australian Bureau of Statistics 2011), means that this very large number of people, along with their caretakers and families, could benefit from new and safe mobility options. Developments towards solutions for the many people living with severe physical disability are therefore extremely important and could drastically improve independence and quality of life.

Artificial sensory systems commonly used in mobile robotics were looked into and camera systems, which have become more accessible, inexpensive, and feasible for real-time operation in recent years, are a stand-out gap in the market. In particular, stereoscopic cameras, conventionally used in smaller mobile robotic applications, and spherical vision camera systems, an extended application of monocular vision, appear to be two interesting camera configurations that could potentially be utilised as primary sensors for effective environmental perception by the TIM smart wheelchair. Stereoscopic cameras can be used to create maps of the local environment, and the spherical vision system can be used in

conjunction to increase the range of vision to 360º, assist the user with navigation selection through the graphical user interface, and assist in dynamic obstacle detection.

Common obstacle avoidance techniques for autonomous mobile robotic systems were reviewed and separated for discussion into two categories: 1) those requiring prior environmental information, and 2) those for use when navigating in unknown environments. For the application of this project, the techniques requiring prior environmental information were discounted, due to the lack of adaptability, the need for environmental modifications, and for generally not fitting in with the aims and objectives of this project. Obstacle avoidance methods designed for navigating unknown environments require a higher level of sophistication and intelligent algorithm design, and this does not place large restrictions on locations for wheelchair navigation, nor the need to modify environments in any way. Hence, these algorithms will be further assessed for use in this project to allow the TIM smart wheelchair to carry out user intentions whilst, in conjunction, executing safe obstacle avoidance tasks. These will be modified to suit the design and ensure safety, which is of utmost importance when considering autonomous navigational assistance of a smart wheelchair.

Computational intelligence, particularly multi-layer delta-error back-propagating neural networks, is discussed and will be utilised in this project. They will be mainly designed to assist in image processing and classification for assisting the operations of the wheelchair and providing added intelligence towards dynamic obstacle detection and optimising environmental adaptability. Implementation into the system for real-time operation during navigation will also be ensured.

A range of commercial user control interfaces for controlling wheelchairs were reviewed, and the designs in this project will be aimed at easy integration with any control system, but primarily those that are hands-free to provide options for the many people who cannot adequately use current commercial control systems. The main aims will be for the TIM smart wheelchair to be able to effectively integrate with any hands-free device, even potentially difficult-to-use devices which have only recently been developed in research.

Other popular smart wheelchair designs were researched and the advantages and downfalls exposed. Some of the good ideas are taken into consideration for this project, such as the *NavChair's* inexpensive design and ability to classify situations of change in the environment,

and the *Hephaestus* wheelchair system''s ideas of potentially being a stand-alone system to attach and implement into any power wheelchair system. Improvements on their inabilities to effectively handle dynamic obstacles from any direction will be addressed in this project, along with replacing the primary sensor designs of ultrasonic arrays with unique camera configurations. This is due to their ability to attain significantly more useful information about surrounding environments than ultrasonic sensor arrays are capable of.

The TIM smart wheelchair designed in this project will take into consideration the research done in this chapter to produce a unique, effective, adaptable, safe, and easy-to-use semi-autonomous system that can execute user intentions in real-time, and via any hands-free control method. This will contribute towards providing solutions to a much larger range of people than is currently accounted for, especially for those who cannot adequately control power wheelchairs through currently available technologies.

Chapter 3

Adaptive Real-time Vision Mapping System Utilising Stereoscopic Cameras

"Disability is a matter of perception. If you can do just one thing well, you're needed by someone." - Martina Navratilova

3.1 Introduction and Aims

Artificial sensors generally play an important role in the design of autonomous systems, such as smart wheelchair applications. They provide data about the environment and objects within it to the processing unit, allowing it to make assistive decisions based on the level of autonomy inbuilt into the system. In order for a smart wheelchair to make assistive decisions during navigation, the information acquisition, processing, and decision-making abilities must

all be executed accurately and reliably in real-time. The application of a smart wheelchair design is to assist people with severe disabilities and provide safe navigational assistance, along with collision avoidance capabilities, which means the reliable source of real-time information is essential.

As discussed in §2.5, stereoscopic cameras are mostly used in small-scale robotics applications, but have here been adapted for reliable use in a smart wheelchair, being a relatively larger application with more risks involved in the event of collisions. However, due to the fact that cameras are increasingly becoming more accessible and inexpensive, they are an attractive choice for such an application, especially when taking into consideration the amount of environmental information they are capable of providing. Stereoscopic cameras can be used to obtain real-time 3-dimensional (3D) representations of environment features, in particular objects and people.

This chapter explores the use of stereoscopic cameras for adaptive mapping vision in the „TIM" smart wheelchair system design. A Point Grey Research company"s Bumblebee XB3 stereoscopic camera system was attached to an Invacare „TDX A" power wheelchair, along with a laptop processing unit and additional hardware to create the Stage 1 TIM semi-autonomous wheelchair prototype. This chapter discusses the real-time stereoscopic vision strategies developed for object mapping in various environments. Advanced methods for optimising the mapping performance through adaptive stereo processing parameter selection are also presented, along with methods for correcting wheel measurement parameters. Experimental results are provided for the methods and strategies developed and explored through this chapter. These results are then discussed and concluded in relation to the aims.

The aims of the research presented in this chapter are to investigate and understand:

1. The feasibility of stereoscopic cameras as a primary sensory system for environmental mapping in smart wheelchair design
2. The accuracies in 3D local environment map construction resulting from disparity image creation.
3. The ability to construct maps in real-time.
4. The use of wheel shaft encoders for wheelchair odometry change calculations, resulting in remapping of local environment features outside the boundaries of stereoscopic vision range.

5. The performance of an adaptive stereo processing parameter selection system, designed using neural networks.

6. The correction process of wheel alignment and specific diameter calculations which affect the wheel shaft encoder readings and resulting environment maps.

3.2 Instrumentation

Invacare 'TDX A' Power Wheelchair

The underlying power wheelchair that was modified into the smart wheelchair „TIM" of this project was an Invacare „TDX A" model. This is a centre wheel drive power wheelchair designed for indoor and outdoor use (Independent Living Centre NSW 2009).

Figure 3-1: Invacare „TDX A" Power Wheelchair

Main Specifications of the Invacare „TDX A" power wheelchair:

Feature	Specification
Load Capacity (supplier stated):	180kg
Overall Length:	1067mm
Overall Height:	870mm (min) – 972mm (max)
Seat Depth:	280mm – 510mm
Seat Width:	255mm – 510mm
Tilt in Space Angle:	3 – 50 degrees
Diameter castor:	75mm
Diameter wheel:	300mm – 355mm

Table 3-1: Invacare „TDX A" Power Wheelchair Main Specifications

The main features of the TDX A wheelchair are as follows:

- Wheels and Castors: The drive wheels of the TDX A are pneumatic and set to the centre of the base, allowing on-the-spot rotations to reduce the turning circle, with two sets of solid rubber pivoting castors at the front and rear. It has a mechanism where the front castors lift vertically when they hit an obstacle or step, up to approximately 75mm. The rear wheels are designed to push down to remain on the ground which can reduce rocking.

- Frame: Rigid frame with the seating fit so the user's centre of gravity is over the centre drive wheels. The base has independent suspension and is designed to remain stable without the use of anti-tip bars. The rear wheels have a stability lock designed to prevent them rising off the ground. This aims to reduce rocking.

- Seat: Standard solid padded foam seat allows adjustable seat width and seat depth, and is generally customisable.

- Backrest: Solid padded back with adjustable height. Backrest angle is manually operated in this model.

- Armrests: Standard padded and upholstered armrests, adjustable in height and width, and removable. The armrests are on a hinge and can swing up and out of the way.

- Leg rests: Swing away and removable.

- Foot plates: Two piece footplates, ability to swing up to move out of the way.

- Controls: Dynamic and DX controllers are used with this base as standard. Joystick controller.

- Batteries: Two 50amp sealed batteries with charge point on the joystick controller.

Bumblebee XB3 Stereoscopic Camera System

Figure 3-2: PGR Bumblebee XB3 Stereoscopic Camera System

The Bumblebee XB3 is a 3-sensor multi-baseline IEEE-1394b (800Mb/s) stereoscopic camera. It features 1.3 mega-pixel sensors and has two baselines available for stereo processing. The extended baseline and high resolution provide more precision at longer ranges, while the narrow baseline improves close range matching and minimum range limitations (Point Grey Research Inc. 2003). The main specifications of the Bumblebee XB3 are displayed in Table 3-2.

The Bumblebee XB3 stereoscopic camera system has two baseline pair combinations, out of the three cameras it can utilise, being a 12cm baseline width between the middle and right camera or a 24cm baseline width between the outer two cameras. The purpose of the stereoscopic camera system in this research is to map out the visible area ahead of the wheelchair for obstacle detection, collision avoidance, and general wheelchair guidance assistance. For these reasons the wide 24cm baseline was selected which utilises the outer two cameras of the Bumblebee XB3 for stereoscopic vision. This allows for further vision away from the cameras as well as wider ranges in mapping, increasing the vision range from about 42° in the 12cm baseline to around 66° in the 24cm baseline of the Bumblebee XB3. This increased horizontal range of vision is very useful taking into consideration the constraints associated with the limited vision of these camera systems. This does, however, increase the dead-band distance from the camera for which no depth can be perceived, but it is still adequate to detect obstacles up to collision because the front of the wheelchair extends 40cm out from the camera, which is the distance the dead-band was able to be calibrated and reduced to whilst using the wide baseline.

Feature	Specification	
Image Sensor Type	Sony® 1/3" progressive scan CCD ICX445 (1280x960 max pixels)	
Baseline Options	12 cm	24 cm
Aperture	f/2.5	f/2.0
Focal Lengths	6mm with 43° HFOV	3.8mm with 66° HFOV
A/D Converter	12-bit analog-to-digital converter	
White Balance	Auto / Manual (Colour model) Manual (Colour model)	
Frame Rates	Up to 16 FPS	
Interfaces	2 x 9-pin IEEE-1394b for camera control and video data transmit / 4 general-purpose digital input/output (GPIO) pins	
Voltage Requirements	8-30V via IEEE-1394 interface or GPIO connector	
Power Consumption	4W at 12V	
Gain	Automatic/Manual	
Shutter	Automatic/Manual, 0.01ms to 66.63ms at 15 FPS	
Signal To Noise Ratio	54dB	
Dimensions	277 x 37 x 41.8mm	
Mass	505 grams	
Camera Specification	IIDC 1394-based Digital Camera Specification v1.31	
Lens mount	3 x M12 microlens mount	
Emissions Compliance	Complies with CE rules and Part 15 Class A of FCC Rules	
Operating Temperature	Commercial grade electronics rated from 0° to 45°C	
Storage Temperature	-30° to 60°C	

Table 3-2: PGR Bumblebee XB3 Stereoscopic Camera System Main Specifications

Overall Stage 1 Prototype Hardware Design

The prototype design (Figure 3-3) uses a Mac Mini PC for the computer processing and a TFT Colour Monitor screen display. Wheel shaft encoders are used to track odometry changes in the wheelchair, and the Bumblebee XB3 stereoscopic camera system is connected via a Firewire connection to the Mac Mini. A National Instruments USB-6008 multifunctional DAQ (Data Acquisition) card is used as the digital to analog converter for sending control signals to the wheelchair motors. Figure 3-4 shows a photo of how this integrated hardware system.
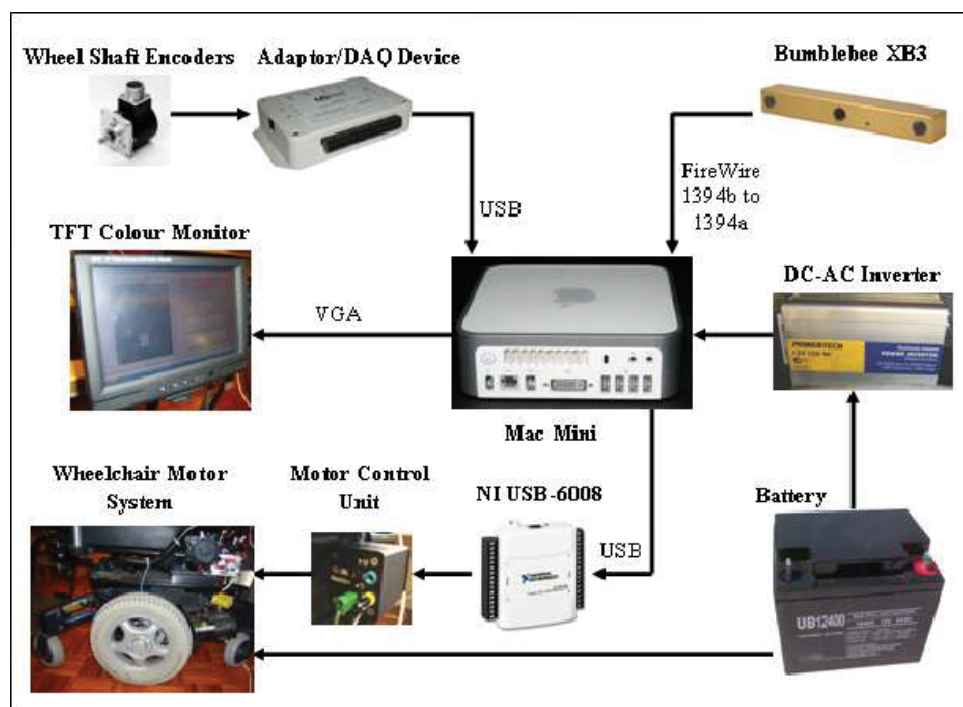
Figure 3-3: Overall Stage 1 Prototype Hardware Design Using Stereoscopic Cameras
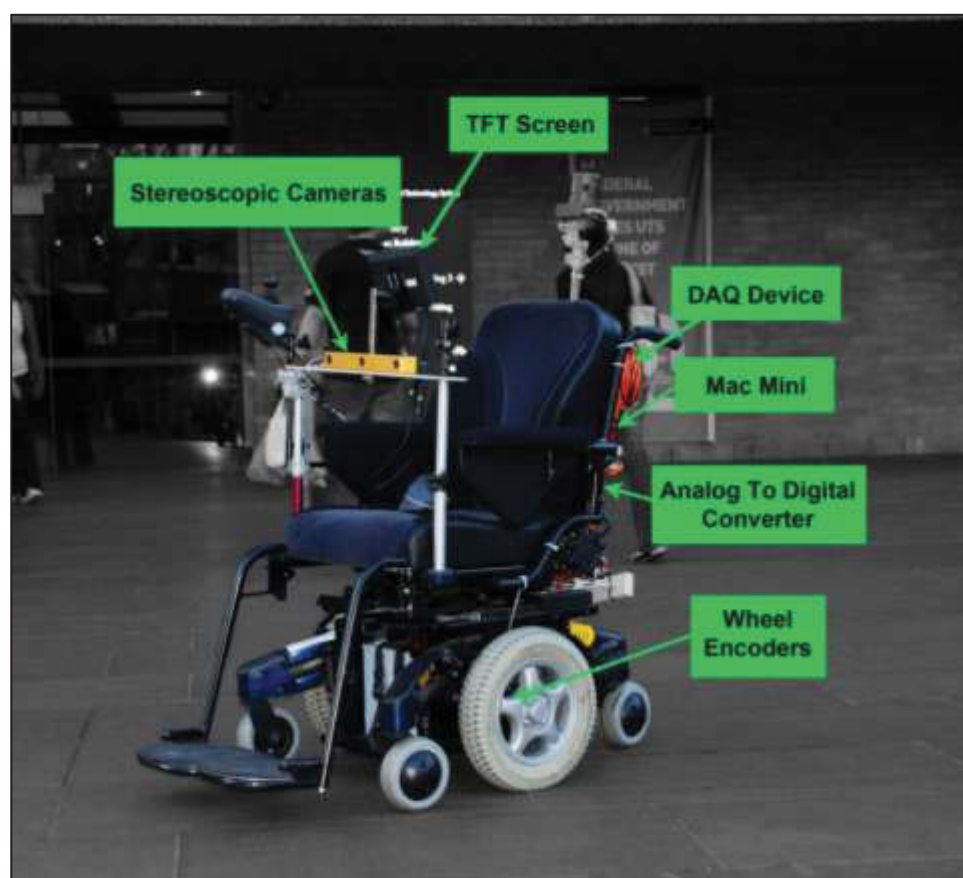
Figure 3-4: TIM Stage 1 Prototype: Integrated Wheelchair Hardware with Stereoscopic Cameras

3.3 Real-time Vision Mapping Strategies

The stereoscopic cameras were selected for mapping the local environment in order to provide the wheelchair with enough information to assist the user through autonomous navigation guidance and obstacle avoidance. To achieve this, the system undergoes a process of image acquisition, individual image pre-processing, combined stereo processing, 3D point mapping, vertical point range filtering, and finally conversion to a 2-dimensional (2D) birds-eye view map. This map contains information about objects and free-space ahead of the wheelchair within the stereoscopic camera system's vision range. Wheel shaft encoders are then also utilised to calculate wheelchair odometry changes, and adjust previously mapped points accordingly, as they move out of vision range, to construct a local static environment map all around the wheelchair.

3.3.1 Stereoscopic Vision Background

Stereo Image Pre-processing

Pre-processing prepares the raw left and right images for stereo processing. This allows processing resolution specification, and options for filtering, rectification, and edge detection of the image. It is important to smooth images if the image rectification is to be performed. It is also good practice to perform low-pass filtering because although rectification can be achieved without low-pass filtering, which would speed up the process, aliasing effects are likely be exhibited.

Rectification is the process of correcting raw input image distortions caused from the camera lenses. For example, straight lines in a scene will often appear curved in the raw image. This effect is particularly noticeable in the corners of the image. Rectification corrects these types of distortions so that both the rows and the columns of the images, digitised from the horizontally-displaced cameras, are correctly aligned. Searching along rows and columns for correspondence would not produce correct results without this feature.

Edge detection is an optional pre-processing feature that allows matching on the discontinuities in the brightness and intensities rather than the absolute values of the pixels in the images. If auto gains inherent in the Bumblebee stereoscopic cameras do not change identically, the absolute brightness between images may not be the same, however, the change

in intensities stays constant. So using edge detection will help in environments where there are significant changes in lighting conditions. Edges are discontinuities of intensity in an image and can be due to many causes such as discontinuities in surface normal, surface colour, depth, or illumination (Kodagoda, 2007).
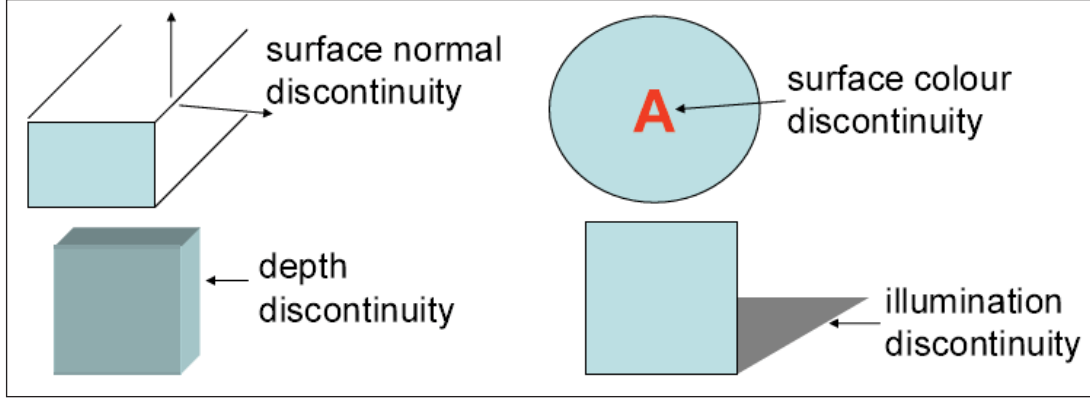
Figure 3-5: Edge Examples (Kodagoda 2007)

Edges correspond to the local maxima of image gradients, which can be computed by convolution, where a local gradient in an image is found as

$$\Delta f = \left[\frac{\partial f}{\partial x}, \frac{\partial f}{\partial y}\right] \tag{3.1}$$
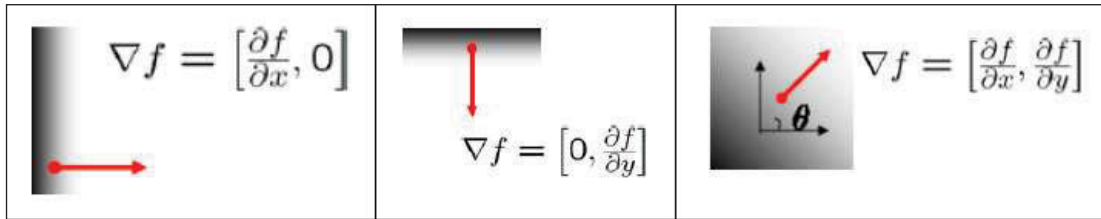
Figure 3-6: Local Gradient Changes (Kodagoda 2007)

So the gradient direction is

$$\theta = tan^{-1}\left(\frac{\frac{\partial f}{\partial x}}{\frac{\partial f}{\partial y}}\right) \tag{3.2}$$

and the gradient magnitude is

$$\|\Delta f\| = \sqrt{\left(\frac{\partial f}{\partial x}\right)^2 + \left(\frac{\partial f}{\partial y}\right)^2} \qquad (3.3)$$

Furthermore, image smoothing before edge detection is effective to minimise the noisy effect that can be produced in an edge image.
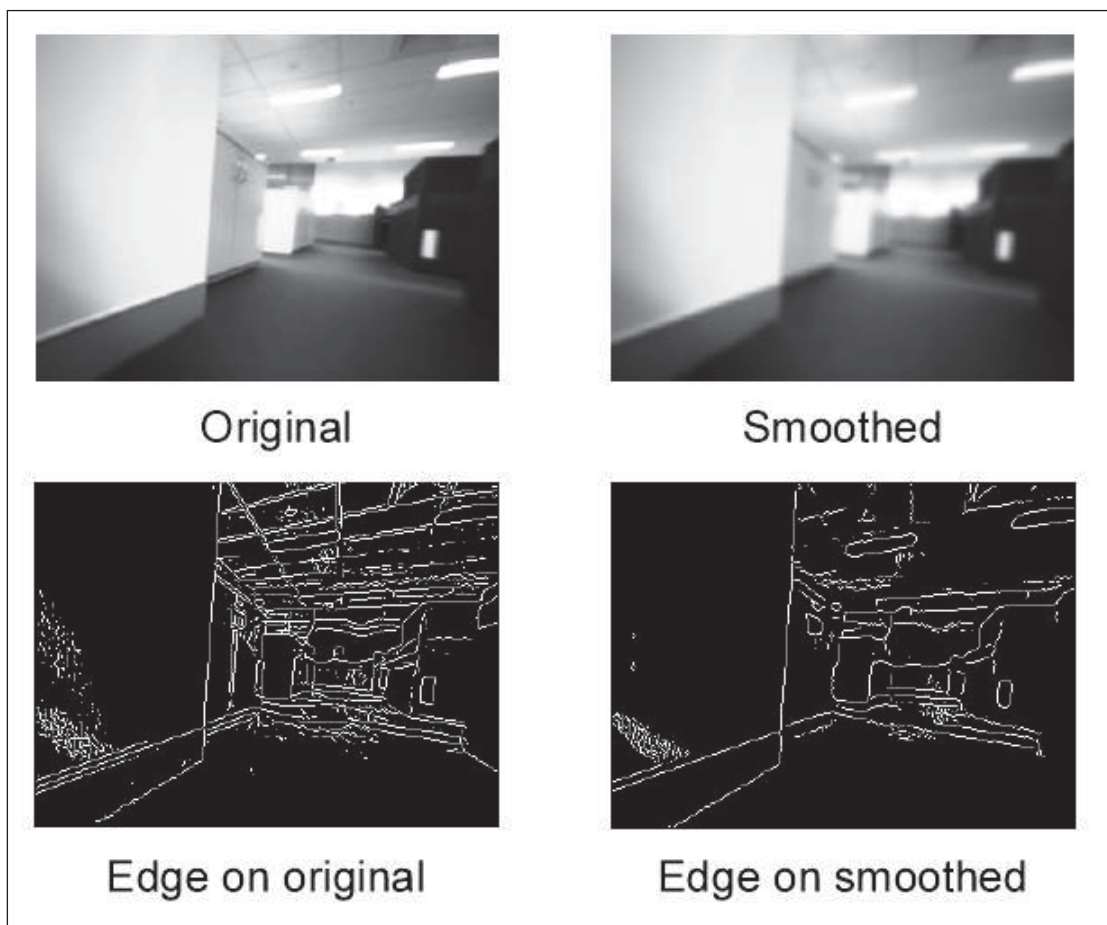
Figure 3-7: Raw Image and Edge Image Comparison (Kodagoda 2007)

Edge detection, especially with smoothing beforehand, will improve results and accuracies in obstacle detection, however, there is additional processing cost associated with it. For the purposes of this project the improvements are desirable and the processing cost is not significant, so edge detection is used as a pre-processing technique.

Epipolar Geometry

As a specific example of multi-view geometry, epipolar geometry, which has been extensively studied in computer vision, is the only available geometric constraint between a stereo pair of images taken of a single scene (Hartley & Zisserman 2000). An example stereo image setup is shown in Figure 3-8, where C_L and C_R are the optical centres of the left and right cameras and I_L and I_R are the left and right image planes, respectively. According to epipolar geometry, for a given image point p_R in the right image, its corresponding point p_L in the left image is constrained to the line l_L, which is called the epipolar line of p_R (Lu et al. 2007).
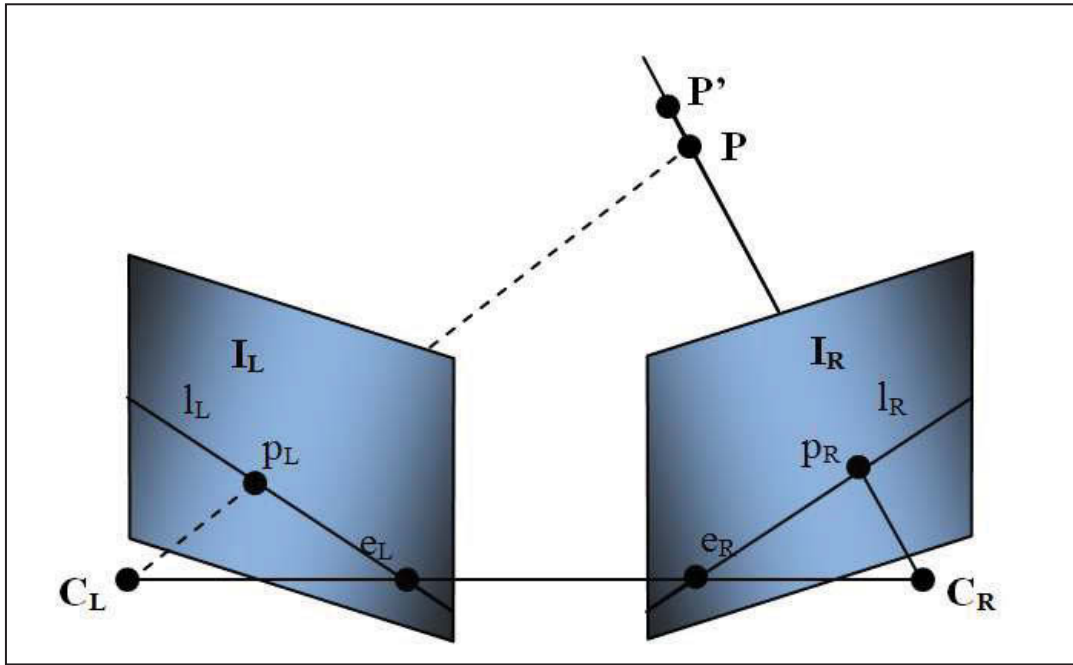
Figure 3-8: Epipolar Geometry

The epipolar constraint can be formulated as

$$l_L = F \cdot \tilde{p}_R \qquad (3.4)$$

$$\tilde{p}_L^T \cdot F \cdot \tilde{p}_R = \tilde{p}_L^T \cdot l_L = 0 \qquad (3.5)$$

where $\tilde{p}_L$ and $\tilde{p}_R$ are the homogeneous coordinates of p_L and p_R, and F is referred to as the *fundamental matrix* (FM). From Equation 3.4 it can be seen that once F is available the equation of epipolar line l_L can be computed in order to significantly reduce the search space

of correspondence by following the obtained epipolar constraint (Lu et al. 2007). If the camera geometry is calibrated, in such a manner that both intrinsic and extrinsic parameters are known, the FM can be precisely calculated as a result of a few matrix manipulations (Zhang 1998), being found as

$$F = A_L^{-T}[t] \times RA_R^{-1} \qquad (3.6)$$

where A_L and A_R are the intrinsic matrices of the left and right cameras, respectively, and *(R,t)* is the rigid transformation (*rotation* and *translation*) which brings points expressed in the right camera coordinate to the left one. It is common practice for multi-view camera systems to first have their camera geometry calibrated before real capture sessions (Zitnick et al. 2004; Lou et al. 2005).

Disparity and Correlation Matching Approaches

An important problem in stereoscopic vision is that of the approach for computing image feature matching to produce a disparity image and calculate pixel depths. Moving pixel windows (or pixel neighbourhoods), used in the matching process between the left and right stereo image pair, must be small enough to avoid effects of projective distortion, and large enough to adequately pick up on intensity variations for reliable matching.
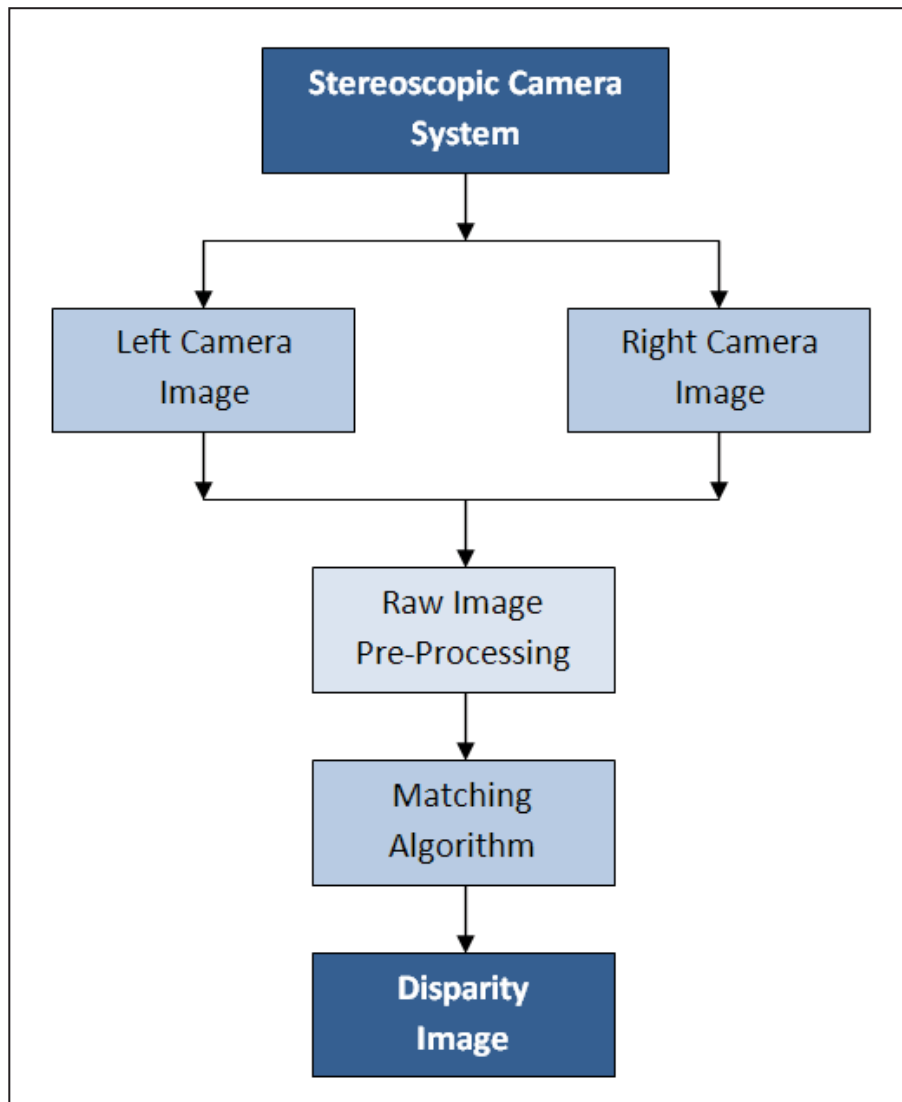
Figure 3-9: Basic Block Diagram for Stereo Images to Disparity Image Process

Generally, when disparity and, hence, depth of image features are required from stereo images, pixel windows in one image are correlated with pixel windows in the other image to obtain a match and determine the disparity values thereof. There are many matching algorithm approaches, used to compute disparity in stereo image pairs, that have arisen since stereoscopic image processing became an area of research, some popular examples are displayed as follows in Table 3-3 (Banks et al. 1997; Brown et al. 2003), where, for each example, *(i,j)* are the pixel coordinates in pixel window W of left and right images I_L and I_R, respectively:

Matching Algorithm Approach	Algorithm
Sum of Squared Difference (SSD)	$$\sum_{(i,j)\in W} \left(I_R(i,j) - I_L(i+d,j)\right)^2$$
Zero-mean Sum of Squared Differences (ZSSD)	$$\sum_{(i,j)\in W} \left((I_R(i,j) - \bar{I}_R) - (I_L(i+d,j) - \bar{I}_L)\right)^2$$
Normalised Sum of Squared Differences (NSSD)	$$\sum_{(i,j)\in W} \left(\frac{(I_R(i,j) - \bar{I}_R)}{\sqrt{\sum_{(i,j)\in W}(I_R(i,j) - \bar{I}_R)^2}} - \frac{(I_L(i+d,j) - \bar{I}_L)}{\sqrt{\sum_{(i,j)\in W}(I_L(i+d,j) - \bar{I}_L)^2}}\right)^2$$
Sum of Absolute Differences (SAD)	$$\sum_{(i,j)\in W} |I_R(i,j) - I_L(i+d,j)|$$
Zero-mean Sum of Absolute Differences (ZSAD)	$$\sum_{(i,j)\in W} |(I_R(i,j) - \bar{I}_R) - (I_L(i+d,j) - \bar{I}_L)|$$
Normalised Cross Correlation (NCC)	$$\frac{\sum_{(i,j)\in W} I_R(i,j+y)I_L(i+d,j)}{\sqrt{\sum_{(i,j)\in W} I_R^2(i,j) \sum_{(i,j)\in W} I_L^2(i+d,j)}}$$
Zero-mean Normalised Cross Correlation (ZNCC)	$$\frac{\sum_{(i,j)\in W}(I_R(i,j) - \bar{I}_R)(I_L(i+d,j) - \bar{I}_L)}{\sqrt{\sum_{(i,j)\in W}(I_R(i,j) - \bar{I}_R)^2 \sum_{(i,j)\in W}(I_L(i+d,j) - \bar{I}_L)^2}}$$
Rank	$$\sum_{(i,j)\in W} \left(I'_R(i,j) - I'_L(i+d,j)\right)$$ $$I'_k(i,j) = \sum_{(m,n)\in W} I_k(m,n) < I_k(i,j)$$

Table 3-3: Pixel Window Matching Algorithms for Stereo Image Correlation

With the use of appropriate pixel window matching algorithms, useful disparity images can be created as a result of stereo image correlation. These can then be converted into 3D point

maps and further processed to create environmental maps relative to the wheelchair. These will be important in assisting with autonomous navigational decisions of the smart wheelchair design. However, stereoscopic vision can be limited by its vision range, so this means either more systems are required to be setup, or additional sensors such as the proposed spherical vision system for increasing the vision range of the smart wheelchair, and also providing very useful assistance directly to the user via the graphical user interface.

3.3.2 Local Environment Mapping Process
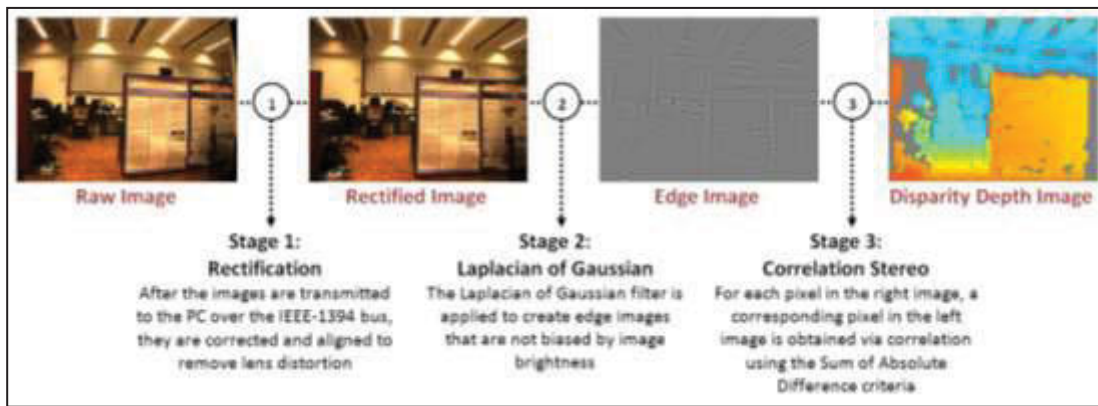
Figure 3-10: Stereoscopic Main Processing Steps

The three main stereo processing steps to get from left and right raw images to a disparity image are introduced in Figure 3-10. These steps are 1) rectification, 2) Laplacian of Gaussian edge detection, and 3) correlation of the stereo pair.

A wider 24cm baseline width between the stereo camera pair was selected based on the fact that it was being utilised for detecting objects in a large open space. A narrower baseline would be appropriate for detecting surface features and contours of an immediate object in front of the cameras, such as those of a person‏‏‏‏'s face, given the smaller range of vision and finer feature matching capabilities. Determination of the local environment mapping methods followed this, for which sample obstacle scenes were setup as the first step of the process. Figure 3-11 shows left and right raw stereoscopic camera images of the example scene setup.
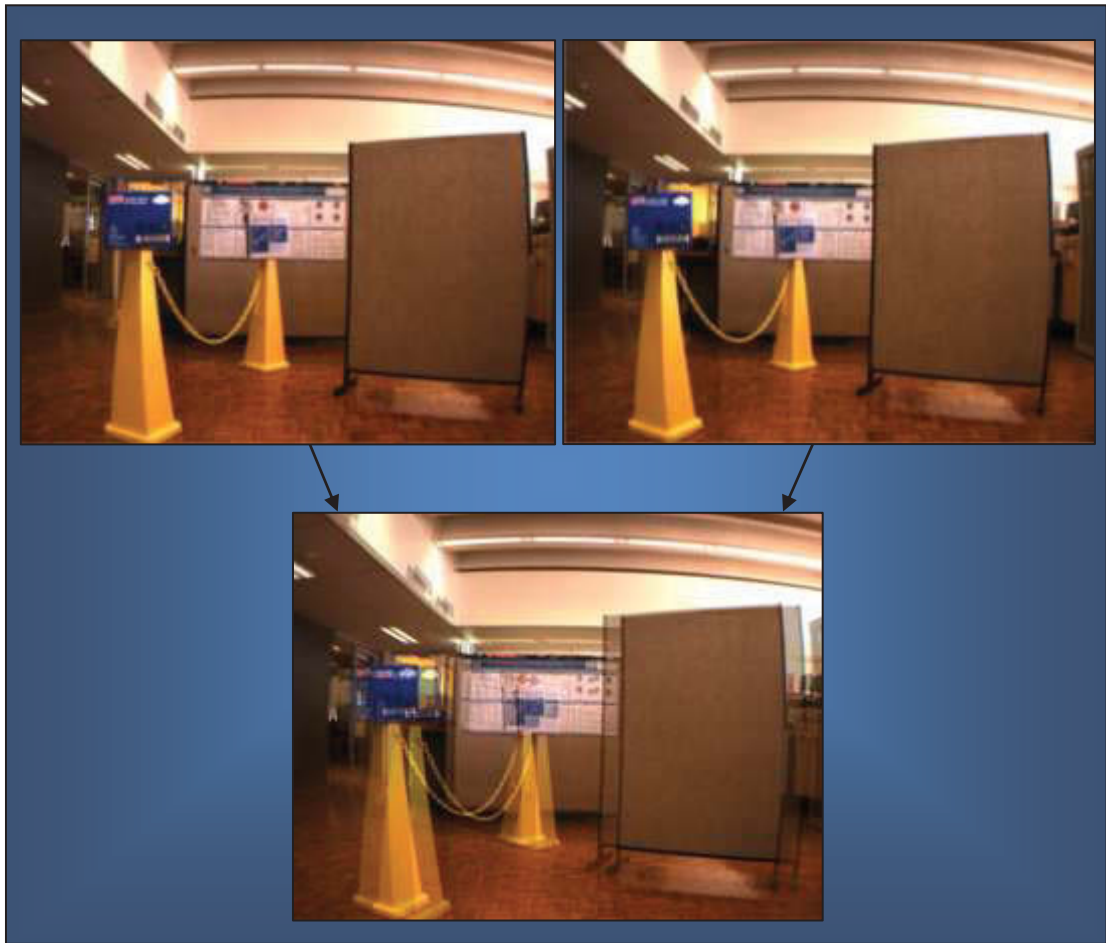
Figure 3-11: Stereoscopic Raw Left and Right Images of Example Scene Setup

Notice the lens distortion slightly curving each raw input image around their centre point before rectification. These left and right images are then correlated using the Sum of Absolute Differences (SAD) algorithm to establish correspondence between the two images. The idea behind this method is that for every pixel in the reference image a given square-size neighbourhood of pixels around the reference pixel is selected, and this neighbourhood is compared to a number of neighbourhoods along the same horizontal row in the other image. An example of this, displaying correlation of 3x3 pixel neighbourhoods between the images, is shown in Figure 3-12.
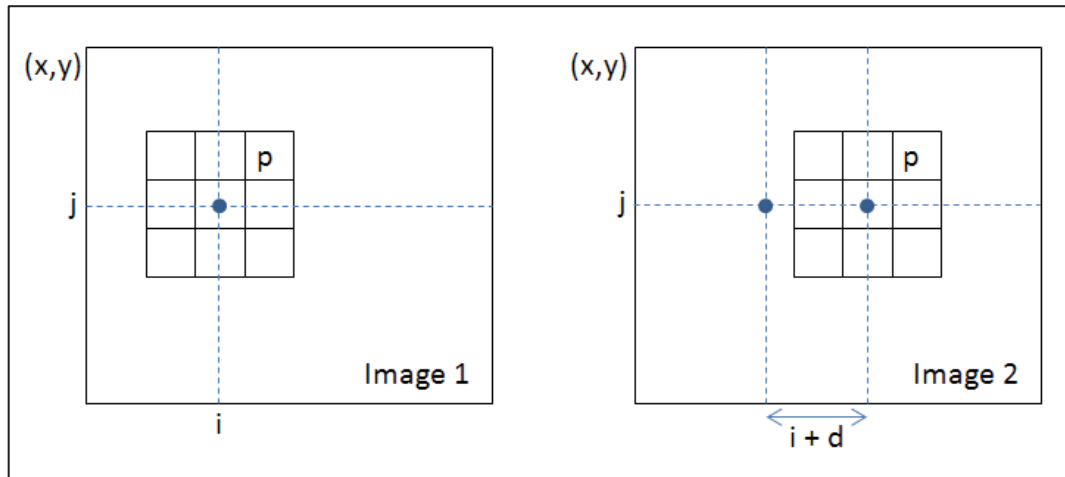
Figure 3-12: Correlation of two 3x3 pixel neighbourhoods along corresponding epipolar lines

The best match is selected and the offset determined, and the process is then repeated for every reference image pixel. This allows depth projection of matched pixels into the third dimension, adding the z-plane to the existing x and y axes. The comparison of neighbourhoods or "masks" is done using the following SAD correlation formula:

$$SAD = \min_{d-d_{min}}^{d_{max}} \sum_{i-\frac{m}{2}}^{\frac{m}{2}} \sum_{j-\frac{m}{2}}^{\frac{m}{2}} \left| I_{right}[x+i][y+j] - I_{left}[x+i+d][y+j] \right|$$

(3.7)

where: d_{min} and d_{max} are the minimum disparity (corresponding to the furthest object) and the maximum disparity (corresponding to the closest object).

m is the mask size.

I_{right} and I_{left} are the right and left images.

Once the SAD algorithm has been executed a disparity image can be produced as a result of all the correlated neighbourhoods of pixels. The larger the horizontal displacement, known as disparity, of a correlated pixel neighbourhood between the left and right stereo images, the closer to the camera system that pixel neighbourhood is located in the z-plane. The distance away from the camera can be calibrated to relate directly to the produced disparity value. For disparity image creation, the determined distance away from the camera system is then colour-coded, with hotter colours (red) being allocated to the closest objects, cooler colours (dark blue) being allocated to the furthest objects, and a smooth gradient of corresponding distance colours in between. The disparity image produced from the example scene setup of Figure 3-11 is displayed in Figure 3-13.

Figure 3-13: Produced Disparity Image of Example Scene Setup

The main stereo processing parameters used to affect the produced disparity image are correlation mask size, disparity range, texture validation, uniqueness validation, surface validation, and a back-forth noise filter.

- Correlation Mask Size: Increasing a stereo correlation mask can increase the density of pixels in the created disparity image. This makes objects appear larger than they are, so decreasing the stereo correlation mask decreases density of the object, making it appear like it has small holes and allowing repetitive patterns in a scene to be more easily mismatched. However, this also makes objects appear closer to their actual dimensions, so the stereo correlation mask needs to be set to an adequate balance point where object dimensions and outlines are as clear as possible without losing too much environmental data or allowing correlation mismatching.

- Disparity Range: This range setting simply limits the z-plane distance minimum and maximum values for the created disparity image. It is basically a focus type camera setting, where the objects within range will be matched much more accurately than those outside the range, for which the outliers usually become dead-bands. A smaller range takes up less processing and shorter processing time whereas a larger range will naturally take longer. The range will be application specific, however is set quite

large given the application, with the main band of z-plane interest lying between 0.3m to 5.5m ahead of the camera system's front edge, which is located 0.5m behind the front edge of the wheelchair.

- Texture Validation: This parameter affects the amount of importance the stereo matching process places on validating perceived texture between the two images. Smooth surfaces such as the back of plastic chairs were the hardest to identify, whereas rough surfaces such as cardboard boxes were easily identified on most settings. This parameter will vary based on how the environment is being perceived, as it will have a greater impact on stereo matching in smaller and more crowded environments in which objects are closer to the cameras, whereas it will not have as much effect in more open environments.

- Uniqueness Validation: This validation method determines whether the best match for a particular pixel is significantly better than other matches within the correlation mask. Increasing this until observed incorrect matching in various scenario of many different objects was performed. It was not a greatly noticeable change, however some noise due to mismatching was reduced and this is desirable.

- Surface Validation: This type of validation was very useful in removing noise referred to as spikes. It attempts to distinguish between surfaces as spikes can occur when there are great contrasts between lighting within a single scene. Surface validation can reduce the noise present on a single perceived surface. However, it can also adversely combine surfaces of different distances from the cameras. A balance in various situations is important.

- Back-Forth Setting: This additional setting eliminates many forms of flickering spikes when they are changing distances from the camera rapidly due to mismatching. It slows the matching process but is very useful in noise filtering so is an important setting to keep activated.

Raw images from the stereoscopic cameras are pre-processed as described in §3.3.1, including low-pass filtering, rectification, and edge detection, before they undergo the above stereo processing methods to produce a disparity image.
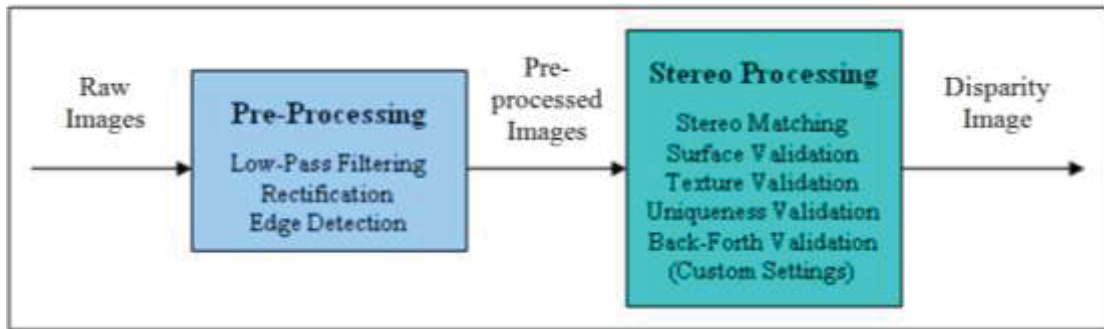
Figure 3-14: Disparity Image Creation Process

Once a disparity image is produced, a 3D point map can be created which maps each of the depth-determined pixels from the disparity image onto a 3-dimensional plane. This is very useful in determining the types of environments and areas that produced noise spikes, and which parameter configuration settings improved the 3D point cloud for the purposes of accurate obstacle detection and depth analysis. The representation of the image and coordinate system which produces disparity images before 3D Point Cloud conversion is shown in Figure 3-15.
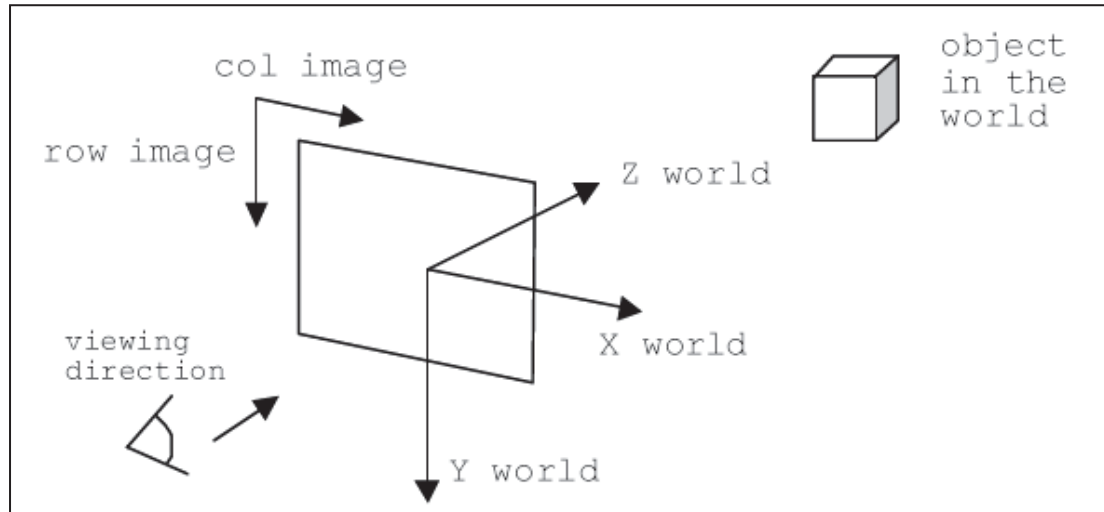
Figure 3-15: Image and World Coordinate Systems

The 3D depth map created from the example scene setup images in Figure 3-11, and resulting disparity image in Figure 3-13, with an added baseline image (no obstacles present), is displayed in Figure 3-16. This has been displayed on a 3D plane, with all matched pixels from the disparity image plotted and highlighted with colours from the corresponding area in the original image:
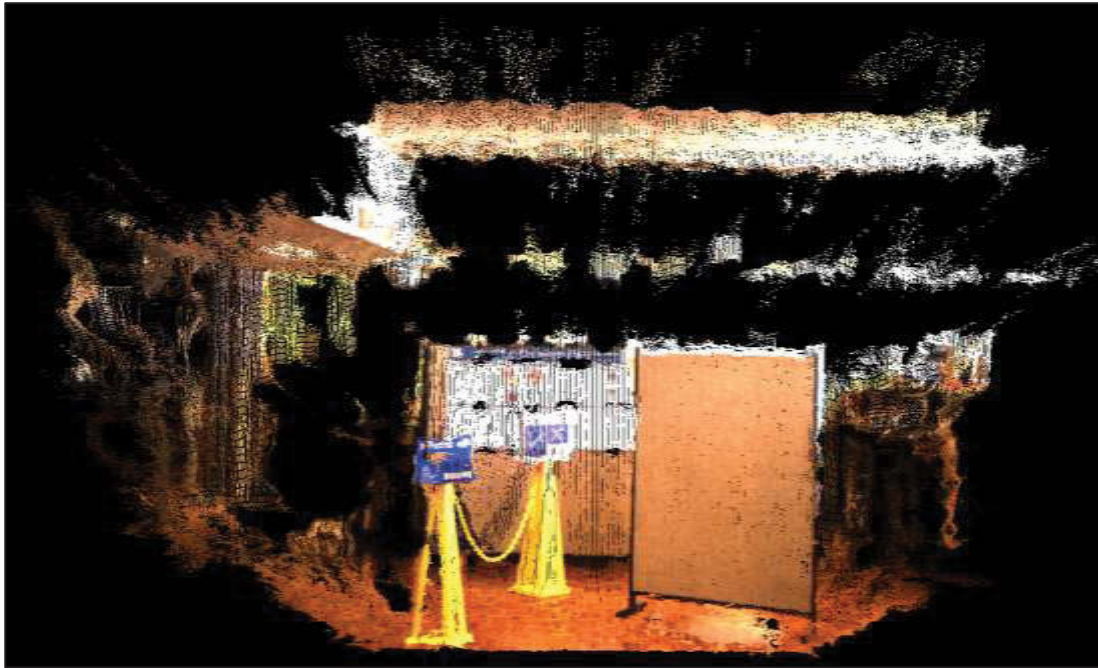
Figure 3-16: Created 3D Point Map of Example Scene Setup

As shown in Figure 3-16, 3D point map creation contains a denser distribution of plotted pixels resulting from correlation in the regions closer to the camera system, with an increasingly sparser distribution of pixels in the regions further away from the camera system. This is due to the correlation errors increasing with distance. However, inaccuracies do not have as significant an impact on performance of the environmental mapping method as noise artifacts which alias distant objects as close objects. The main task is to identify objects in the scene and their locations for 2D bird"s-eye view mapping.

Of course, only the parts of the scene that can be seen from the cameras can appear in the 3D map, so all objects are represented by the visible points, appearing as a front „shell" of the object as opposed to appearing solid. However, this is useful in determining the closest surfaces of objects in the scene which constitute the information required by the TIM smart wheelchair. Being mapped into 3D space, the point map of Figure 3-16 can be rotated to view placement of objects in the scene, rotating the camera-observed scene to the right both 45 degrees (Figure 3-17) and 90 degrees (Figure 3-18) shows the placement of objects in the scene.
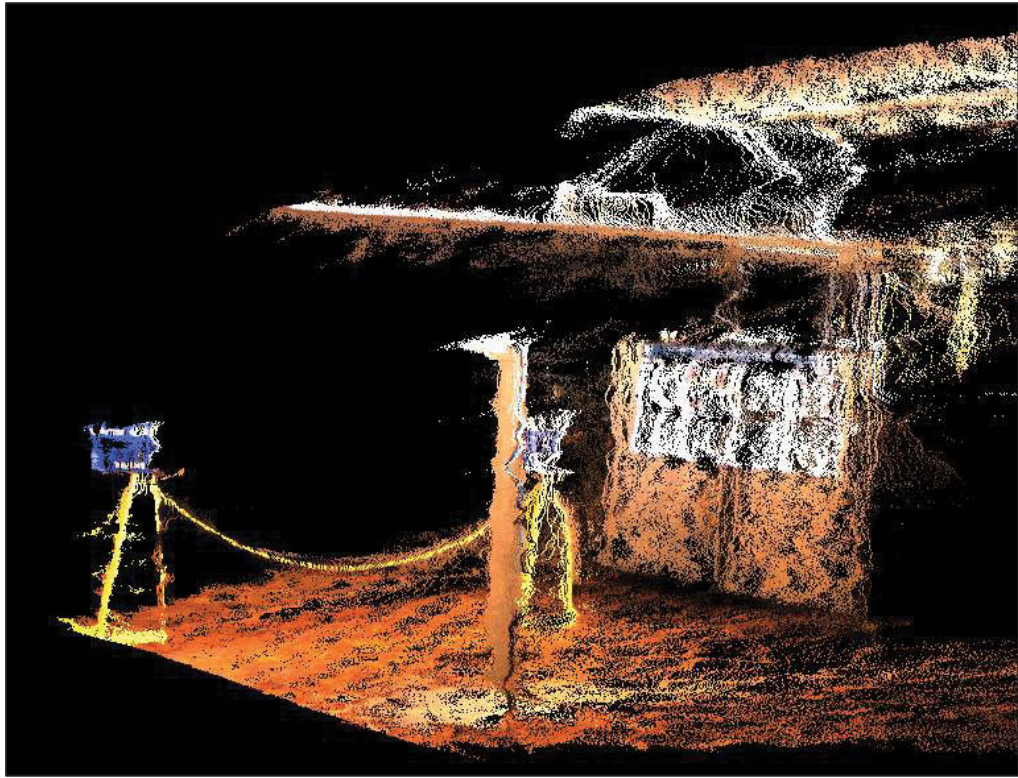
Figure 3-17: Example Scene Setup 3D Point Map Rotated 45 Degrees to the Right
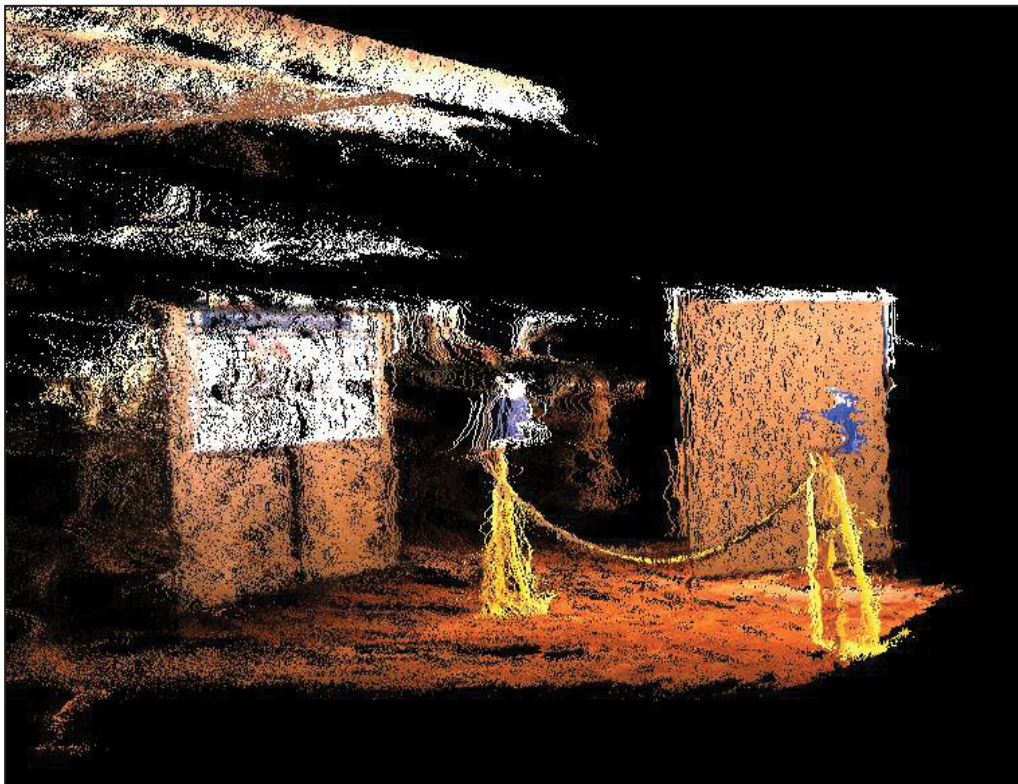
Figure 3-18: Example Scene Setup 3D Point Map Rotated 45 Degrees to the Left
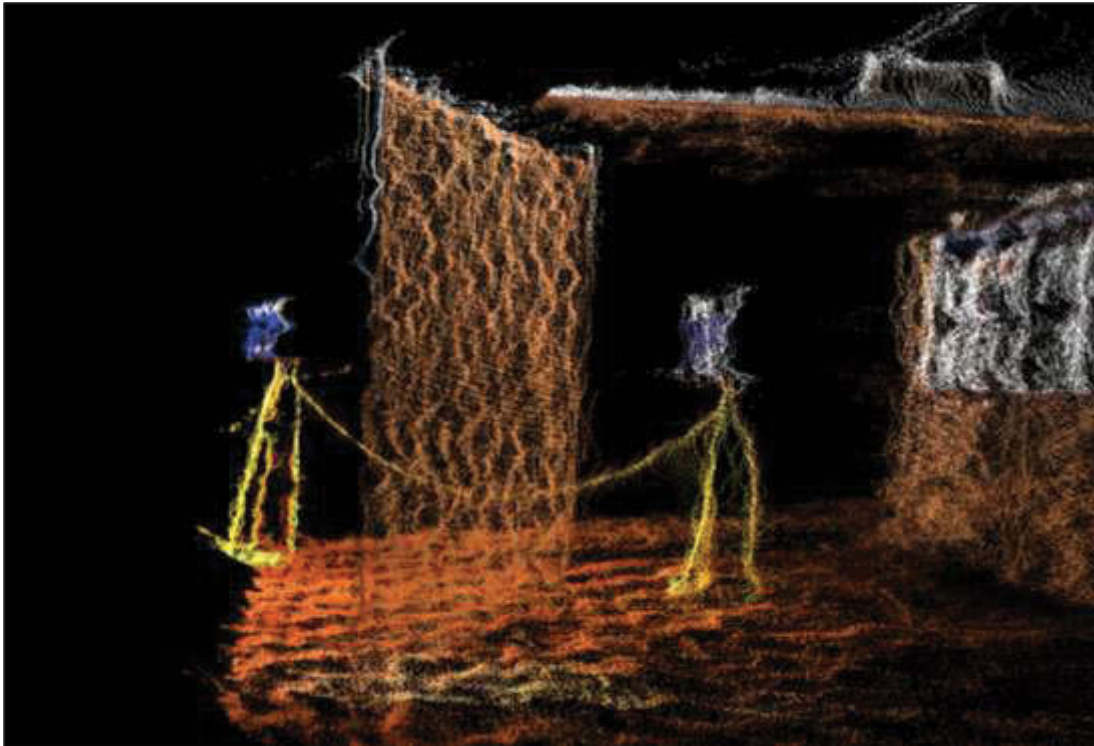
Figure 3-19: Example Scene Setup 3D Point Map Rotated 90 Degrees to the Right

Figure 3-20: Example Scene Setup Comparison Photo taken from Same Angle as Figure 3-19
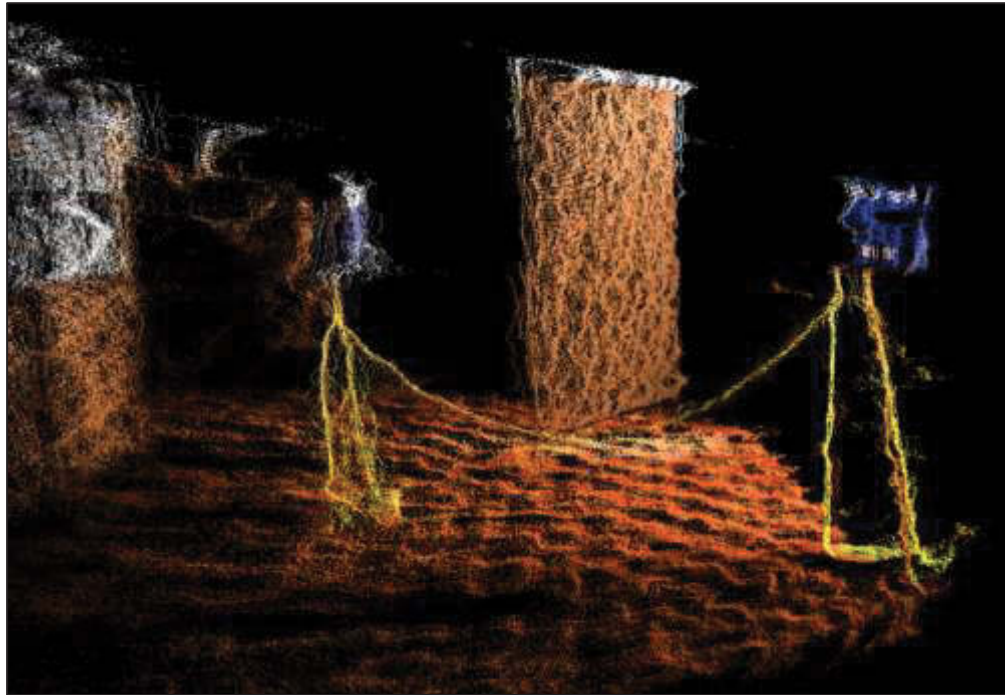
Figure 3-21: Example Scene Setup 3D Point Map Rotated 90 Degrees to the Left

Figure 3-22: Example Scene Setup Comparison Photo taken from Same Angle as Figure 3-21

Figure 3-19 displays that the general depth positioning of pixels in 3D space are clustered in local areas for any given object, showing adequate depth estimation of correlated pixels from the stereo pair of images. Observational comparison against the photo taken from the same

angle in Figure 3-20 shows correct placement of objects in the 3D point map. Even the chain inbetween the two yellow plastic pyramids is correctly correlated, with the position and link intact between the pyramids and the height off the ground able to be seen from the side, which is not easy to estimate from the original raw images of Figure 3-11.

Comparing the rotated 3D point map on the other side in Figure 3-21 against the photo taken from that same angle in Figure 3-22 again confirms correct placement of objects by observation in the 3D point map. To convert this to a useable representation for the wheelchair, in this case being a 2D bird's eye view map, this scene should be viewed from above to see the placement of obstacles in the local environment (Figure 3-23).
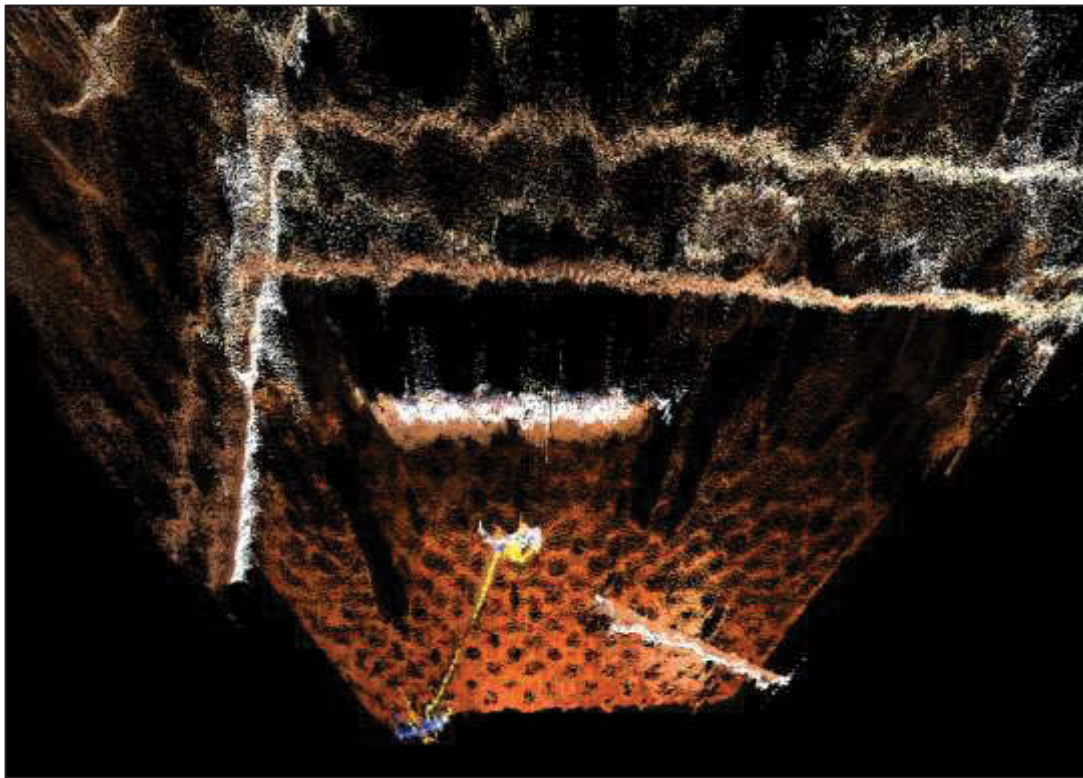
Figure 3-23: Example Scene Setup 3D Point Map Rotated to Bird's Eye View from Above

Filtering out the floor and everything above the highest point of the wheelchair results in only the objects which pose as obstacles being left in the scene. This remaining data is then grouped by pixel density so that stray artifact pixels are not treated as whole objects. The grouped data can then be converted into a 2D bird's eye view representation of the local obstacles, which only plots the closest object points for each visible angle to save memory and processing time. The example scene setup result is shown in Figure 3-24.
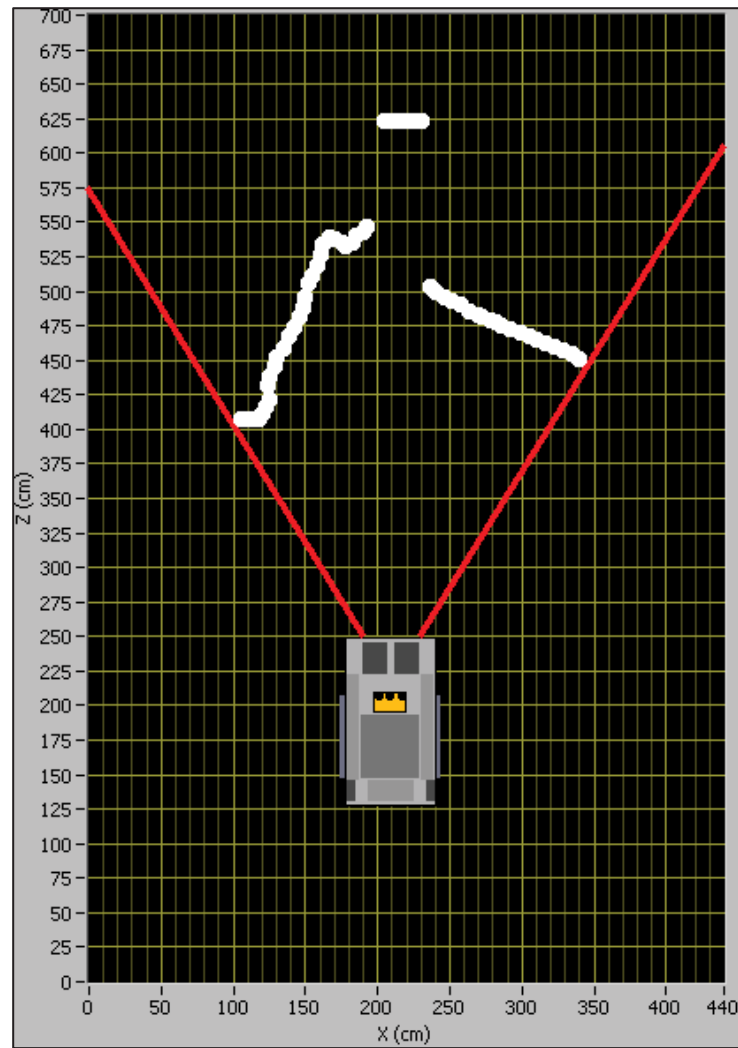
Figure 3-24: Example Scene Setup 2D Bird's Eye View Map Representation

This form of mapping allows the wheelchair to view the space available in its local environment and determine where objects are placed. The red lines in Figure 3-24 represent the field-of-view (FOV) using the stereoscopic cameras, and the white plotted points represent the determined placement of objects points in the scene. This mapping process is absolute in nature, where object points placed on the map are considered definite objects, all space directly between each point and the wheelchair are considered free space, and all space in the same line past the object are considered unknown. This is a simpler and more specific mapping approach as opposed to the probability maps commonly created using sonar and ultrasonic sensors, which allocate probabilities of object placement in the map based upon movements of the sensors, due to their associated uncertainties.

3.3.3 Wheelchair Odometry Change Calculations

Memory depth mapping is necessary for this application as the wheelchair can potentially collide with obstacles once they move out of the range of vision. So if the position of objects out of the range of vision can be recalculated and assumed to be static, then the wheelchair can use memory depth mapping to avoid collisions with these objects.

Design Method

In many mobile robotic applications, position estimation methods used are usually either absolute or relative positioning. The absolute positioning method generally relates the vehicle's position to external environmental features, such as beacons or landmarks. However, this may involve prior knowledge or other information processes that are not required for this wheelchair as it navigates through unknown territory. The relative positioning method is more applicable here, where odometry and changes thereof can be obtained for the wheelchair as it moves. This data is acquired from wheel encoders, which individually measure rotation of the two drive wheels. This allows odometry changes in real-time to be determined, making it a simple, inexpensive, and appropriate solution for this project.

The wheelchair model assumes that wheel revolutions can be translated into linear displacement relative to the floor. This means that movements of the wheels are recorded and do not take into account conditions of slippage. However, for the short distance ranges involved, these small and rarely-occurring inaccuracies in data processing do not impact heavily on operations for this project.

Movements of the wheelchair as a whole are represented by position and orientation changes to the midpoint of the driving axis connecting the two main wheels. Figure 3-25 displays a diagram representing movements of the wheelchair. The left and right wheel positions are denoted by A and C, the midpoint of the drive axis is denoted B, forming the reference point of this wheelchair (Wang, 1988):
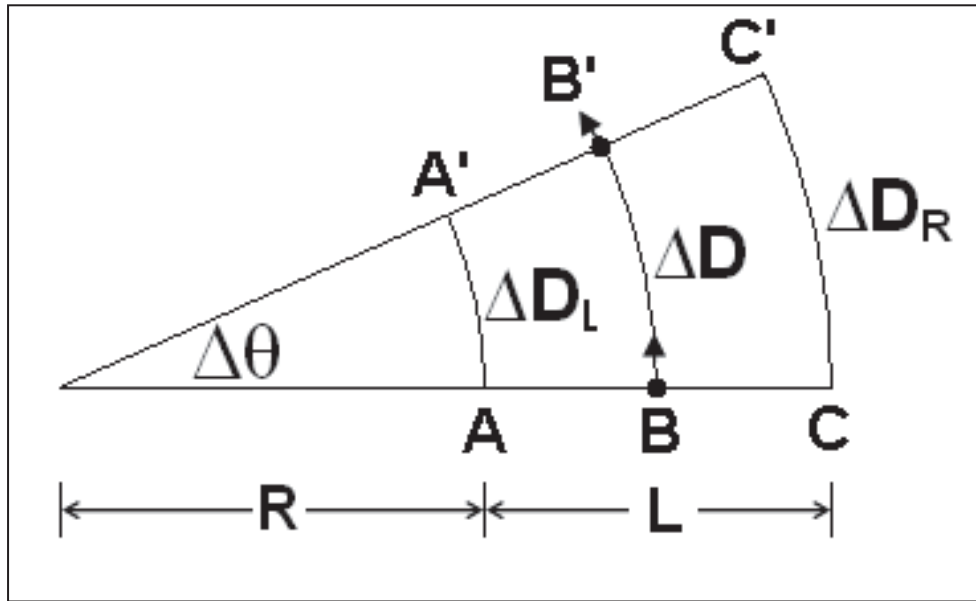
Figure 3-25. Illustration of Movement

In Figure 3-33, the length of the axis is denoted by L such that $L = AC = A'C'$. Whenever the wheelchair moves, the left wheel moves from A to A', the right wheel moves from C to C', and the reference point moves from B to B'. The change in distance ΔD and the change in angle $\Delta\theta$ resulting from the movement can be calculated in terms of the separate distances covered by the left wheel ΔDL and by the right wheel ΔDR. This data is acquired from the wheel encoders and then decoded into distance measurements for calculating these odometric changes. Using the equation for the length of an arc, the distances covered by the left and right wheels are

$$\Delta D_R = (L + R)\Delta\theta$$

(3.8)

$$\Delta D_L = R\Delta\theta$$

The distance covered by the reference point is the average of the inner and outer arcs, being the distances covered by the left and the right wheels. Furthermore, the change in angle is proportional to the difference of the outer and inner arcs, as found from rearranging the above equations to eliminate the unknown distance R.

Thus,

$$\Delta D = \frac{(\Delta D_R + \Delta D_L)}{2}$$

(3.9)

$$\Delta \theta = \frac{(\Delta D_R - \Delta D_L)}{L}$$

In 2-dimensional Cartesian space, the state of the wheelchair at time t is represented by a triplet *(Xt, Yt, θt)* forming the wheelchair‟s position coordinates and orientation. This triplet is what needs to be determined. Using the above equations the new orientation θ_t at time t can be simply updated from the previous orientation θ_{t-1} at time *t-1* plus the calculated change in angle $\Delta \theta$, ie. $\theta_t = \theta_{t-1} + \Delta \theta$. However, the wheelchair‟s position coordinates *(Xt, Yt)* are not yet known because to achieve a total arc length ΔD and change of orientation $\Delta \theta$, any path could be taken. Figure 3-26 will be used to illustrate how the wheelchair‟s position coordinates can be determined assuming circular paths (Wang 1988):

Figure 3-26. Illustration of Position Change

In Figure 3-26, beginning at point *O* and oriented in the direction of point *A,* the wheelchair moves to point *P* oriented in the direction of point *G*. Assuming a circular path, *ΔD=arc(OP)*

and $\Delta\theta = \angle ABP$. It can be shown that BC, parallel to DE and to OP, bisects the angle $\angle ABP$ such that

$$\angle ABC = \angle ADE = \angle AOP = \frac{\Delta\theta}{2} \qquad (3.10)$$

Therefore,

$$\angle POF = \angle AOF - \angle AOP = \theta_{t-1} + \frac{\Delta\theta}{2} \qquad (3.11)$$

For an arbitrary path where the length OP is not known, a method for approximating the position change ΔX and ΔZ is to approximate P by P' (Wang 1988) , such that the length OP' $= arc\ OP = \Delta D$. Using this, we have

$$\Delta X \approx \Delta D \cos\left(\theta_{t-1} + \frac{\Delta\theta}{2}\right)$$

$$\Delta Z \approx \Delta D \sin\left(\theta_{t-1} + \frac{\Delta\theta}{2}\right) \qquad (3.12)$$

and the new wheelchair state (X_t, Y_t, θ_t) at time t for an arbitrary path is approximated by

$$X_t = X_{t-1} + \Delta X \approx X_{t-1} + \Delta D \cos\left(\theta_{t-1} + \frac{\Delta\theta}{2}\right)$$

$$Z_t = Z_{t-1} + \Delta Z \approx Z_{t-1} + \Delta D \sin\left(\theta_{t-1} + \frac{\Delta\theta}{2}\right) \qquad (3.13)$$

$$\theta_t = \theta_{t-1} + \Delta\theta$$

For a circular path, the relationship between the length of OP and $arc(OP)$ can be determined as (using L and R notations from Figure 3-25)

$$\frac{OP}{arc(OP)} = \frac{2\left(\frac{L}{2}+R\right)\sin\left(\frac{\Delta\theta}{2}\right)}{\left(\frac{L}{2}+R\right)\Delta\theta} = \frac{\sin\left(\frac{\Delta\theta}{2}\right)}{\left(\frac{\Delta\theta}{2}\right)} \qquad (3.14)$$

That is,

$$OP = \frac{sin\left(\frac{\Delta\theta}{2}\right)}{\left(\frac{\Delta\theta}{2}\right)} \Delta D \qquad (3.15)$$

Using this, we have

$$\Delta X = \frac{sin\left(\frac{\Delta\theta}{2}\right)}{\left(\frac{\Delta\theta}{2}\right)} \Delta D \, cos\left(\theta_{t-1} + \frac{\Delta\theta}{2}\right)$$

$$\qquad (3.16)$$

$$\Delta Z = \frac{sin\left(\frac{\Delta\theta}{2}\right)}{\left(\frac{\Delta\theta}{2}\right)} \Delta D \, sin\left(\theta_{t-1} + \frac{\Delta\theta}{2}\right)$$

and the new state of the wheelchair (X_t, Z_t, θ_t) at time t for a circular path is given by

$$X_t = X_{t-1} + \frac{sin\left(\frac{\Delta\theta}{2}\right)}{\left(\frac{\Delta\theta}{2}\right)} \Delta D \, cos\left(\theta_{t-1} + \frac{\Delta\theta}{2}\right)$$

$$Z_t = Z_{t-1} + \frac{sin\left(\frac{\Delta\theta}{2}\right)}{\left(\frac{\Delta\theta}{2}\right)} \Delta D \, sin\left(\theta_{t-1} + \frac{\Delta\theta}{2}\right) \qquad (3.17)$$

$$\theta_t = \theta_{t-1} + \Delta\theta$$

It should be noted that *(sin α) / α→1* as *α→0*. The term *sin[(Δθ/2)/(Δθ/2)]* can be viewed as an adjustment factor for the wheelchair"s change in position due to the circular movement.

These algorithms allow not only the movements of the wheelchair to be recorded, but can also be built upon to provide „memory" mapping capabilities, as described in the next section §3.3.4. Here, the movements of the wheelchair and odometry changes are used to recalculate the coordinates of mapped object points, relative to the wheelchair, once they are no longer in the wheelchair cameras" field of vision.

3.3.4 Real-time Environment Map Construction

As shown in Figure 3-4 in §3.2, the stereoscopic cameras are mounted on a frame in front of the user, placing them directly in the centre of the wheelchair. A problem here, however, is that the horizontal range of vision is only about 66º wide. This is adequate for avoiding objects directly ahead of the wheelchair when in the range of vision, but when these objects move outside the range of vision they are forgotten. The wheel odometry change calculations of §3.3.3 can be used here to reposition the mapped object points once they move out of the range of vision, effectively „remembering" the objects. The same coordinate system used in the mapping process, defined in the 3D point map construction as shown in Figure 3-15, is applied here, whereby the y-axis is in the direction from the above straight downward to the below, the x-axis is in the direction from the left straight across to the right, and the z-axis is in the direction from the back straight to the front of the wheelchair. The environment in front of the TIM wheelchair is updated whilst inside the range of vision, and the positions of objects are remembered as they move outside of that range of vision.
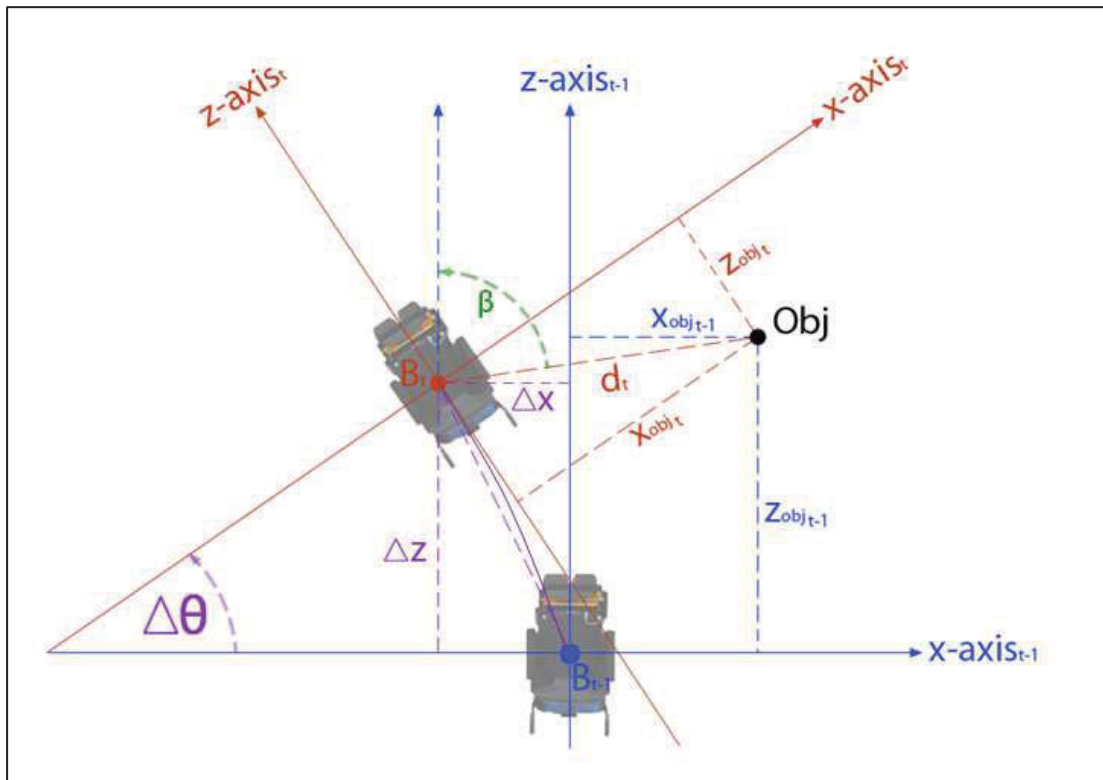
Figure 3-27: Coordinate Changes of TIM Relative to Environment
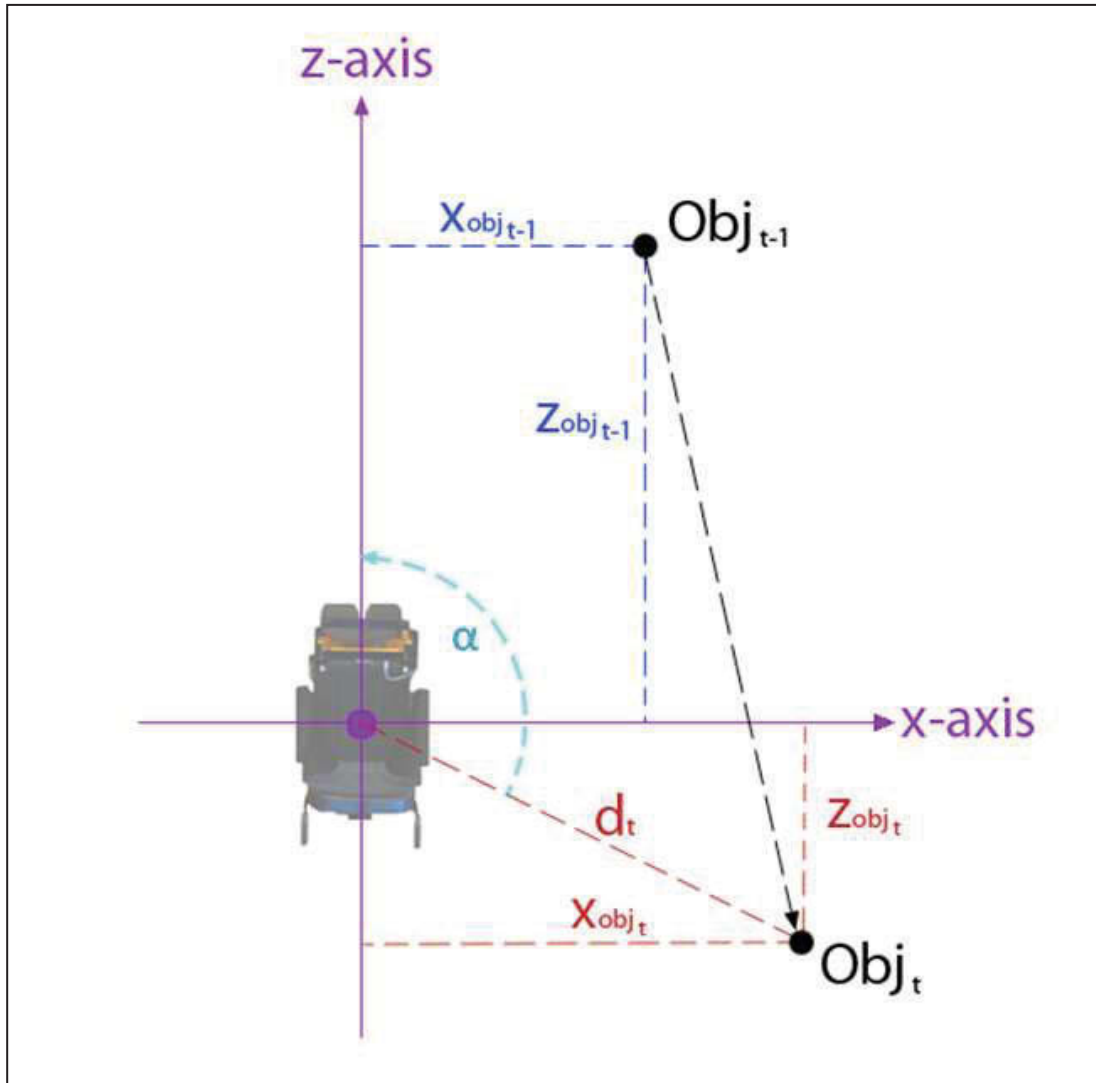
Figure 3-28: Updating Position of Objects Relative to TIM

The principle of real-time 2D environment map construction is illustrated in Figure 3-27 and Figure 3-28, whereby object points can be remembered when the wheelchair cameras can no longer see them. Figure 3-27 displays the movement of the wheelchair relative to the environment and objects. The position of the wheelchair can be seen in the prior computational cycle at instant *t-1*, at which time the mapped object point *obj* is within vision range of the cameras. When the wheelchair moves forward and to the left, the next computation cycle at instant *t* results, and the new location and angle vector of the wheelchair is determined from the wheelchair's change in odometry triplet *(ΔX, ΔZ, $\Delta \theta$)*.

At this time instant t, the object point obj is no longer in view as the wheelchair has moved and turned away from it. Relative to the wheelchair the object point obj_{t-1} has moved from inside the range of view to outside the range, and resulting in the object at this instant in time obj_t now being located behind the wheelchair, a concept illustrated in Figure 3-28. In order to remember this object point, the position can be recalculated relative to the wheelchair's drive shaft centre point at this instant B_t, which can be seen in Figure 3-27. The recalculation estimation is performed in the following algorithms. The changes in odometry as previously presented in Equation 3-7 are

$$\Delta X = X_t - X_{t-1}$$

$$\Delta Z = Z_t - Z_{t-1}$$

$$\Delta\theta = \theta_t - \theta_{t-1}$$

Considering the changes in odometry of the wheelchair and the changes in position of the object point relative to the wheelchair, the next step is to calculate the distance of the line d_t between the object obj_t and the wheelchair drive shaft centre point B_t at time instant t, which is found as

$$distance_{d_t} = \sqrt{\left(X_{obj_{t-1}} - \Delta X\right)^2 + \left(Z_{obj_{t-1}} - \Delta Z\right)^2} \tag{3.18}$$

The angle β between the line of the z-axis at time $t-1$ and the line d_t, is calculated as

$$\beta = tan^{-1}\left(\frac{X_{obj_{t-1}} - \Delta X}{Z_{obj_{t-1}} - \Delta Z}\right) \tag{3.19}$$

The angle α between the line of the z-axis at time t and the line d_t, is calculated as

$$\alpha = \beta + \Delta\theta \tag{3.20}$$

The recalculation estimate of the coordinates of object point obj_t at time instant t, can now be calculated as

$$X_{obj_t} = distance(d_t).(sin\ \alpha)$$

(3.21)

$$X_{obj_t} = \sqrt{\left(X_{obj_{t-1}} - \Delta X\right)^2 + \left(Z_{obj_{t-1}} - \Delta Z\right)^2}.\sin\left[\tan^{-1}\left(\frac{X_{obj_{t-1}} - \Delta X}{Z_{obj_{t-1}} - \Delta Z}\right) + \Delta\theta\right]$$

$$Z_{obj_t} = distance(d_t).(cos\ \alpha)$$

(3.22)

$$Z_{obj_t} = \sqrt{\left(X_{obj_{t-1}} - \Delta X\right)^2 + \left(Z_{obj_{t-1}} - \Delta Z\right)^2}.\cos\left[\tan^{-1}\left(\frac{X_{obj_{t-1}} - \Delta X}{Z_{obj_{t-1}} - \Delta Z}\right) + \Delta\theta\right]$$

where:

(X_{obj_t}, Z_{obj_t}):   coordinates of object obj_t at new time instant t,

$(X_{obj_{t-1}}, Z_{obj_{t-1}})$:   coordinates of object obj_{t-1} at prior time instant $t-1$,

$distance(d_t)$:   distance of the line d_t.

These algorithms are applied to each step in depth mapping to reposition all mapped object points. The repositioned data is scanned and all points that remain ahead of the wheelchair within the range of vision limits are removed as that area is continuously populated with new depth data updates from the processed camera images. Only the repositioned points outside vision limits of the camera system are stored and displayed on the depth map along with the updated depth data. This alone, without further methods of data gathering, is useful for mapping static environments containing static objects, as the remapped objects are „remembered" in the exact positions within which they were last seen.

3.4 Advanced Methods for Optimising Intelligent Vision Mapping Performance

Of particular concern in this application is how the stereo processing parameters affect the mapping process as many external influences, especially brightness and contrasts in environmental lighting conditions, determine the accuracy of stereo matching for disparity image creation. Extreme changes in lighting when moving from one environment to another tend to introduce large amounts of noise into the disparity images and hence produce noise artifacts in the wheelchair's local environment map. To overcome this problem, a method for adaptive online stereo processing parameter selection is introduced in an effort to reduce noise, increase mapping accuracies, and generally produce the most appropriate configuration at all times.

3.4.1 Environmental Lighting Type Categories

The process described in §3.3.2 for processing stereoscopic images into a 2D local environment depth map requires a reasonable configuration of the stereo processing parameters. These have a significant influence over the ability of the method to accurately correlate image pixel neighbourhoods between the stereo images. However, it is unfortunate that no single configuration is adequate for all many types of environments and lighting conditions, calling for it to be tuned individually to various scenarios, which can be time-consuming and requires trial-by-error tuning. Brightness and contrast features in images acquired from varying environments all impact upon the image quality and, hence, parameter configuration required. Furthermore, there are a number of parameters (different mask sizes, disparity range values, and various validation parameters) which all affect the performance and cannot be treated individually. For this reason a strategy for an adaptive stereo processing parameter selection is proposed, whereby the cameras can deal with a large range of potentially encountered environments and conditions, and the wheelchair is made capable of selecting the most appropriate configuration of four category options based on perceived environmental conditions at any given time.

Image Feature Quantisation

Alongside the ability to produce depth maps from acquired stereoscopic images, the rectified colour images can also be analysed directly for desired features. Depth mapping from stereo

images is greatly affected by the lighting conditions in a scene. In particular, the brightness and contrast contained within a single scene has the most impact on accuracies in depth mapping. Consistency in these parameters produces higher accuracies most of the time, whereas scenes with highly contrasting areas of brightness, such as those containing sunlight reflections as well as dark spaces, can prove very difficult for accurate depth mapping and will usually introduce noise artifacts due to correlation mismatches.

To address this issue, quantisation of appropriate image features is the first step. Quantisation here is the conversion of desired image features to discrete values. The image feature of interest here is illumination, which is a fundamental component in the process of image formation. The strength of the sensation which illumination excites in the human eye is referred to as brightness, which is proportional to the logarithm of luminous flux, F (Acharya & Ray 2005). Fechner's Law defines brightness B by the relation:

$$B = k \log\left(\frac{F}{F_o}\right) \tag{3.23}$$

where: k is a constant and F_o is a reference luminous flux, measured in lumane (lm).

Unfortunately, imaging processes can be complicated by specular reflections, whereby two nearby areas of a single surface can produce very different illumination intensities depending on the varying angles of light sources as well as the inclination of the surface. As such, the term "reflectivity" is used to signify the proportion of intensity reflected towards the camera when objects are illuminated from a particular direction.

By convention, digitised grey-scale images represent black pixels as zero and white pixels as the maximum, usually 255 (each pixel represented with a single byte of data, being 0 to 255). All other grey levels are accordingly represented as numbers in between this minimum and maximum. Large differences in reflectivity or illumination intensity in adjacent areas of an image produces a high contrast. This is a crucial element of image quality and measures the difference in image intensity between adjacent areas (Lacey 1998). The image carries no information without the presence of contrast, which arises in, but is not fixed to, the acquisition process.
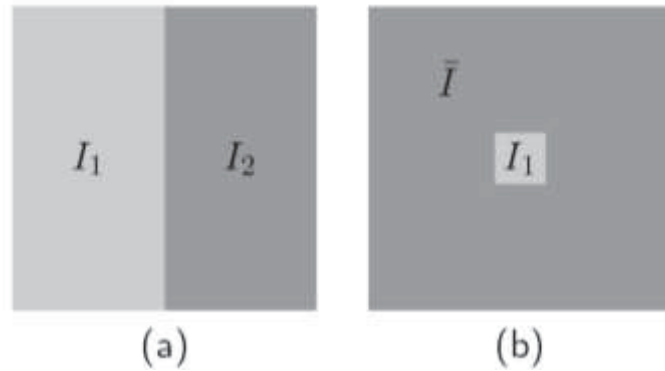
Figure 3-29: Contrast for Two Cases: (a) Areas of Similar Size, and (b) Areas of Different Size

Figure 3-29 displays two simple cases of contrast within an image that are frequently encountered. Contrast is most commonly defined relative to the mean intensity. Case (a) looks at the contrast between two adjacent areas of about the same size, I_1 and I_2. The mean intensity in this case is $(I_1 + I_2)/2$ and the deviation from mean is $|I_1 - I_2|/2$, giving the contrast

$$C = \frac{|I_1 - I_2|}{|I_1 + I_2|} \tag{3.24}$$

Case (b) looks at the contrast between a smaller foreground, I_1, and a larger background, $\bar{I}$. The mean intensity is approximately the same value as $\bar{I}$, provided by the large background area and the difference is $\Delta I = |I_1 - \bar{I}|$, giving the relative contrast

$$C = \frac{\Delta I}{\bar{I}} = \frac{|I_1 - \bar{I}|}{\bar{I}} \tag{3.25}$$

So, brightness and contrast are important factors when considering the quality of an image, and these are both features that can be quantified. Brightness of environments will vary based on the lighting sources, from poorly lit rooms to rooms with adequate man-made light sources to outdoor areas illuminated by sunlight. Contrast will also vary in different environments based on the number of light sources and reflective surfaces. Fewer light sources in a single indoor room generally produces lower contrasts whereas rooms with more light sources, such as those allowing less lit areas inside and reflected sunlight from outside to be seen in a single image, generally produce higher contrasts. To address the variances in these factors, which affect both image quality and stereoscopic matching performance, a real-time adaptive stereo processing parameter selection technique is produced to find the most appropriate

stereoscopic parameter configuration based on the brightness and contrasts being viewed in any given environment at any instant in time.

Environmental Lighting Conditions Categories

Originally, a single configuration of stereo processing parameters was determined which performed best across all types of environment areas. However, it was soon realised that the stereo processing would produce higher levels of noise artifacts in areas that had different lighting conditions to those most commonly navigated by the wheelchair during testing. For this reason the real-time adaptive configuration of stereo processing parameters would be very beneficial for the process of autonomous navigation using these cameras by the wheelchair. Upon taking the wheelchair to many different types of areas, the environmental lighting conditions found were categorised into four different conditions which were each manually configured with the most appropriate corresponding stereo processing parameters. In addition to that discussed back in §3.3.2, these parameters have the following value ranges:

Stereo Parameter	Value Range
Stereo Mask Size	0 – 23
Edge Mask Size	0 – 11
Minimum Disparity Range	0 – 499
Maximum Disparity Range	0 – 499
Texture Validation	0.00 – 4.00
Surface Difference	0.00 – 3.00
Surface Size	0 – 400
Uniqueness Threshold	0.00 – 3.00
Back-Forth Setting	Off/On

Table 3-4: Stereo Processing Parameter Value Ranges

Since it is necessary to change these parameters to meet different environmental lighting conditions, the categories had to first be defined. Grey-scaling the image aids in this process as this format for images contains the illumination intensity information only. The default environmental condition is that most commonly encountered, exhibiting a general mix of contrasting illuminations within the one image frame. The main variance found that actually required reconfiguration of the stereo processing parameters where areas with extreme contrasts between the light and dark illuminations in the scene, mostly when indoors in a

relatively dark area and bright sunlight is entering from outdoors, resulting in perceived silhouetting of objects indoors. Other variances from the default condition were areas of consistent lighting within the single image, either consistently dark areas or consistently bright areas. These different environmental lighting conditions made up the set of four categories for encountered areas, along with their allocated stereo parameter configurations, are as follows:

- **Category 1**: General Illumination Contrast (default)
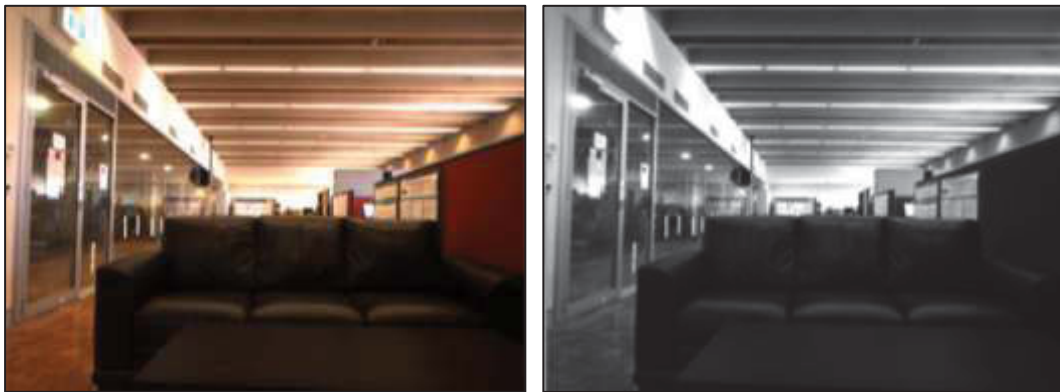
Figure 3-30: Category 1: General Illumination Contrast Areas Example

This is the default setting and is most commonly encountered, since most environments navigated by wheelchair feature a range of contrasts and lighting differences within the single perceived scene. The stereo parameter configurations for this category are

Stereo Parameter	Value Range
Stereo Mask Size	13
Edge Mask Size	5
Minimum Disparity Range	0
Maximum Disparity Range	115
Texture Validation	0.77
Surface Difference	1.44
Surface Size	230
Back-Forth Setting	On

Table 3-5: Category 1 Stereo Processing Parameter Values

- **Category 2**: Extreme Illumination Contrast
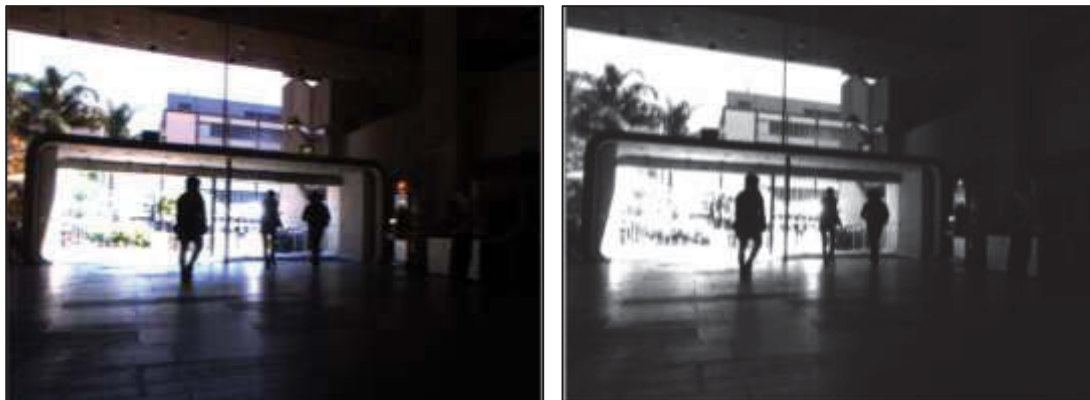
Figure 3-31: Category 2: Extreme Illumination Contrast Areas Example

This category is most often encountered when the cameras situated indoors looking at indoor objects but are also able to see significant amounts of bright sunlight reflections from outdoors, causing an extreme contrast in illumination within the single image view. The stereo parameter configurations for this category are

Stereo Parameter	Value Range
Stereo Mask Size	15
Edge Mask Size	9
Minimum Disparity Range	0
Maximum Disparity Range	115
Texture Validation	0.44
Surface Difference	0.62
Surface Size	315
Back-Forth Setting	On

Table 3-6: Category 2 Stereo Processing Parameter Values

- **Category 3**: Consistent Dark

Figure 3-32: Category 3: Consistent Dark Example

This category is encountered most when the cameras are closer to objects or walls in darker rooms or corridors. Although not often found, this category is necessary for the times when the wheelchair does venture into poorly lit areas. The stereo parameter configurations for this category are

Stereo Parameter	Value Range
Stereo Mask Size	13
Edge Mask Size	5
Minimum Disparity Range	0
Maximum Disparity Range	115
Texture Validation	0.55
Surface Difference	0.93
Surface Size	323
Back-Forth Setting	On

Table 3-7: Category 3 Stereo Processing Parameter Values

- **Category 4**: Consistent Bright

Figure 3-33: Category 4: Consistent Bright Areas Example

This category is encountered generally less in testing than the other three categories, being that of bright areas that are consistently bright throughout the acquired image. Generally well lit areas are also contrasted to some degree by darker spaces in the image. However, open outdoor areas on a sunny day are the most common environments that call for the configurations of this category. The stereo parameter configurations for this category are

Stereo Parameter	Value Range
Stereo Mask Size	13
Edge Mask Size	9
Minimum Disparity Range	0
Maximum Disparity Range	115
Texture Validation	0.27
Surface Difference	1.03
Surface Size	285
Back-Forth Setting	On

Table 3-8: Category 4 Stereo Processing Parameter Values

3.4.2 Neural Network Classification for Adaptive Stereo Processing Parameter Selection

To classify which of these categories the cameras are observing at any instant in time, during real-time operation of the wheelchair, a neural network is utilised for the classification process. The neural network method of classification utilised is introduced in §2.3.3. A pre-processed modification of the grey-scale image is used as the inputs for this. The greyscale image is reduced in resolution to a 40x56 matrix (40 rows and 56 columns) by taking the average pixel value in each cell of the reduced resolution grid. For example, the image in Figure 3-34 is grey-scaled, and the reduced-resolution overlay setup is shown in Figure 3-35, producing the reduced-resolution image in Figure 3-36.
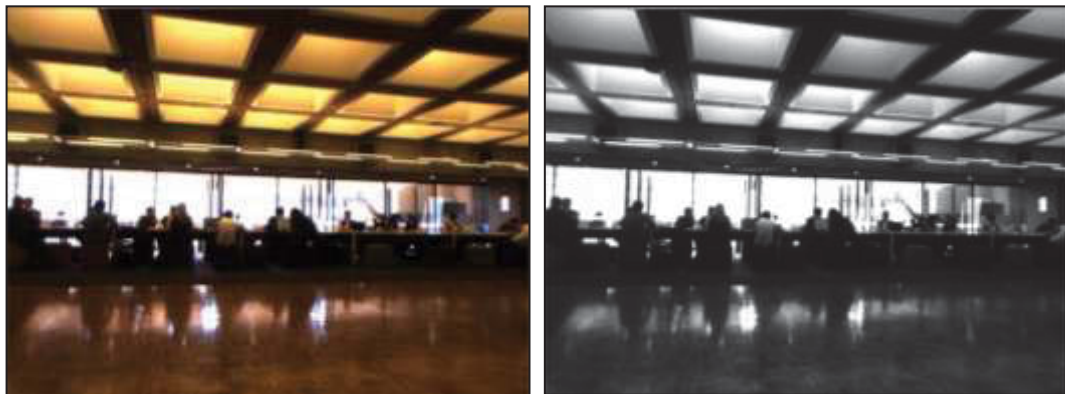
Figure 3-34: Neural Network Input Setup: Grey-scale Step

Figure 3-35: Neural Network Input Setup: Grid overlay Step
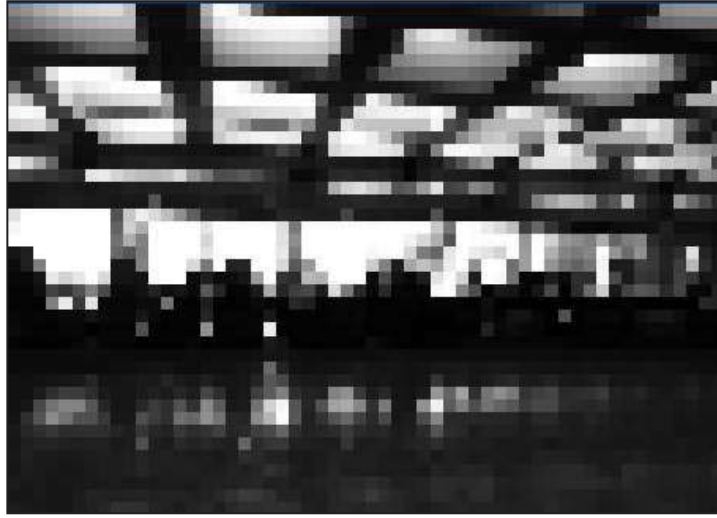
Figure 3-36: Neural Network Input Setup: Reduced-resolution Step

This reduced-resolution image, shown in Figure 3-36, contains adequate information about the illumination intensities for the different pixel neighbourhoods. The data contained in this image is then converted into a 1D (1-dimensional) array to create a useable neural network input. All data element values are between 0 and 255, inclusive, for the 8-bit grey-scale representation (8bits = 2^8 = 256 values). The data is normalised through the process of dividing each element by 128, which places all values to between 0 and 2, and then subtracting 1 from these values, resulting in all data element values normalised to floating point numbers between -1 and 1. Normalisation is an important process to help prevent over-growth of weights by holding numbers that are too large to be processed efficiently. The neural network used for this is two-layer, utilising a generalised Delta learning rule for error back-propagation training, and a bipolar activation function. Each of the images is represented as a 1D array in the following manner:

- Denoting the number of pixel rows (*r*) in the image as *n* and the number of pixel columns (*c*) as *m*, the top left pixel is (r_0,c_0) and the bottom right pixel is (r_{n-1},c_{m-1}). As previously mentioned here the image is reduced to a resolution of 56x40 pixels, giving *m*=56 and *n*=40.

- Beginning with the top left pixel of the image (r_0,c_0), scanning right to the top right pixel (r_0,c_{m-1}), then moving down one row and again scanning from the left (r_1,c_0) to (r_1,c_{m-1}), and so on until the input array for the Neural Network is filled as a single column. This produces a 1D array of 2240 normalised pixel values. So,

$$x = \begin{bmatrix} (r_0, c_0) \\ (r_1, c_1) \\ \vdots \\ (r_0, c_{m-1}) \\ (r_1, c_0) \\ \vdots \\ (r_{n-1}, c_0) \\ \vdots \\ (r_{n-1}, c_{m-1}) \end{bmatrix} \tag{3.26}$$

The inputs of this Neural Network are made up of a number of patterns, being the number of images for each of the training, validation, and testing phases. For this 400 patterns (images) were used for each of the training, validation, and testing phases. The number of output classes (output neurons) are $K = 4$, here representing environmental categories 1 to 4. Due to the neural network being two-layer, this means there is a hidden layer and an output layer. The variable parameters that affect the training process are the number of hidden neurons J^*; the number of hidden neurons with the added dummy neuron J, where $J = J^*+1$; the learning constant η; and the momentum constant α. These parameters can be varied and an optimised configuration of such is required to be found. The equations for the training phase of this method are described below.

Initialisation:

Input vectors x are defined in Equation 3.26, and are all augmented by assigning -1 to each, resulting in a total of I elements for each input vector x_{aug}. On the other end, the 4 output categories produce the 4 class memberships

$$d_1 = \begin{bmatrix} 1 \\ -1 \\ -1 \\ -1 \end{bmatrix}, d_2 = \begin{bmatrix} -1 \\ 1 \\ -1 \\ -1 \end{bmatrix}, d_3 = \begin{bmatrix} -1 \\ -1 \\ 1 \\ -1 \end{bmatrix}, d_4 = \begin{bmatrix} -1 \\ -1 \\ -1 \\ 1 \end{bmatrix} \tag{3.27}$$

Initialisation of weights are done by generating random matrices for the hidden layer weights $\overline{W}$ and the output layer weights W, with $\overline{W}$ dimensions being set as J^* rows by I columns, and W dimensions being set as K rows by J columns. Each element in these random matrices are randomly generated to between the values of -1 and 1. Once initialised the following calculations are performed for every step which each looks at one pattern at a time.

Recursive Training Steps:

The hidden layer is addressed first, between the input neurons and the hidden neurons. The hidden layer activation vector $\bar{v}$ is expressed as

$$\bar{v} = \overline{W}x_{aug} \tag{3.28}$$

A bipolar activation function is used to find the output value of the hidden layer y, where

$$y = \frac{2}{(1 + e^{-\bar{v}})} - 1 \tag{3.29}$$

This hidden layer output y is augmented by assigning -1 to the vector producing y_{aug}, which then becomes the input for the output layer.

Now the output layer goes through the same process as the hidden layer, except it is between the hidden neurons and the output neurons. The output layer activation vector v is expressed as

$$v = Wy_{aug} \tag{3.30}$$

A bipolar activation function is again used to find the output value of the output layer z, where

$$z = \frac{2}{(1 + e^{-v})} - 1 \tag{3.31}$$

This output value z is used to determine the learning signal, which is the error between the target output d and the calculated output z, and is aimed to be minimised as the network is trained. The learning signal term as such is defined as

$$e = d - z \tag{3.32}$$

After each step, an output layer error, known as pattern error, is produced for that run. This is found by looking at each vector element k separately, and is calculated, for each pattern P, as

$$E_P = \frac{1}{2}e_k^2 = \frac{1}{2}\sum_{k=1}^{K}(d_k - z_k)^2 \tag{3.33}$$

The learning signal term is then used to calculate the error signal term δ, used for weight modification, which is found as

$$\delta = -\frac{\partial E_P}{\partial v_k} = -\frac{\partial E_P}{\partial z_k} \cdot \frac{\partial z_k}{\partial v_k} = (d_k - z_k)\frac{\partial z_k}{\partial v_k} \tag{3.34}$$

The updated weights for the proceeding step, such that W_{P+1} is the next weight vector from W_P, under the delta training rule can now be found from

$$W_{P+1} = W_P - \eta\frac{\partial E_P}{\partial W_P} = W_P + \eta\delta y'_{aug} \qquad \text{where } \boldsymbol{\delta} = \begin{bmatrix} \delta_1 \\ \delta_2 \\ \vdots \\ \delta_K \end{bmatrix} \tag{3.35}$$

The momentum method is also employed here to accelerate the convergence of the error back-propagation learning algorithm. The method involves supplementing the current weight adjustments with a fraction of the most recent weight adjustment. Adding this into Equation 3.35 is done so as follows

$$W_{P+1} = W_P - \eta\frac{\partial E_P}{\partial W_P} = W_P + \eta\delta y'_{aug} + \alpha(W_P - W_{P-1}) \qquad \text{where } \boldsymbol{\delta} = \begin{bmatrix} \delta_1 \\ \delta_2 \\ \vdots \\ \delta_K \end{bmatrix} \tag{3.36}$$

Introducing this momentum term typically helps to speed up convergence as well as achieve a more efficient and reliable profile. Note that $\mathbf{w}^0 = \mathbf{w}^1$. Now the delta error back-propagates through to the hidden layer for hidden layer weight modification. This error signal term for the hidden layer $\overline{\boldsymbol{\delta}}$ is found as

$$\bar{\delta}_j = -\frac{\partial E_P}{\partial \overline{v}_j} = -\frac{\partial E_P}{\partial y_j} \cdot \frac{\partial y_j}{\partial \overline{v}_j} \tag{3.37}$$

Note that

$$\frac{\partial E_P}{\partial y_j} = \frac{\partial}{\partial y_j}\left[\frac{1}{2}\sum_{k=1}^{K}(d_k - z_k)^2\right] = -\sum_{k=1}^{K}\frac{\partial E_P}{\partial z_k}\frac{\partial z_k}{\partial v_k}\frac{\partial v_k}{\partial y_j} \qquad (3.38)$$

$$\frac{\partial E_P}{\partial y_j} = -\sum_{k=1}^{K}(d_k - z_k)\frac{\partial z_k}{\partial v_k}w_{Pkj} = -\sum_{k=1}^{K}\delta_k w_{Pkj} \qquad (3.39)$$

This error signal term for the hidden layer $\overline{\delta}$ is now found as

$$\delta_j = -\frac{\partial E_P}{\partial y_j}\cdot\frac{\partial y_j}{\partial \overline{v_j}} = \frac{\partial y_j}{\partial \overline{v_j}}\sum_{k=1}^{K}\delta_k w_{Pkj} \qquad \text{where } \overline{\delta} = \begin{bmatrix}\bar{\delta}_1\\\vdots\\\bar{\delta}_{J*}\end{bmatrix} \qquad (3.40)$$

In a similar manner to the output layer weights update, the modified weights of the hidden layer can be expressed as

$$\overline{W}_{P+1} = \overline{W}_P - \eta\frac{\partial E_P}{\partial \overline{W}_P} = \overline{W}_P + \eta\bar{\delta}x'_{aug} + \alpha(\overline{W}_P - \overline{W}_{P-1}) \qquad (3.41)$$

This process, from Equation 3.28 to Equation 3.41, is repeated for every step which trains each of the training set patterns sequentially. Each step produces a pattern error, as in Equation 3.33, and every K, or in this case every 4, patterns together form a cycle. The accumulative error, known as cycle error E_c, can be calculated over the error back-propagation training cycle with P patterns and K output neurons as

$$E_c = \frac{1}{2}\sum_{p=1}^{P}\sum_{k=1}^{K}(d_{pk} - z_{pk})^2 = \sum_{p=1}^{P}E_P \qquad (3.42)$$

Optimisation Process:

Cycle error is used in the neural network optimisation process to determine the best parameter configuration and highest achievable classification accuracies. The above Equations 3.28 to 3.42 are all used and repeated throughout the training phase, but to optimise and prevent over-fitting as described in §2.3.3, a simultaneous validation phase is also used, whereby the weights at all steps of the training phase are applied to the validation set, using Equations 3.28 to 3.33 and cycle error Equation 3.42. The cycle error is observed in the validation phase and the early-stopping technique is employed for when this cycle error decreases, hits a local minimum, and starts increasing for a number of cycles sufficient enough to assume that the error will not reduce below the minimum already seen. When this is determined, training and validation both stop. The weights stored at the early stopping point, being the cycle exhibiting minimum validation cycle error, are determined as the optimal weights for this neural network training process.

Figure 3-37: Example Test Patterns of Category 1: General Illumination Contrast Areas
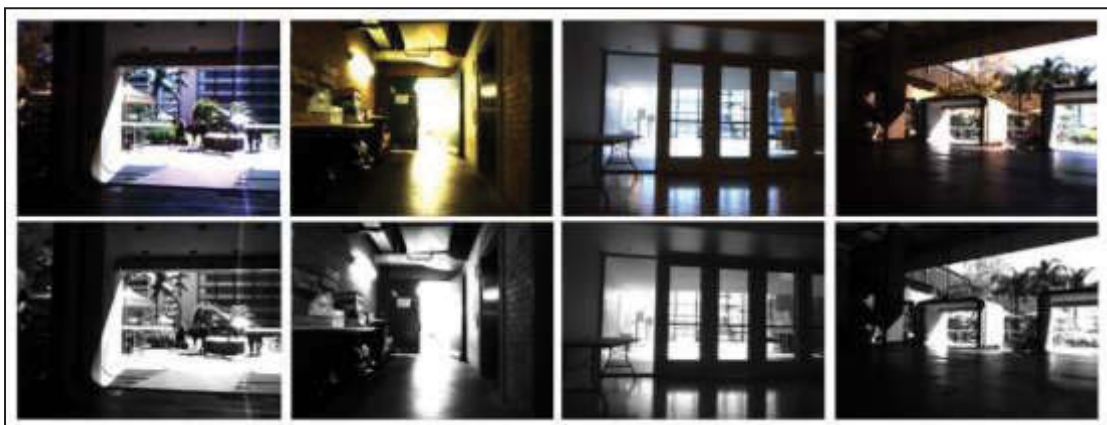
Figure 3-38: Example Test Patterns of Category 2: Extreme Illumination Contrast Areas
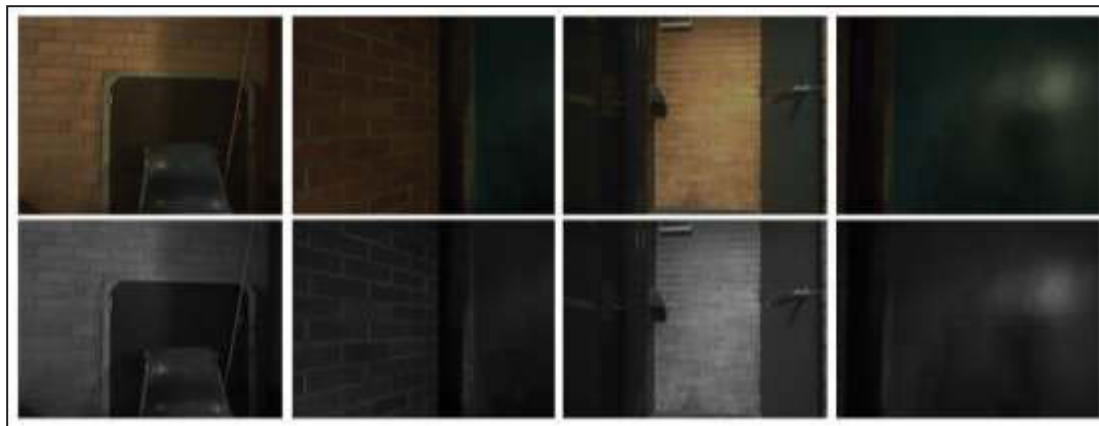
Figure 3-39: Example Test Patterns of Category 3: Consistent Dark Areas

Figure 3-40: Example Test Patterns of Category 4: Consistent Bright Areas

Figure 3-37 to Figure 3-40 display examples of the test set image samples used to analyse the performance of the neural network. The test set consists of 400 images, being made up of 100 test images for each category, and these have been acquired from various locations and environments as can be seen in the above figures. The optimised trained neural networks will be given each of the 400 test images and will classify each, and the best performing network will become the solution for real-time classification of environmental categories.

3.4.3 Correction of Wheel Measurement Parameters for Memory Mapping Rectification

It is common practice to use wheel shaft encoders to estimate a mobile robot‟s position due to its simplicity in computation and implementation. This reason combined with navigation in unknown environments, meaning no known landmarks, is why wheel shaft encoders have been implemented into this wheelchair design. However, problems arise when using these to estimate changes in the wheelchair‟s position and update the map accordingly. There are inaccuracies when errors in these estimates accumulate and unfortunately they have no bounds which can lead to very large inaccuracies over time and distance travelled. These errors result from imperfections in both the software design and the electrical and mechanical implementations (systematic errors), and operating conditions such as wheel slippage (non-systematic errors) (Borenstein & Feng 1996). The main sources of these systematic and non-systematic errors can be summarised as follows:

- Systematic Errors:
    - Unequal wheel diameters
    - Wheel misalignment
    - Actual wheelbase uncertainty (due to non-point wheel contact with the floor)
    - Limited wheel shaft encoder sampling rate
    - Limited wheel shaft encoder resolution

- Non-systematic Errors:
    - Movement over surfaces which are rough or grooved
    - Movement over unexpected objects on the floor
    - Wheel-slippage due to moving on smooth or slippery floors, and fast acceleration or turning (skidding)

In the case of the TIM wheelchair prototype in this research, most work is done indoors and on even floors with flat surfaces, so the majority of errors are systematic. Borenstein and Feng (1996) introduced the University of Michigan Benchmark (UMBmark) to aid in correcting the uncertainties in the actual wheelbase and unequal driving wheel diameters, being the largest contributors to systematic errors.

A bi-directional square path experiment is conducted to achieve correction, as in Figure 3-41. The vehicle follows a square path in both a clockwise (CW) direction and counter-clockwise (CCW) direction a number of times each. The final estimated position, actually being the same as the starting position, is recorded. Based on the set of final estimated positions and their errors from the starting position, the actual diameters of the left and right driving wheels and wheelbase are corrected. This method can significantly improve the accuracy of the odometry change calculations.
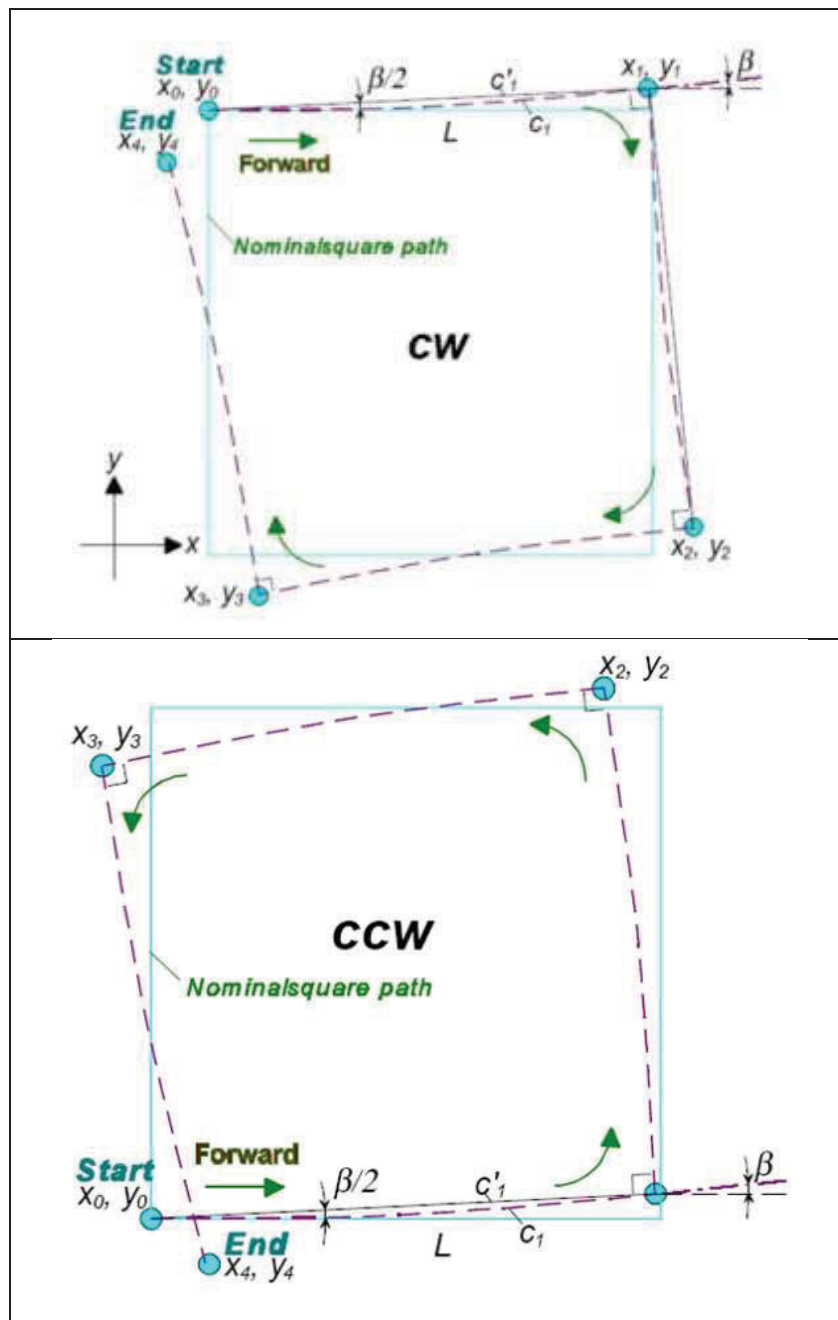
Figure 3-41: Bi-directional Square Path Experiment, UMBmark method (Borenstein & Feng 1996)

Following the experiments, the coordinates of the centre of gravity error from the final positions is defined as:

$$x_{CW/CCW} = \left(\frac{1}{n}\right) \sum \varepsilon x_{i,CW/CCW}$$

(3.43)

$$y_{CW/CCW} = \left(\frac{1}{n}\right) \sum \varepsilon y_{i,CW/CCW}$$

where

n: is the number of experiment runs in each CW/CCW direction,

$\varepsilon x, \varepsilon y$:   are return position errors

This method then estimates the left and right wheels" actual diameters as:

$$D_{alw} = \frac{2D_{avg}}{E_D + 1}$$

(3.44)

$$D_{arw} = \frac{2D_{avg}}{\frac{1}{E_D} + 1}$$

where

$D_{alw/arw}$: are the actual diameters of the left and right wheels respectively,

D_{avg}:   is the average of the left and the right nominated diameters, such that
$D_{avg} = (D_L + D_R)/2$,

D_L, D_R: are the nominated left and right wheel diameters provided by the producer,

E_D: is the error caused by unequal wheel diameters.

This error, E_D, is estimated by the following equation:

$$E_D = \frac{D_{arw}}{D_{alw}} = \frac{R + \frac{b_{nom}}{2}}{R - \frac{b_{nom}}{2}} \qquad (3.45)$$

where

b_{nom}:   is the nominated wheelbase of the wheelchair provided by the wheelchair''s producer

R: is the radius of path curvature

The radius of path curvature, R, is calculated as follows:

$$R = \frac{\frac{L}{2}}{sin\left(\frac{\beta}{2}\right)} \qquad (3.46)$$

where

L: is the length of one straight leg of the square

β: is the incremental orientation error gained from the curved motion along each straight leg

The incremental orientation error, β, is calculated as:

$$\beta = \frac{x_{CCW} - x_{CW}}{4L} \qquad (3.47)$$

The actual wheelbase, b_{actual}, is estimated by the following equation:

$$b_{actual} = b_{nom}\left(\frac{90}{90 - \alpha}\right) \qquad (3.48)$$

where

$$\alpha = \frac{-(x_{CCW} + x_{CW})}{4L} \qquad (3.49)$$

There are two main steps for this correction process in the design of the wheelchair in this research:

- Step 1: Data Acquisition

  The wheelchair is controlled to follow a square in both CW and CCW directions several times. The error in absolute position for each run is used to calculate the centre of gravity, as in Equation 3.43.

- Step 2: Correction of Wheel Measurements

  The actual wheelbase, actual left wheel diameter, and actual right wheel diameter are estimated by Equations 3.44– 3.49.

This correction procedure is important as the wheel calibration inaccuracies will create large errors in mapping, increasing over time, if not rectified. This is evident when maps are created over a length of time, producing visible distortions as a result of the wheelchair algorithms incorrectly calculating rotations of the wheels and associated travelled distances.

3.5 Experimental Results

3.5.1 Depth Mapping Calculation Accuracies

The stereoscopic cameras were first configured in a lab environment with minor lighting contrasts, later to be placed into environmental lighting „Category 1‟. The configurations were manually set to suit the environment and reduce noise artifacts in the disparity readings. The aim here was to determine the accuracy performance of the depth calculation process. This process, described in §3.4.1, was optimised through 1) stereo parameter adjustments for the conversion from stereoscopic images to disparity image and then to a 3D depth map, and 2) determining pixel cluster densities in the 3D map before producing the 2D bird‟s eye view environmental map. Once these optimisations were employed the cameras effectively mapped the placement of objects in the local environment.

The actual distance to different types of objects were measured and varied to compare against the depth calculation results from the stereoscopic mapping process. The cameras were repositioned so that the distance between the centre of the camera system and the selected

objects ranged from 0.5m to 5m with 0.5m increments. In this lab environment the available objects for testing were a wall, a door, a garbage bin, a fire hydrant, another wheelchair, a cleaner who was in the lab at the time, and a trolley. These formed a sufficient set of varying object types, sizes, and surface textures. The results of calculated depths and associated uncertainties, over 10 seconds of stationary mapping and recording, are compared against the actual distances in Table 3-9.

Actual (m)	Wall	Door	Garbage Bin	Fire Hydrant	Wheelchair	Cleaner	Trolley
0.5	0.50±0.02	0.50±0.02	0.50±0.02	0.50±0.02	0.50±0.01	0.50±0.02	0.50±0.02
1	1.00±0.02	1.00±0.02	1.00±0.02	1.02±0.02	1.00±0.02	1.00±0.02	1.00±0.02
1.5	1.50±0.02	1.50±0.02	1.50±0.03	1.52±0.03	1.50±0.03	1.50±0.03	1.50±0.03
2	2.00±0.03	2.00±0.03	2.00±0.03	2.01±0.03	2.00±0.03	2.00±0.03	2.00±0.03
2.5	2.49±0.01	2.49±0.04	2.49±0.03	2.52±0.02	2.50±0.02	2.49±0.02	2.50±0.03
3	2.98±0.03	2.98±0.04	3.02±0.02	3.05±0.01	3.01±0.02	3.00±0.02	3.01±0.03
3.5	3.48±0.03	3.48±0.02	3.52±0.03	3.53±0.03	3.48±0.02	3.51±0.01	3.52±0.04
4	3.98±0.03	4.02±0.03	3.99±0.03	4.02±0.03	3.97±0.03	4.01±0.03	4.02±0.04
4.5	4.47±0.03	4.48±0.04	4.48±0.03	4.59±0.05	4.48±0.03	4.52±0.04	4.51±0.03
5	4.99±0.04	4.99±0.05	4.98±0.02	5.00±0.06	5.00±0.04	5.01±0.03	4.99±0.05

Table 3-9: Stereoscopic Camera Depth Mapping – Object Calculated vs Actual Distances (m)

These results found the depth mapping of all object types were sufficiently accurate for the needs of the project. They showed that the accuracy decreases and uncertainty ranges increase the further away the objects are from the stereoscopic camera system, however, the errors are low regardless. The highest errors seen were with the fire hydrant, due to the shiny and smooth curved surface, producing an error of ±0.06m even at a distance of 5m from the camera system.

3.5.2 Real-time Environment Mapping Results

Real-time vision mapping strategies were discussed in §3.3, and the combination of these strategies allows the wheelchair to construct a 2D bird‟s eye view environmental map in which object points can be plotted onto the map and „remembered‟ once they move out of the range of vision. Observation of the memory depth maps, whilst manually pushing the wheelchair around an office environment, showed correct repositioning of obstacle depth data once they had moved outside the vision range. Tests were conducted and the following set of photos and depth map screen captures resulted, shown in Figure 3-42 to Figure 3-49.
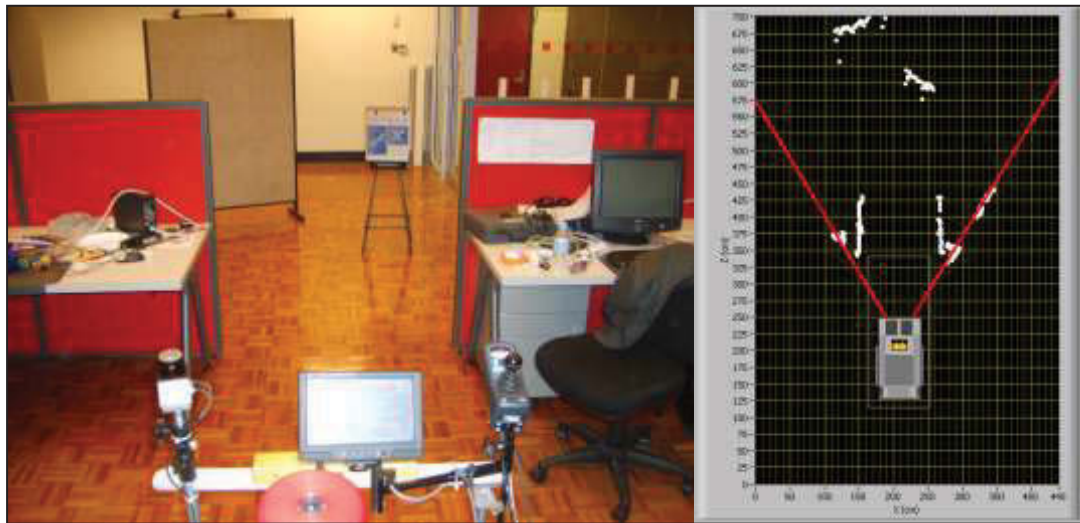
Figure 3-42. Memory Depth Map Construction Test: Position 1
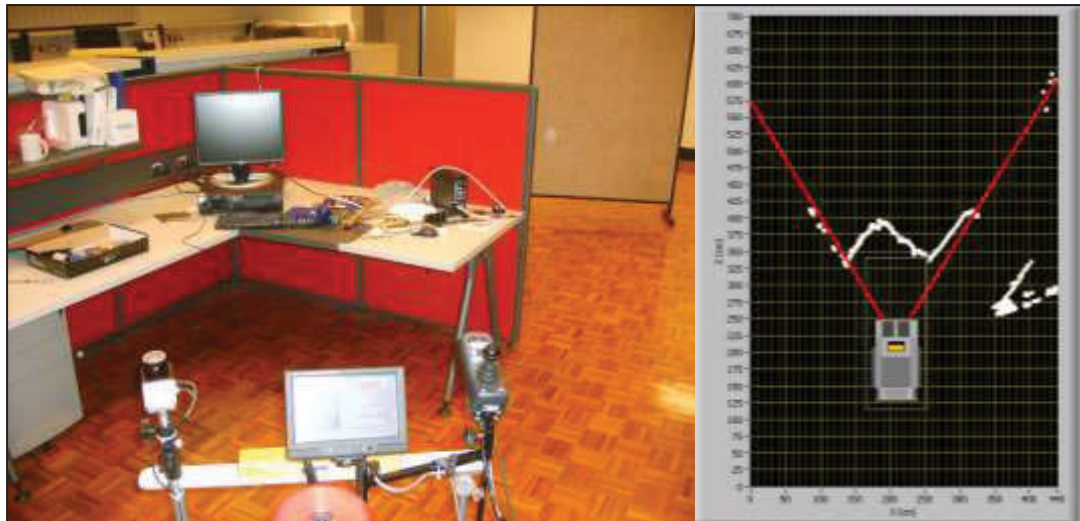
Figure 3-43. Memory Depth Map Construction Test: Position 2

Figure 3-44. Memory Depth Map Construction Test: Position 3
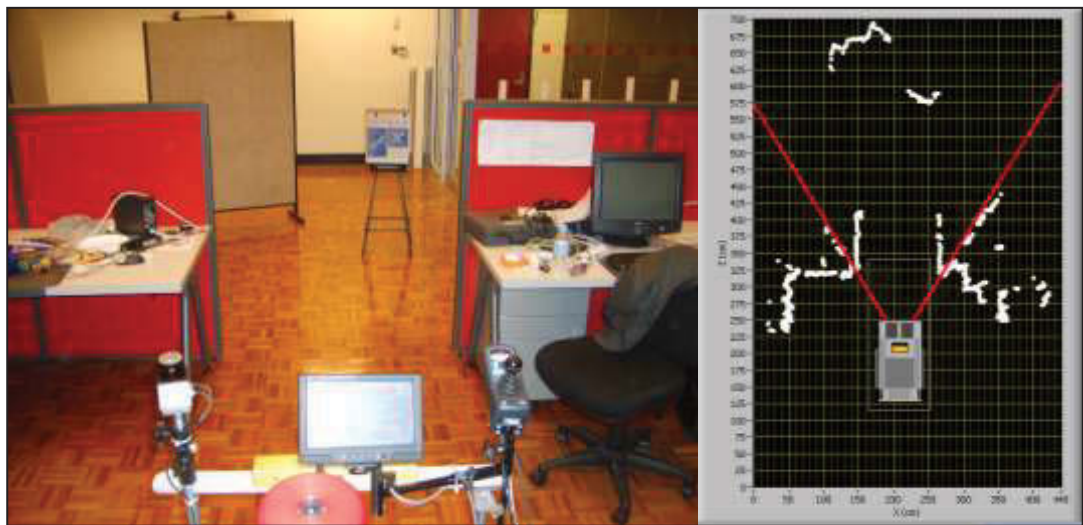
Figure 3-45. Memory Depth Map Construction Test: Position 4
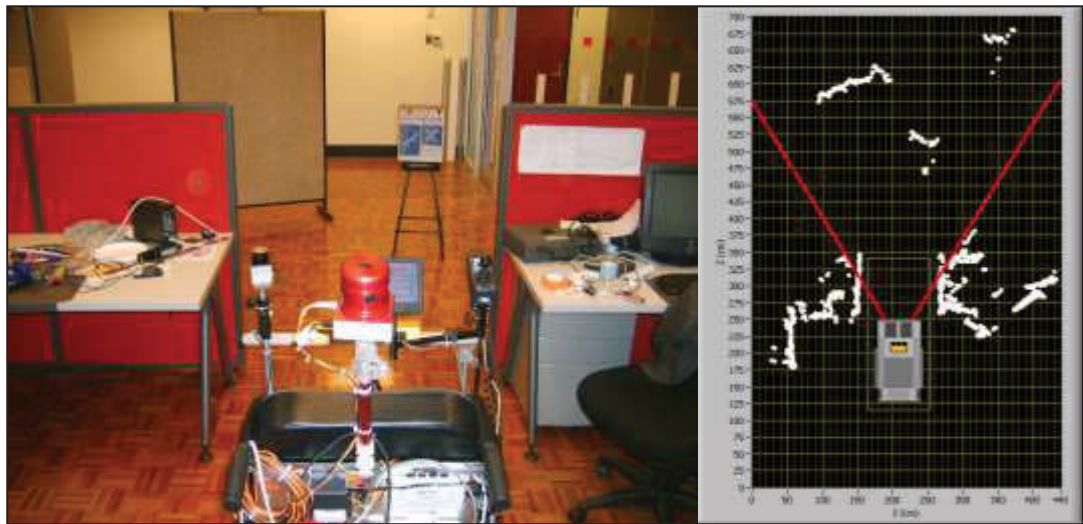
Figure 3-46. Memory Depth Map Construction Test: Position 5
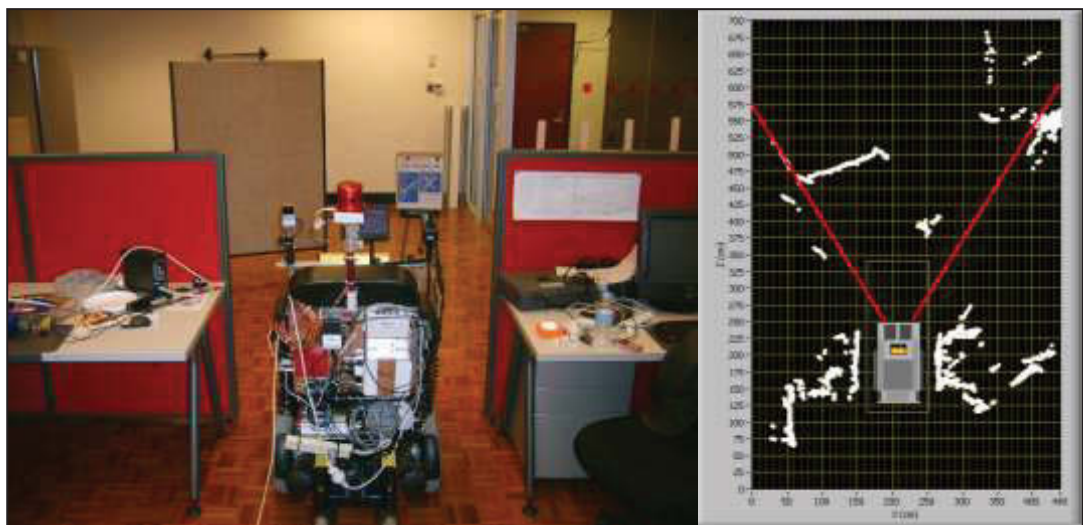
Figure 3-47. Memory Depth Map Construction Test: Position 6
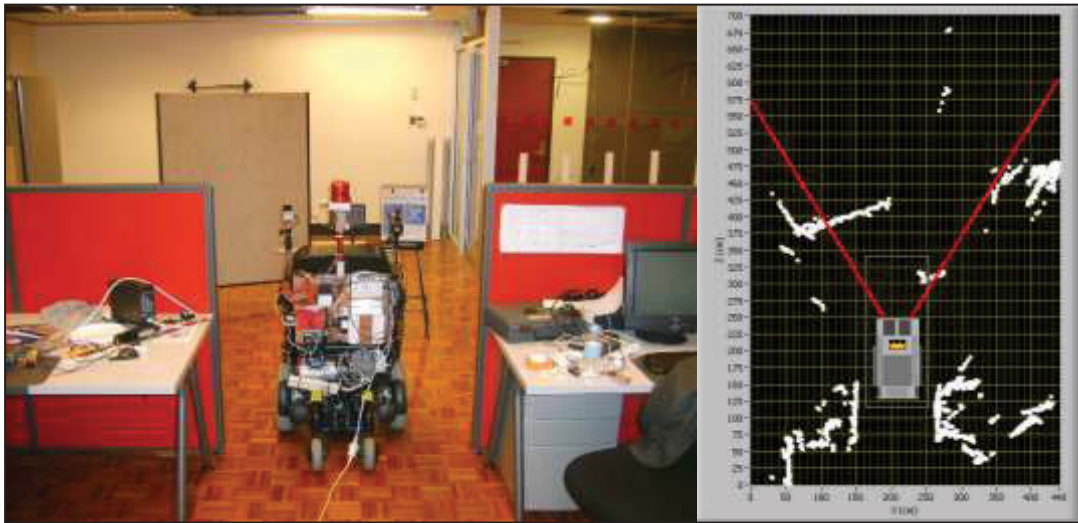
Figure 3-48. Memory Depth Map Construction Test: Position 7
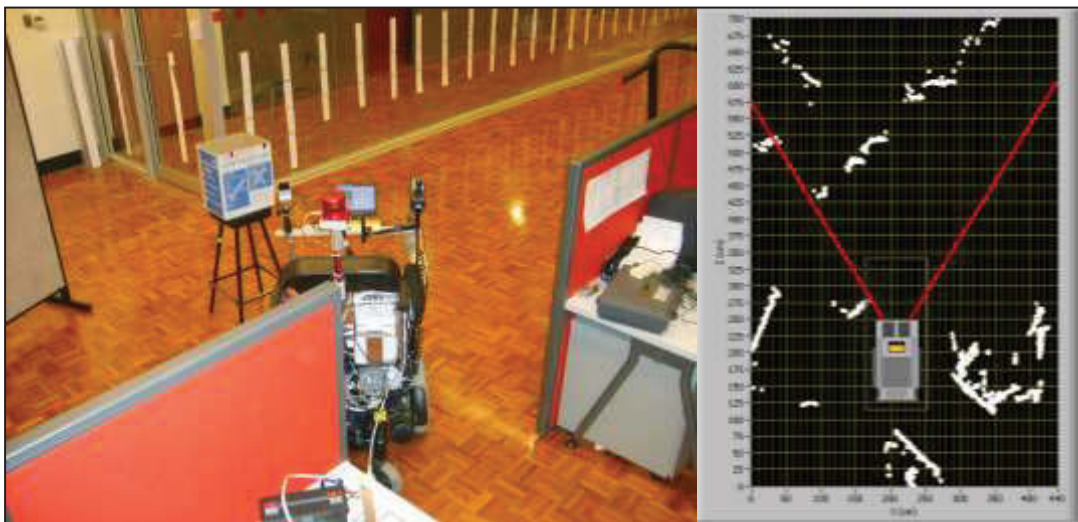
Figure 3-49. Memory Depth Map Construction Test: Position 8

The idea of this test was to observe the repositioning of mapped object points when they moved outside the range of vision of the stereoscopic cameras, and to also make a number of comparisons between measured features and corresponding mapped features. This is to help determine if the memory mapping recalculations of environmental features is performed correctly. It can be seen from the screen shots that an icon of the wheelchair along with the vision limits drawn in red have been placed on the 2D depth map. Mapped object points are displayed on the map in white. The following findings were made from the test:

- Position 1 (Figure 3-42) shows the wheelchair in a small work area with inner edges of the desks to the left and to the right, and a box on a stool and a board further ahead. These are all mapped into the vision range area on the depth map. Note that because

there has been no movement there is no map point population of memory space outside the vision range.

- In Position 2 (Figure 3-43) the wheelchair has been rotated to the left, and the shape of the desk originally to the left can now be seen in the vision range on the 2D depth map. It can also be seen that memory mapping has started, as the part of the desk originally to the right in the field of vision in Position 1 is now outside the vision range, but is still visible on the map. These map points have been recalculated and repositioned on the 2D depth map based on the sensed movements of the wheelchair calculated by the wheel encoders.

- In Position 3 (Figure 3-44) the wheelchair has been rotated to the right, now with the desk originally on the right and the chair in front of it in vision range on the 2D depth map. The desk on the left can still be seen in the memory map section.

- Position 4 (Figure 3-45) shows the wheelchair back in its original starting position, the same as in Figure 3-42, however now it has populated part of its memory map with depth information about the two desks and chair.

- In Position 5 (Figure 3-46) the wheelchair has moved forward so that the front of the wheelchair is in line with the closest edges of the desk. This is also displayed on the 2D memory depth map.

- In Position 6 (Figure 3-47) the wheelchair has been moved further forward so that its centre is in line with the centre of the desks, which are now completely outside the vision range. At this point some measurement tests were carried out, with the results shown in the following table:

Measured Feature	Actual Measurement (cm)	Memory Map Calculation (cm)
Length of desk on the left	84	89
Length of desk on the right	84	81
Width between desks	121	119
Gap between left desk and WC	29	28
Gap between right desk and WC	27	26
Length from front of left desk to front of WC	18	16
Length from front of right desk to front of WC	18	20
Length from back of WC to back of left desk	23	20
Length from back of WC to back of right desk	23	24

Table 3-10. Memory Depth Map Calculations vs Actual Feature Measurements

It can be seen here that all calculations in the memory depth map are very close to the actual measurements, all within an accuracy of ±5cm.

- In Position 7 (Figure 3-48) the wheelchair was moved further forward so the length from the back of the wheelchair to the front of each of the desks was measured as 28cm, being calculated by the memory map as 27cm for the left desk and 25cm for the right desk, which are both very close to the actual values.

- In Position 8 (Figure 3-49) the wheelchair has been rotated about 45º to the right, relative to Position 7. In accordance with this rotation the objects have moved position and rotation on the map, as the memory depth map is relative to the wheelchair's position and orientation. The lines of the desk edges, which were parallel to the sides of the wheelchair in Position 7, are now on a 45º angle slanted to the left on the depth map, corresponding to the 45º rotation to the right that the wheelchair has made between Position 7 and Position 8.

These results have displayed correct recalculations in object mapped point positions into the memory map. Equation 3.8 to Equation 3.22 calculate both wheelchair odometry changes and recalculation of the mentioned point positions, so the observations in this section have confirmed the equations to be true to their purpose.

Despite these desired results, minor skewing of the memory mapping was also observed over larger ranges of movement, and noise artifacts were observed in various environments of testing. These led to the advanced methods for optimising intelligent vision mapping performance, presented in §3.4 and the results of which are provided in the next sections, §3.5.3 and §3.5.4.

3.5.3 Adaptive Stereo Parameter Selection Results

These results above are found when the stereo parameters are configured for the specific environmental lighting conditions. As described in §3.4.2, the settings here, whilst still producing the same accuracies to most objects, were also found to also exhibit noise artifacts in other lighting conditions, such as in the environments featuring extreme brightness contrasts. When the stereo parameter settings were changed to suit the environment and reduce the noise artifacts, the same all-round depth calculation accuracies were achieved as in Table 3-9. This need for changing of parameter settings led to the four different

environmental lighting categories described and the associated adaptive stereo parameter selection technique.

The neural network for environment category classification was trained and validated a number of times for optimisation. The first step was to determine the most suitable number of hidden neurons J^* in the network structure. This was done by setting the learning constant and the momentum constant, and only varying the number of hidden neurons. Based on the result differences from the random initial weights each time the network is trained, the same training configuration (keeping the number of hidden neurons constant) is run 20 times for each, with the resulting maximum, minimum, and average validation classification accuracies across all 4 categories recorded for that hidden neuron number. Following this the number of hidden neurons is incremented and the process is repeated, which is performed on the number being set from 2 to 20, inclusive. The results of this selection process are shown in Table 3-11 and plotted in Figure 3-50.

No. Hidden Neurons	Min Accuracy (%)	Average Accuracy (%)	High Accuracy (%)
2	45.00	46.477	48.00
3	61.25	72.159	75.00
4	76.25	80.682	86.25
5	77.50	81.875	87.50
6	80.75	83.875	86.00
7	81.25	83.875	86.25
8	81.75	85.000	88.50
9	81.00	82.750	85.00
10	77.50	80.625	83.00
11	75.00	78.000	80.00
12	73.75	76.477	80.00
13	72.50	74.545	77.50
14	72.50	74.886	77.25
15	71.25	74.432	77.00
16	71.50	74.432	76.25
17	71.25	74.318	76.50
18	72.50	74.205	76.25
19	68.75	74.432	77.5
20	71.25	73.977	76.25

Table 3-11: Table of Optimal Number of Hidden Neurons Analysis for Training and Validating
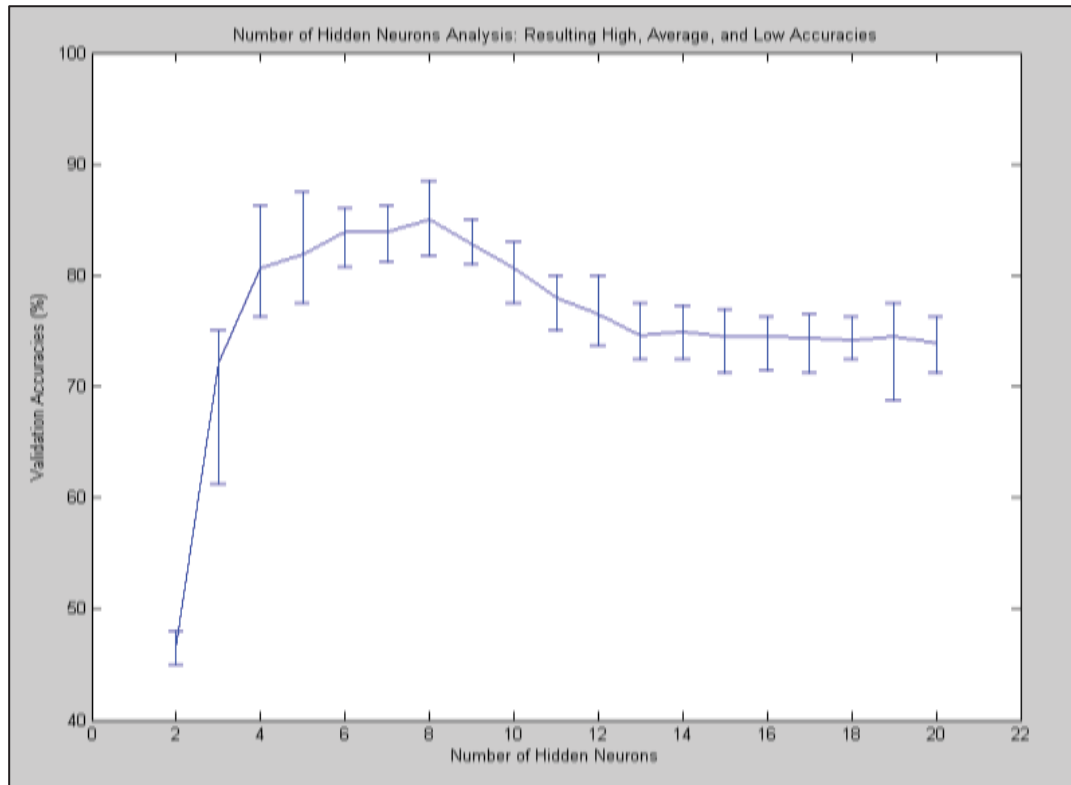
Figure 3-50: Plot of Optimal Number of Hidden Neurons Analysis for Training and Validating

It can be seen from the plot that 8 hidden neurons is the optimal number resulting from the analysis, providing the highest average accuracy, the highest overall accuracy, and a sufficient stability margin. This is now selected as the value, so from here the learning constant and validation constant are both varied, followed by another analysis to further optimise results. The learning constant was varied from 0.001 to 0.5 with increments of 0.001, and the momentum constant was varied from 0.01 to 0.5 with increments of 0.01. All combinations of these were run to determine the best performing regions of combination, with only high accuracy combinations being recorded. Resulting from this, the region of combination that produced the highest consistent accuracies was when the learning constant was set to 0.03 and the momentum constant was set to 0.1. So the final settings for this optimised configuration were:

NN Learning Parameter	Final Value Setting
Number of Hidden Neurons	$J* = 8$
Learning Constant	$\eta = 0.03$
Momentum Constant	$\alpha = 0.1$

Table 3-12: Neural Network Final Optimised Learning Parameter Settings
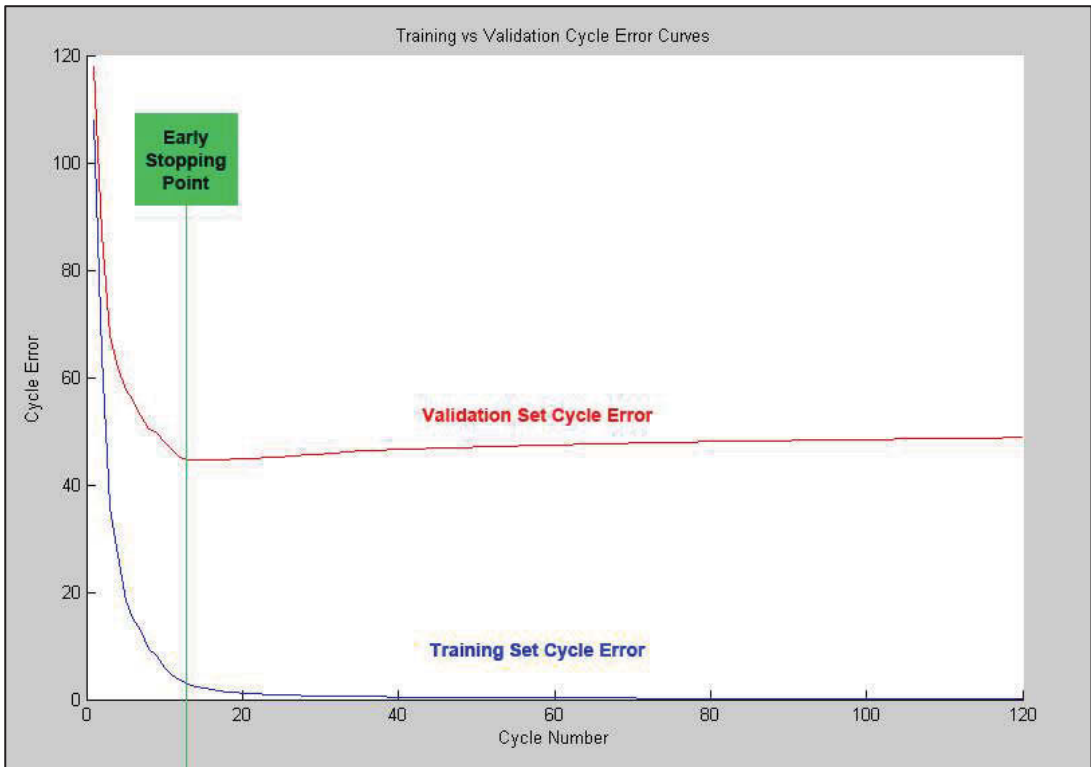
Figure 3-51: Early Stopping Method Employed for Optimisation of Training and Validation

This optimised configuration was run a number of times, with the cycle error curves shown in Figure 3-51, along with the employed early stopping technique at minimum validation cycle error, to prevent over-fitting of the network. The weights found at this point are taken as the optimised weights for this run of training and validation. The optimised weights are then applied to a separate test set of data to view the performance of the neural network results and how adaptable it is to different data which can still be categorised into any of the four available.

Class		Test Results (T)		
		Positive	Negative	
Actual	Positive	TP	FN	TP+FN
Status (S)	Negative	FP	TN	FP+TN
		TP+FP	FN+TN	Total

Table 3-13: Neural Network Results Table

Table 3-13 displays how results of neural network testing are to be tabulated for analysing each class or category. The actual result status (S), in this case being whether or not a pattern actually belongs to the class being tabulated, is compared against the test results (T), showing whether or not the neural network thinks that pattern belongs to the class. The terms used in this table layout are described below:

- True Positive (TP): This is the number of test patterns the neural network correctly classifies as belonging to the class of the table.
- False Positive (FP): This is the number of test patterns the neural network incorrectly classifies as belonging to the class of the table, when in fact they belong to a different class.
- False Negative (FN): This is the number of test patterns the neural network incorrectly classifies as belonging to a different class, when in fact they belong to the class of the table.
- True Negative (TN): This is the number of test patterns the neural network correctly classifies as belonging to a different class than that of the table.

Further analysis is that of finding, for each category class, the sensitivity, specificity, false positive rate, and false negative rate. These are defined as follows:

- Sensitivity: This is the probability that the test says a pattern belongs to a class when in fact it does. So it is a measure of the how likely it is for the neural network to correctly classify a pattern as being in the analysed class. This should ideally be a high value of probability, as

$$P(T^+|S^+) = \frac{TP}{TP + FN} \tag{3.50}$$

- Specificity: This is the probability that the test says a pattern does not belong to a class when in fact it does not. So it is a measure of the how likely it is for the neural network to correctly classify a pattern as not being in the analysed class. This should ideally be a high value of probability, as

$$P(T^-|S^-) = \frac{TN}{TN + FP} \tag{3.51}$$

- False Positive Rate: This is the probability that the test says a pattern belongs to a class when in fact it does not. So it is a measure of the how likely it is for the neural network to incorrectly place a pattern in the class being analysed. This should ideally be a low value of probability, as

$$P(S^-|T^+) = \frac{FP}{FP + TP} \tag{3.52}$$

- False Negative Rate: This is the probability that the test says a pattern does not belong to a class when in fact it does. So it is a measure of the how likely it is for the neural network to incorrectly place a pattern in a different class to that being analysed. This should ideally be a low value of probability, as

$$P(S^+|T^-) = \frac{FN}{FN + TN} \tag{3.53}$$

For the testing phase, 400 image samples were used, in which 100 images belonged to each of the four class categories. The optimised weights were applied to this test set and the output classification of each pattern compared against the actual category the test pattern belonged to. When selecting the classified category, the neural network outputs a percentage of probability for each of the four categories, based on the extent it believes the pattern belongs to each. The category exhibiting the highest of the four percentages is taken as the test classification output for that test pattern. The results of this testing are shown in Table 3-14.

Category 1:		Test Results		
		Positive	Negative	
Actual	Positive	77	23	100
Status	Negative	16	284	300
		93	307	400

Category 2:		Test Results		
		Positive	Negative	
Actual	Positive	94	6	100
Status	Negative	11	289	300
		105	295	400

Category 3:		Test Results		
		Positive	Negative	
Actual	Positive	100	0	100
Status	Negative	7	293	300
		107	293	400

Category 4:		Test Results		
		Positive	Negative	
Actual	Positive	90	10	100
Status	Negative	5	295	300
		95	305	400

Table 3-14: Neural Network Testing Results for Environmental Category Classification

ANALYSIS		Category Number			
		1	2	3	4
Sensitivity (%)	TP/(TP+FN)	77.00	94.00	100.00	90.00
Specificity (%)	TN/(TN+FP)	94.67	96.33	97.67	98.33
False Pos rate (%)	FP/(FP+TP)	17.20	10.48	6.54	5.26
False Neg rate (%)	FN/(FN+TN)	7.49	2.03	0.00	3.28

Table 3-15: Analysis of Testing Results for Environmental Category Classification

Analysis of these results shows that Category 1 (General Illumination Contrast) exhibits the lowest sensitivity, at 77%, and the lowest specificity, at 94.67%, of the four categories. It also has the highest false positive rate and the highest false negative rate, being 17.2% and 7.49% respectively. This means that out of the four categories, images that belong to this category get wrongfully classified more than others, and this is likely due to the uncertain and diverse nature of the category, being the most general of all four. Images belonging to this category can have a large range of variances, and because these images are the least distinctly different images to other categories.

Category 2 (Extreme Illumination Contrast) has a high sensitivity, at 94%, and a high specificity, at 96.33%. It also has reasonably low false positive and false negative rates, being 10.48% and 2.03% respectively. This means that images from environments of extreme contrast are mostly correctly classified, with a small number of other category images wrongfully being classed into this category too.

Category 3 (Consistent Dark) is the best performing category, with a perfect sensitivity, at 100%, and high specificity, at 97.67%. It also has a low false positive rate and a perfect false negative rate, being 6.54% and 0% respectively. This means that all images belonging to this category were correctly identified, since a consistently dark area is easier to determine than any of the other categories.

Category 4 (Consistent Bright) also exhibited high sensitivity, at 90%, and high specificity, at 98.33%. It also has a low false positive and false negative rate, being 5.26% and 3.28% respectively. This means that all images belonging to this category were correctly identified, since a consistently dark area is easier to determine than any of the other categories. This means that images from environments of consistent brightness are mostly correctly classified.

The overall result attained for this optimised neural network was **90.25% classification accuracy** across all four categories. This is a high accuracy result and is useful for determining what type of environmental conditions are being perceived by the cameras, and hence, what type of environment the wheelchair is in at any given time. This classification accuracy, however, was found to be improved upon through placing a minimum certainty level on each pattern classification.

Whenever a test image sample is provided to the neural network it outputs a percentage of how closely the image matches its understanding of each category. The category class that has the highest percentage match for that image sample is the category the neural network classifies that image into. Out of the four possible categories in this classification system, the most commonly encountered is Category 1 (General Illumination Contrast), which is also the configuration setting that performs best across all environments. For this reason Category 1 is made the default classification for when the neural network is uncertain about which category an image sample belongs to. Specifically, if the matched category for a given image is found with less than a 60% certainty, then the image is classified as being in the default Category 1.

With this strategy implemented, the testing results for the neural network are improved to the following results shown in Table 3-16 and Table 3-17.

Category 1:		Test Results		
		Positive	Negative	
Actual	Positive	91	9	100
Status	Negative	16	284	300
		107	293	400

Category 2:		Test Results		
		Positive	Negative	
Actual	Positive	94	6	100
Status	Negative	3	297	300
		97	303	400

Category 3:		Test Results		
		Positive	Negative	
Actual	Positive	100	0	100
Status	Negative	3	297	300
		103	297	400

Category 4:		Test Results		
		Positive	Negative	
Actual	Positive	90	10	100
Status	Negative	2	298	300
		92	308	400

Table 3-16: Improved Neural Network Test Results for Environmental Category Classification

ANALYSIS		Category Number			
		1	2	3	4
Sensitivity (%)	TP/(TP+FN)	91.00	94.00	100.00	90.00
Specificity (%)	TN/(TN+FP)	94.67	99.00	99.00	99.33
False Pos rate (%)	FP/(FP+TP)	14.95	3.09	2.91	2.17
False Neg rate (%)	FN/(FN+TN)	3.07	1.98	0.00	3.25

Table 3-17: Analysis of Improved Test Results for Environmental Category Classification

The overall result attained for this optimised neural network, combined with the employed default category strategy, was increased to **93.75% classification accuracy** across all four categories, meaning a 3.5% improvement on the prior classifications.

The sensitivity of Category 1 was raised significantly, placing it at 91%, up from 77%, the associated false positive rate was decreased from 17.2% to 14.9%, and the false negative rate was also decreased from 7.49% to 3.07%. This shows that previously when images belonging to Category 1 were wrongfully classified as belonging to other classes, most of them had less than 60% certainty values, allowing this default strategy to improve the overall performance of the adaptive system.

Category 2 had a rise in specificity from 96.33% to 99%, a significant decrease in false positive rate from 10.4% to 3.09%, and a slight decrease in false negative rate from 2.03% to 1.98%. Category 3 had a rise in specificity from 97.67% to 99%, and a decrease in false positive rate from 6.54% to 2.91%. Category 4 had a rise in specificity from 98.33% to 99.33%, a decrease in false positive rate from 5.26% to 2.17%, and a slight decrease in false negative rate from 3.28% to 2.25%.

Overall, this default category for uncertainty in classification has improved the performance of the neural network in adapting stereo processing parameter selections to the environmental lighting conditions present at any point in time. This strategy significantly improves the performance and accuracy of environmental mapping by the smart wheelchair system, reducing noise artifacts and correctly identifying both objects and traversable free space in the perceived environment.

The method of real-time operation employed for this technique is that every time the environment map is updated from the stereoscopic cameras image acquisition and the wheelchair odometry change calculations, the design is run to provide a category classification. At the end of each set of 10 updates, which is a time span of around 1.5 seconds, the stereo processing parameters are set to the category with the highest number of classifications in the set. This means that the stereo processing parameters are not unnecessarily changing up to 7 times a second, nor are they changing to match incorrect classifications. Out of the set of 10, an incorrect classification, or even a few, would not affect the majority number, further increasing the performance of this system during real-time wheelchair navigation.

3.5.4 Results for Correction of Wheel Measurement Parameters

The two main steps for the wheelbase correction process were executed in a large open-space indoor area. For the first step involving data acquisition, the wheelchair was controlled to follow an 8x8m square path in both a clockwise (CW) direction and a counter-clockwise (CCW) direction. This was repeated 10 times for each and all data which was recorded. The second step involved the correction of wheel measurements, whereby the effective wheelbase, effective left wheel diameter, and effective right wheel diameter are estimated from the data gathered, improving on the slightly inaccuracies of the nominated wheel measurements from the producer. Following this the data acquisition step was repeated and data collected for comparison against the original trial results.

The nominated wheel measurements from Invacare, the producers of the „TDX A‟, were set as the original wheelbase and drive wheel diameter parameters when programming the wheel shaft encoder conversions to wheelchair odometry changes whenever it performs movements. These nominated wheel parameters were as follows:

$$\text{Nominated Left Wheel Diameter:} \qquad D_L = 0.35m$$

$$\text{Nominated Right Wheel Diameter:} \qquad D_R = 0.35m \qquad\qquad (3.54)$$

$$\text{Nominated Wheelbase:} \qquad b_{nom} = 0.55m$$

Following the first CW and CCW data acquisition trials, the overall finish point error results of the UMBmark experiment, before applying the wheel measurement parameter corrections, are shown in Figure 3-52. The final calculated position of the wheelchair at the end of the 8x8m square path run, which is actually positioned exactly where it started, is recorded relative to the starting position and direction of travel. If the starting position is allocated as the point (0,0) on the xz plane, and the initial direction of travel is along the z-axis in the positive direction, then the calculated final positions are plotted. In Figure 3-52, the red circles represent calculated final positions for the CW directions, with the associated CW centre of gravity displayed as a red square, and the blue crosses represent calculated final positions for the CCW, with the associated CCW centre of gravity displayed as a blue square.
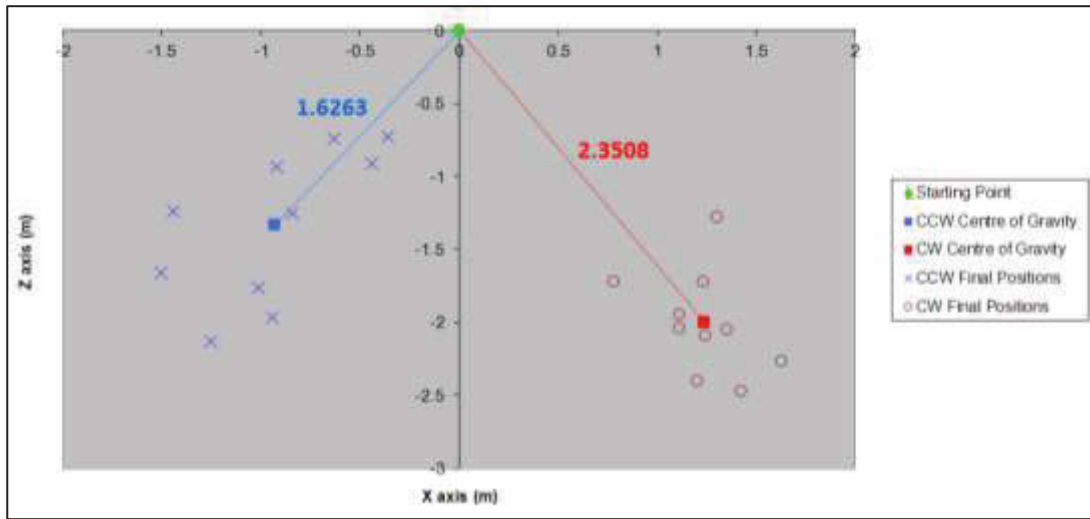
Figure 3-52: UMBmark Experiment Results Prior to Wheel Parameter Correction

The errors in final positions are a result of the inaccurate nominated values for wheelbase and wheel diameters. The centre of gravity error for the CW trials is about 2.35m, which is further away from the starting point than the CCW centre of gravity error, being about 2.63m. In this experiment, non-systematic errors are considerable, however, these results are predominantly caused by systematic errors.

Following these experimental results, the centre of gravity errors for both directions are calculated from Equation 3-37. The CW trial centre of gravity error results are:

$$x_{CW} = \left(\frac{1}{n}\right) \sum \varepsilon x_{i,CW} = 1.237$$

$$z_{CW} = \left(\frac{1}{n}\right) \sum \varepsilon z_{i,CW} = -1.999$$

The CCW trial centre of gravity error results are:

$$x_{CW} = \left(\frac{1}{n}\right) \sum \varepsilon x_{i,CW} = -0.933$$

$$z_{CW} = \left(\frac{1}{n}\right) \sum \varepsilon z_{i,CW} = -1.332$$

For improving the accuracy of the method, the error of the wheelchair's model is defined as follows (Borenstein & Feng 1996):

$$E_{sys} = \max(R_{i,CW}; R_{i,CCW}) \tag{3.55}$$

Where $R_{i,CW}$ and $R_{i,CCW}$ are the centre of gravity error from the starting point for CW and CCW directions respectively, such that

$$R_{i,CW/CCW} = \sqrt{x_{i,CW/CCW}^2 + z_{i,CW/CCW}^2} \tag{3.56}$$

The error of the wheelchair in this situation, before correction, is

$$E_{uncorrected\_sys} = 2.3508 \tag{3.57}$$

Applying Equations 3-38 to 3-43, the correcting procedure is carried out and the values for the actual left and right wheel diameters, as well as the actual wheelbase value, are found to be:

Actual Left Wheel Diameter: $D_{alw} = 0.350219m$

Actual Right Wheel Diameter: $D_{arw} = 0.349667m$ (3.58)

Actual Wheelbase: $b_{actual} = 0.531103m$

To evaluate the accuracy of the corrected wheel measurement parameters, the UMBmark experiment is repeated using the new values for comparison against the original performance. The results of the trials are shown in Figure 3-53, which present final positions and centre of gravity values that are a significant improvement on the original results. These show the final positions are scattered much closer to the starting position.
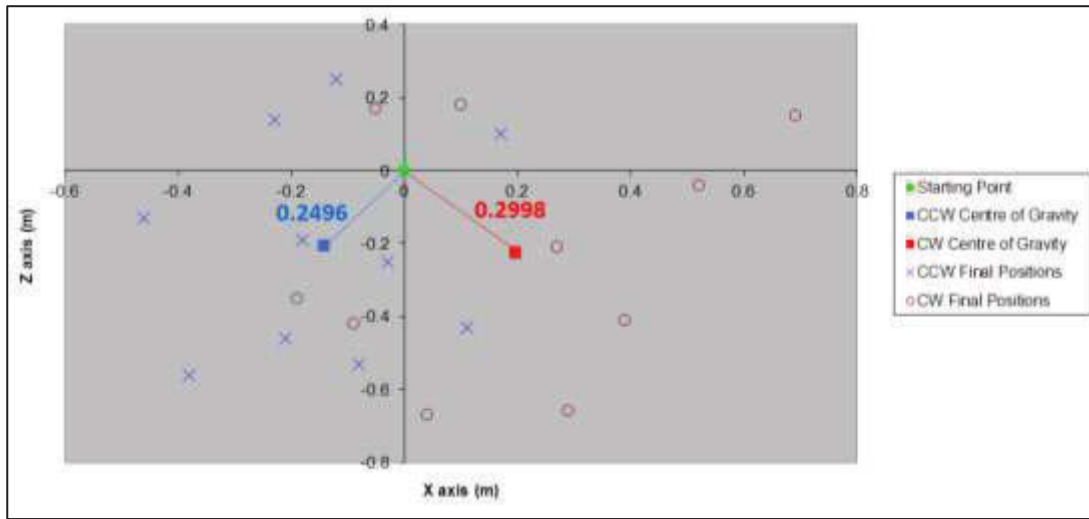
Figure 3-53: UMBmark Experiment Results After Wheel Parameter Correction

The centre of gravity errors are both significantly lower than before the corrections, with the CW error down from 2.3508m to 0.2998m, and the CCW error down from 1.6263m to 0.2496m. As a result the wheelchair error is now

$$E_{corrected\_sys} = 0.2298 \qquad (3.59)$$

This has shown a significant improvement in accuracy of about 10-fold with the corrected wheel measurement parameters resulting from the UMBmark experiment.

$$N = \frac{E_{uncorrected\_sys}}{E_{corrected\_sys}} = \frac{2.3508}{0.2298} \approx 10$$

This improved mapping performance resulting from the UMBmark experiments can be seen in the example shown in Figure 3-54. The mapped path resulting from the original wheel parameters is displayed in Figure 3-54(A) and the mapped path produced after the correction process is displayed in Figure 3-54(B). Object plot points are black while the pink path represents that calculated to be taken by the wheelchair.

(A)   (B)
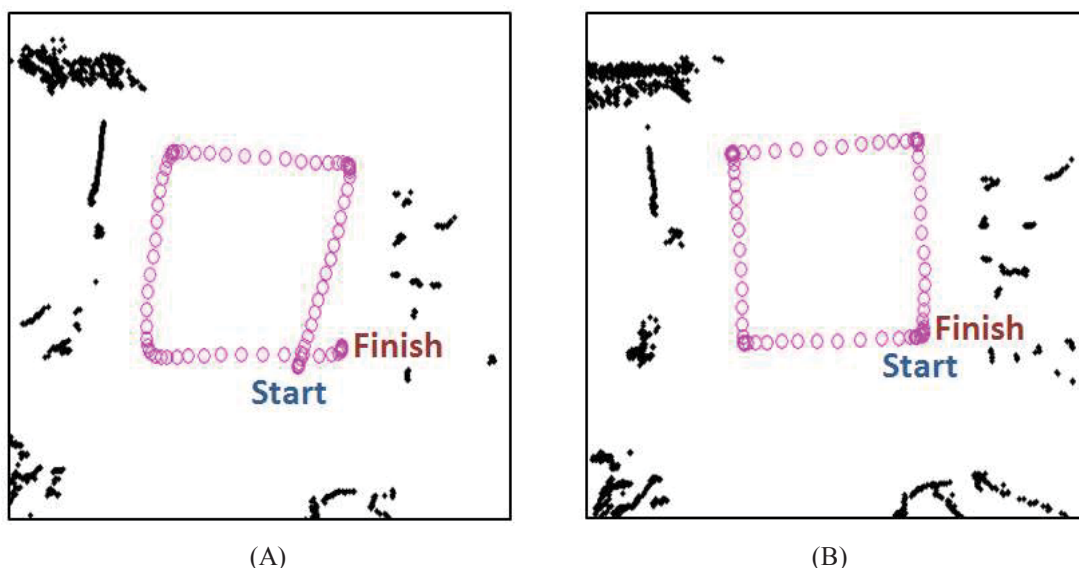
Figure 3-54: UMBmark Run (A) Before and (B) After Wheel Parameter Correction

Figure 3-54 is an example of a counter-clockwise 8x8m square UMBmark run where the start and finish points were in the exact same location. Figure 3-54(A) displays an example of where the wheelbase error causes the created map to incorrectly calculate a larger degree of turning angle than is actually performed, resulting in the calculated finish point being offset from the start point. Figure 3-54(B) displays the same example after the wheel parameters have been corrected, resulting in the calculated finish point being very close to the start point. An example of how this correction can affect mapping performance over larger distances is shown in Figure 3-55. This is an appropriate display of how error can increase over time, since in this case the wheelchair maps a sharp U-shaped area, whilst travelling a total of about 40m through it.

(A)   (B)
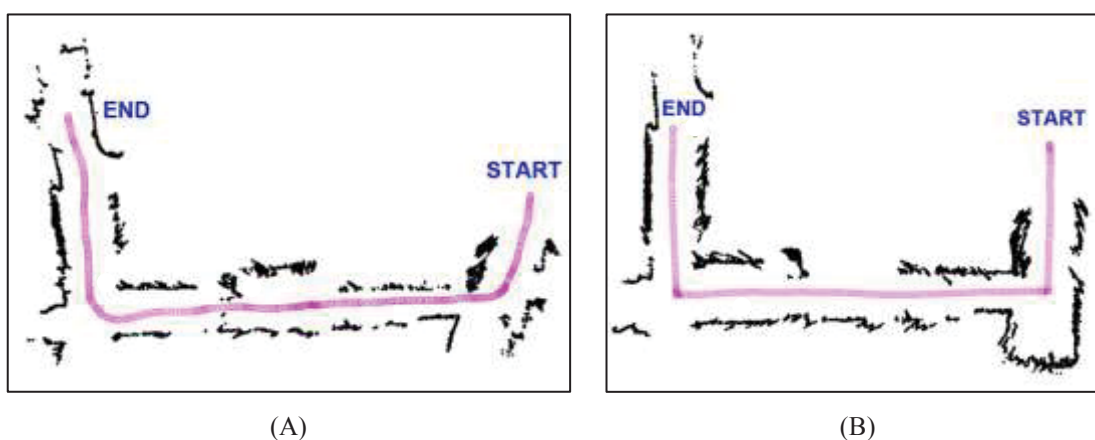
Figure 3-55: Mapping Results (A) Before and (B) After Wheel Parameter Correction

It can be seen from the two figures above that the black points mostly represent walls of the corridor through which the wheelchair was being navigated. The corridors, like many commonly found, have 90˚ turns, so the lines of the walls should generally be perpendicular to each other on the corners of connecting corridor passages. The map produced before the wheel parameter corrections, in Figure 3-55(A), displays moderately skewed angles in the lines of the walls and turns where the walls appear to be at angles greater than 90˚, even greater than 120˚ in some cases. The map produced after the correction process, displayed in Figure 3-55(B), shows a significant improvement in the mapping, where the corridor passages and connecting walls take turns that are well represented, as approximately 90˚. With the wheel parameters corrected, accurate environment maps such as this are made feasible.

3.6 Discussion and Chapter Conclusion

This chapter has introduced a reliable method of constructing real-time 2D bird's eye view environment maps by combining data from stereoscopic cameras and wheel encoders. These maps are updated synchronously with the processing time required to acquire and convert stereoscopic raw images to the 2D map, which is performed at a rate of about 6Hz. This is a sufficient update speed to allow fast decisions to be made confidently during navigation.

The results from the experiments conducted have confirmed that stereoscopic cameras as a primary sensory system are definitely feasible for real-time environment mapping. This has been made accurate and reliable through the strategies implemented in this chapter.

The first important strategy involved converting raw stereo images through to 2D environment maps, in an effort to allow the TIM wheelchair to adequately perceive its local environment and use the information to carry out safe navigational decisions. This mapping process involved:

- Raw image acquisition from the left and right stereoscopic pair of cameras;
- Image pre-processing, consisting of low-pass filtering, rectification to eliminate image distortion, and Laplacian of Gaussian edge detection;
- Stereo processing to produce a disparity image, which was achieved using stereo matching, surface validation, texture validation, uniqueness validation, and back-forth validation techniques;

- Conversion from the disparity image into a 3D point map, which places mapped pixels of environmental features into a 3D plane;
- Removal of the floor and areas above the highest point of the TIM wheelchair, and extraction of object placement in the local environment for mapping onto a 2D bird's eye view environment map, allowing the wheelchair to make intelligent navigational decisions based on the relative placement of these objects.

Performing wheelchair odometry change calculations was the next strategy deployed, which facilitated the ability of the system to „remember‟ objects previously mapped and passed outside the range of stereoscopic vision. This was made possible through the acquisition of wheel encoder data from each of the two drive wheels and the calculations which converted these readings into specific odometry changes of the wheelchair, consisting of change in position coordinates ΔX and ΔZ as well as change in angle of the wheelchair $\Delta\theta$. These parameters are constantly updated during real-time operation, which provide a number of uses in mapping and automated navigational guidance operations.

Once the odometry changes of the wheelchair are determined they can be adapted to recalculate the placement of all mapped object points outside the range of vision, relative to the wheelchair. This is performed frequently to construct a real-time environment map, and to remember the placement of objects that have moved out of the range of vision, in order to further avoid collisions. This is mostly applicable to static objects that are not moving and, hence, their placement will not change as the wheelchair navigates past. It is also useful for the purposes of creating maps of the environment for reporting and presenting purposes, as well as the potential to later create and remember maps of known environments.

Improving the accuracy of these environment maps was also performed through correction of wheel measurement parameters. This assumed reasonably even surfaces of varying types, and does not include uneven surfaces, which are rarely found in indoor environments. Odometry change calculations were initially based upon vendor specifications of the drive wheel diameter, which was used to translate wheel encoder data to determine changes in wheelchair odometry. However, even small errors between the vendor specification and the actual drive wheel diameters can cause distortions to the memory mapping process, skewing maps and representing remembered objects in incorrect locations relative to the wheelchair. To overcome this problem the wheel measurement parameters were corrected with the use of UMBmark experiments, whereby the actual wheelbase and actual left and right wheel

diameters were calculated. This was achieved by running the wheelchair many times along set paths to determine the wheel parameter errors from the resulting maps. Correcting these errors helped optimise the memory mapping process.

It was discovered that the quality of disparity images was heavily dependent on the stereo processing parameters, and these could be set to work well in one type of environment but produce problems, such as artifacts in mapping, when operated in another type of environment. This is an issue that occurs frequently in stereo processing due to the fact there is no „one-size-fits-all" set of parameters that will work equally well in different environments and lighting conditions. In response to this issue, a process for intelligent stereo processing parameter selection was designed, which involves classifying environmental categories in real-time, based on image data available, and adapting the parameters accordingly. The environment types were separated into four categories to account for most encountered environmental situations, being 1) „General Illumination Contrast", 2) „Extreme Illumination Contrast", 3) „Consistent Dark", and 4) „Consistent Bright".

Classification, at any single instant in time, of the environmental category was optimised to 93.75% accuracy across the four categories. However, the system takes the most occurring classification at the end of each set of 10 classifications, increasing the accuracy, very rarely making errors, whilst maintaining a very low impact on operation of an incorrect classification (due to it only lasting about 2 seconds before the next update).

Overall, this chapter has presented an effective implementation of stereoscopic cameras in a smart wheelchair for environmental mapping. Due to the limited range of vision of the stereoscopic cameras, this stage of the TIM smart wheelchair prototype is ideally operated in a static environment. Although it will still avoid dynamic obstacles, such as people moving around, it will not detect them in the case where they move near the wheelchair from a rear or side angle without first being seen ahead of the wheelchair. In this case they cannot be seen and can potentially be knocked by extremities of the wheelchair during rotations. The limited vision of the stereoscopic cameras requires more supplementing sensors to reduce blind spots, which is an issue addressed with the wide 360º vision range of the spherical vision camera system and accompanying vision strategy designs, detailed in the next chapter.

Chapter 4

Utilisation of a Spherical Vision Camera System for Real-time Obstacle Detection over a Wide Vision Range

"No pessimist ever discovered the secret of the stars, or sailed to an uncharted land, or opened a new doorway for the human spirit." - Helen Keller

4.1 Introduction and Aims

Spherical vision, given its inherent large field-of-view, is an attractive addition to the primary sensors in this project for the reasons of providing 1) 360° of obstacle detection at any given time, and 2) real-time video streams to the user, allowing them to view what is happening around the wheelchair. Laser rangefinders, sonar sensors, ultrasonic sensors, and infrared

sensors are the conventional type of sensor used for detecting objects in close proximity surrounding a mobile robot in a dynamic environment. However, since vision can provide a wealth of information, including the direct video stream to the user operating the wheelchair, it has been made a primary sensor choice for the TIM smart wheelchair developments in this project.

This chapter presents the methods developed for extending the capabilities of a spherical vision camera system to allow real-time detection of surrounding dynamic obstacles within any given environment, during autonomous navigation of the smart wheelchair. A Point Grey Research (PGR) Ladybug2 spherical vision camera system was attached to the „TDX A‟ power wheelchair to provide complete 360º surrounding vision. This is so the Ladybug2 spherical vision camera system can provide information about dynamic obstacle placement all around the wheelchair, to help with the automated decision-making process involved when the wheelchair needs to navigate. This assistive technology aids in the range of vision, with instantaneous detection of obstacles surrounding the smart wheelchair, as well as providing the user with a direct visual video stream on their personal graphical user interface.

Having made these further hardware modifications to the TIM smart wheelchair, the aims of the research presented in this chapter are to investigate and understand:

1. The feasibility of spherical vision cameras in this smart wheelchair design.
2. The advantages and disadvantages of using spherical vision in this type of application.
3. An effective approach for instantaneous dynamic obstacle detection around the wheelchair, within predefined „traffic light‟ virtual safety zones, using the acquired spherical camera images. These „traffic light‟ zones are generally defined as follows:
    a. Red – Stop (obstacles too close to move)
    b. Yellow – Caution (obstacles near, move slowly)
    c. Green – Go (no obstacles near, clear to move)
4. How spherical vision can be used to provide a real-time control interface for the user.
5. The real-time performance of the spherical vision for a surrounding obstacle detection system, with performance quantification.

4.2 Instrumentation

Ladybug2 Spherical Vision Camera System

Figure 4-1: PGR Ladybug2 Spherical Vision Camera System
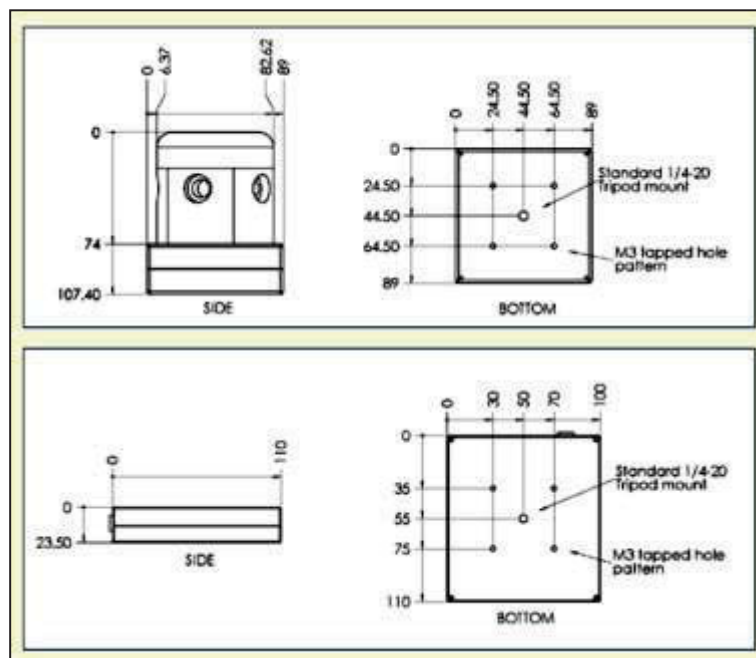
Figure 4-2: Ladybug2 Dimensional Drawings (Point Grey Research Inc. 2005).

The PGR Ladybug2 (figure 4-1) is an omni-directional camera system for acquisition of high
quality hemispherical video. There are six cameras in this system: five are in a horizontal ring
configuration and the sixth points vertically upwards. The cameras are packed tightly together

such that the distance between adjacent cameras is less than 20mm, enabling the system to collect video from more than approximately 80% of the full sphere and almost the same apparent point of view (Point Grey Research Inc. 2005).

The Ladybug2 is composed of a head unit and a storage unit (Figure 4-2). The storage unit is connected to the camera head via a high-speed fiber-optic connection, and can record up to 20 minutes of full frame, raw, uncompressed video. Any standard PC with an IEEE-1394 (Firewire) capability can be used to acquire from, or send controls to, this camera system. Alternatively, expansion cards (such PCMCIA or ExpressCard) with Firewire expansion can be utilised. The main specifications of the Ladybug2 spherical vision camera system are as follows:

Feature	Specification	
Overview	360º spherical IEEE-1394b digital video camera system	
Imaging Sensor	6 Sony ICX204AK 1/3" 1024x768 progressive scan CCDs	
A/D Converter	6 Analog Devices AD9849 12-bit analog-to-digital converters	
Data Output	Head Unit	30FPS raw, uncompressed 8bpp (Y8) Bayer-tiled data
Interfaces	Head Unit	1.2Gbps optical link for data transfer to Compressor
	Compressor	1.2Gbps optical link for data transfer from Head
		800Mbps IEEE-1394b link for data transfer to PC
Voltage Requirements	8-32V	
Power Consumption	Head Unit	Less than 6.5W
	Compressor	Less than 4.7W
Gain	Automatic/Manual Gain modes 0 to 26dB	
Shutter	Automatic/Manual Shutter modes 0.06ms to 34ms at 30FPS	
Dimensions	Head Unit	90mm x 90mm x 110mm
	Compressor	39mm x 43mm x 10mm
Mass	Head Unit	920g
	Compressor	270g
Camera Specification	IIDC 1394-based Digital Camera Specification v1.31	
Emissions Compliance	FCC and CE Class A device	
Operating Temperature	Commercial grade electronics rated from 0° to 45°C	
Storage Temperature	-30° to 60°C	

Table 4-1: PGR Ladybug2 Spherical Vision System Main Specifications

Overall Stage 2 Prototype Hardware Design
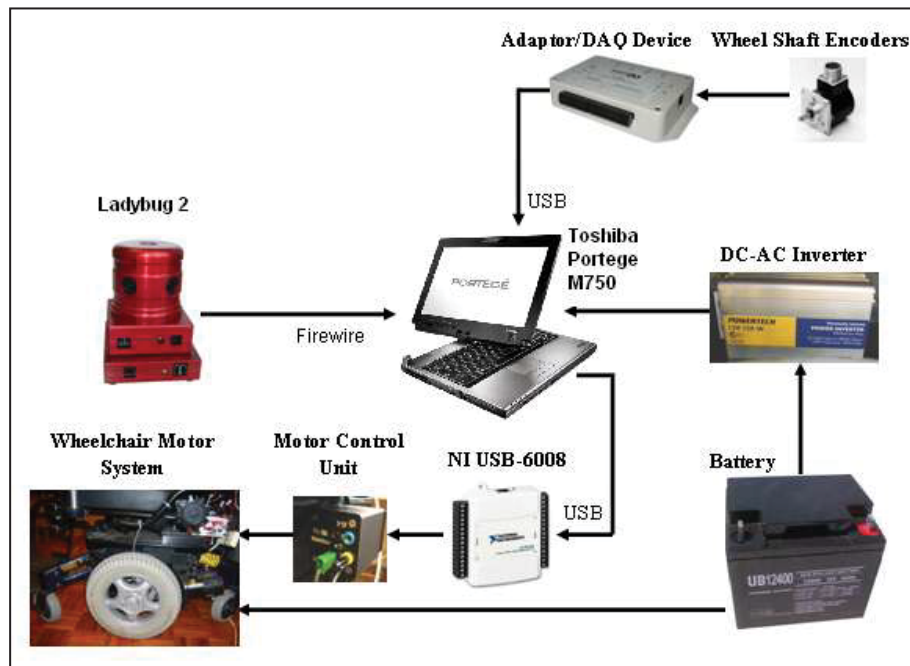
Figure 4-3: Overall Stage 2 Prototype Hardware Design Using Spherical Vision Cameras

Figure 4-4: TIM Stage 2 Prototype: Integrated Wheelchair Hardware with Spherical Vision Cameras

The Stage 2 prototype design (Figure 4-3) features the addition and integration of the
Ladybug2 spherical vision camera system, which was installed on a metal support shaft above

the back of the wheelchair. The Bumblebee XB3 stereoscopic camera system was disconnected for this phase of the TIM smart wheelchair design. A Toshiba Portege M750 tablet PC was introduced for the computer processing and graphical user interface display. Wheel shaft encoders are again used to track odometry changes in the wheelchair, and the Ladybug2 spherical vision camera system is connected via a Firewire IEEE-1394b connection to the Toshiba tablet PC, which had a custom metal frame built to house it. Figure 4-4 shows a photo of how this hardware system looked when integrated.

4.3 Spherical Vision Image Processing Strategies

The methods discussed in this section involve image processing techniques, applying methods used for monoscopic vision to spherical vision, as the concepts are essentially the same. These methods involve parallax variance analysis between sequential image frames taken before and after each movement of the spherical vision camera system (due to movements in the wheelchair it is attached to). This allows perceived environmental changes as the wheelchair moves to be used in determining how close dynamic obstacles may be positioned relative to the wheelchair.

Digital image analysis is a key factor in solving any given computer imaging problem. In such an application as this smart wheelchair design, acquisition of a sample image database taken from the spherical camera system in varying environments, and examination of these images, is the first step towards developing an obstacle detection imaging solution. Image analysis involves manipulating the image data to determine required information, and is typically part of a larger process, which raises a number of application-specific questions to be answered (Umbaugh 2011):

- How much spatial and brightness resolution is required?
- Will existing methods solve the problem?
- Is colour information needed?
- Does any of the image data need to be transformed into the frequency domain?
- Do the images need to be segmented to find object information?
- What are the important features in the images?
- Is the hardware fast enough for the application?

To answer these questions and determine the most appropriate approach to obstacle detection around the wheelchair using the spherical camera system, a range of image analysis possibilities were examined. Images contain very large amounts of data, and often much of the data is not essential in solving a specific imaging problem, so a primary challenge here was to determine exactly what information was necessary to adequately detect obstacles. To begin with, images are acquired from the spherical vision camera system (Figure 4-5) and the most relevant forms of display views are observed. These display views are the individual camera views from each of the surrounding cameras (Figure 4-6), and the 360º stitched panoramic view (Figure 4-7).
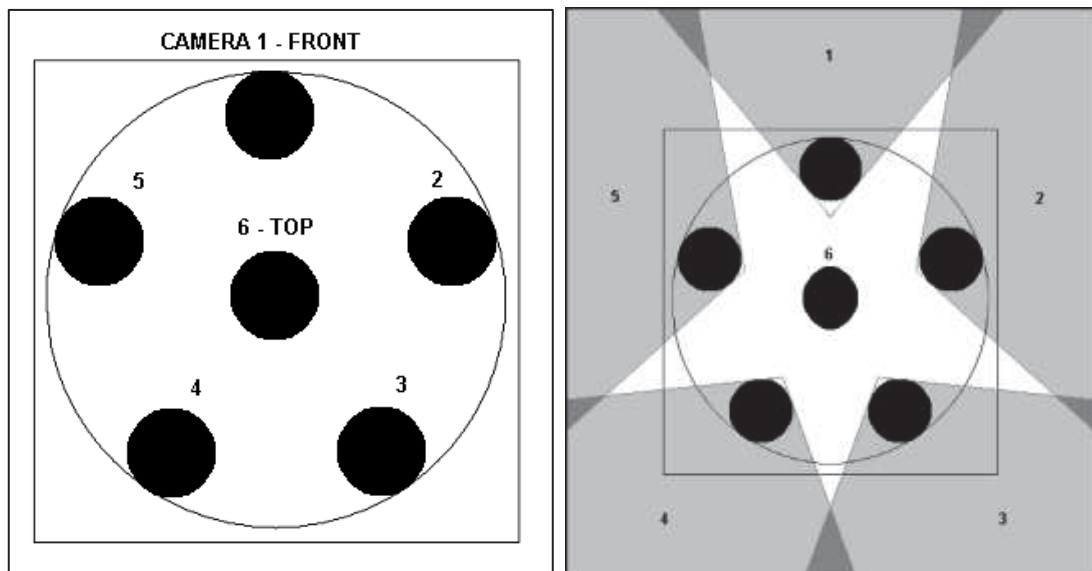
Figure 4-5: Spherical Vision Camera Configuration (Left) and Fields of View (Right) from Above
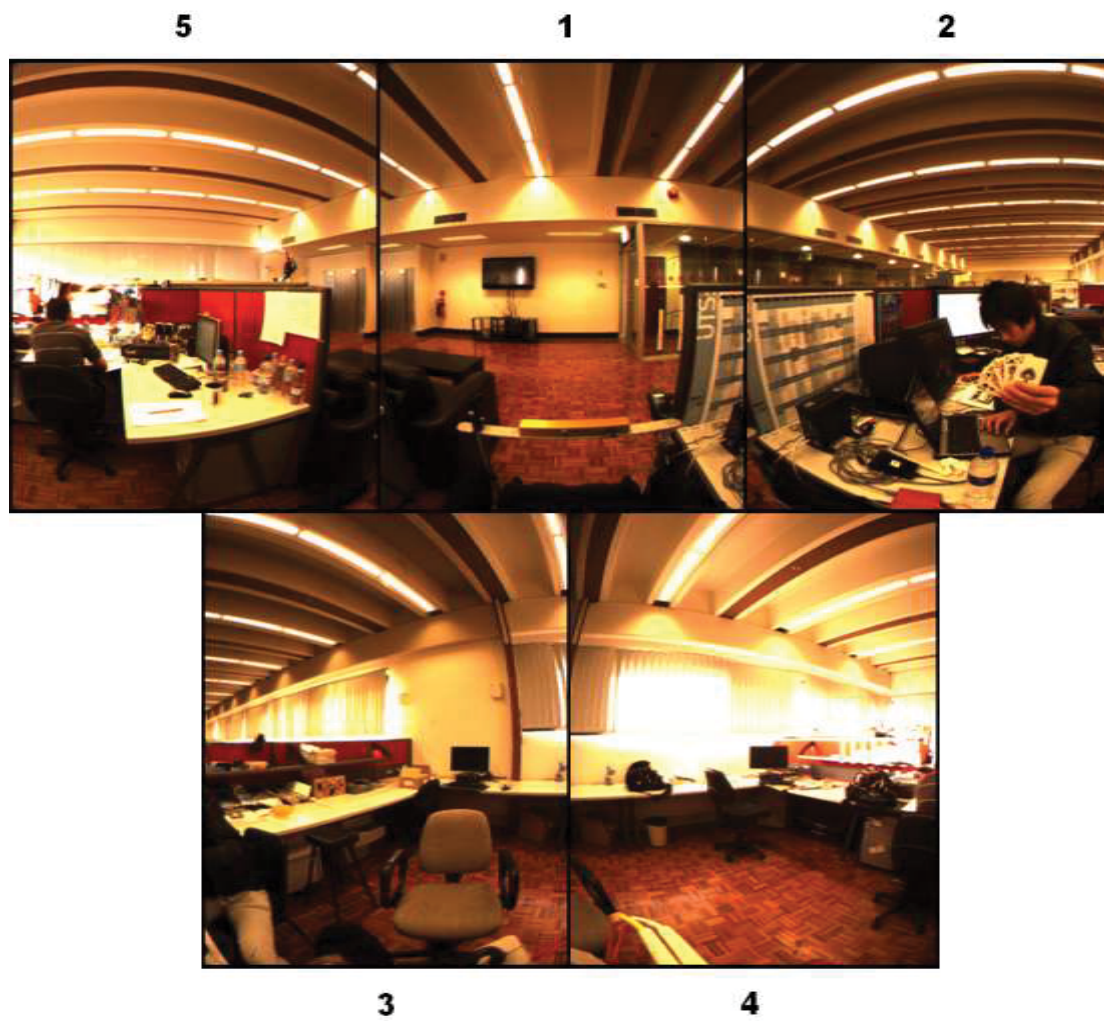
Figure 4-6: Individual Surrounding Camera Views of the Spherical Vision System

Figure 4-7: Spherical Vision – 360º Stitched Panoramic View

These two image representations suit different types of image processing, so both were considered in an effort to determine the most appropriate approach for detecting the obstacles that breach the virtual safety zones, at any one time, around the wheelchair. To answer the question about existing methods solving the problem, parallax variances between sequential image frames was an approach investigated due to its use in monocular SLAM (Simultaneous Localisation and Mapping) applications in static environments (Civera et al. 2008). Although this method is adapted for the purposes required here in this project, the ideas of determining parallax variance completely spawn from such monocular camera image processing strategies.

4.3.1 Distortions in Spherical Vision

Spherical vision inherently exhibits image distortions, especially when dealing with stitched panoramic images, as it bends and distorts 360º of space into a single image. However, due to the fact that it is an effective method of viewing a large vision range in a single streaming feed, it is very useful for a user to become familiar with perceiving the whole environment panorama as the wheelchair moves. The horizontal axis of the panoramic view correlates to a linear spread of angles across the 360º of vision. This range of vision angles are allocated to match the birds-eye view x-z map of Figure 3-24 (§3.3.1). As such, the positive half of the x-axis correlates to positive angles and the negative half correlates to negative angles. Relative to the spherical camera system, which is mounted on the wheelchair, the 0º angle begins directly to the right side of the system, 90º is directly in front, 180º / -180º is directly to the left, and -90º is directly behind . This angle allocation is displayed in Figure 4-8 with respect to the spherical vision cameras from above, and Figure 4-9 displays the angle breakdown in a panoramic image constructed from the spherical camera system.
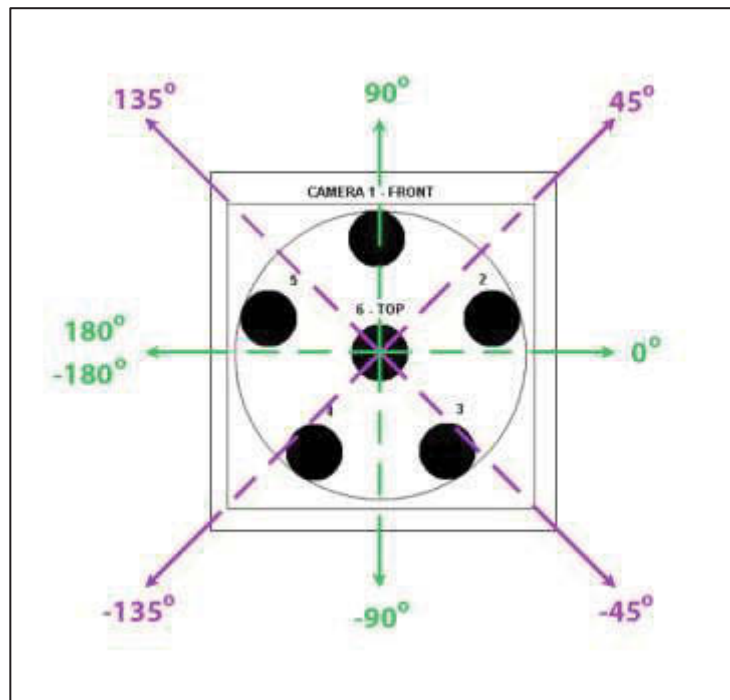
Figure 4-8: Angle Allocation for Spherical Vision Relative to Camera System from Above
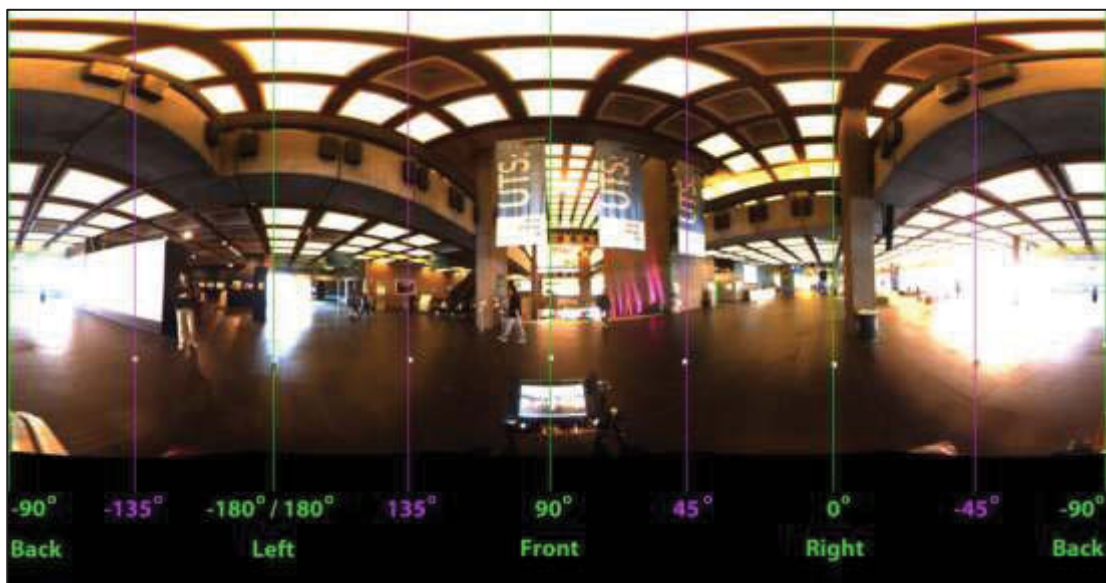
Figure 4-9: Angle Breakdown for Spherical Vision Panoramic Image

As can be seen in Figure 4-9, the stretching of the full 360º space into a single panoramic image feed, with a linear spread of angles, provides an effective method of viewing the wide vision range all at the same time. This is especially the case once accustomed to the apparent distortions, which mostly appear closer to the vertical extremities of the image feed. The panoramic images are created using a spherical coordinate system. The image axes u and v

map to the two spherical angles γ and φ, respectively, which are computed as follows given the *x, y, z* of a point (refer to Figure 3-15 in §3.1.1) in the camera head coordinate frame:

$$D^2 = X^2 + Y^2 + Z^2$$

$$\gamma = atan^2(Z, X) \tag{4.1}$$

$$\varphi = acos\left(\frac{Z}{D}\right)$$

Despite the fact that the pixels become increasingly stretched out towards the poles of the sphere (top and bottom of the image, this simple spherical angle projection maps well to a 2D image display (Point Grey Research 2005). As such, designs for intelligent vision using the panoramic view will be required to take into account these inherent distortions.

4.3.2 Parallax Variances in Sequential Imaging

Similar to the principle of operation for depth mapping involved in stereoscopic cameras (discussed in §3.3.1), it is possible for the spherical vision cameras to also be used to estimate depth of objects in the surrounding environment. However, this is a difficult task as slightly offset views of a scene, such as those produced from stereoscopic cameras, can only be achieved from the spherical camera system by moving its position between screen grabs, calculating the change in odometry, and then comparing the slightly offset images taken before the move and after the move.

Parallax is an effect whereby the apparent position of an object being viewed appears to differ when viewed from two different lines of sight. Objects displaying a high parallax between the two different acquired images reflect a closer position to the camera and objects displaying low parallax reflect a position further away from the camera. Stereoscopic vision requires two cameras to acquire the offset images simultaneously, whereas a monocular camera can only achieve a parallax effect by taking an image, moving a known distance, and taking another image to produce offset perspectives of a target scene. This principle is here investigated, along with the odometry change calculations, to estimate the depth of objects surrounding the wheelchair in its local environment.

When looking at parallax variances between frames of stitched panoramas, information about the environment all around the wheelchair can be obtained. The idea was to develop this particular approach with the panoramic view of the spherical cameras. Images from a single camera were, however, reviewed first to easily view parallax variances between frames taken before and after the camera was moved (Figure 4-10).
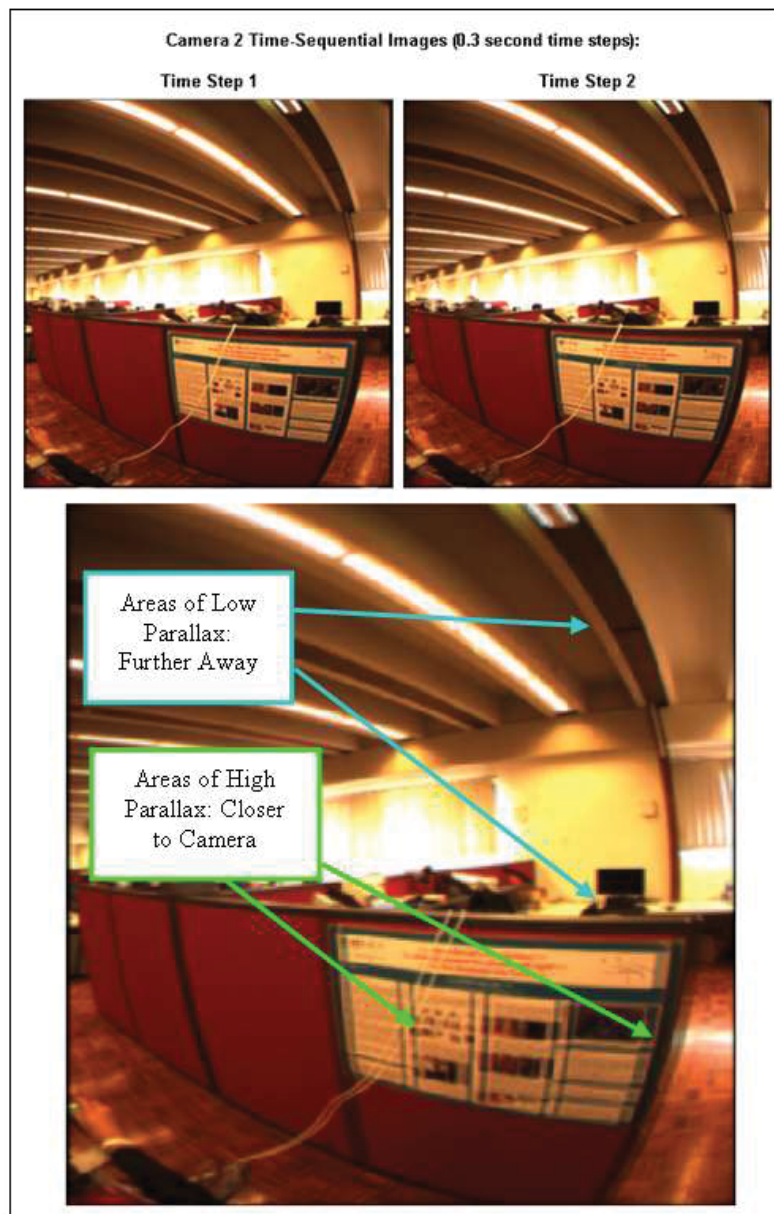
Figure 4-10: Sequential Imaging from Spherical Camera #2 and Combination View

It can be seen in Figure 4-10, that whilst the wheelchair was moving, a photo (Time Step 1) was taken from Camera 2, then another taken 0.3 seconds later (Time Step 2). Combining the two images has shown closer objects in the scene exhibit higher parallax than those further

away, showing this method can be useful in estimating depth of objects in the surrounding environment. Following this, sequential images were then acquired when the wheelchair was moving forward, analysed in panoramic view (Figure 4-11), and combined for parallax variance analysis (Figure 4-12).

Figure 4-11: Sequential Time-step Scene Panorama When Moving Forward

Figure 4-12: Combined Scene Panoramas Displaying Parallax Variances

Parallax variances are evident through the whole combination scene. When moving straight ahead, static objects exhibiting high parallax between scene captures are closer to the wheelchair than objects exhibiting low parallax between scene captures. The amount of this is determined by how far the wheelchair has moved between each capture, which is determined by the wheelchair odometry change calculations presented in §3.3.2. However, another problem occurs when the wheelchair is turning, in which even distant objects will appear to exhibit high parallax between scene captures, as displayed in Figure 4-13 and Figure 4-14.

Figure 4-13: Sequential Time-step Scene Panorama When Turning Right

Figure 4-14: Combined Scene Panoramas Displaying Parallax Variances

The apparent high parallax of all objects between scene captures when the wheelchair is turning can be corrected using the calculated angle of rotation of the wheelchair from the wheel encoders, again referring to §3.3.2. The second scene capture can then be accordingly phase-shifted back so that two scene captures are in phase, which will then mean that only objects close to the wheelchair will continue to exhibit high parallax between scene captures (Figure 4-15).

Figure 4-15: Phase-corrected Combined Scene Panoramas Displaying Parallax Variances

The change in angle calculated is used to phase correct sequential images in comparison, allowing for parallax variances to be determined. Position change can then be used to determine baseline changes of the camera system between image captures, allowing for increased reliability in estimating object depths in the scene by correlating parallax variance with depth regions.

This raises the following steps for analysing the image and detecting obstacles surrounding the wheelchair:

- Using panoramic view, images are taken and each image is compared to its predecessor
- Calculate odometry changes in the camera for each movement, using the wheel encoders and odometry change calculations of the wheelchair as presented in §3.3.2.
- Correction of the prior image follows this, based on angle change of the wheelchair, and hence cameras, by shifting it into phase with the latter image
- Use changes in odometry of the wheelchair to calculate distance change of the camera system between image captures
- Determine parallax variance for objects between frames in the environment when different movements are made to the wheelchair

- Using a Sum of Absolute Differences (SAD) algorithm, similar to creating a disparity image, convert sequential images to a parallax map and use calculated focal lengths to assist in estimating correlations between parallax variance and depth regions.

This method will likely provide a few problems in obstacle detection, since the amount of parallax variance will change based on the movements of the wheelchair, so it will all be a relative measure. Furthermore, if the wheelchair is stationary and an obstacle is very close to the wheelchair, and also stationary, then there will be no parallax variance present, which will be problematic for the objectives of reliable obstacle detection.

4.4 Advanced Methods for Real-time Dynamic Obstacle Detection

Following analysis on the parallax variance method for obstacle detection, a new method was developed and investigated as a more appropriately tailored approach for this imaging problem and application. This method involves instantaneous obstacle detection utilising neural networks in dynamic environments, in an effort to allow obstacles to be detected regardless of whether the wheelchair is stationary or in motion.

4.4.1 Obstacle Detection using Neural Networks

The method of instantaneous obstacle detection using neural networks was developed in this research for the purpose of moving further beyond the shortfalls of parallax variance when dealing with dynamic environments, along with providing an instantaneous form of obstacle detection in the „traffic light" virtual safety zones (Figure 4-16). This method makes use of artificial neural networks to classify images into one of the three virtual safety zone categories.

The objective of this method is to observe the spherical view segments and classify each into the „Red", „Yellow", or „Green" zones based on the presence of any obstacles being detected. If there is, for example, a person standing very close to the wheelchair within the „Red" zone of segment 1, then that segment will be classified as „Red", meaning that the wheelchair cannot rotate in either direction whilst it is still allocated that classification, otherwise a collision with the person would result. If that person was standing in the „Yellow" zone of segment 1, then that segment would be classified as „Yellow", meaning that the wheelchair

can turn in that direction but to take caution because the person is still fairly close to the wheelchair. If the person was standing outside of the „Yellow" zone or was not even visible at all in segment 1, then that segment would be classified as „Green", meaning it is clear to move in that direction.

Instantaneous obstacle detection utilising neural networks has the purpose of classifying virtual safety zone breaches by obstacles. The idea behind the virtual safety zones is to restrict the wheelchair moving (especially turning) into objects, providing a collision avoidance system that takes into account all angles around the wheelchair. The virtual safety zones and segmentation of the spherical vision range are displayed, from a bird's eye view representation, in Figure 4-16:
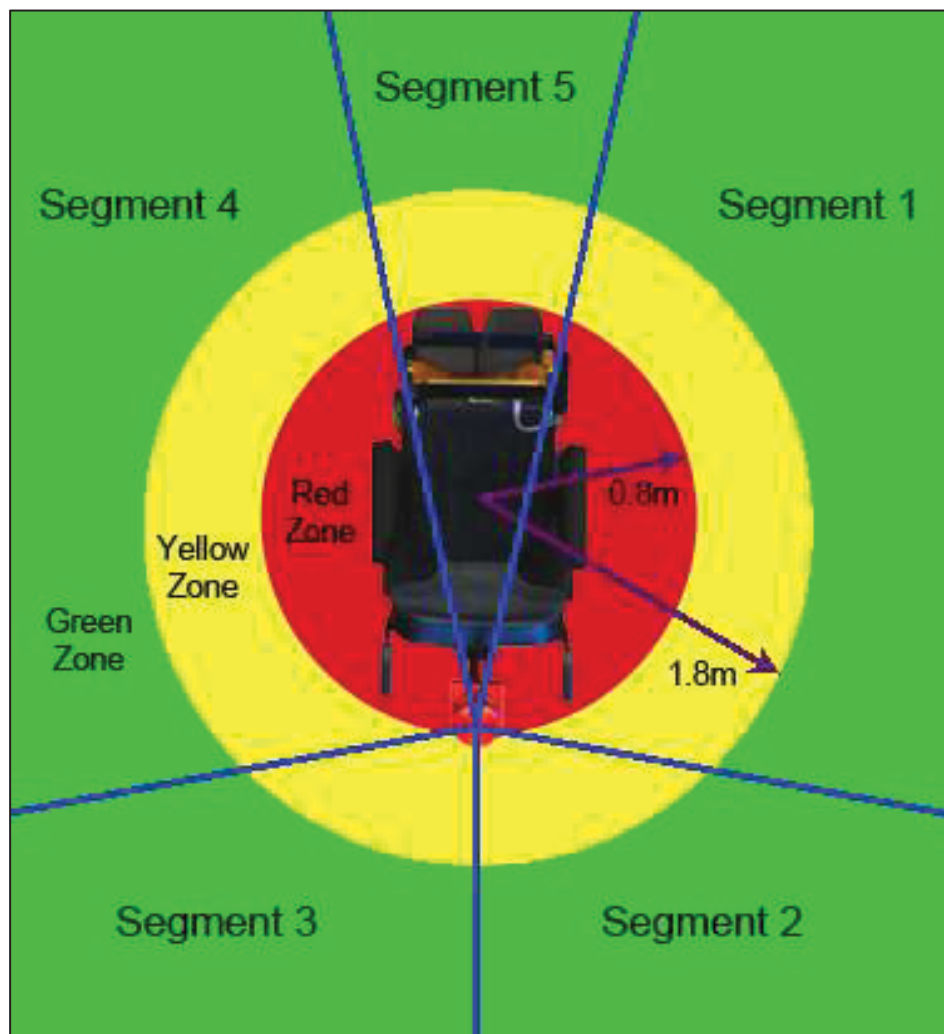
Figure 4-16: Wheelchair „Traffic Light" Zones and Vision Range Segmentation for Obstacle Detection

As displayed in Figure 4-16, the carefully-planned segmentation of the 360º spherical panoramic vision has been done in a manner that separates the right and the left sides of the wheelchair symmetrically. Segments 1 and 4, consisting of 85º of vision each, are of primary concern in this method, as these are the segments that contain the main „Red Zone" areas which must be able to detect obstacle breaches. These segments also contain the „Yellow Zone" and the „Green Zone", and as such, are the most important segments for classification into the three zone categories. Segments 2 and 3, consisting of 70º of vision each, are behind the wheelchair and any object in these zones cannot be collided with as a result of wheelchair rotation, and hence they only contain two zone categories, Yellow and Green. Segment 5, consisting of 50º of vision, is not included in zone classification strategies, as it is directly ahead of the wheelchair and also contains visual obstructions at all times from the user"s head and wheelchair components.

This method of segmentation takes into account the general movements of the wheelchair and where dynamic obstacles, people in particular, are likely to position themselves relative to the wheelchair when moving near or past the system. An example photo was taken to further display the safety zones and segmentation concepts in a real-world setting, displayed in Figure 4-17, with an associated spherical vision panorama image displayed in Figure 4-18. Here the „Red Zone" can be seen as representing the turning radius of the wheelchair, within which a collision would occur with a breaching obstacle if the wheelchair were to rotate. The „Yellow Zone" can be seen to be an area of caution, being close to the wheelchair but not yet being a threat for collision, and all areas outside this is the „Green Zone". Segments 1 to 5, here labelled as S1 to S5, are also displayed for relevance to this method. In this photo a person is standing next to the wheelchair in Segment 4 and is breaching the „Red Zone", and as such the wheelchair must be able to instantaneously determine this fact and not allow rotation, otherwise a collision would result.

Figure 4-17: „Traffic Light" Zones and Vision Range Segmentation Photo Display

Figure 4-18: Associated Spherical Vision Panoramic Segmentation Photo Display

The segmentation process has been determined in a way that also reduces computation and complexity of this obstacle detection method. The symmetrical nature of the method allows for grouping of segments for classification, as instantaneous images of Segment 1 can be horizontally flipped to look the same as Segment 4, and, likewise, Segment 2 can be horizontally flipped to have the same orientation as Segment 3. This means that one neural network classification system will be created for the Segment 1 and Segment 4 group (S1/S4),

containing three zone categories being the Red, Yellow, and Green zones, and another neural
network classification system will be created for the Segment 2 and Segment 3 group (S2/S3),
containing two zone categories being the Yellow and Green zones.

Furthermore, any part of the panoramic image above the highest point of the wheelchair is not
required, since there is no chance for collision. To reduce processing costs associated with the
image processing, these parts of the image that are not required are removed from the
classification process. Taking all these points into account results in the panoramic image
shown, in Figure 4-18, being split and prepared for processing into the individual S1/S4
images shown in Figure 4-19, and individual S2/S3 images shown in Figure 4-20.
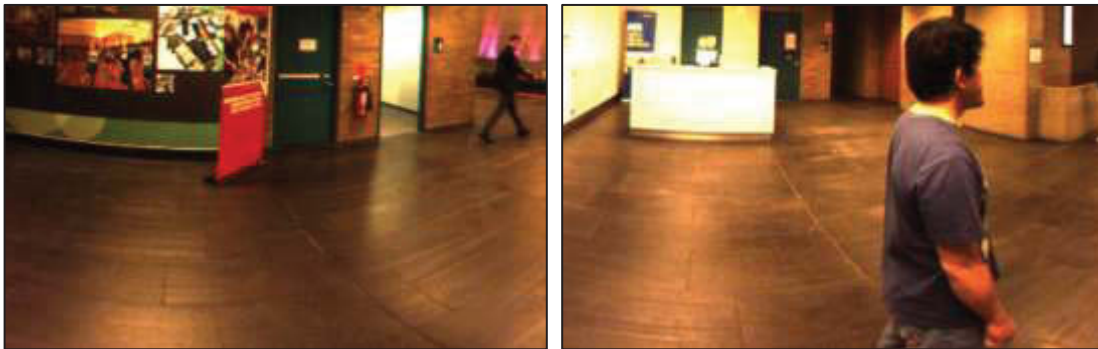
Figure 4-19: S1/S4 Panoramic Image Segments Prepared for Processing and Classification
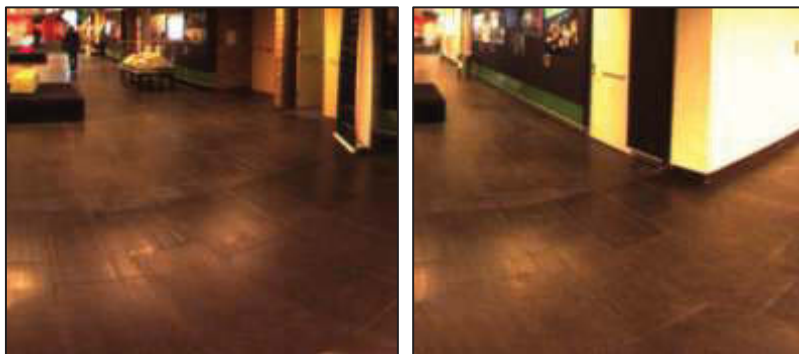
Figure 4-20: S2/S3 Panoramic Image Segments Prepared for Processing and Classification

These images then undergo basic pre-processing to prepare them for neural network input,
specifically, 8-bit grey-scaling and resolution adjustment. The S1/S4 resolutions are adjusted
to 134x85 pixel images, and the S2/S3 resolutions are adjusted to 96x85 pixel images.
Segment 4 for S1/S4 and Segment 3 for S2/S3 of these photos will be used to display
examples of these, with 8-bit grey-scaling shown in Figure 4-21, and resolution adjustment
shown in Figure 4-22.

Figure 4-21: 8-bit Grey-scaling Step Example (Left - S1/S4, Right - S2/S3)

Figure 4-22: Resolution Adjustment Step Example (Left - S1/S4, Right - S2/S3)

Similar to §3.4.1, the image data is then normalised through the process of dividing each element by 128, which places all values to between 0 and 2, and then subtracting 1 from these values, resulting in all data element values normalised to floating point numbers between -1 and 1. Each of the images are represented as a 1D array in the following manner:

- Denoting the number of pixel rows (r) in the image as n and the number of pixel columns (c) as m, the top left pixel is (r_0,c_0) and the bottom right pixel is (r_{n-1},c_{m-1}). The S1/S4 images are reduced to a resolution of 134x85 pixels, giving m=134 and n=85, and the S2/S3 images are reduced to a resolution of 96x85 pixels, giving m=96 and n=85.

- Beginning with the top left pixel of the image (r_0,c_0), scanning right to the top right pixel (r_0,c_{m-1}), then moving down one row and again scanning from the left (r_1,c_0) to (r_1,c_{m-1}), and so on until the input array for the Neural Network is filled as a single column. This produces a 1D array of 11390 normalised pixel values for S1/S4, and 8160 normalised pixel values for S2/S3. So,

$$x = \begin{bmatrix} (r_0, c_0) \\ (r_1, c_1) \\ \vdots \\ (r_0, c_{m-1}) \\ (r_1, c_0) \\ \vdots \\ (r_{n-1}, c_0) \\ \vdots \\ (r_{n-1}, c_{m-1}) \end{bmatrix} \qquad (4.2)$$

For these neural networks, 930 patterns (images) for S1/S4 and 600 patterns (images) for S2/S3 were used for each of the training, validation, and testing phases. The number of output classes (output neurons) for S1/S4 are $K = 3$, representing „Traffic Light" zone categories Red, Yellow, and Green, and the number of output classes for S2/S3 are $K = 2$, representing zone categories Yellow and Green.

Figure 4-23: Example S1/S4 Category „Red Zone" Images
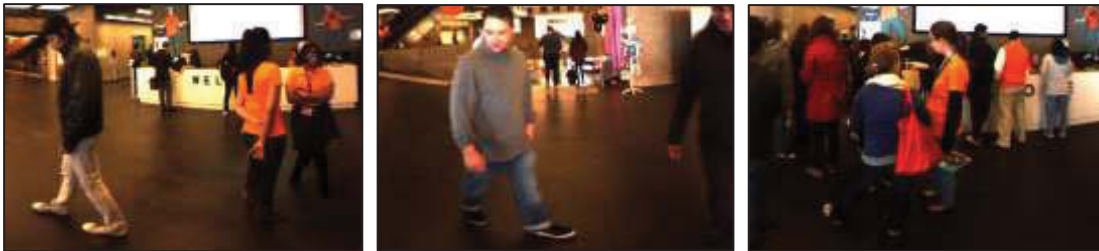
Figure 4-24: Example S1/S4 Category „Yellow Zone" Images

Figure 4-25: Example S1/S4 Category „Green Zone" Images

Some examples of the S1/S4 images used in the neural network learning process are displayed in Figure 4-23 (Red Zone), Figure 4-24 (Yellow Zone), and Figure 4-25 (Green Zone), and some examples of the S2/S3 images are displayed in Figure 4-26 (Yellow Zone) and Figure 4-27 (Green Zone):

Figure 4-26: Example S2/S3 Category „Yellow Zone" Images

Figure 4-27: Example S2/S3 Category „Green Zone" Images

These neural networks were trained, validated, tested, and optimised using the method discussed in this section. The performance of the classification system produced was assessed and following this an improved method expanding on the techniques in this section was investigated. This proposed system involved introducing a combination of image processing techniques for pre-processing the spherical images, and then conducting neural network classification on the modified images. Pre-processing with image analysis techniques can aid in the process by enhancing appropriate image features relevant in obstacle detection applications and this idea was used to improve the performance of the classification systems.

4.4.2 Improved Obstacle Detection Method

A number of image processing methods were employed for pre-processing the database of images, prior to neural network training as described in the previous section. These methods were designed to help find object edges, separating objects from environment, and overlay onto the original image segment, assisting the neural network to determine similarities and differences between images. Although these image processing techniques are conducted on

the individual segments of the spherical image separately, the process is shown here using the entire panoramic image display. The process starts with the panoramic image (Figure 4-28), and separated into segments using region of interest masks, which has been omitted here in the process display.

Figure 4-28: Advanced Obstacle Detection Processing: Panoramic Scene

The idea here is to remove the details in the image that are not important, such as texture on surfaces like the floor and walls, and to attempt to do so whilst preserving the object edges in the image. This can be a difficult task but the following processes were able to achieve this objective. The brightness, contrast, and gamma settings are first adjusted (Figure 4-29), mainly to produce less contrast in the image and increase the brightness. This is an initial step in helping to gently „wash out" some of the detail in the image without degrading the object edges.

Figure 4-29: Advanced Obstacle Detection Processing: Brightness and Contrast Adjustment

Gaussian blur is then applied to the image with a 3x3 filter mask to softly blur the image space and further smooth out some of the detail, again without damaging the object edges in the image. The image space Gaussian filter for 2D images is an NxN-tap convolution filter (uses a square-shaped footprint of NxN pixels) that weights all the pixels inside its footprint, based on the Gaussian function (Umbaugh 2011):

$$G(x, y) = \frac{1}{2\pi\sigma^2} e^{-\frac{x^2+y^2}{2\sigma^2}} \tag{4.3}$$

The Gaussian function (Figure 4-30) provides values for weighting the pixels inside the filter footprint, resulting in a blur effect. The associated special representation, sometimes referred to as the "bell surface", demonstrates how much pixels can be affected by the filter, especially with larger filter mask sizes.
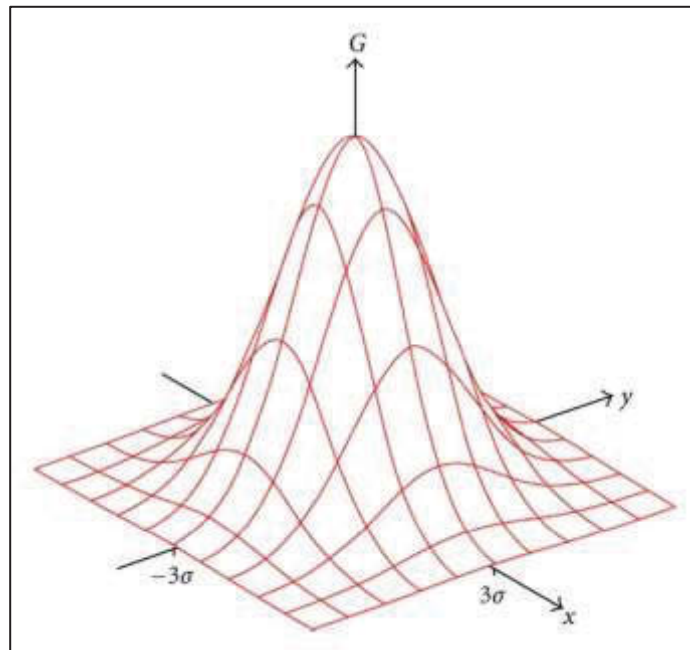
Figure 4-30: 2D Gaussian Function

Applying the 3x3 Gaussian filter to the image in Figure 4-29 produces the following, softly blurred panoramic image:
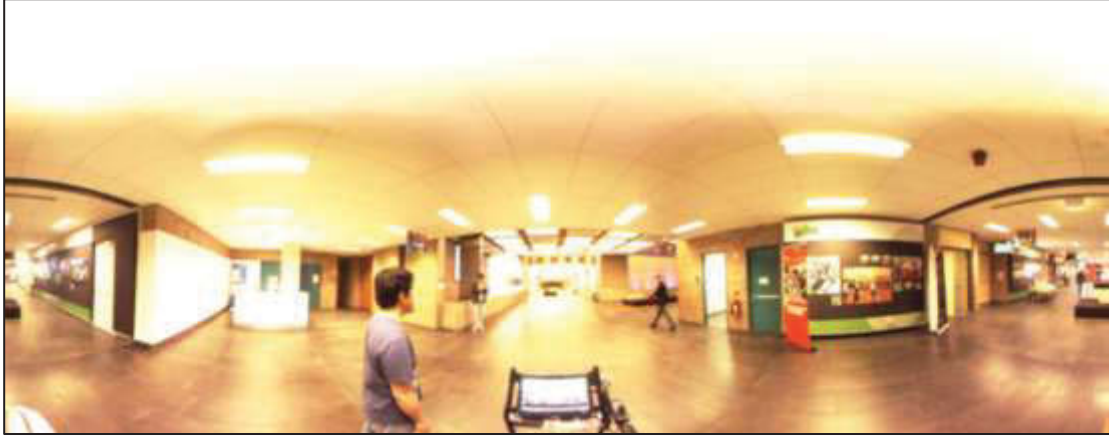
Figure 4-31: Advanced Obstacle Detection Processing: 3x3 Gaussian Filter Blur Affect

Following these steps of gently blurring the image, a Kuwahara filter is applied, which is an adaptive, edge-preserving, smoothing filter (Umbaugh 2011). The Kuwahara filter is here implemented with a square window, of size given by:

$$H = W = 4L + 1 \qquad (4.4)$$

where H is the window height, W is the window width, and L is an integer.

This window is divided into four regions, each of size:

$$s_r = \frac{H+1}{2} \times \frac{W+1}{2} \qquad (4.5)$$

Using a 5x5 window size, the Kuwahara filter can be explained with the following points:

- As shown in Figure 4-32, the 5x5 window is divided into four 3x3 regions with some overlap.
- The average brightness, m_i, and the standard deviation, σ_i, is found for each of the four regions.
- The filter outputs the average region value that has the smallest standard deviation.
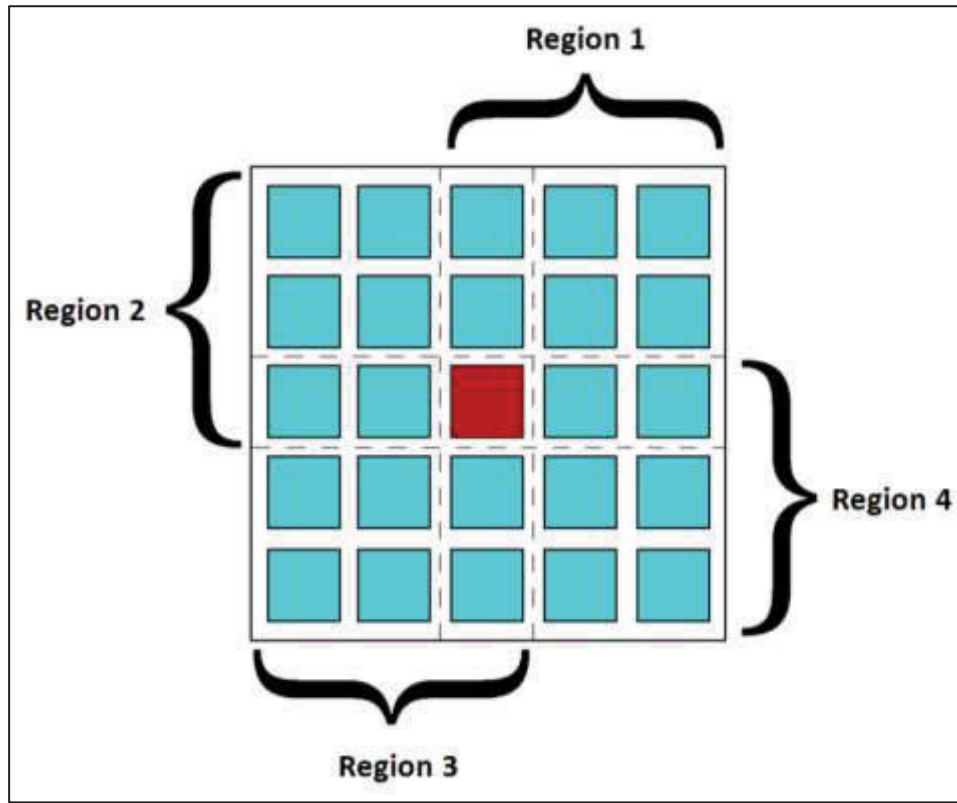
Figure 4-32: Kuwahara Filter 5x5 Example

The means and standard deviations of this edge-preserving filter are defined as follows:

$$m_i = \frac{1}{\frac{H+1}{2} \times \frac{W+1}{2}} \sum_{I(r,c) \in i^{th} Region} I(r,c) \tag{4.6}$$

$$\sigma_i = \sqrt{\frac{1}{\left(\frac{H+1}{2} \times \frac{W+1}{2}\right) - 1} \sum_{I(r,c) \in i^{th} Region} [I(r,c) - m_i]^2} \tag{4.7}$$

This concept is applied to the image in Figure 4-31, continuing the process towards obstacle detection, and the Kuwahara filter window size was varied to observe the affect. A 15x15 window size was selected to almost completely remove detail in the images through the smoothing filter, whilst retaining the object boundaries. This produced the image displayed in Figure 4-33:
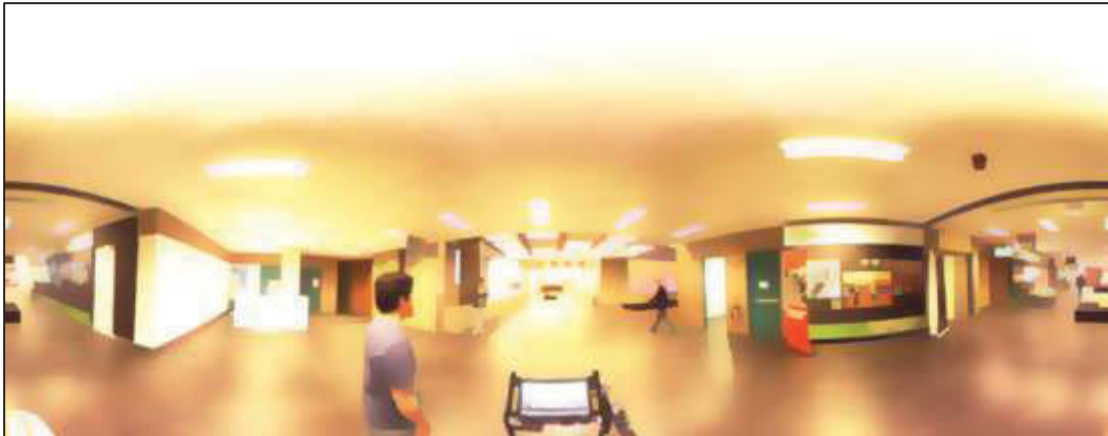
Figure 4-33: Advanced Obstacle Detection Processing: 15x15 Kuwahara Filter

The next step involves finding the object edges in the image through edge detection algorithms. These methods are performed on a grey-scaled image representation of that shown in Figure 4-33. The Prewitt edge detection operator is an appropriate choice for this task; however, an improved version of this algorithm was investigated for the benefits it provides (Yang et al. 2011). The traditional Prewitt operator only uses two pixel templates with horizontal and vertical edge detection. For the purpose of detecting edges in a number of directions, as opposed to limiting the detection to the horizontal and vertical, this improved method proposed an operator with eight pixel template directions (Figure 4-34) in an effort to detect more edges on more angles.

The traditional algorithm calculates the gradient of each point in the image in the specified directions, and takes the maximum value of the gradient magnitudes as the edge pixel value. This can be very sensitive to noise in the image. The improved method uses two types of threshold methods, being 1) an adaptive threshold using the average of the pixel neighbourhoods, and 2) a gradient magnitude threshold. For each pixel, the average value of the eight neighbourhoods of grey-scale pixels is taken and multiplied by a constant k.
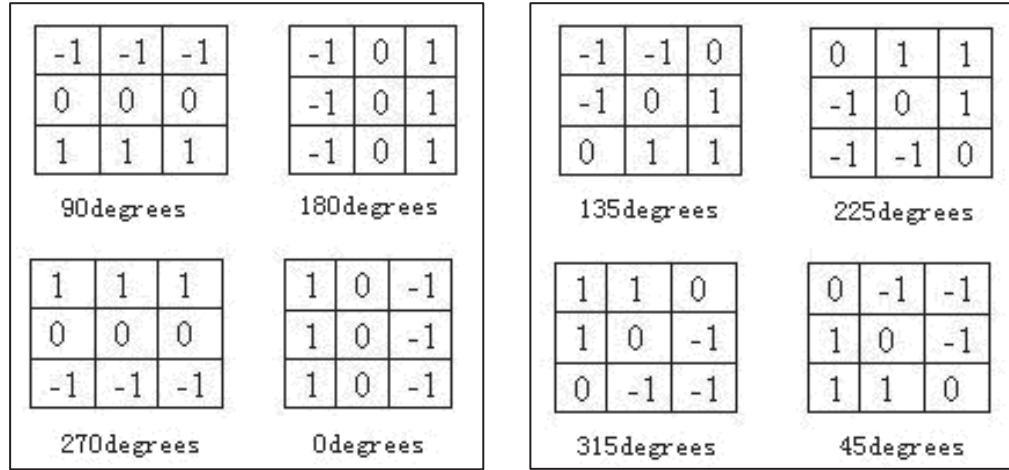
Figure 4-34: Improved Prewitt Edge Detection Directions Template

Given the total number of image pixels, N, the grey-scale range is defined as $[0, L\text{-}1]$. The grey values of these pixels are divided into two categories C_0 and C_1, whereby C_0 represents the pixel values in the range $[0, T\text{-}1]$, and C_1 represents those in the range $[T, L\text{-}1]$ (Yang et al. 2011). The probability of C_0 and C_1, respectively, are denoted w_0 and w_1, and the mean values of each are denoted u_0 and u_1. The mean grey value of all image pixels is denoted u. The class variance σ^2 is defined as:

$$\sigma^2 = w_0(u_0 - u)^2 + w_1(u_1 - u)^2$$
$$= w_0 w_1 (u_0 - u_1)^2$$

(4.8)

To improve the detection of edges, an optimal threshold T_o is found from using the constant k and another threshold value T, which is found when class variance σ^2 reaches the maximum value. This optimal threshold value is simply found as:

$$T_o = T \times k$$

(4.9)

Experiments were performed by Yang et al. (2011) which determined the edge detecting effect is best when constant k is between the values 0.25 and 0.45. The results of this from the mentioned paper are summarised in the following images shown in Figure 4-35:

Figure 4-35: Edge Detection Example: Original Images with Random Noise (Yang et al. 2011)

Figure 4-36: Edge Detection Example: Traditional Prewitt Edge Detection (Yang et al. 2011)
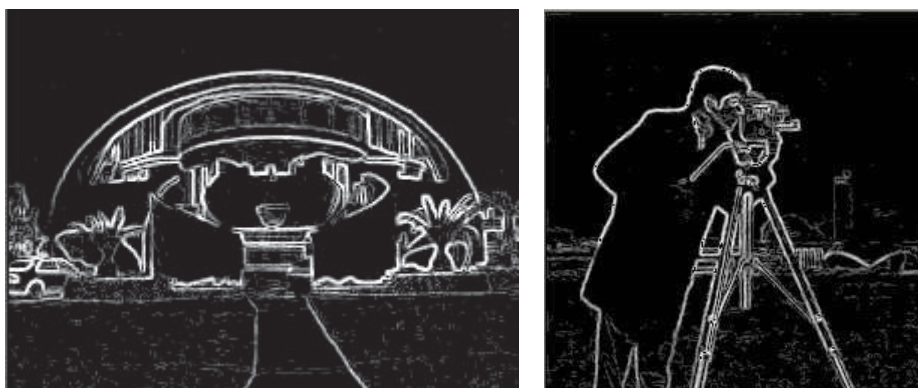
Figure 4-37: Edge Detection Example: Improved Prewitt Edge Detection Results (Yang et al. 2011)

It can be seen that without a smoothing step in the paper, the edge detection in Figure 4-37 is effective. The original two images (Figure 4-35), with random noise, are displayed, followed by the results from traditional Prewitt edge detection (Figure 4-36), and this can be compared with the improved Prewitt edge detection method results (Figure 4-37). This improved method applied here in this project to the already smoothed image in Figure 4-33, yielded the following image shown in Figure 4-38:

Figure 4-38: Advanced Obstacle Detection Processing: Improved Prewitt Edge Detection

Having already smoothed using the Kuwahara filter allows objects to be easily found through the edge detection method, as displayed in Figure 4-38. It can be seen that not many surface textures are producing edges, resulting in mostly object outlines being highlighted. This is very desirable in the process of obstacle detection. Another display of this is shown in Figure 4-39, whereby the edges detected are highlighted in pink to be easily seen, and overlayed onto the colour image of Figure 4-33:

Figure 4-39: Advanced Obstacle Detection Processing: Edge Overlay on Smoothed Colour Image

It can be seen wherever the objects in the scene are located, there is edge detection all around them, which was the objective of this task. As this edge detection method was actually performed on a grey-scale representation of the image in Figure 4-33, the overlay of edges on the grey-scale representation is also displayed in Figure 4-40:

Figure 4-40: Advanced Obstacle Detection Processing: Edge Overlay on Smoothed Grey-scale Image

Moving back from this edge detecting method and just taking the edges found, this is actually overlayed onto a grey-scale representation of the original image, and this is the final image that is segmented and used as input into the neural network. The idea is that the edges have now been found through the steps presented in this section and these are added to the image data being sent to the neural network, in an effort to improve classification results and correctly detect the presence of obstacles in the „Traffic Light" virtual safety zones. This final panoramic image display with edge overlay is shown in Figure 4-41:

Figure 4-41: Advanced Obstacle Detection Processing: Edge Overlay on Grey-scale Original Image

Similar to the neural network setup in §4.4.1 and Equation 4.2, each of the segments is converted into a 1D array for neural network input, however there is a difference here in the normalisation process. Because these images are still represented by 8-bit grey-scale images, the original pixel values are still between 0 and 255 inclusive. So when normalised the pixels are each divided by 128, which again puts all pixel values in the range between 0 and 2. Then

the answer minus 1 places all values in the range -1 to 1, however, a maximum pixel value of 255, once normalised, yields an answer of approximately 0.9928. This results in a range of -1 to 0.9928 once normalised. So this is where the edge overlay can be included, replacing all pixels they are overlaying with a normalised value of 1, providing a clear strategy of separating the values allocated to the detected edges. The images are now ready for neural network input.

4.5 Performance Results

4.5.1 Parallax Variance Approach Results

Parallax variance was an approach investigated for attempting to detect obstacles during movement of the wheelchair, based on correlation algorithms applied to two sequential panoramic images at a time during operation. The feasibility of this method was investigated through acquiring sequential panoramic image frames, grey-scaling, and applying correlation algorithms to two consecutive frames. An example of how the parallax variance was assessed is shown in Figure 4-42 to Figure 4-45.

In Figure 4-42, the wheelchair is moving forward, and this frame grab displays a person standing alongside the wheelchair. Figure 4-43 shows the next panoramic frame in the sequence, whereby the wheelchair has moved forward slightly in its motion path, and the environment has appeared to alter slightly in relation to this movement. The theory here is that the person standing is closer to the wheelchair than any other object in the scene, so he should have a greater horizontal displacement between the two frames than objects further away from the wheelchair.

Figure 4-44 displays a visual result of the correlation algorithm. The pixel neighbourhoods compared between the images are allocated a colour code, similar to disparity imaging concepts in §3.3.1. Pixel neighbourhoods found to have a greater horizontal displacement between the two images are deemed as being closer to the wheelchair and are applied hotter colours (red). Pixel neighbourhoods with smaller horizontal displacement are applied cooler colours (blue). The degree in between is a gradual change between the blue and red, based on the relative horizontal pixel neighbourhood displacements.

Figure 4-42: Parallax Variance Approach: Forward Movement Panoramic Image at Time *t*

Figure 4-43: Parallax Variance Approach: Forward Movement Panoramic Image at Time *t+1*
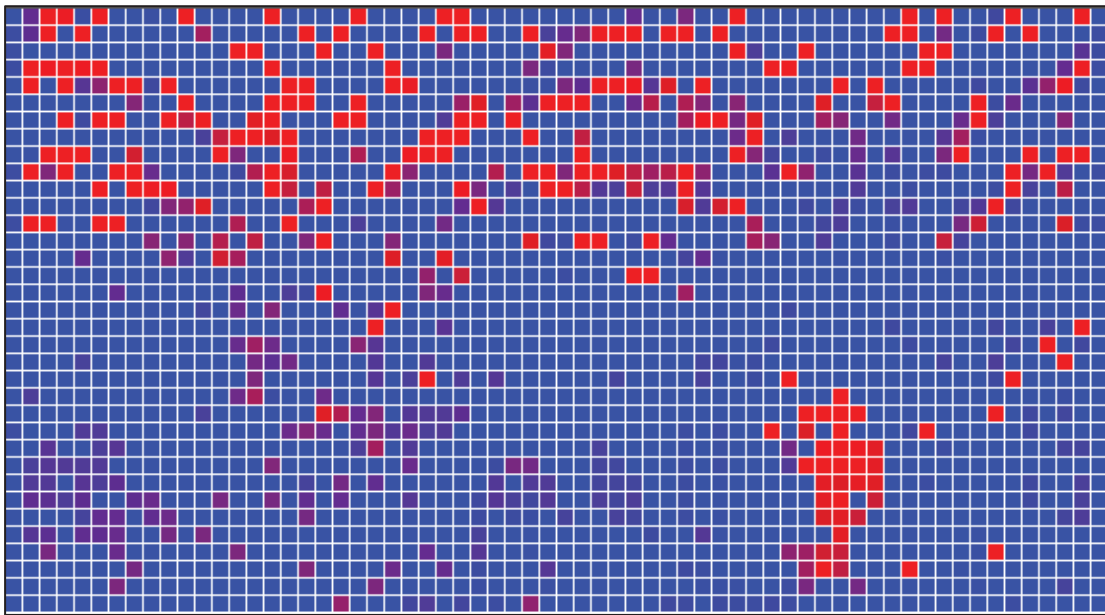
Figure 4-44: Parallax Variance Approach: Forward Movement Panoramic Images Correlation Result

To view how this relates to the areas of the original images, the visual correlation result image from Figure 4-44 is overlaid onto the image in Figure 4-43, as displayed in Figure 4-45.
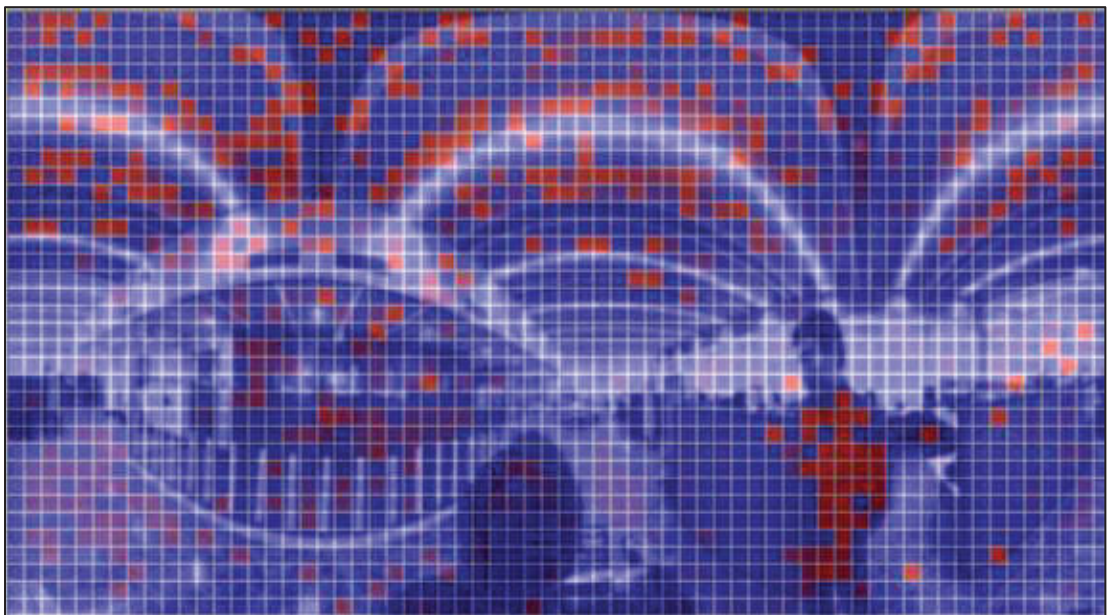
Figure 4-45: Parallax Variance Approach: Panoramic Images Correlation Result Overlay

It can be seen here that there is a relatively dense group of hotter red colours gathered on the person standing alongside the wheelchair, meaning that the person was detected as a closer object. However, there are also many hotter colours scattered around the entire image too, and

this was found to be so because of the distortions in the panoramic representation. This is the reason why stereoscopic images undergo a rectification process before correlation.

This idea was worth the investigation, so a number of situations that could potentially be encountered by the wheelchair were assessed and results reviewed for feasibility. All situations included people, either stationary or moving, and varying between being close to the wheelchair and being further away.

These main situations, where two consecutive frames in a sequence were extracted for review, were:

1) forward movement of the wheelchair through a static environment
2) forward movement of the wheelchair through a dynamic environment
3) turning movement of the wheelchair through a static environment
4) turning movement of the wheelchair through a dynamic environment
5) wheelchair remaining stationary in a stationary environment
6) wheelchair remaining stationary in a dynamic environment

The first situation reviewed involved the forward movement of the wheelchair as in Figure 4-42 to Figure 4-45. In a static environment, where there was no movement other than the wheelchair, close objects produced dense clusters of hot colours for pixel neighbourhood correlations. It was generally found that a high number of scatted areas exhibit hot colours too based on the object movements through distorted areas of the panoramic image representation. However, this case can determine where relatively close objects are located.

The second situation included dynamic objects in the environment as the wheelchair moved forward. Of interest here were people who were also moving in addition to the wheelchair"s forward movements, which presented a few sub-situations for review. When a person is walking alongside the wheelchair in the same direction with approximately the same velocity, it is sometimes very difficult for this method to adequately determine if there is an object there at all. Movements of such parts as the person"s arms would sometimes produce minor clusters of hot colours, but generally these would be scattered and produce uncertain results about the object being close to the wheelchair. When the person is walking in the opposite direction and is away from the wheelchair it creates the illusion they are displaced further apart in the image frames, and hence produce hot colours indicating they are much closer to the wheelchair when in fact they are further away. This appears to produce a number of problems when people are moving around in the wheelchair"s local environment.

The third situation involved the wheelchair turning in a static environment, such as that shown in the phase-corrected, combined scene in Figure 4-15. This worked well at producing clusters of hot colours, gradually getting hotter the closer the parts of the objects were to the wheelchair. Unfortunately, it also produced clusters of hot colours for objects a distance away from the wheelchair too.

In addition to this, the fourth situation included dynamic objects, so people were moving in different manners. Whether the person was walking straight past the wheelchair in either direction, close or far away, the correlation produced hot colours in all cases. This was the situation with most uncertainty involved and many errors throughout the correlation procedure.

The fifth situation involved the wheelchair remaining stationary in a stationary environment. Predictions for this situation were proven correct as no movements within the scene provided no horizontal displacements between matched pixel neighbourhoods. Hence, regardless of whether objects were close to, or far away from, the wheelchair, only cool colours were produce and no objects were detected.

The last situation reviewed added dynamic objects to this situation. People walking past the wheelchair, close or far, as well as walking towards or away from the wheelchair, all produced clusters of hot colours, which was an adequate method for detecting which angles, relative to the wheelchair, the dynamic objects were located, but not adequate for detecting how close they were located.

Upon reviewing these situations, it was quickly realised that this could work well in detecting objects when they are stationary and the wheelchair is moving, or when the wheelchair is stationary and the objects are moving, but any other situation causes too many errors that would not be worth attempting to overcome. This meant that sequential image frames when both objects and wheelchair are moving could be a difficult approach to the problem, and so it was decided that instantaneous image frame analysis may be a more adequate approach. This led to the design of the instantaneous dynamic obstacle detection method using neural networks.

4.5.2 Performance of Neural Network Obstacle Detection Methods

4.5.2.1 Performance of Initial Method Design

The neural networks for instantaneous obstacle detection were trained and validated a number
of times for optimisation. The first step was to determine the most suitable number of hidden
neurons J^* in the network structure, and this was done by setting the learning constant and the
momentum constant, and only varying the number of hidden neurons. Based on the result
differences from the random initial weights each time the network was trained, the same
training configuration (keeping the number of hidden neurons constant) was run 20 times for
each, with the resulting maximum, minimum, and average validation classification accuracies
recorded across all 3 „Traffic Light" zone categories in the S1/S4 and likewise for the 2 zone
categories in the S2/S3 panoramic image segments. As the S1/S4 group was of priority
importance in this application due to the results actually affecting real-time navigational
operation, this group was analysed here. Following this the number of hidden neurons was
incremented and the process repeated, which was performed on the number being set from 2
to 20, inclusive.

No. Hidden Neurons	Min Accuracy (%)	Average Accuracy (%)	High Accuracy (%)
2	40.04	44.086	47.31
3	60.00	68.172	79.14
4	68.92	74.958	81.29
5	74.19	77.515	81.18
6	76.24	80.117	84.52
7	75.05	79.910	83.87
8	79.14	82.031	84.30
9	80.75	82.269	84.84
10	83.66	85.914	87.31
11	83.12	85.772	86.88
12	84.41	86.947	88.38
13	84.95	87.143	88.92
14	84.52	85.682	87.10
15	82.04	85.008	86.34
16	81.29	83.399	84.52
17	76.34	81.173	85.91
18	80.32	82.981	84.62
19	80.00	82.606	84.19
20	78.49	80.728	83.01

Table 4-2: Optimising Number of Hidden Neurons for Initial S1/S4 „Traffic Light" Zone Classification
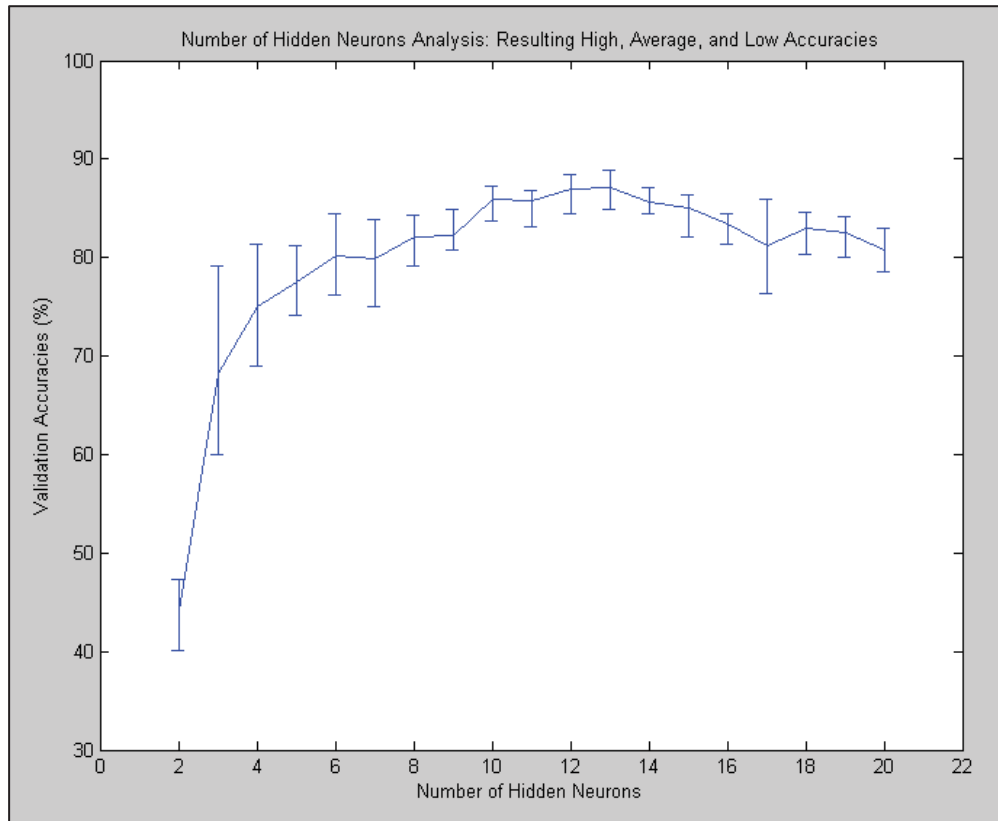
Figure 4-46: Hidden Neurons Analysis Plot for Initial S1/S4 „Traffic Light" Zone Classification

It can be seen from the plot that 13 hidden neurons is the optimal number resulting from the analysis, providing the highest average accuracy, the highest overall accuracy, and a sufficient stability margin. This is now selected as the value and from here the learning constant and validation constant are both varied and another analysis is done to further optimise results. The learning constant was varied from 0.001 to 0.5 with increments of 0.001, and the momentum constant was varied from 0.01 to 0.5 with increments of 0.01. All combinations of these were run to determine the best performing regions of combination, with only high accuracy combinations being recorded. Resulting from this, the region of combination that produced the highest consistent accuracies was when the learning constant was set to 0.01 and the momentum constant was set to 0.02. So the final settings for this optimised configuration were:

NN Learning Parameter	Final Value Setting
Number of Hidden Neurons	$J^* = 13$
Learning Constant	$\eta = 0.01$
Momentum Constant	$\alpha = 0.02$

Table 4-3: Neural Network Optimised Learning Parameter Settings for Initial S1/S4 Classification

For the testing phase, 930 image samples were used for S1/S4 classification, in which 310 images belonged to each of the three class categories. The optimised weights were applied to this test set and the output classification of each pattern compared against the actual category the test pattern belonged to. When selecting the classified category, the neural network outputs a percentage of probability for each of the three categories, based on the extent it believes the pattern belongs to each. The category exhibiting the highest of the three percentages is taken as the test classification output for that test pattern. The results of this testing are shown in Table 4-4 (for table structure, refer to Table 3-13 in §3.5.3).

Category 1: RED ZONE		Test Results		
		Positive	Negative	
Actual Status	Positive	281	29	310
	Negative	41	579	620
		322	608	930

Category 2: YELLOW ZONE		Test Results		
		Positive	Negative	
Actual Status	Positive	261	49	310
	Negative	19	601	620
		280	650	930

Category 3: GREEN ZONE		Test Results		
		Positive	Negative	
Actual Status	Positive	292	18	310
	Negative	36	584	620
		328	602	930

Table 4-4: Neural Network Testing Results for Initial S1/S4 „Traffic Light" Zone Classification

ANALYSIS		Category Number		
		1	2	3
Sensitivity (%)	TP/(TP+FN)	90.65	84.19	94.19
Specificity (%)	TN/(TN+FP)	93.39	86.94	94.19
False Pos rate (%)	FP/(FP+TP)	12.73	6.79	10.98
False Neg rate (%)	FN/(FN+TN)	4.77	7.54	2.99

Table 4-5: Analysis of Testing Results for Initial S1/S4 „Traffic Light" Zone Classification

Analysis of these initial S1/S4 classification results shows that Category 1 (Red Zone) exhibits a sensitivity of 90.65%, and a specificity of 93.39%. It has the highest false positive rate, being 12.73%, with a more reasonable false negative rate of 4.77%. This means that out

of the three categories, images that belong to this Red Zone category get wrongfully classified more than others.

Category 2 (Yellow Zone) has the lowest sensitivity, at 84.19%, and the lowest specificity, at 86.94%. It also has reasonably low false positive and false negative rates, being 6.79% and 7.54% respectively.

Category 3 (Green Zone) is the best performing category, with the highest sensitivity, at 94.19%, and the highest specificity, at 94.19%. It does, however, have a false positive rate of 10.98%, with a better false negative rate of 2.99%. This seems to be the easiest category to classify, mostly due to the fact that the Green Zone exhibits more open spaces and less image intensity variances towards the lower parts of the images, where objects closer to the cameras appear to generally affect.

The overall result attained for this optimised neural network was **89.68% classification accuracy** across all three categories. This is a reasonably high accuracy result and is useful for determining whether or not objects are near the cameras in the traffic light zones, at any instant in time.

For the initial S2/S3 group, the best configuration yielded 9 hidden neurons, a learning constant of $\eta=0.03$ and a momentum constant of $\alpha=0.01$. Between the two categories in this group, Yellow Zone (Category 1) and Green Zone (Category 2), an overall classification accuracy of 93.50% was attained.

These classification accuracies were adequate for instantaneous obstacle detection. However, through the addition of the edge-detection overlay strategies, all results were drastically improved. Since safety is of utmost importance in this application, higher accuracies in these instantaneous obstacle detection methods will yield better real-time performance of the smart wheelchair during navigation.

4.5.2.2 Performance of Improved Method Design

The neural networks for instantaneous obstacle detection were retrained and again validated a number of times for optimisation. This was done in the same fashion as previous, however, with the additional pre-processing performed on the input images, namely the edge-detection

strategies and the overlay approach, this improved system can also be compared to the initial design. For this strategy the optimal number of hidden neurons was found as follows:

No. Hidden Neurons	Min Accuracy (%)	Average Accuracy (%)	High Accuracy (%)
2	60.11	62.154	64.95
3	74.30	79.668	86.02
4	88.71	91.989	95.16
5	91.94	94.187	96.45
6	94.19	95.922	96.77
7	93.23	94.505	95.38
8	93.12	94.001	95.05
9	93.23	94.130	94.95
10	92.47	93.928	95.59
11	92.26	93.732	95.59
12	91.18	93.308	95.05
13	91.94	92.964	94.52
14	90.75	92.787	94.41
15	90.32	92.599	94.62
16	88.28	92.110	94.19
17	89.03	92.318	93.98
18	86.67	91.375	93.66
19	87.20	90.881	93.87
20	87.10	90.709	93.66

Table 4-6: Optimising Number of Hidden Neurons for Improved S1/S4 Classification
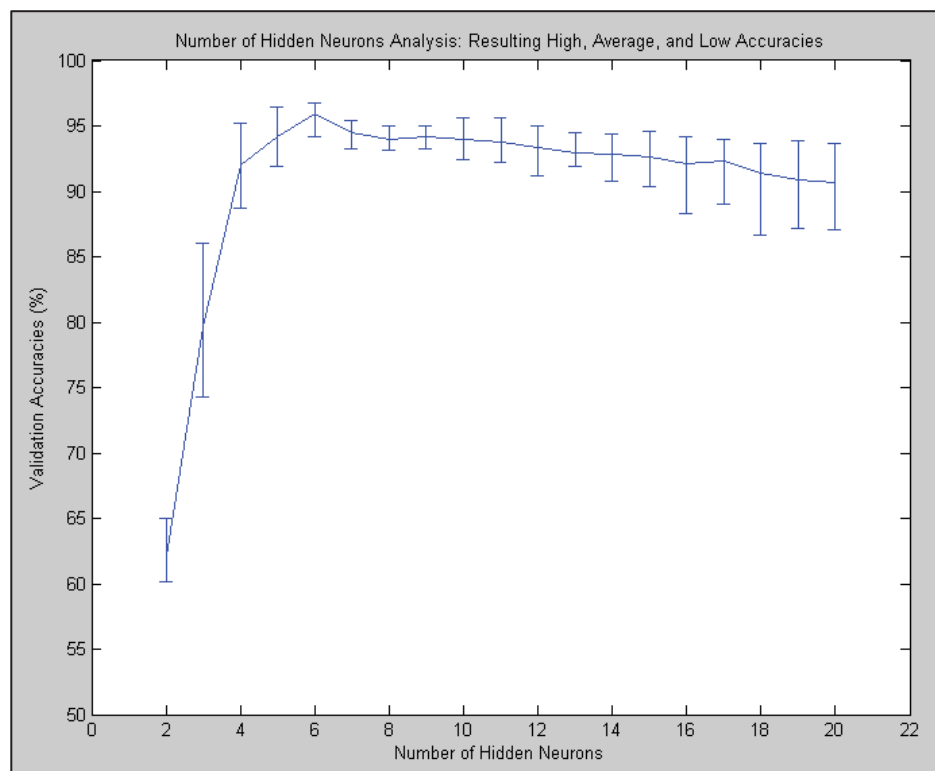
Figure 4-47: Hidden Neurons Analysis Plot for Improved S1/S4 „Traffic Light" Zone Classification

It can be seen from the Table 4-6 and Figure 4-47 that 6 hidden neurons is the optimal number resulting from the analysis, providing the highest average accuracy, the highest overall accuracy, and a sufficient stability margin. The analysis continues from here in the same fashion as §4.5.2.1. Resulting from this, the region of combination that produced the highest consistent accuracies was when the learning constant was set to 0.008 and the momentum constant was set to 0.006. So the final settings for this optimised configuration were:

NN Learning Parameter	Final Value Setting
Number of Hidden Neurons	$J* = 6$
Learning Constant	$\eta = 0.008$
Momentum Constant	$\alpha = 0.006$

Table 4-7: Neural Network Optimised Learning Parameter Settings for Improved S1/S4 Classification

Again for the testing phase, 930 image samples were used for S1/S4 classification, in which 310 images belonged to each of the three class categories. The results of testing this improved S1/S4 zone classification system are shown in Table 4-8.

Category 1: RED ZONE		Test Results		
		Positive	Negative	
Actual	Positive	305	5	310
Status	Negative	11	609	620
		316	614	930

Category 2: YELLOW ZONE		Test Results		
		Positive	Negative	
Actual	Positive	297	13	310
Status	Negative	8	612	620
		305	625	930

Category 3: GREEN ZONE		Test Results		
		Positive	Negative	
Actual	Positive	302	8	310
Status	Negative	7	613	620
		309	621	930

Table 4-8: Neural Network Testing Results for Improved S1/S4 „Traffic Light" Zone Classification

ANALYSIS		Category Number		
		1	2	3
Sensitivity (%)	TP/(TP+FN)	98.39	95.81	97.42
Specificity (%)	TN/(TN+FP)	98.23	98.71	98.87
False Pos rate (%)	FP/(FP+TP)	3.48	2.62	2.27
False Neg rate (%)	FN/(FN+TN)	0.81	2.08	1.29

Table 4-9: Analysis of Testing Results for Improved S1/S4 „Traffic Light" Zone Classification

Analysis of these improved S1/S4 classification results shows that Category 1 (Red Zone) now exhibits the highest sensitivity at 98.39%, and also a very high specificity of 98.23%. It still has the highest false positive rate, now 3.48% which is considerably lower than the initial design which gave 12.73%, and now also has a much lower false negative rate of 0.81% compared to the previous 4.77%. This means that out of the three categories, images that belong to this Red Zone category are most likely to be accidentally classified and least likely to be missed, which is desirable because it is better to make sure as many obstacles breaching the Red Zone are detected as possible.

Category 2 (Yellow Zone) has the lowest sensitivity, at 95.81%, which is much higher than the previous 84.19%, and also a much higher specificity, at 98.71% compared to the previous 86.94%. It now also has very low false positive and false negative rates, both being significantly reduced to 2.62% and 2.08% respectively.

Category 3 (Green Zone) is still a high performing category, with an increased sensitivity of 97.42%, up from 94.19%, and remains the highest specificity, now 98.87%, up from 94.19%. The false positive rate has now been drastically reduced from 10.98% to 2.27%, and still exhibits a very low false negative rate of 1.29%, down from 2.99%.

The overall result attained for this optimised neural network was **97.20% classification accuracy** across all three categories. For the improved S2/S3 group, the best configuration yielded 5 hidden neurons, a learning constant of $\eta=0.01$ and a momentum constant of $\alpha=0.01$. Between the two categories in this group, Yellow Zone (Category 1) and Green Zone (Category 2), an overall classification accuracy of **98.67%** was attained.

These results have displayed conclusively that 1) the „Traffic Light" Zones neural network classification approach to instantaneous obstacle detection is feasible and appropriate, and 2)

with the use of the edge-detection overlay strategy designed in §4.4.2, very high classification accuracies can be achieved.

4.5.3 Real-time Interface Results

The optimised neural network was implemented into the real-time operation of the wheelchair. This is done by providing the panoramic video feed directly onto the user's screen so they can see everything around surrounding the wheelchair, have the option to visually see the zone breaches through the allocation of zone colour beneath the segment areas on the panoramic feed (Figure 4-48), as well as the automated guidance system being able to use the information for navigational decisions.

When being used for navigational decisions, the system takes the highest occurring classification for each segment out of a moving window of three consecutive frames, making each classification the majority of an image triplet. If all three are different (only possible for the S1/S4 group), then the closest zone is taken (Red Zone) for safety. This provides an even higher chance of correct classification than just taking the segment zone classifications from each single panoramic image frame, given that there is a still small chance an error will occur in individual classifications.

Using this addition in real-time whilst navigating through a crowd over approximately 20 seconds, offline post-analysis of the online sequence provided results about the segment classifications. In this filmed sequence there were 108 panoramic image frames, providing 106 classified frames (as the first 2 are not classified until a group of 3 has been seen) for each of the segments S1 to S4. The separations of these are shown in Table 4-10.

Segment	Red	Yellow	Green	Total
S1	20	53	33	106
S2	N/A	79	27	106
S3	N/A	41	65	106
S4	32	36	38	106

Table 4-10: Real-time Test: Category Numbers

The S1 segment classified all 33 image triplets with majority Green Zone, and made 2 classification errors, both incorrectly classifying Yellow Zone as Red Zone image triplets.

This is due to the slightly higher false-positive rate of the Red Zone category, however these few incorrect classifications only resulted in a total of less than half a second of extra caution and no option to rotate.

The S2 segment classified only one image triplet incorrectly, being a Green Zone as a Yellow Zone majority. This does not, however, provide any effect on the operation of the wheelchair in any way. The S3 segment classified all image triplets correctly into the Yellow and Green Zone categories.

The S4 segment incorrectly classified one Green Zone as a Yellow Zone, and correctly classified all Red Zone categories. This is preferable for the few incorrect classifications to be made as a closer category to the wheelchair rather than further away, meaning extra caution than necessary is taken in the majority of mistaken classifications.

Overall these real-time results are very positive, with accuracies across all four segments staying above 98%. With these accuracies, the few incorrect classifications are only made generally in less than a quarter of a second at a time, so the effect they have becomes negligible anyway. In this test, results proved the effectiveness of this system in a crowded dynamic environment. Figure 4-48 shows a frame from the user interface during this test.

Figure 4-48: User Interface Visual Panoramic Video Feed with Real-time „Traffic Light" Zone Results

It can be seen in this interface example that the segments each have a colour beneath them to show the closest zone being breached, as the results of the neural network at any instant provide. Here, segment S1 has a person breaching the Red Zone (of the Red/Yellow/Green possibilities), S2 has a person breaching the Yellow Zone (of the Yellow/Green possibilities), S3 does not have a Yellow Zone breach, so is classified as the Green Zone, and S4 has a Yellow Zone breach (of the Red/Yellow/Green possibilities).

The advantage of displaying the interface in this manner is to provide the user with more information about what is happening around the wheelchair, with the addition of implementing it as a control mechanism too. The intention was to use this panoramic feed to make directional selections for travel, using any hands-free control system, by controlling a cursor at the top of the video feed to move anywhere along the entire 360º of vision and be used to make the selections.

4.6 Discussion and Chapter Conclusion

This chapter has introduced a spherical vision camera system into the hardware configuration of the TIM smart wheelchair design. The strategies for utilising this camera system were designed and validated with the intention of being able to adequately detect obstacles in real-time all around the wheelchair, and hence optimise the vision range to provide 360º of obstacle detection in both static and dynamic environments.

It was found that panoramic vision from spherical cameras has the disadvantage of not being able to effectively use some common monocular vision strategies, such as parallax variance through movement, due to the distortions inherent in the panoramic representations which make it difficult to process these methods. It was, however, found to be feasible and effective through the designed strategy of the instantaneous „traffic light" zone classification system. This involved the panoramic image being segmented into five different segments and pre-processed, before neural network classification of the four main surrounding segments. These were grouped into horizontally-mirrored pairs (S1/S4 group and S2/S3 group), and classified at any instant in time into one of the following „traffic light" zone categories:

- Red – Stop (obstacles too close to move in that direction)
- Yellow – Caution (obstacles near, move slowly if moving in that direction)
- Green – Go (no obstacles near, clear to move in that direction)

The advanced and improved method of this strategy involved a combination of image processing methods for effective edge-detection of objects in the image. This was then overlayed onto the lower-resolution, grey-scale version of the original panoramic image, before being rearranged based on pixel values into a 1-dimensional input array for neural network classification. At any instant in time, roughly 5 times a second, each of the four main segments (S1 to S4) are classified individually by two pre-trained neural networks. This

method produced an optimised overall classification accuracy of 97.20% for the S1/S4 group across the Red, Yellow and Green Zone categories, and 98.67% for the S2/S3 group across the Yellow and Green Zone categories.

Real-time performance of this displayed the effectiveness of the system in a crowded and dynamic environment. Classification is done on each segment in a moving window of 3 consecutive frames, which produces an image triplet for a majority classification approach, further increasing the chance of correct classifications. Upon moving through a crowd of people walking in different directions around the wheelchair, the overall accuracies across all four segments stayed above 98% in this real-time test. Any given instantaneous result is not only displayed on screen, but also potentially used in the decision-making process of the automated guidance system in the wheelchair, ultimately providing it with more information about the surroundings to assist in avoiding collisions.

Furthermore, the colour version of the panoramic video feed is displayed visually on the screen for a few reasons. The first is so the user, who is likely to not have a large range of physical movement for looking around, can see everything going on around the wheelchair in a manner that does not take long to become familiar with. The second reason is the intention for it to assist in controlling the wheelchair. As the video feed visually displays the 360º of space all around the wheelchair, it is intended that a cursor above the feed will be used to select directions for travel via hands-free controls. This provides a simple implementation possibility of a more continuous spread of directional commands than such common discrete selections as „left‟, „forward-left‟, „forward‟, „forward-right‟, „right‟, and other such commands.

Resulting from the work in this chapter, spherical vision has been found as an effective contributor to the camera systems used for intelligent vision in the design of the TIM smart wheelchair. It assists in obstacle-detection, helps the decision-making process of the automated guidance system, provides the user with an efficient visual feed of the surrounding environment, and opens up a very useful option for a graphical user interface in hands-free control of the smart wheelchair.

Chapter 5

Real-time Operational Performance of a Hands-free Smart Wheelchair System using a Unique Camera Configuration Biologically Inspired by Equine Vision

"Each handicap is like a hurdle in a steeplechase, and when you ride up to it, if you throw your heart over, the horse will go along too." - Lawrence Bixby

5.1 Introduction and Aims

Both the stereoscopic and the spherical camera vision systems have been separately analysed and strategies towards intelligent vision designed for each. The stereoscopic system, combined with the wheel encoders, provides birds-eye view mapping of the local environment ahead of the wheelchair, with the ability to remember placement of objects once they move out of the 66° range of stereoscopic vision, based on the movements of TIM's

wheels. This is appropriate for constructing maps of static environments. The methods designed for the spherical vision cameras, however, provide 360º of instantaneous obstacle zone classifications, allowing TIM to determine when static or dynamic objects are located close to the wheelchair in segmented surrounding areas. These two different camera systems, and designed vision strategies, now need to be combined to work together in both the hardware and software integration of the TIM wheelchair for real-time implementation.

Robotics techniques play a large role in intelligent system design such as smart wheelchairs. Many modern artificial sensors used in intelligent robotic applications are biologically inspired and modelled on real sensors in living systems such as humans, animals, and insects (Dario et al. 2005). This concept has been taken here and applied to the overall camera vision design and integration of the TIM smart wheelchair, for the purpose of being able to model the design of the vision system on an effective version in nature.

This chapter presents the biological inspiration of equine vision along with the final hardware and software implementations of the TIM smart wheelchair. The overall system integration design is provided, with hands-free control interfaces included, and performance testing of the system through experimental study. A real-time operational system is produced to allow users to select directions for travel via hands-free control systems, and the wheelchair must carry out these commands whilst detecting and avoiding obstacles along the way, automatically doing the finer manoeuvres, and ultimately making the travel safe. A total of 10 participants completed the experiments on the TIM smart wheelchair, using a head-movement system (HMC) and a brain-computer interface (BCI), separately, as two methods of hands-free control. The experiment protocol and results are presented and analysed in this chapter, with a discussion and chapter conclusion in relation to the aims.

The aims of the research presented in this chapter are as follows:

1. Find biological inspiration for the vision system design model, to allow effective integration of the combination of stereoscopic and spherical vision cameras.
2. Design the overall software architecture for the TIM smart wheelchair, including communication with all integrated hardware components. This must encompass all final strategy designs and constitute the intelligence of the smart wheelchair.
3. Design advanced real-time obstacle avoidance system, which is required to be semi-autonomous to work with the user‟s commands from the hands-free controls.

4. Implement the TIM smart wheelchair into a functional and operational real-time system.

5. Construct testing protocol and conduct experimental studies with a range of participants, both able-bodied (AB) and non-able-bodied (Non-AB), to gather such information about the wheelchair implementation as feasibility, ease-of-use, operation, safety, and other information necessary to be gained from the experimental study.

5.2 Instrumentation and Final Stage Prototype Design

The final prototype was based on the biological inspiration of equine vision, with the hardware modelled on this. Everything required for the final TIM smart wheelchair prototype was assembled and the system integration began. Careful thought was taken in the placement of the hardware, with many components being required on the wheelchair in specific locations. Attention was given to the sensor placement, computer screen location and orientation, and how all parts would be moved out of the way to allow a person to get in and out of the wheelchair.

5.2.1 Biological Inspiration: Equine Vision System

The combination of stereoscopic and spherical vision is not something previously found in literature, and in fact, spherical vision alone was rarely found in literature searches. As such it was not initially obvious as to how it was going to be implemented into the single smart wheelchair system. Biological inspiration for the overall vision system was sought after, since nature provides many characteristics that have stood the test of time thought genetic evolution and natural selection. Since this wheelchair needs to be safe and observant in dynamic situations, research on animals with effective vision systems, used to aid in self-protection, was assessed. The most adequate vision system found, of the researched candidates, was the equine vision system, particularly that of horses.

Horses in nature spend approximately 50-60% of their time grazing with their heads lowered and eyes near ground level (Figure 5-1). This leaves them vulnerable to predation from such threats as wolves, lions, and snakes. However, horses inherently have a large range of vision which provides early warning of approaching, and potentially threatening, dynamic

movements outside of their binocular vision range. This allows for quick instinctual assessment of the local environment and a speedy escape from imminent danger (Murphy et al. 2009).

Similarly, the wheelchair‟s vision system being modelled on this allows for the stereoscopic vision to map static objects ahead of the wheelchair in real-time and use obstacle avoidance strategies for both static and dynamic objects. The spherical vision, in addition, provides dynamic obstacle detection all around the wheelchair, preventing collisions with moving objects which have not already been mapped.

The equine eye is large and prominent, being housed within enclosed orbits located laterally in the skull (Samuelson 1991). Using measurements based on the position and dimensions of the equine eye, the retinal field of view of each eye in the vertical plane has been estimated to be about 178º (Hughes 1997), whilst that in the horizontal plane is slightly greater, being about 200º (Harman 1999). The horizontally elongated pupil in the equine eye facilitates wider lateral vision than, for example, the circular pupil of the human eye (Roberts 1992).

The binocular overlap of the visual field is located down the nose of the horse and has been found to have a width of around 65º (Crispin et al. 1990). Two blind spots have been identified within the equine visual field, being one in front of the forehead, and one (approximately 25º) directly behind the horse (Roberts 1992). Visual field characteristics and the extent of blind spots do vary between different horse breeds (McGreevy 2004), however, the overall ideas of the equine visual system have been a sufficient inspiration for the vision system developed for the TIM smart wheelchair.

Figure 5-1: Horse Grazing; Photo Showing the General Position and Orientation of Horse‟s Eyes

5.2.2 TIM Smart Wheelchair Hardware Design and Camera Combination

The novel combination of stereoscopic cameras and spherical vision cameras mimics the binocular and monocular fields of view inherent in the equine visual system, whilst also minimizing the blind spots (Figure 5-2). The stereoscopic cameras at the front of the wheelchair provide approximately 66º of vision similar to the binocular vision of a horse, and the spherical vision cameras above the back of the wheelchair provide complete 360º monoscopic vision, similar to the monocular vision of the horse without the posterior blind spots. This allows 3D mapping of the local environment ahead of the wheelchair and detection of obstacles posing as potential collision dangers (dynamic in particular) all around the wheelchair.
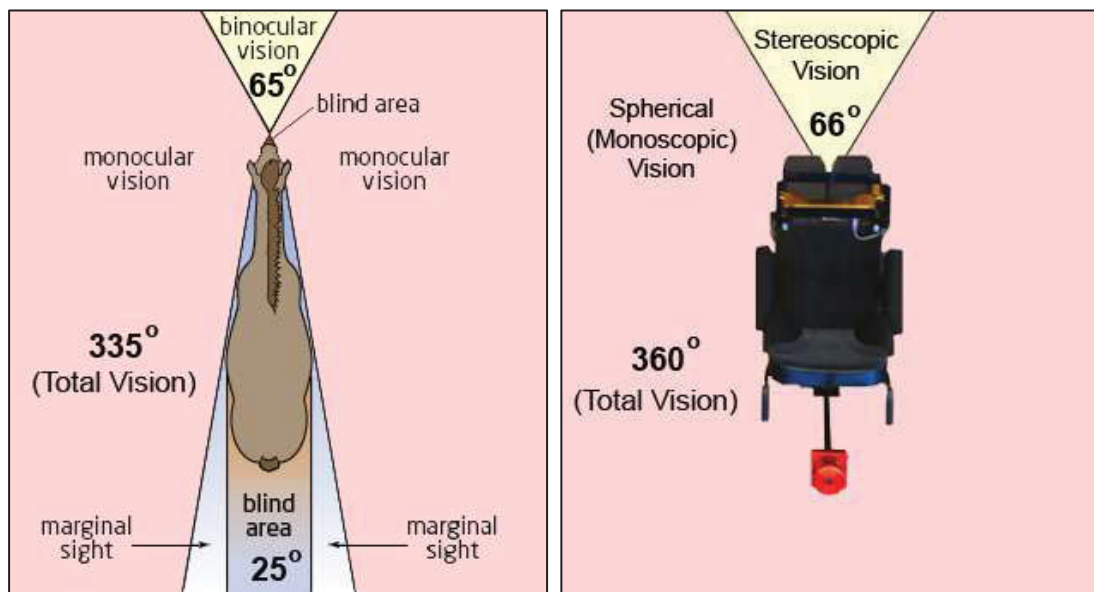
Figure 5-2: Visual System of a Horse; Inspired Vision System of the TIM Smart Wheelchair

The location of the camera systems relative to the wheelchair provide a modelled overall vision system, with the improvements of minimising the blind spots inherent in the equine vision system. The final TIM smart wheelchair prototype design required all necessary hardware to be finalised and implemented onto the wheelchair. Figure 4-3 shows the overall final stage prototype hardware design.

Chapter 5: Real-time Operational Performance of a Hands-free Smart Wheelchair System
using a Unique Camera Configuration Biologically Inspired by Equine Vision
196
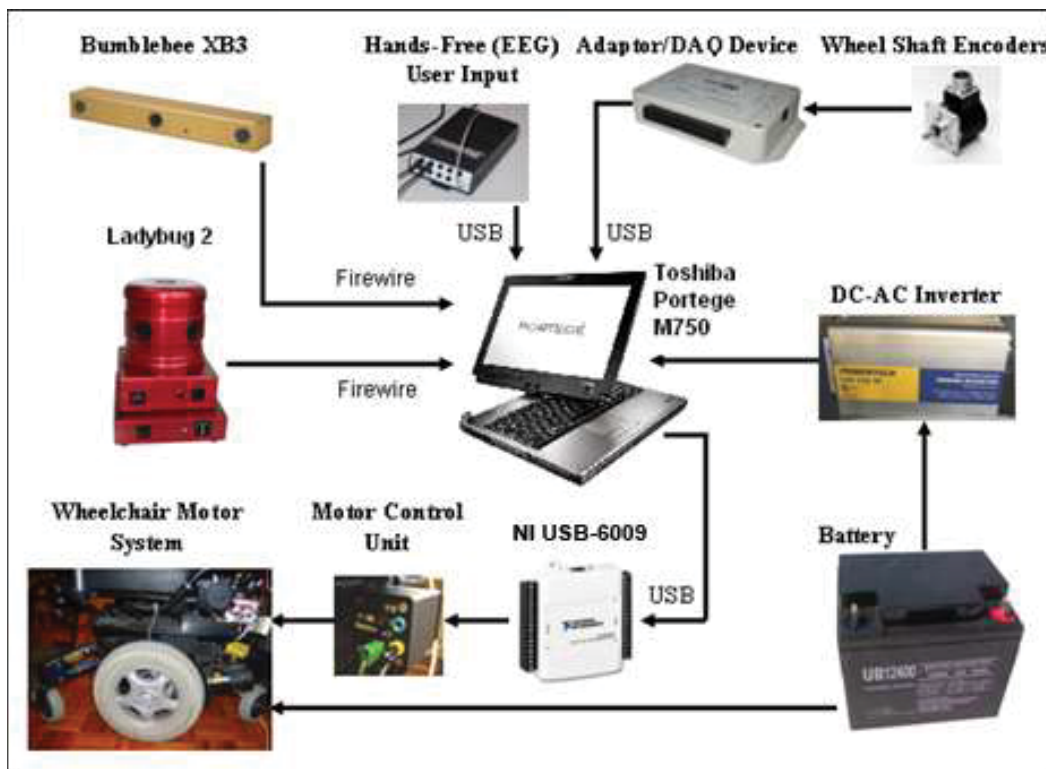
Figure 5-3: Overall Final Stage Prototype Hardware Design

Both the Bumblebee XB3 stereoscopic cameras and the Ladybug2 spherical vision cameras communicate the data via a Firewire IEEE-1394b connection to the Toshiba table PC. The Mac Mini and TFT screen of the Stage 1 prototype design have been completely removed now, as all processing and graphical user interface displaying are performed by the Toshiba Portege M750 tablet PC. Hands-free user input (eg. EEG data for the BCI interface) is acquired via USB, and likewise with the wheel shaft encoder data from the DAQ device. The National Instruments (NI) USB-6008 multifunctional DAQ card was replaced with an NI USB-6009 card, which is very similar except it is an updated model and slightly faster. This is used as the digital to analog converter on the wheelchair to send voltages to the wheel motors via the motor control unit. The Toshiba tablet PC, both camera systems, wheel encoder DAQ device, and the „TDX A" power wheelchair are all powered by the „Gel-Tech 8GU1H Sealed Gel maintenance-free" rechargeable 12V battery located in the tray underneath the wheelchair.
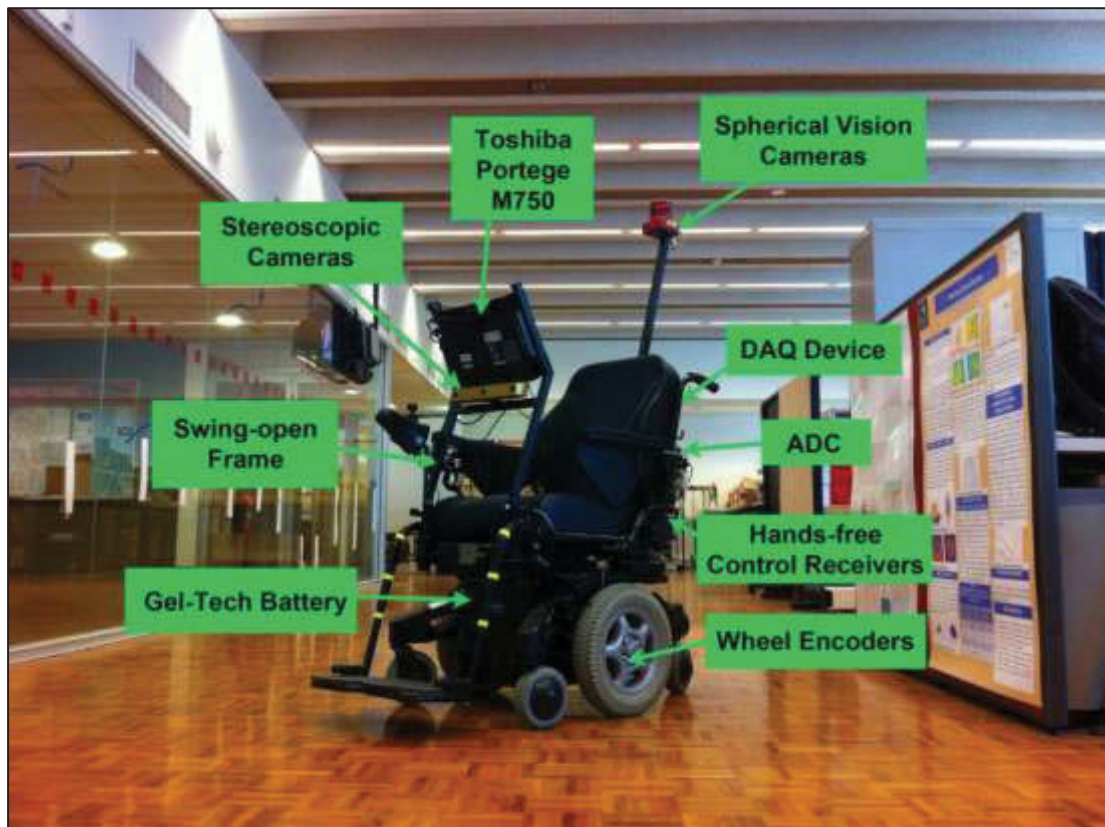
Figure 5-4: TIM Final Stage Prototype

The final stage prototype of the TIM smart wheelchair in the Centre for Health Technologies at UTS is shown in Figure 5-4, along with the hardware features and where they are located on the wheelchair. There is a neat layout and appearance to this prototype design. Most hardware components that do not require specific placement on the wheelchair are neatly mounted to the metal panel on the back.

Careful and specific placement of the hardware on the final stage prototype was carried out to allow an overall configuration that is modelled according to the vision requirements, as well as making the chair as ergonomic as possible for a prototype under development. The main dimensional measurements are displayed in Figure 5-5 (Front View), Figure 5-6 (Side View), and Figure 5-7 (Rear View).

Chapter 5: Real-time Operational Performance of a Hands-free Smart Wheelchair System
using a Unique Camera Configuration Biologically Inspired by Equine Vision

198
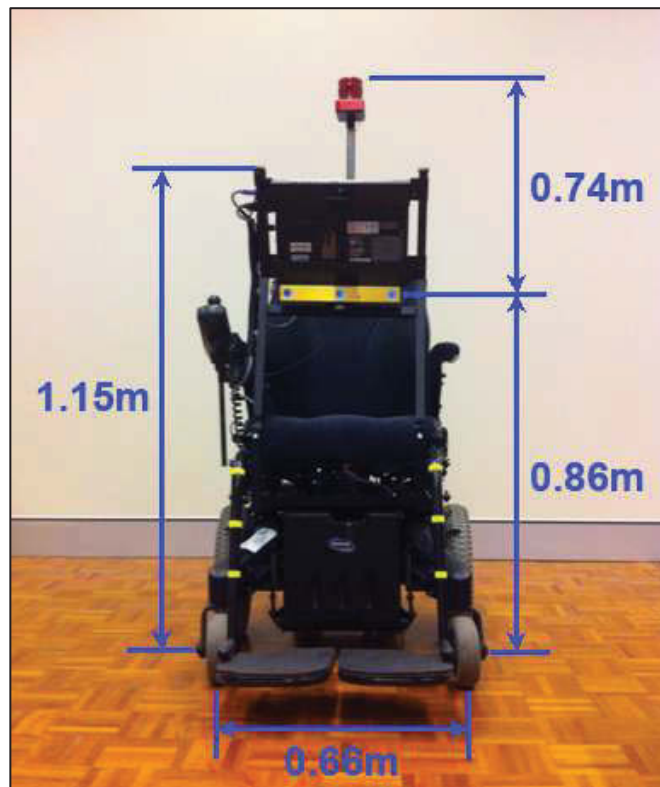
Figure 5-5: TIM Final Stage Prototype Hardware Dimensional Measurements: Front View

Figure 5-6: TIM Final Stage Prototype Hardware Dimensional Measurements: Side View
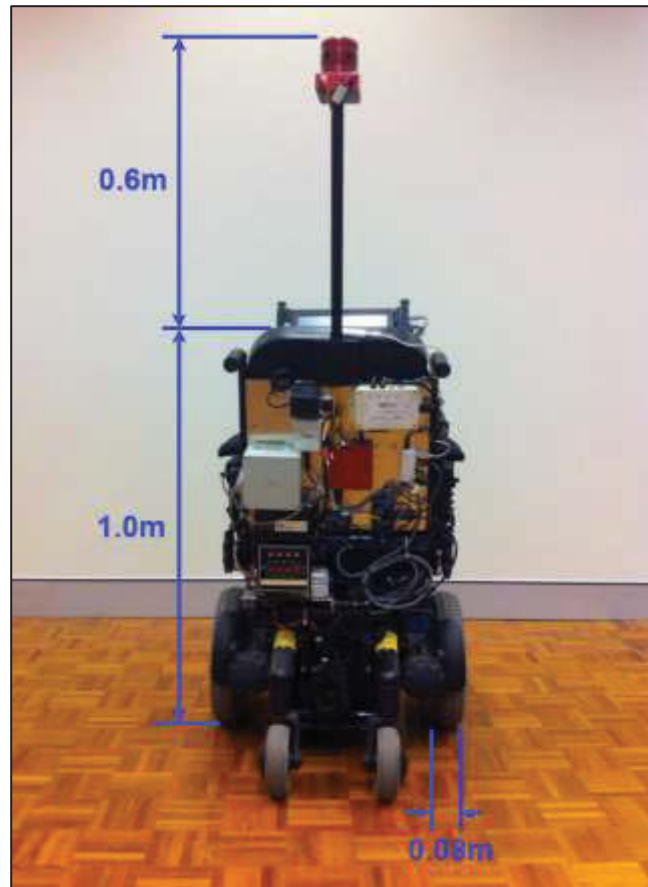
Figure 5-7: TIM Final Stage Prototype Hardware Dimensional Measurements: Rear View

In addition to the placement and dimensional considerations of the TIM smart wheelchair design, consideration was also taken for the opening features of the hardware to allow adequate access for a user to move in and out of the wheelchair without all the equipment and frames getting in the way (Figure 5-8).

Figure 5-8: TIM Final Stage Prototype Opening Design

5.3 Software System Design

Following on from the specific hardware design considerations, the entire software system of the TIM smart wheelchair required an overall software architecture design to be created, taking into account all interactions with the input and output hardware system. This required complete system integration, bringing all hardware-software interactions and communication into a single functional system, and all inner processing to be broken down into software modules. The flow of data between these software modules was also determined carefully to minimise data transfers, improve processing speeds, and optimise the overall process.

5.3.1 Software Architecture

The software architecture was created as a modular programming approach to integrating the entire system of the TIM smart wheelchair. As shown in Figure 5-9, all interactions between software and hardware are displayed, and the software modules have been separated for individual processing, only passing required data to other modules. This software architecture takes inputs from stereoscopic cameras, spherical vision cameras, hands-free user input devices, and wheel encoders. It sends outputs to the Toshiba tablet PC screen for displaying the graphical user interface (GUI) and also sends voltage controls via digital-to-analog conversion (using the NI USB-6008) to the wheelchair motors.

The camera image processing (both for stereoscopic and spherical vision processing) was mostly programmed in a Microsoft Visual C++ environment, whereby the input taken from the cameras, the management of the Firewire bus, synchronisation between the two types of cameras systems, pre-processing, and map data array production are all executed in the Dynamic Link Library (DLL) produced here. This allows the main programs produced in a National Instruments (NI) LabVIEW environment to call the DLL file during each main loop run when the next instant of camera data is required. All other software modules here were produced in LabVIEW, including the main control of all software modules, hands-free input acquisition and processing, graphical user interface, odometry change calculations, local environment map creation and updating, shared control program, automated guidance system, and controls to send all voltage outputs to the wheelchair motors.

Chapter 5: Real-time Operational Performance of a Hands-free Smart Wheelchair System using a Unique Camera Configuration Biologically Inspired by Equine Vision

201
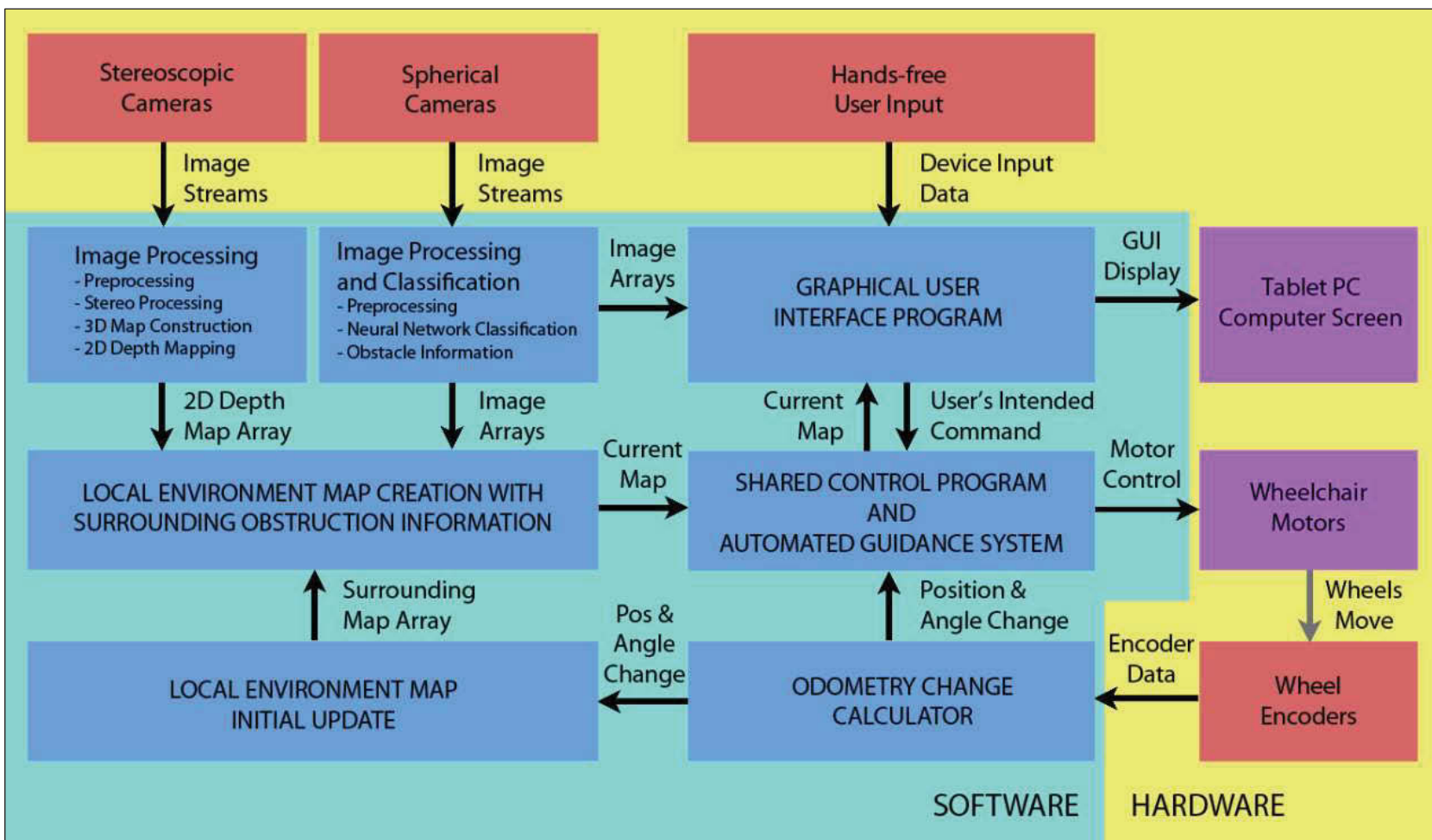
Figure 5-9: TIM Software Architecture

The odometry change calculations module, as discussed in §3.3.2, sends the position and angle change data between updates to the local environment map update module, assisting in the update of object positions on the map, as well as sending the data to the shared control program to help determine the wheelchairs movements during automated guidance. This allows the wheelchair to utilise the data produced from its own movements to improve performance in its environmental perceptions and in the decision-making process for automated steering.

The local environment mapping modules populate and update the mapping of objects in the local environment, as a result of new camera sensor data updates and wheelchair odometry change calculations. The most recent map information is then sent to the shared control program to make its decisions for movement, based on both the users intentions and the obstacle information extracted from the maps. This provides the automated guidance system with the decisions necessary to carry out the required navigation at any instant in time.

The graphical user interface module is the communication link between the software's intelligence and the user, allowing the user to make decisions on navigational commands, and the software to accept these decisions, combine them with the map information, and make the most appropriate real-time manoeuvres as a result of processing all the given data. This needs to be easy to view and understand for the user, contain appropriate commands, and be responsive to the provided instructions. The general operations flowchart for the software updates, which occur around 5 times per second, is displayed in Figure 5-10.
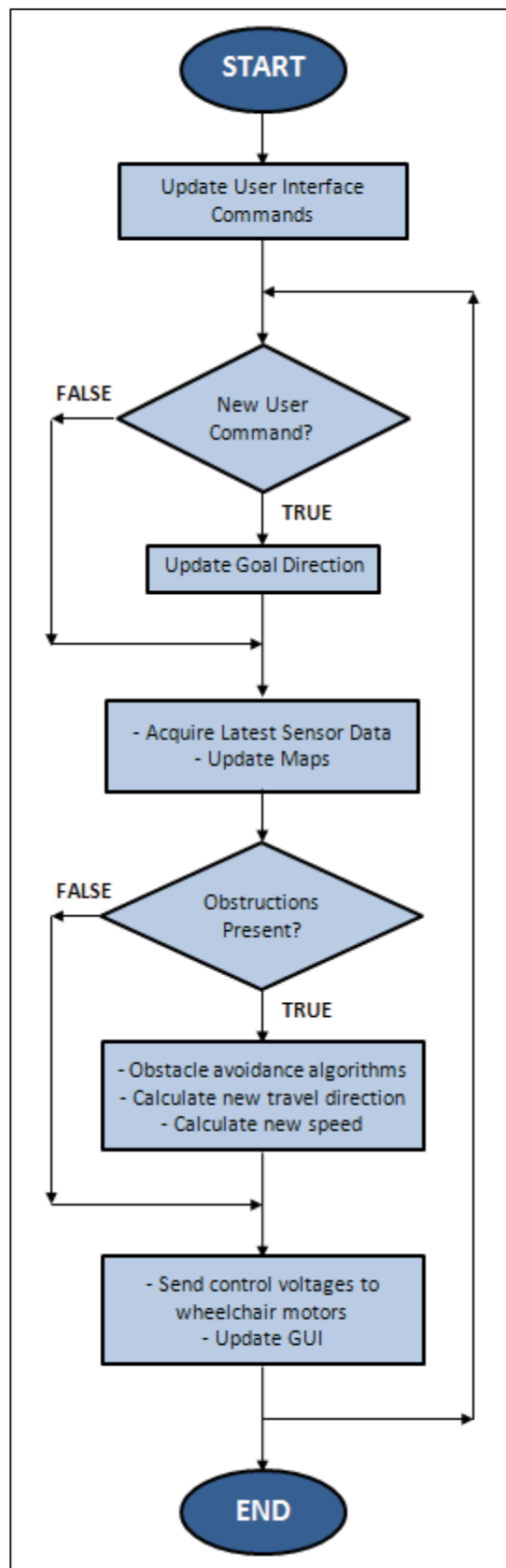
Figure 5-10: TIM Software Main Loop Overview Flowchart

Chapter 5: Real-time Operational Performance of a Hands-free Smart Wheelchair System
using a Unique Camera Configuration Biologically Inspired by Equine Vision
204

5.3.2 System Integration with Hands-free Control Technology

Research in recent years has seen a number of control interfaces for wheelchairs produced without yet being made available via commercialisation. For people who cannot adequately control any of the commercial products discussed, alternative control products in research include voice control systems (Simpson & Levine 2002; Nishimori et al. 2007), a wireless, digital head-movement controller (Nguyen et al. 2006), and non-invasive brain-computer interfaces (Skinner et al. 2007; Aviator 2012).

Joseph and Nguyen (1998) introduced the use of neural networks in classifying head-movement tasks. A wireless head-movement controller (HMC) developed at UTS, shown in Figure 5-11, basically uses a small 3D accelerometer mounted into a cap worn by the user to track the movements of their head. This can allow users to calibrate any head movements that are comfortable and repeatable to them and translate these into directional commands for the wheelchair. This is a simpler version of the commercial head actuated control systems, except easier to use, able to be calibrated, can provide a continuous and proportional signal, and is a physically subtle control device.
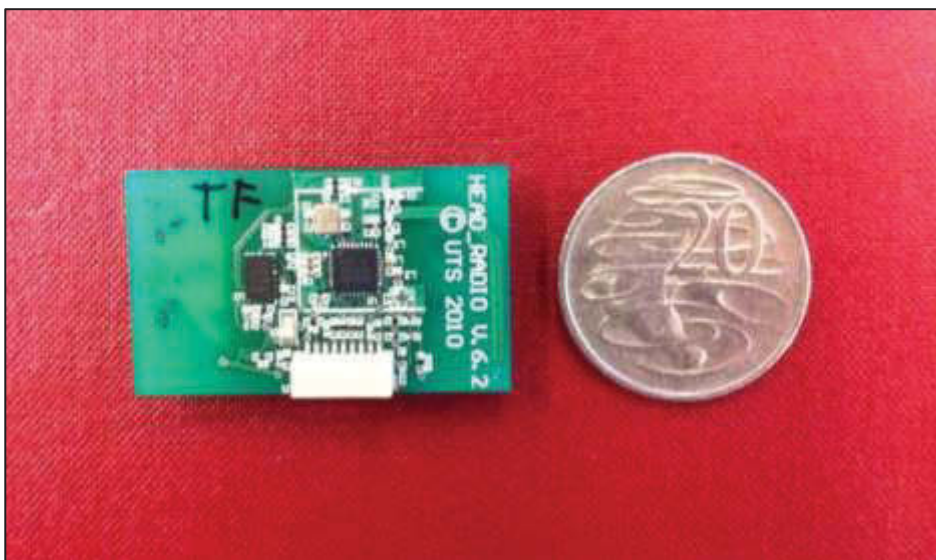
Figure 5-11: Wireless Head Movement Controller Developed at UTS

This technique accommodates a wide range of users, however, for people on the higher end of severe physical disability, such as those with LIS, who cannot control any movements nor communicate adequately, a brain-computer interfaces (BCI) can provide a possible solution. Aviator (2012), developed as a venture spun out of UTS, features a small, non-invasive, and

wireless electroencephalography (EEG) acquisition device, which can be used to facilitate brain-computer interfaces (Figure 5-12). This can be worn discretely in a cap, headband, or headgear setup. The signals are acquired with electrodes and conductive gel, amplified and filtered, and wirelessly transmitted to a receiver USB dongle, which feeds the signals into the central processing unit (CPU) for analysis. These signals are analysed to obtain the user‟s intentions and allow them control over devices, however, many further developments are required for BCI techniques in general to improve accuracies for high levels of applicability.

Figure 5-12: „Aviator‟ EEG Device Prototype Developed at UTS; User Wearing the Prototype

The graphical user interface program module of software architecture (Figure 5-9) provides easy methods of interfacing hands-free controls to the wheelchair. The main idea is to allow the user to provide directional and operational commands to the TIM smart wheelchair via the hands-free control system. In this project the two control methods investigated separately are 1) the head-movement controller (HMC), and 2) the brain-computer interface (BCI) using the „Aviator‟ EEG acquisition device prototype.

Initial Hands-free Technology Integration Design

Initial GUI designs featured discrete selector controls, such as that displayed in Figure 5-12, where the selections were „Stop‟, „Left 10‟ degrees, „Right 10‟ degrees, „Left 45‟ degrees, „Right 45‟ degrees, „Left 90‟ degrees, „Right 90‟ degrees, „Forward‟, and „Forward to Object‟. This format allowed the user to scroll through the discrete directional selections and make selections for movements.
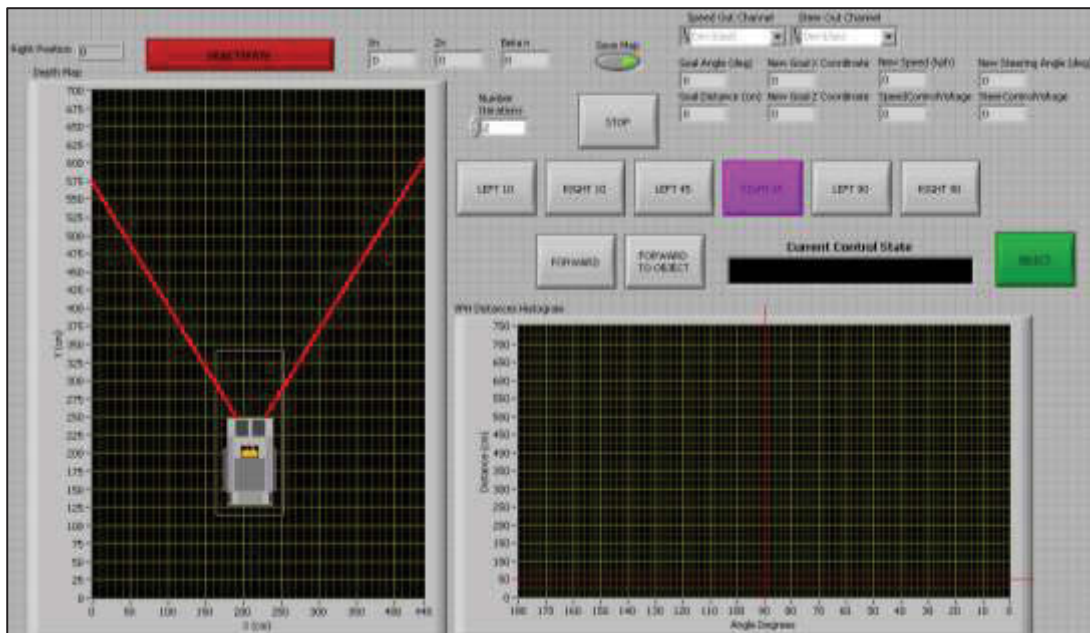
Figure 5-13: Screenshot of Initial (Discrete) Graphical User Interface Design for Controlling TIM

The HMC control allows the user to tilt their head in directions that are comfortable and can be calibrated to associate any easy movements with specific commands. Depending on the level of control the user is able to gain over this system there are two modes of operation:

1. Continuous directional control: This mode basically makes the user‟s head the joystick for the wheelchair, whereby tilts in any given direction control the wheelchair to move in that direction. This is only useful if the user has a reasonably high level of controlled movement to their head.

2. Screen control by movement association: This mode allows any comfortable movement, once associated with a screen command, to move the highlighted direction selector on the screen around (Figure 5-13). Another movement, such as a nod, is allocated to selecting the current highlighted direction. This is similar to having a few arrow keys and an „Enter‟ key on the keyboard, with movements associated to the arrow keys for moving the selector, and a nod associated to the „Enter‟ key selection.

The BCI control system allows the user to associate thoughts (mental tasks) with selecting commands. Through a process of EEG acquisition, picking up on the user‟s „brainwaves‟, the interface design gives the user the ability to associate a mental command, such as focussing on visualising a Rubik‟s cube rotating, with selector movements (arrow keys), and closing

their eyes for between half-a-second and one second to select („Enter" key). This is integrated in a similar fashion to the HMC screen control by movement association method.

Tests on these initial hands-free technology integration designs showed that the methods were feasible, however, the discrete selector approach had the following shortcomings:

- Trade-offs between the number of discrete selections and the time taken to move the selector between the different selections, more directional selections take more time to move the selector between.

- Difficult to direct the wheelchair in specific directions due to the user having to judge degree differences such as 10 degrees to the left. This caused accidental overshoots or short falls when turning, and hence frustration in directing the wheelchair in the desired directions.

- Generally, not a very intuitive and user-friendly interface form.

This led to the design of a continuous selector design, which incorporated a panoramic video feed from the spherical vision cameras. This was produced in an effort to overcome the disadvantages of this initial discrete selector interface design.

Continuous Hands-free Technology Integration Design

The continuous selector design, for integrating hands-free technology with the TIM smart wheelchair, was produced as another application of the spherical vision cameras. A panoramic video feed is streamed to the screen in the GUI, allowing the user to easily view everything around the wheelchair (taking into account their potentially limited physical movement range), whilst also being used as the continuous selector control method.

The idea here is the arrow keys and „Enter" key commands, provided via the HMC or BCI, moves the triangular selector, shown in Figure 5-14, along the panoramic feed, which represents all 360º of direction selections, and then the user can select when it is in the desired position through visual association with the direction for travel. This is simpler, quicker, more effective, and easier to use than the discrete method. It means that the user is selecting directions based on the visual cues, similar to the way humans typically localise and navigate, mostly using the sense of vision.

Figure 5-14: Screenshot of Final (Continuous) Graphical User Interface Design for Controlling TIM

This form of interfacing is very efficient for controlling the wheelchair via the hands-free control technologies. The user only really needs to focus on moving the green triangular selector and making their selections, allowing them to easily change directions on the fly, and actually choose their desired directions based on the visual feed. The operation includes the function to easily move to the „Stop‟ command, and the selector can scroll off the right side of the video feed and reappear on the left side, and vice-versa. Added simplicity here includes setting the selector movement in a direction, such as towards the right, and it continuing in that motion until in the desired location, at which time the user provides the „Enter‟ command to stop the movement of the selector, and repeats the „Enter‟ command to make a command selection in that position. This reduces the number of commands necessary to make selections, and in the case of BCI, requires less mental focus, which can be tiring to the user.

This continuous selector GUI provides an easy method for the user to provide real-time directional commands, and TIM smart wheelchair must then carry out these commands as best it can, whilst performing obstacle avoidance, safe direction selection, and all finer manoeuvres using its automated guidance system.

5.4 Advanced Real-time Obstacle Avoidance System

The obstacle avoidance algorithm investigated for this application was the Vector Polar Histogram (VPH) method (An & Wang 2004), which was a combination, adaptation, and improvement of both the Potential Field Method (PFM) (Borenstein & Koren 1989) and the Enhanced Vector Field Histogram (VFH+) (Gong et al. 2007). PFM and VFH+ were primarily developed for mobile robotic obstacle avoidance applications using sonar and

ultrasonic sensors, whereas VPH was adapted for use with laser rangefinders. Since the TIM smart wheelchair utilises camera systems for environmental perception, the VPH algorithm, with the integration of some VFH+ concepts, has been adapted and improved again for this application, which will be referred to here as TIM-VPH.

These obstacle avoidance algorithms are necessary for the real-time navigational intelligence of the TIM smart wheelchair system. Once a desired directional command is received from the user, the wheelchair must attempt to safely travel in that direction, whilst automatically avoiding both static and dynamic obstacles along the way. This is particularly useful for hands-free control technologies, such as BCIs, which can be used effectively to provide commands to the wheelchair, however, can also be very difficult to provide controls frequently throughout the navigation process.

The TIM-VPH method here takes on the general structure of the VPH algorithm, replaces some concepts with those of VFH+, and makes improving adaptations to suit the equine vision-inspired camera configuration used by the TIM smart wheelchair. A producer-consumer control loop was deployed whereby the hands-free control commands from the user, such as via BCI controls, are acquired through its own timed „producer" loop, and the command data is then sent to the TIM wheelchair"s data processing and control „consumer" loop. The producer loop typically runs at a slightly faster rate than the consumer loop, thus resulting in the consumer loop utilizing only the most recently transmitted data. After image acquisition and processing from the two camera systems has completed in each cycle, the instantaneous local environment obstacle map is updated accordingly. Following this map update, the main steps of the TIM-VPH algorithm, all still included in the consumer loop, are:

1. **Grid representation:** Convert the „active area" (being the local updating range of the environment map) to a grid form, similar to VFH+ except with binary values representing free or occupied cells, as opposed to certainty values.

$$
\begin{aligned}
m_{i,j} = 0 \quad & if \quad cell\ is\ empty \\
m_{i,j} = 1 \quad & if \quad cell\ is\ occupied\ by\ object
\end{aligned}
\tag{5.1}
$$

2. **Safety to a single point:** Displayed in Figure 5-15, this is another included VFH+ concept, being the expansion of objects and reduction of wheelchair representation, adapted here to a non-circular model representation, since the TIM wheelchair model is more

adequately represented by a rectangle. Without this step the rectangular model representation would otherwise present further problems, in dimensional accountability, for the algorithms providing automated obstacle-avoiding navigational manoeuvres. With the inclusion of this step, the model of the wheelchair does not need to be taken into account in further steps. This is made possible due to the fact that if the reduced point representation can move through any given space following object expansion, then the wheelchair can move through the space in the actual setting.
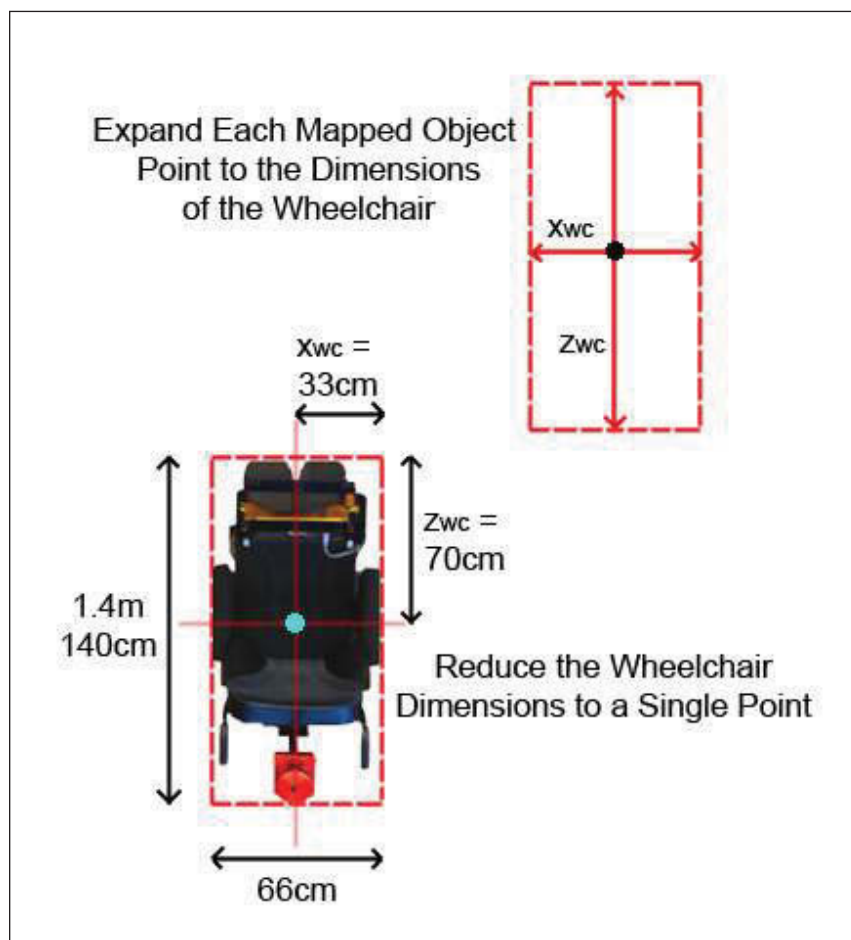
Figure 5-15: TIM Representation Reduction and Correlating Object Expansion

3.   **Goal direction creation:** Whenever a command is given to the wheelchair a target cell can placed at the nearest object location in the goal direction, or further past the objects, in the goal direction, depending on what the user commands. As with all other active obstacle cells, the vector direction and magnitude from the wheelchair centre point (WCCP) can be found as follows:

Vector direction of active cell from wheelchair centre point:

$$\beta_{i,j} = arctan\left(\frac{z_i - z_{wccp}}{x_i - x_{wccp}}\right) \tag{5.2}$$

Vector distance of active cell from wheelchair centre point:

$$d_{i,j} = \sqrt{\left(x_i - x_{wccp}\right)^2 + \left(z_i - z_{wccp}\right)^2} \tag{5.3}$$

where: (x_{wccp} , z_{wccp}) = coordinates of the WCCP

(x_{ac}, z_{ac}) = coordinates of active cell

4.   **Creation of a vector polar histogram:** Sector segmentation is done to convert the active area matrix into a polar histogram displaying closest object distance as opposed to obstacle density for each sector, with any sectors that do not contain objects within sight being allocated the maximum vision range distance d_{v_max} away from the wheelchair, indicating large amounts of free space in that direction. For each sector corresponding to each direction angle α (here being 0 to 180 degrees), the polar obstacle magnitude is the distance to the nearest object for that sector $d_{x,z}(\alpha)$, which represents the maximum distance $D(\alpha)$ in that direction that the wheelchair can reach. This is defined as:

$$D(\alpha) = min\left(d_{x,z}(\alpha)\right) \qquad \alpha = 0,1,2,\dots,180 \tag{5.4}$$

5.   **Reduction of the polar histogram:** This is done by a threshold function into a binary histogram providing candidate directions for possible navigation. As in VPH this takes into account the wheelchair's real-time velocity, acceleration and deceleration parameters, allowing the necessary time and space to stop the wheelchair to be obtained:

$$t = \frac{V(t)}{a}$$

$$\tag{5.5}$$

$$S(t) = V(t)a - \frac{1}{2}at^2 = \frac{V^2(t)}{2a}$$

For each direction angle α, the function can be rewritten as:

$$V(\alpha, t) = \frac{V_t . d_1}{D(\alpha, t)} = \begin{cases} V_t . cos^2(\theta(t) - \alpha) & ; \quad |\theta(t) - \alpha| \leq 90 \\ 0 & ; \quad |\theta(t) - \alpha| > 90 \end{cases}$$ (5.6)

$$S(\alpha, t) = \frac{V^2(\alpha, t)}{2a} = \begin{cases} \dfrac{V_t^2 . cos^2(\theta(t) - \alpha)}{2a} & ; \quad |\theta(t) - \alpha| \leq 90 \\ 0 & ; \quad |\theta(t) - \alpha| > 90 \end{cases}$$ (5.7)

Then, taking into consideration an additional general safety distance between wheelchair and obstacles (D_s), we define a time-varying threshold function for each angle as:

$$D_T(\alpha, t) = S(\alpha, t) + D_s = \begin{cases} \dfrac{V_t^2 . cos^2(\theta(t) - \alpha)}{2a} + D_s & ; \quad |\theta(t) - \alpha| \leq 90 \\ D_s & ; \quad |\theta(t) - \alpha| > 90 \end{cases}$$ (5.8)

where:

V_t is the real-time speed of the wheelchair,

$\theta(t)$ is the steering direction of the wheelchair,

a is the deceleration of the wheelchair.

By comparing the polar histogram and the threshold function, a binary histogram can be produced, where each angle candidate in the polar histogram that is further (higher distance) than the threshold value for that angle becomes a candidate ($H=1$) in the binary histogram. All other angles closer than this threshold value are blocked off as angles that cannot be selected for travel in that particular instant in time ($H=0$). So, the binary histogram is created using the following:

$$\begin{aligned} H(\alpha, t) = 1 && if \ D(\alpha, t) \geq D_T(\alpha, t) \\ H(\alpha, t) = 0 && if \ D(\alpha, t) < D_T(\alpha, t) \end{aligned}$$ (5.9)

6. **Selection of a steering direction from candidate directions:** These candidates are found from the binary histogram where $H(\alpha, t) = 1$, as can be seen in Figure 5-16, which produce a set of candidate angles U. This is adapted and improved from the VPH method. An appropriate cost function C is used to select a direction Ω from the candidate angles, and is represented as a function of each candidate angle α belonging to candidate angles set U.

Seeing as VPH was aimed more towards smaller mobile robotic systems, it was more suitable for the robot to seek a closer way around obstacles, passing them as closely as possible without breaching the constraints of the specified safety distances. However, for a larger application such as this TIM smart wheelchair, passing as close as possible to obstacles is not necessary. So for this reason, as well as the fact that candidate directions exhibiting a larger amount of free space are more desirable, a cost inversely proportional to the amount of free space, up to the maximum vision range distance d_{v_max}, is added to the candidate direction cost function.

$$C(\alpha) = K_1|\alpha - \varphi| + K_2|\alpha - \theta| + K_3\left(\frac{D}{d_{v\_max}}\right), \quad \alpha \in U \tag{5.10}$$

where:

K_1, K_2, K_3 are constants,

φ is the target direction of the wheelchair.

The first term represents the cost associated with deviating from the target direction. The second term represents the cost associated with deviating away from the current heading direction. The third term represents the cost associated with directions that have obstacles up ahead, which will reduce with more free space in any given direction. The constants are undetermined parameters that will facilitate the level of importance placed on each of the associated term.

The best direction is the one that has the least associated cost value, representing the most appropriate balance between the cost terms. So the final selection of steering direction Ω is found as follows:

$$C(\Omega) = \min C(\alpha), \quad \alpha \in U \tag{5.11}$$

7. **Speed control:** This is based on the distance to objects in the selected steering direction Ω, found from Equation 5.11, and will range up to the maximum allowed speed V_{max}:

$$V = \left(1 + \frac{d_{v\_max} - d(\Omega)}{d_{v\_max} - D_s}\right)V_{max} \tag{5.12}$$

Once implemented, these algorithms form the obstacle avoidance in the automated guidance system. They allow the user˝s intentions for travel directions to be taken and carried out, whilst safely avoiding the obstacles along the way. Equation 5.10 provides a means of the wheelchair being able to navigate around objects, commit to the direction of choice when multiple paths around an object are present, and steer further around objects in open spaces. This takes into account general navigational tendencies, whereby a wheelchair user will manoeuvre closer around to objects in cluttered environments and move further around objects when there is more space present. This system integration allows the user, hands-free control technology, and the TIM smart wheelchair to all operate as a coordinated and unified system.

5.5 Experimental Study Protocol

This smart wheelchair has been designed using a combination of stereoscopic and spherical vision cameras for environmental perception during real-time navigation. This is to be controlled by proof-of-concept (POC) hands-free control interfaces. A range of different types of users, particularly people with paraplegia or other such forms of physical disability, should be able to communicate their intentions for navigation through a non-commercial POC Head-Movement Control (HMC) system, which is one new method of a hands-free control interface. A wider range of users, including people with tetraplegia and those on the severe end of physical disability, should be able to communicate their intentions for navigation through a non-commercial POC Brain-Computer Interface (BCI). For some users this may be the only system they can control, but for many this should be able to be controlled as an alternative to the HMC system.

Using either form of hands-free control, in combination with the TIM smart wheelchair˝s shared control system (HMC+TIM and BCI+TIM), the participants will communicate directions for travel, and the wheelchair will be able to effectively carry out these commands. It will do so utilising its vision capabilities and navigational intelligence in real-time, making the travel safe and automatically avoiding all collisions, whilst also carrying out the users intentions. These tasks will be appropriately executed between the user and the wheelchair in a pre-determined static environment, where obstacles will force the wheelchair to make autonomously assistive manoeuvres, which it carry out in a safe manner and avoid all collisions. The user and wheelchair will also be able to handle these same tasks for safe

navigation in a dynamic environment, where collisions with moving obstacles, such as people walking, will all be avoided in addition to the static obstacles.

This experimental study was approved by the University of Technology, Sydney (UTS) Human Research Ethics Committee, approval number 2011-245A. Refer to Appendix D for the application documents.

Experiment Aims:

- Investigate the real-time performance of the entire hands-free smart wheelchair system.
- Conduct the experiments with people not connected to the project, with varying levels of physical mobility.
- Assess the automated assistance of the TIM smart wheelchair using camera systems for vision and navigational strategies employed for safety.
- Use a real setting, being an environment in UTS, where the users will need to control the wheelchair using a hands-free interface, and navigate with the assistance of TIM along corridors and through an obstacle course, avoiding people and obstacles along the way when present.
- Gain statistical feedback following completion of the experiments, using a QUEST (Quebec User Evaluation of Satisfaction with Assistive Technology) survey adaptation, which will be completed by all participants.

Main Test Statements:

- In the Static Course experiments, the assistance from TIM will allow both HMC and BCI control methods across all participants to be carried out in faster times than the HMC Only control.
- In the Dynamic Course experiments, the assistance from TIM will also allow both HMC and BCI control methods across all participants to be carried out in faster times than the HMC Only control.

Experimental Methods:

- Two new types of hands-free control will be utilised to show that this wheelchair can be integrated with varying types of control interfaces. The first is a Head-Movement Control (HMC) system and the second is a Brain-Computer Interface (BCI).

- A range of able bodied test subjects will complete the experiments first, to provide initial statistics and help with improving unforseen control problems and test details. More able-bodied tests will continue once the protocol is finalised, and following this, a few mid-level tetraplegics will complete the tests. Those who can utilise both systems will do so, however, this is not expected of the tetraplegic subjects. The subject numbers are as follows:
    - Able-bodied Subjects: 8
    - Mid-level Tetraplegic Subjects: 2
- The experimental studies are set for being conducted in Building 2, Level 3 of UTS. The user needs to complete 2 different obstacle courses for each hands-free control technique.
- The first obstacle course, referred to as the „Static Course" (Figure 5-16), requiring roughly 39m of travel, is a test of the general static environment navigational capabilities of the wheelchair, as well as testing the shared control strategies between the user and the wheelchair. The obstacles to be avoided in this test included tables, chairs, couches, bins, lockers, doors, walls, and general corridor features. For this test the user will command the wheelchair to complete the following tasks:
    - Command the wheelchair to move forward from the Start Zone to the Check Point 1 (CP1) zone (Figure 5-18) and make a right turn at CP1 to move towards CP2. If CP1 is missed, the wheelchair will navigate into a dead-end and the user will be required to turn the wheelchair around and find their way back to CP1 and navigate towards CP2 (Figure 5-19).
    - The wheelchair passes through CP2 and must then automatically avoid objects by making its way through an obstacle course at CP3, before going through the CP4 doorway (Figure 5-20).
    - Following this, the person must attempt to stop the wheelchair in the Stop Zone (Figure 5-21), which is just before the carpeted area changes floor surface type.
- The second obstacle course, referred to as the „Dynamic Course" (Figure 5-22), requiring roughly 29m of travel, is a test of the general dynamic environment navigational capabilities of the wheelchair, with a smaller emphasis this time on the shared control strategies between the user and the wheelchair. The obstacles to be avoided in this test included tables, chairs, bins, lockers, doors, walls, general corridor features, and walking people. For this test the user will command the wheelchair to complete the following tasks:

- o Starting this time at Check Point 1 (CP1), being the Start Zone in this test, and initially facing CP2 direction (Figure 5-19), the user needs to command forward to the wheelchair.

- o The wheelchair must automatically avoid a person walking across the path of the wheelchair in the CP2 area, before making its way through the CP3 obstacle course and then through the CP4 doorway.

- o Immediately following the passing of the CP4 doorway the wheelchair must automatically avoid another person walking towards the wheelchair, moving in the opposite direction.

- o Following this, the participant must again attempt to stop the wheelchair in the Stop Zone.

- These experiments test both the user‟s ability to control the wheelchair with the hands-free technologies, and more importantly, tests the wheelchair‟s ability to carry out the user‟s intentions, even with such new non-commercial forms of control input from the user. Of particular importance here is for the wheelchair to perceive its environment with the camera systems in real-time and navigate safely, avoiding all obstacles.

- If the user appears competent in the use of either hands-free control interface, HMC and/or BCI, they will repeat the Static Course and Dynamic Course experiments without the automated assistance of the TIM smart wheelchair („HMC Only‟ / „BCI Only‟). If this is the case, the wheelchair will be stopped if a collision is close to occurring, the situation documented, and the wheelchair manually moved by an experiment conductor away from the potential collision before continuing.

- All tests are mapped to display both the map produced as well as the path taken through the experiment location. These results will all be displayed on a common pre-produced environment map for comparison and analysis.

- All forward-back and left-right control voltage efforts will be recorded for each run, as will the times taken between each check point.
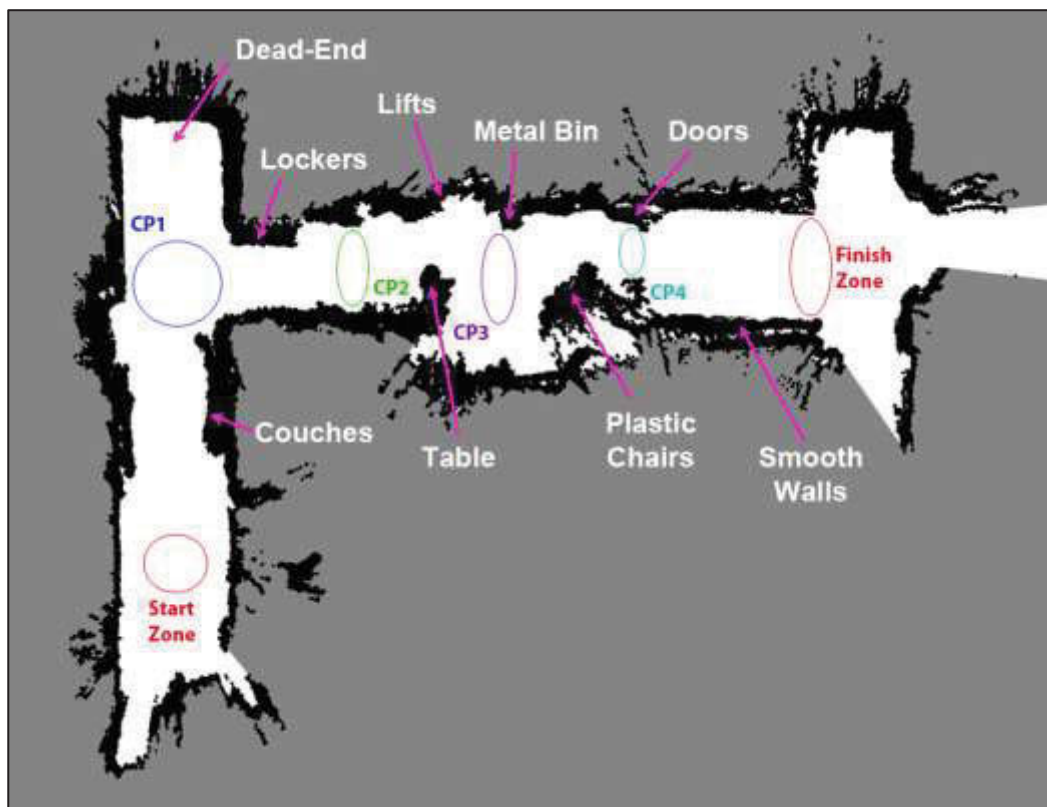
Figure 5-16: „Static Course" Experimental Study Map with Check Point Zones

Figure 5-17: „Static Course" Experimental Study Setup: TIM Smart Wheelchair at the Start Zone
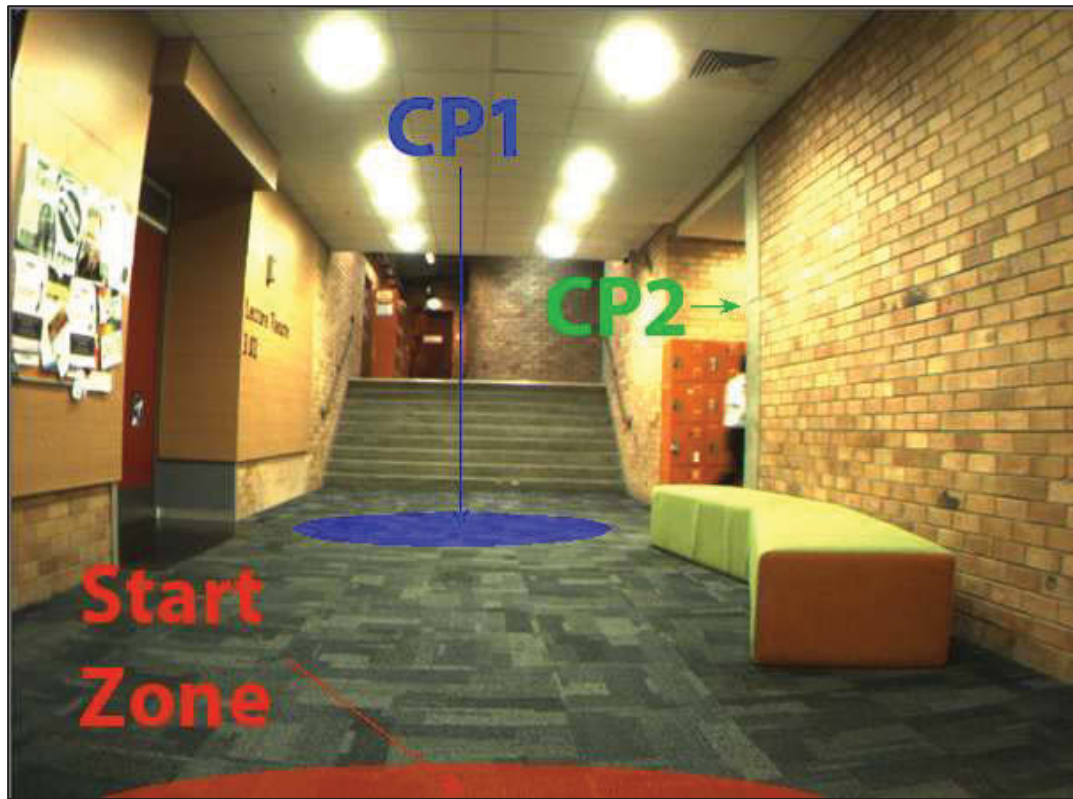
Figure 5-18: „Static Course" Experimental Study Setup: Start Zone to CP1
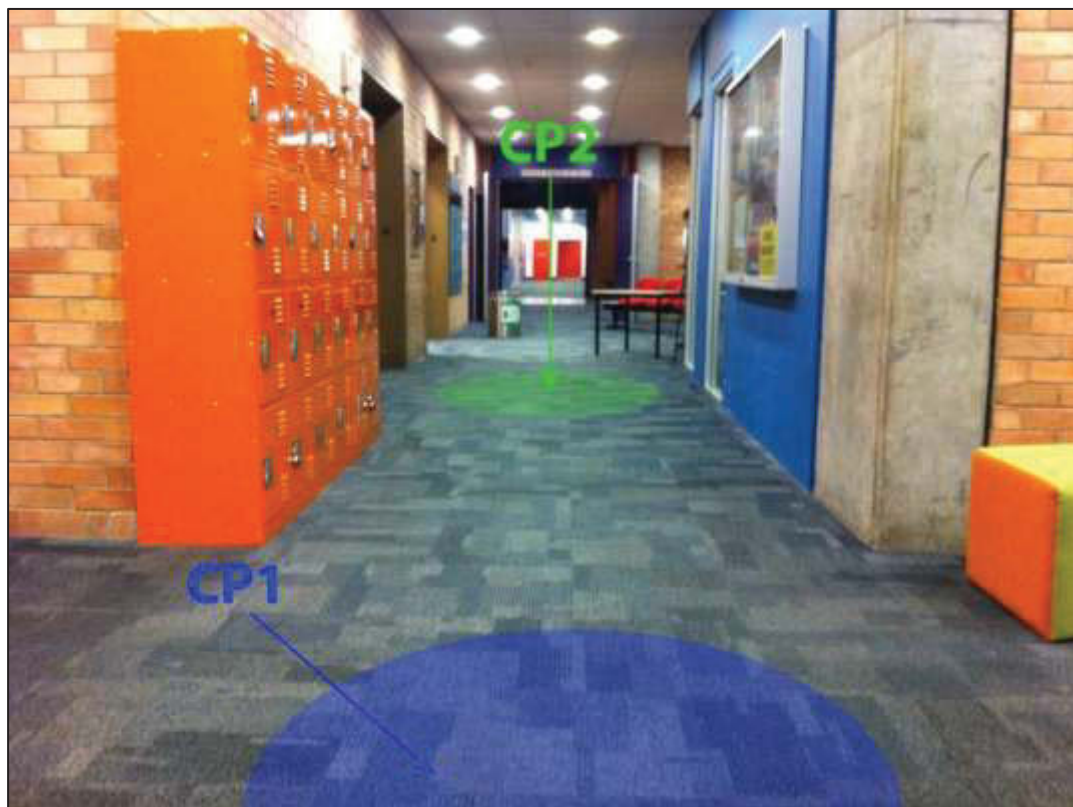
Figure 5-19: Experimental Study Setup: CP1 to CP2

Figure 5-20: Experimental Study Setup: CP2 to CP3 to CP4
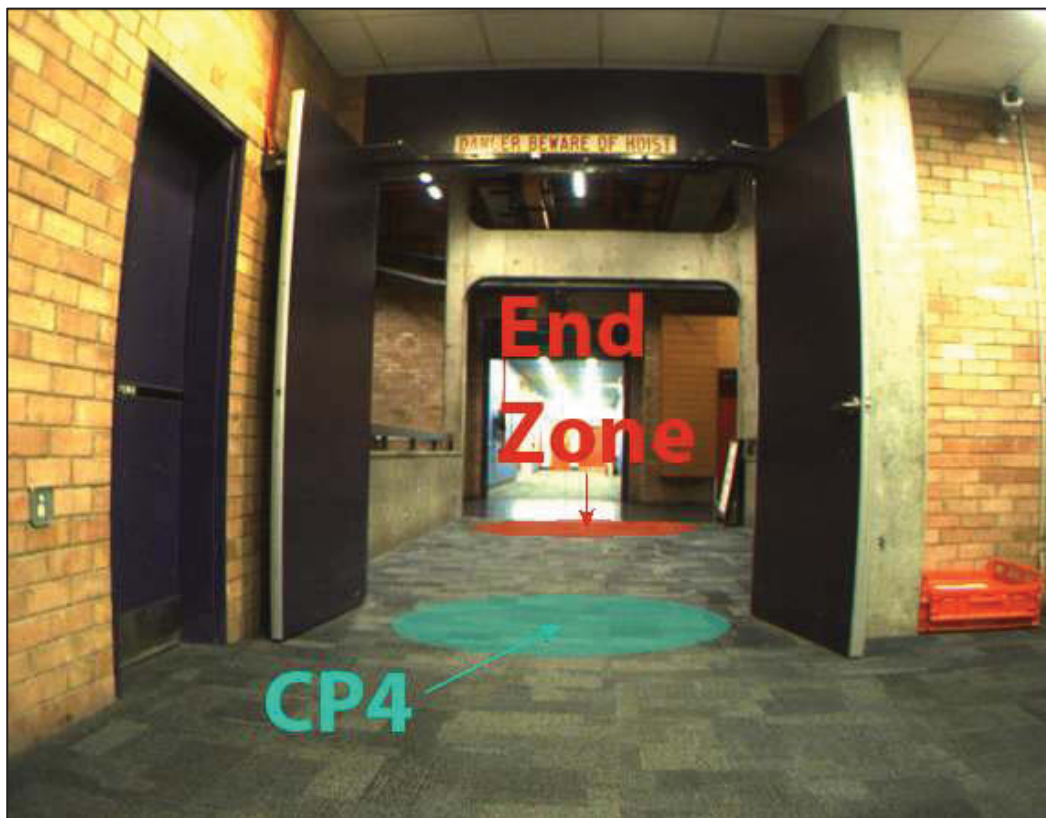
Figure 5-21: Experimental Study Setup: CP4 to End Zone
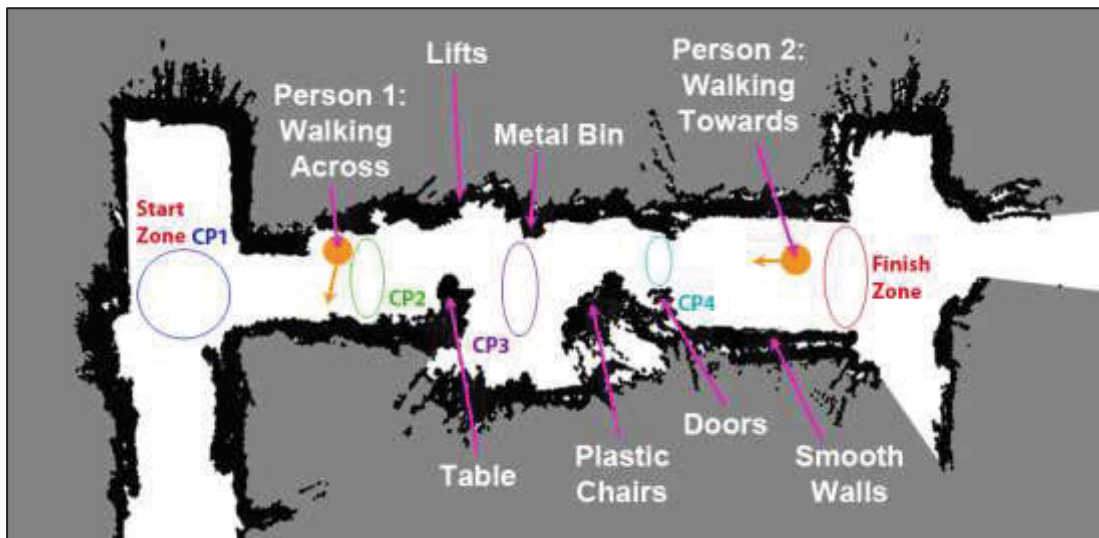
Figure 5-22: „Dynamic Course" Experimental Study Map with Check Point Zones

5.6 Results

The results in this section come from the preliminary testing of the advanced TIM-VPH real-time obstacle avoidance system in varying environment types. This has the purpose of assessing the algorithms in the types of environments likely to be encountered by the wheelchair, and assists in the process of testing leading up to experimental study. The second part of this results section focusses on the experimental studies conducted on 10 participants, and the analysis resulting from these tests.

5.6.1 Advanced Real-time Obstacle Avoidance System

Once optimised and implemented, the advanced real-time obstacle avoidance system proved useful for automated guidance in unknown environments. The process of obstacle-avoiding direction and speed selection, described by Equations 5.1 to 5.12, allow candidate directions to be produced and the most appropriate selected at any instant in time, given the local environment map data and the prior navigational decisions made.

When the wheelchair was set up in an office environment, the TIM-VPH polar histogram, shown in aqua in Figure 2-23, was produced when moving past a wall to the left, a board to the right, and toward the edge of a desk next to free space up ahead. Based on the velocity of the wheelchair and the current heading direction, the threshold function plotted in pink was

also produced. The TIM-VPH binary histogram is then created as a result of the polar histogram and threshold function, whereby any polar histogram angle with a distance-to-object value higher than that of the threshold function value for that angle becomes a candidate direction for travel, whereas all other angles become blocked off for that instant. The binary histogram is allocated a value of *H=1* for each angle that is a candidate for travel and *H=0* for each angle blocked off. These candidate angles range from right (0º) to directly ahead (90º) to the left (180º).
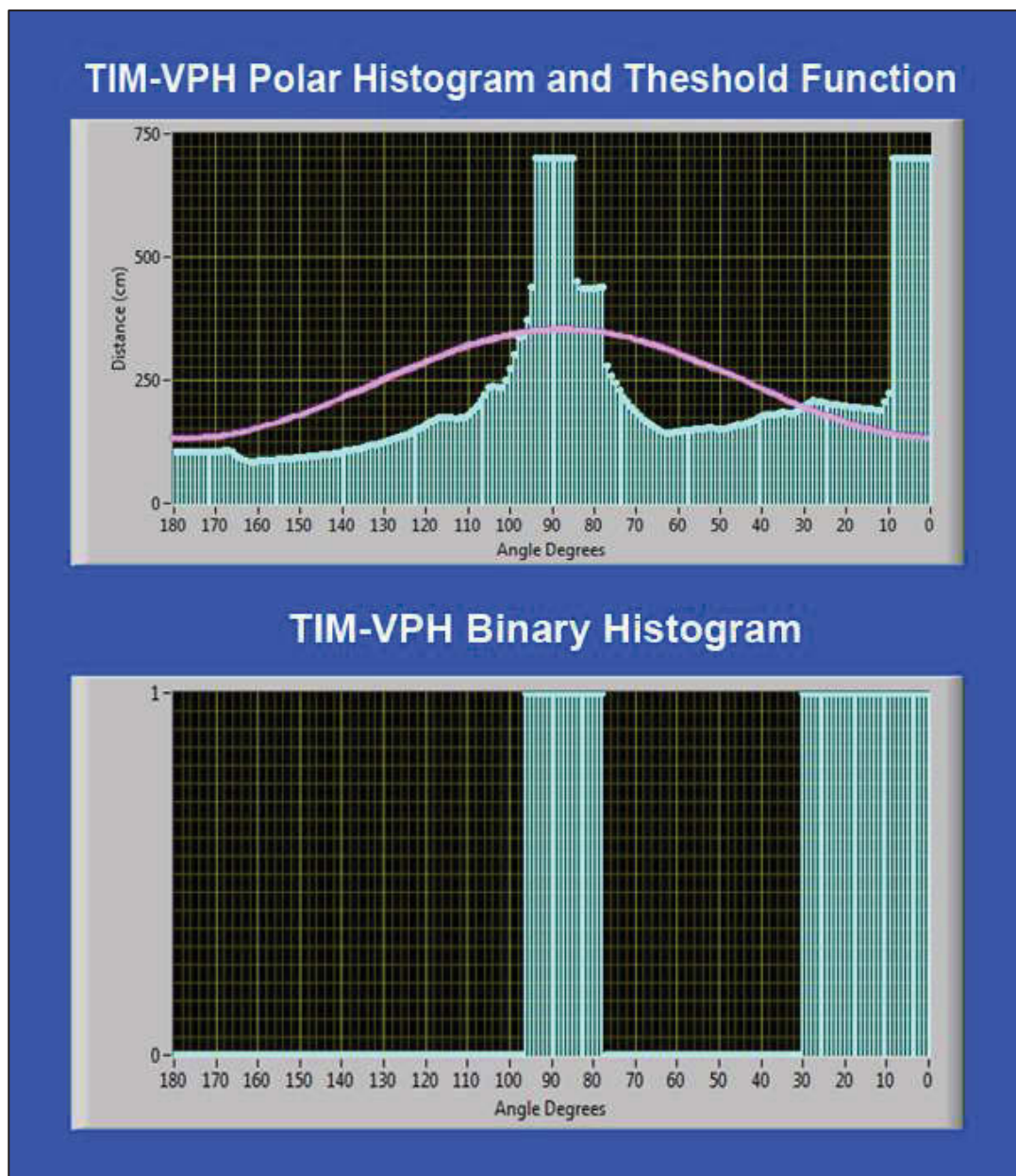
Figure 5-23: Creation of TIM-VPH Binary Histogram from Polar Histogram with Threshold Function

These obstacle avoidance algorithms were tested for real-time operation in a cluttered university office environment, a hospital / rehabilitation centre corridor environment, and a highly-dynamic open university environment. This was done to perform testing in a range of situations this smart wheelchair could potential encounter.

Cluttered University Office Space

The first test was in a cluttered office space where the wheelchair was provided a single forward command via the touchscreen. It was then required to use this command and safely navigate as far as possible around all obstacles in the path. When there is no more space available to move, the TIM wheelchair was then also required to realise this fact and stop.

Figure 5-24: Photos of Cluttered University Office Space Obstacle Avoidance Test

Chapter 5: Real-time Operational Performance of a Hands-free Smart Wheelchair System
using a Unique Camera Configuration Biologically Inspired by Equine Vision

224

In this test the wheelchair passed right around a board (photos 1 and 2 in Figure 5-24), then had to weave left around two desk chairs (photos 3 and 4 in Figure 5-24), manoeuvre in between a couch and the wall (photo 5 in Figure 5-24), and past a TV on a wall before stopping in a corner once the options for travel have run out (photo 6 in Figure 5-24). The map resulting from this obstacle avoidance test is displayed in Figure 5-25.
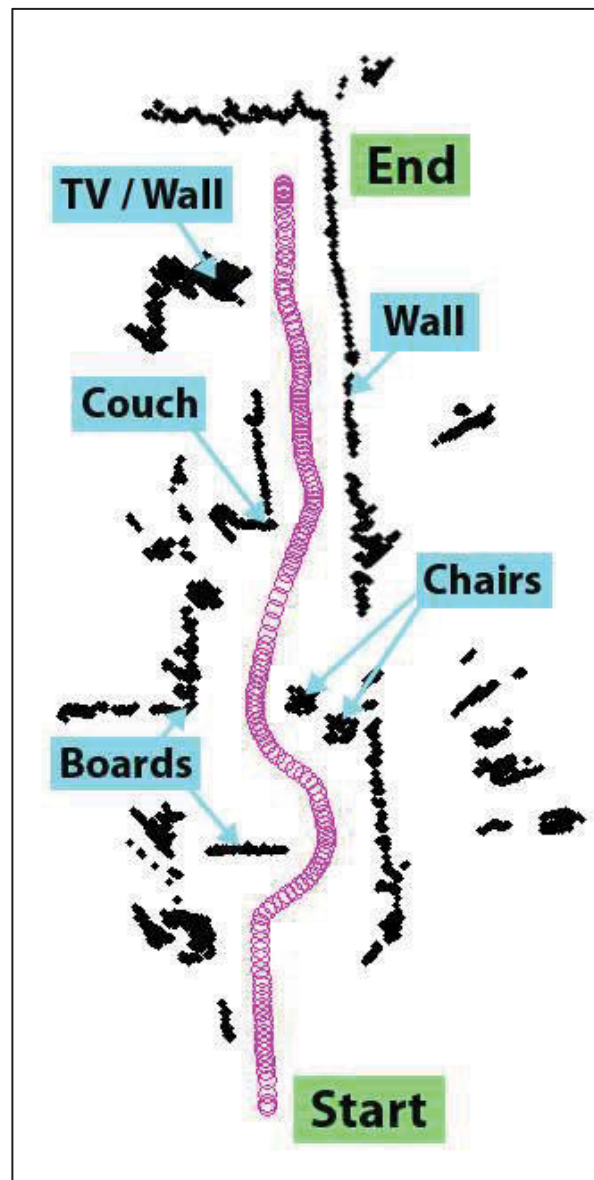
Figure 5-25: Map Produced from University Office Space Obstacle Avoidance Test

This test proved positive in the ability of the obstacle avoidance algorithms to allow the TIM wheelchair to automatically weave around obstacles and safely navigate in a cluttered office space. The average velocity in this test was 1.74km/hr.

Hospital / Rehabilitation Centre Corridor Environment

This obstacle avoidance test was conducted at the Royal Rehabilitation Centre, Sydney (RRCS). The corridors in this centre are an adequate example of typical hospital and rehabilitation centre corridor environments. Figure 5-26 shows photos of the Rehabilitation Studies Unit (RSU) in the RRCS where this testing of TIM"s automated guidance system was conducted.

Figure 5-26: Photos of the RSU at the Royal Rehabilitation Centre, Sydney; and Corridor Testing

In these tests the wheelchair was provided commands via direct touchscreen input into the TIM software programs, simulating hands-free commands. At this early stage in testing, the wheelchair had to be stopped and rotated when multiple directions were present. Starting at the front entrance to the RSU, the wheelchair was provided a forward command where it was then required to automatically navigate around a wall edge and down a short corridor. When it reached the top of a T-intersection it was then provided a stop command, rotate left 90º command, and then another forward command to take it down a longer corridor stretch, where it was required to automatically avoid a static cleaner"s trolley, static rubbish bin, and lastly, a

dynamic person obstacle travelling in the opposite direction to one side of the narrow corridor.

The first run was carried out using a typical power wheelchair joystick controller (dotted aqua line in Figure 5-27) to record for comparison the way this course would likely be navigated by a user able to control the joystick. The test runs then allowed the automated navigation system to operate given the computer commands (red path in Figure 5-27). This 5-minute test was conducted 10 times for repeatability (the first is displayed in Figure 5-27), where results in all cases were positively similar and no collisions were made. The wheelchair consistently passed obstacles with a reasonable smoothness in the manoeuvres, and over the course of all 10 tests maintained an average velocity of 1.95km/hr.
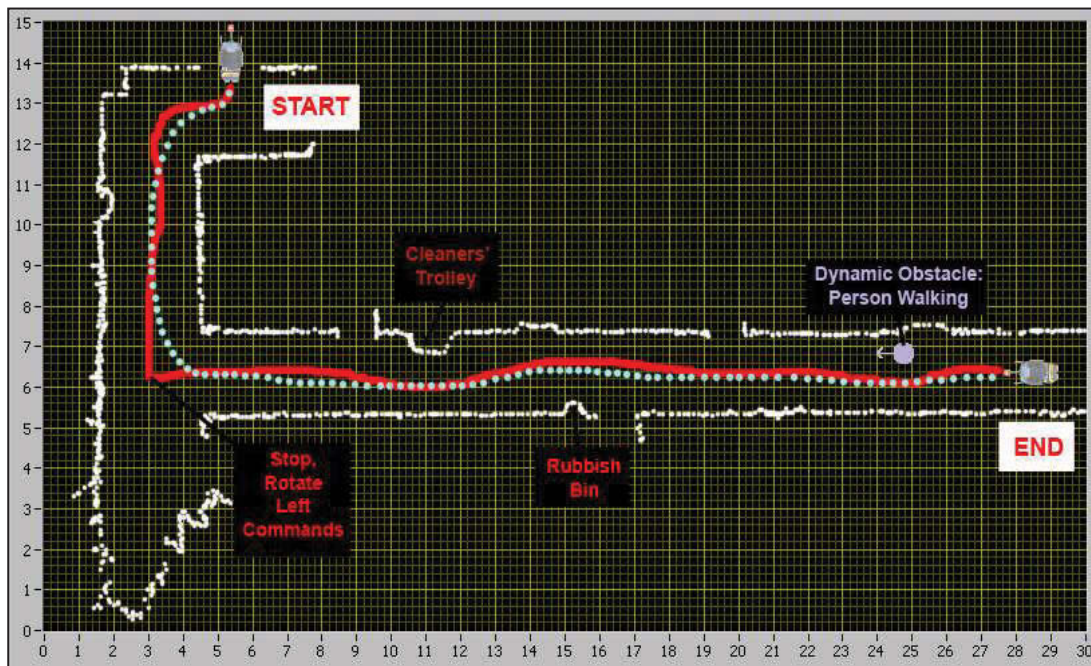
Figure 5-27: Obstacle Avoidance Corridor Test at the Royal Rehabilitation Centre, Sydney

This preliminary testing showed that the wheelchair could handle basic obstacle avoidance in fairly narrow hospital / rehabilitation centre corridor environments. However, it was soon realised that the stopping and rotating for such turns as right-angle turns is inefficient and needed to be resolved. The option to select turns on the fly was then implemented after this set of testing by simply changing the control options in the TIM software programs, whereby any command to change direction would set a new target goal direction and the wheelchair would immediately attempt to navigate in that new direction.

Open and Highly-dynamic University Environment

This set of experiments were conducted at the University of Technology, Sydney (UTS) in the main area of the tower building during peak lunch hours when there were many people walking around. The aim of these experiments were to test the performance of TIM˝s assistive guidance capabilities when navigating through a crowded and highly dynamic environment from one area to another, past pre-defined checkpoints, whilst being controlled via hands-free control technology. For these experiments, the BCI system intended for use in the experimental study was personally tested for control through EEG signal classifications. Since being an experienced user of the personally designed BCI, this became a run-through test of the hands-free technology in combination with the obstacle avoidance system. A drawn map of the area with the checkpoints and paths taken are shown in Figure 5-28.
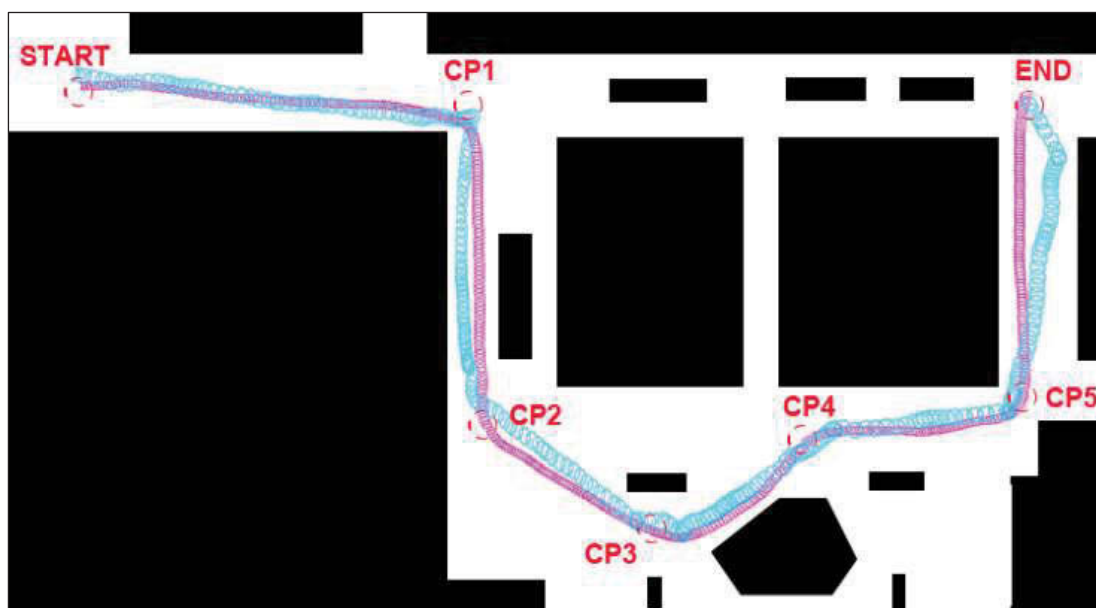
Figure 5-28: University Testing Map: Joystick Control (Pink) vs BCI+TIM (Blue) Paths Executed

From the Start point to the End point, there were five other checkpoints (CP1-CP5) that had to be passed along the way as displayed in Figure 5-28. This was first run using a conventional joystick to control the power wheelchair (pink path in Figure 5-28) with a consistent speed of V_{max} (from Equation 5.12 of §5.4) for comparison purposes. For this joystick run the total distance travelled was about 110m, completed in a total time of 182seconds. This produced an average speed of 2.18km/hr.

Chapter 5: Real-time Operational Performance of a Hands-free Smart Wheelchair System
using a Unique Camera Configuration Biologically Inspired by Equine Vision

228

Figure 5-29: Photos of Open and Highly-dynamic University Environment Obstacle Avoidance Test

The 8 system tests were then conducted, using the BCI for control and TIM''s navigational guidance (BCI+TIM), with the first of these runs being displayed, for comparison against the joystick test, as the blue path in Figure 5-28. Completion times varied, mostly due to the changing crowd density (Figure 5-29) as TIM slowed down and consumed more time when avoiding people in crowded areas. Times of travel between the set check points are displayed in Table 5-1.

Test Run: J = Joystick, Others = BCI+TIM Run Number								
J	1	2	3	4	5	6	7	8
Total Time (sec)	182	212	227	198	206	219	210	214	191
Avg Speed (km/hr)	2.18	1.87	1.74	2.00	1.92	1.81	1.89	1.85	2.07

Table 5-1: Total Time and Average Velocity for University Environment Obstacle Avoidance Tests

Overall, however, the use of BCI in shared-control with TIM''s navigational guidance took an average of 209.63 seconds across the 8 test runs, which only amounted to about 15% more time than the time taken to complete the course using the conventional joystick (Table 5-1). These results were positive and the TIM smart wheelchair was then put into an experimental study to test the performance with a range of participants.

5.6.2 Experimental Study Results

To evaluate the performance of the TIM smart wheelchair, the two difference experimental study tests were setup and conducted, being the Static Course and the Dynamic Course. In addition these were each run using the HMC and BCI separately as the control methods. Each experiment required different skills and levels of control from both the user and TIM. Eight able-bodied (AB) participants and two non-able-bodied (Non-AB) participants were asked to complete as many of the tests as possible. For the AB participants, there were four males and four females, aged from 21 to 56, and for the Non-AB participants, there were two males, aged 20 and 33. Across all participants the mean age ± standard deviation (SD) was found to be 30.3 ± 11.3. All AB participants had no prior experience using wheelchairs, and both Non-AB participants are full-time wheelchair-users.

	Participant Details									
Participant #	1	2	3	4	5	6	7	8	9	10
Gender	Male	Female	Male	Male	Female	Female	Male	Female	Male	Male
Age	24	23	45	34	23	56	21	24	20	33
AB / Non-AB	AB	AB	AB	AB	AB	AB	AB	AB	Non-AB	Non-AB
Disability Level	N/A	N/A	N/A	N/A	N/A	N/A	N/A	N/A	C6-C7	C6-C7
Trial Courses Completed (Y/N)										
HMC Only Static	Y	Y	Y	Y	Y	Y	Y	Y	Y	N
HMC+TIM Static	Y	Y	Y	Y	Y	Y	Y	Y	Y	Y
BCI Only Static	Y	N	N	N	N	N	N	N	Y	N
BCI+TIM Static	Y	Y	Y	Y	Y	Y	Y	Y	Y	Y
HMC Only Dynamic	Y	Y	Y	Y	Y	Y	Y	Y	Y	N
HMC+TIM Dynamic	Y	Y	Y	Y	Y	Y	Y	Y	Y	Y
BCI+TIM Dynamic	Y	Y	Y	Y	Y	Y	Y	Y	Y	Y

Table 5-2: Experimental Study: Basic Clinical and Demographic Characteristics of Participants

5.6.2.1 'Static Course' Test Results

Head-movement Controller (HMC) Hands-free Control System

The Static Course was run using the HMC system for control, and automated guidance assistance from TIM. If able to be controlled well, the user could then opt to also repeat the test with the HMC only, and no automated guidance assistance from TIM. This was also the case with the BCI system, first run with the assistance from TIM and then a few participants were asked to repeat the test again without assistance for basic comparisons. Example results will be displayed for Participant 9, who is Non-AB, being tetraplegic C-6 to C-7, meaning he is a wheelchair-user with paralysis of legs and part of wrists and hands, little finger-dexterity, but relatively preserved shoulder and elbow movement.

Figure 5-30: Participant 9 (Non-AB) Static Course using HMC Only Map

Figure 5-31: Participant 9 (Non-AB) Static Course using HMC+TIM Map
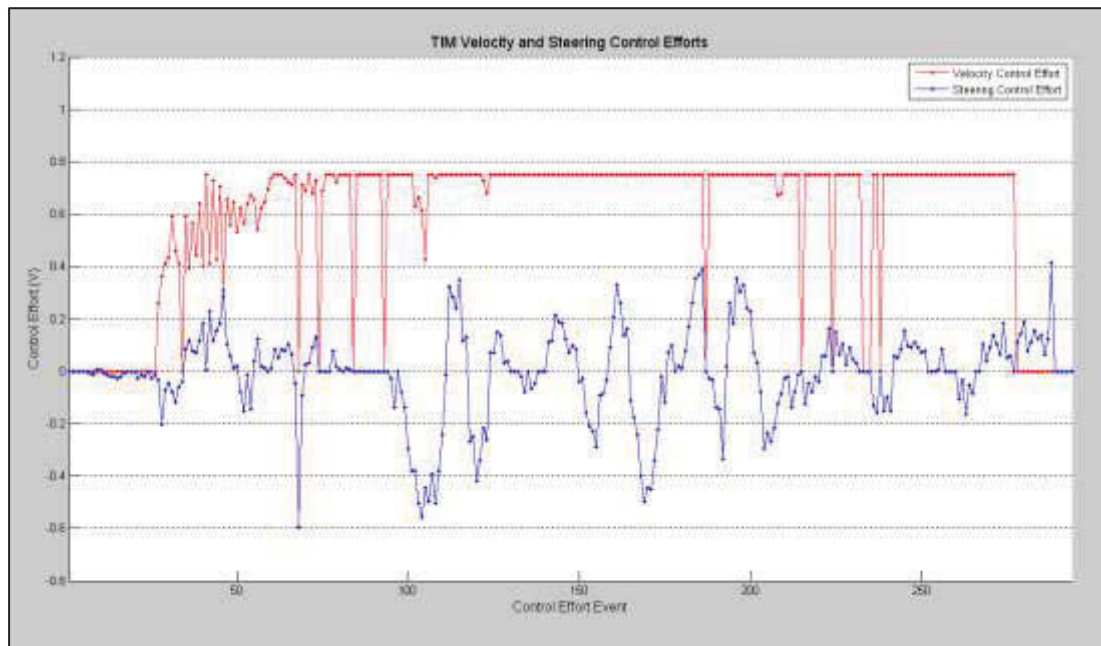
Figure 5-32: Participant 9 (Non-AB) Static Course using HMC Only Control Efforts
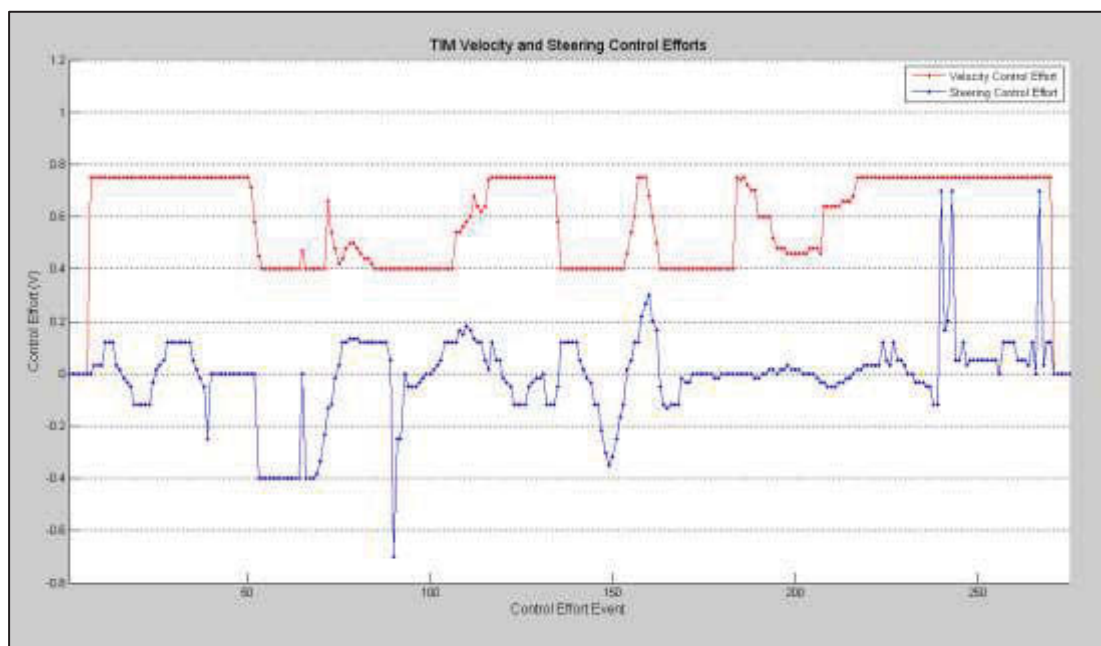
Figure 5-33: Participant 9 (Non-AB) Static Course using HMC+TIM Control Efforts

In both of these test examples, Participant 9 performed well with reasonably smooth control in the HMC Only run. Apart from the slightly late command input for the first right turn in the HMC+TIM, this run was even smoother, evident in the differences between the control efforts graphs shown in Figure 5-32 and Figure 5-33. The HMC Only Static Course run took this

participant 74.4 seconds to complete, whereas the HMC+TIM Static Course took 8.6 seconds less time, at 65.8 seconds.

The average times taken for both participant groups (AB and Non-AB) between each check point in the Static Course using HMC Only and HMC+TIM controls, along with the control run of joystick only are all shown in Figure 5-34. In these Static Course results graphs, the Start Zone is represented by 0 on the check point number, the time taken from there to CP1 is represented at 1, CP1 to CP2 represented by 2, and so on till the CP4 to the End Zone represented at 5. The results were more consistent between the participant groups during the presence of automated guidance assistance from TIM. On average the Non-AB participant group, being wheelchair-users, were able to complete every checkpoint in the course faster than the AB group when using the HMC Only control, which is expected due to their advantage in wheelchair manoeuvring experience.
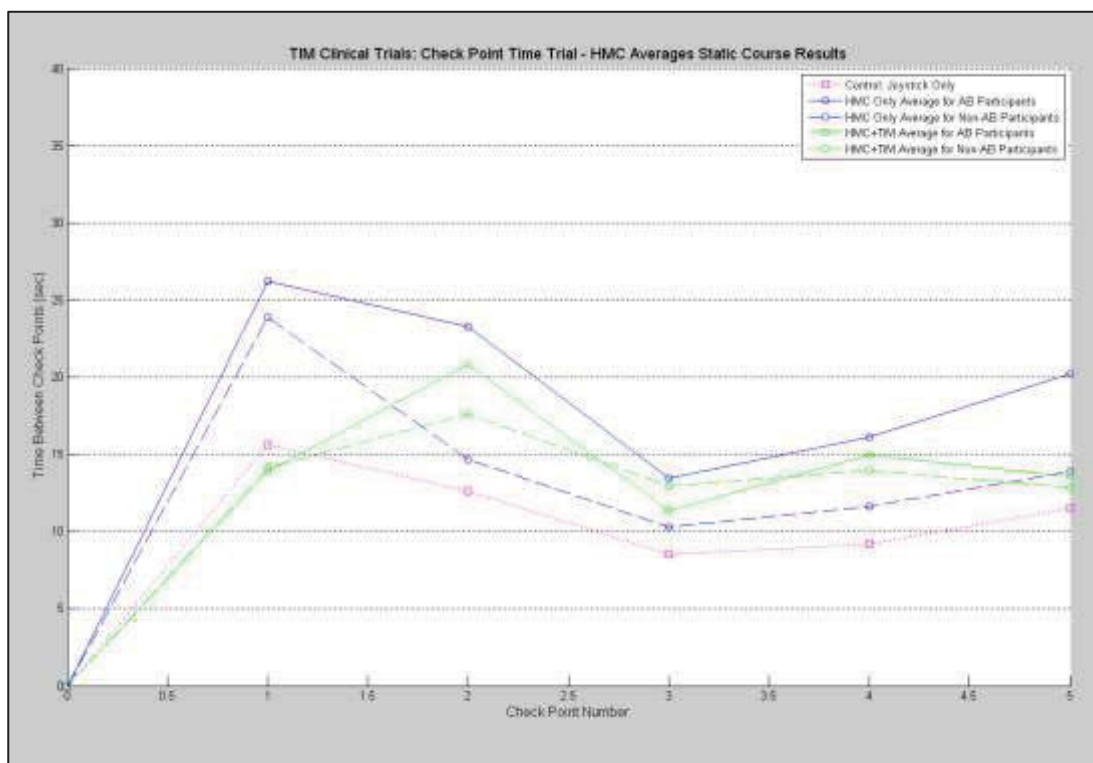
Figure 5-34: Static Course using HMC Results – Check Point Time Averages by Participant Groups

As shown in Figure 5-35, the run from the Start Zone to the CP1 checkpoint was on average performed fastest with HMC+TIM, even beating the Joystick Only control run for that leg. After this CP1 checkpoint obstacles and manoeuvres create a challenge to both the HMC Only and HMC+TIM approaches. On average, however, the automated guidance assistance

from TIM in the HMC+TIM control method provides consistently faster performance between all checkpoints than the HMC Only control method.
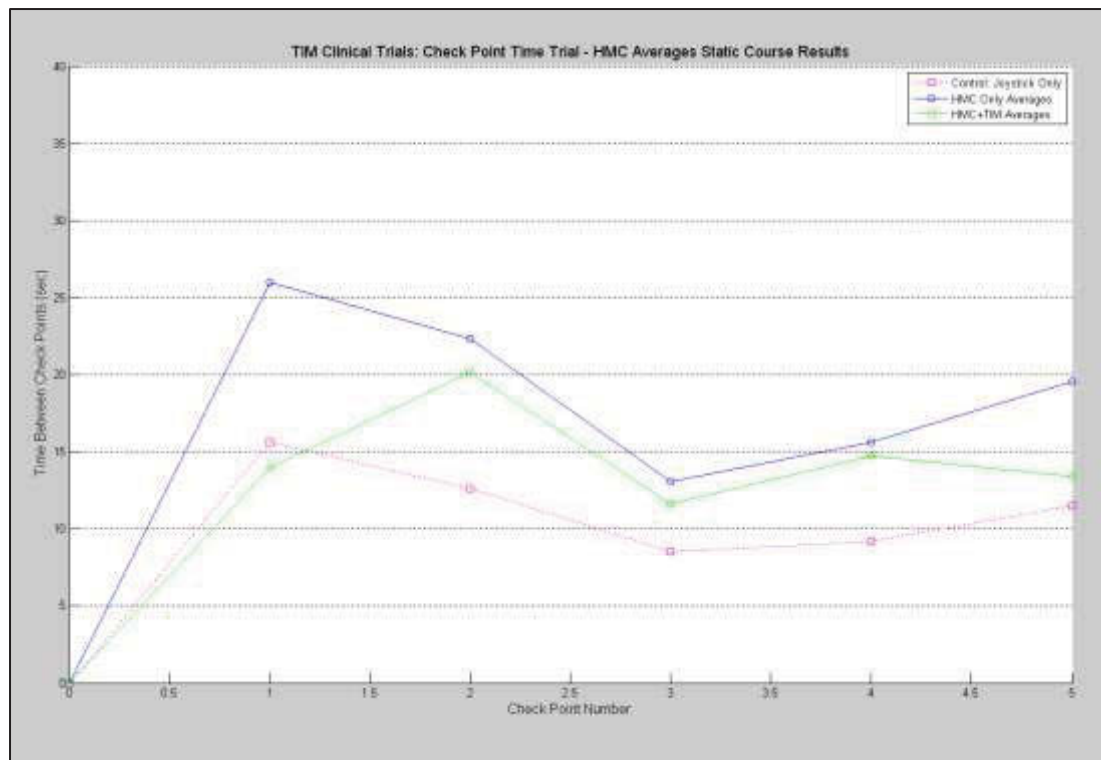
Figure 5-35: Static Course using HMC Results – Check Point Time Averages

Brain-computer Interface (BCI) Hands-free Control System

The Static Course was then run using the BCI system as the hands-free control method. Due to the fact that this system is reasonably simple to use with the assistance of TIM but not so easy to use in real-time without the assistance, only one AB participant and one Non-AB participant undertook the Static Course using BCI Only, and whenever there were any impending collisions the wheelchair was emergency stopped by a test facilitator and manually moved to face away from the collision point and back onto the test path, before continuing with the test.

Since Participant 9 (Non-AB) completed the BCI+TIM and gained fast control over the interface, he was asked to also complete the BCI Only test. The results for this participant are again shown as examples here for the Static Course tests using the BCI hands-free control system.

Chapter 5: Real-time Operational Performance of a Hands-free Smart Wheelchair System
using a Unique Camera Configuration Biologically Inspired by Equine Vision

234
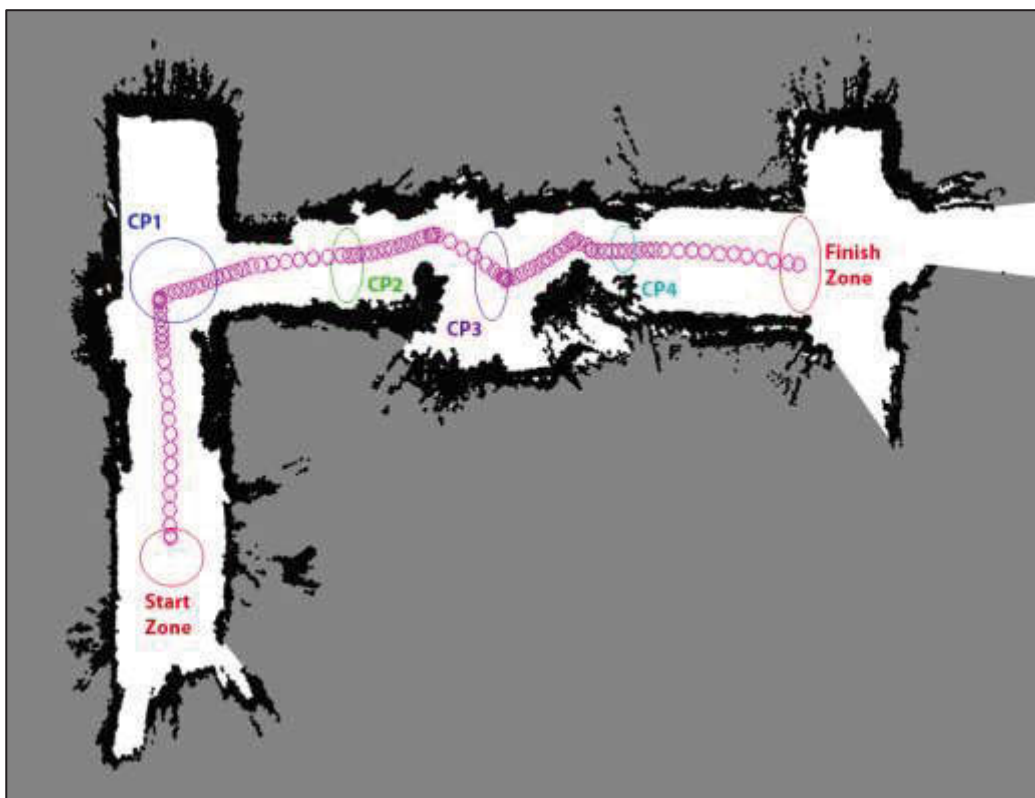
Figure 5-36: Participant 9 (Non-AB) Static Course using BCI Only Map
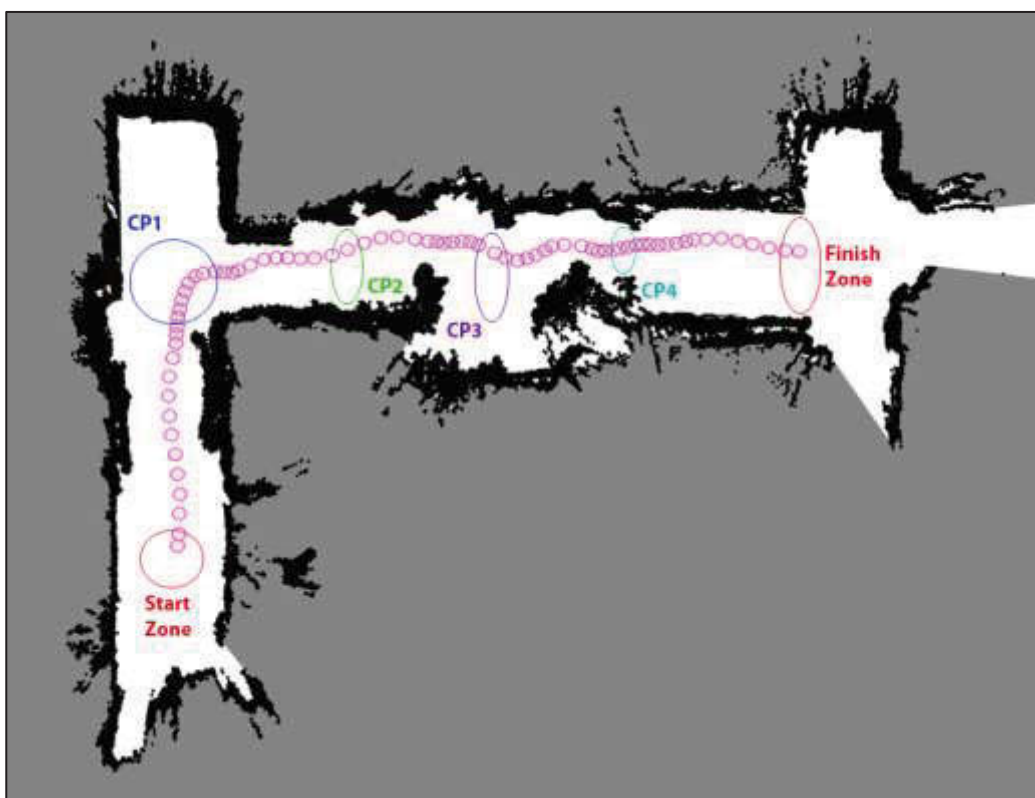
Figure 5-37: Participant 9 (Non-AB) Static Course using BCI+TIM Map
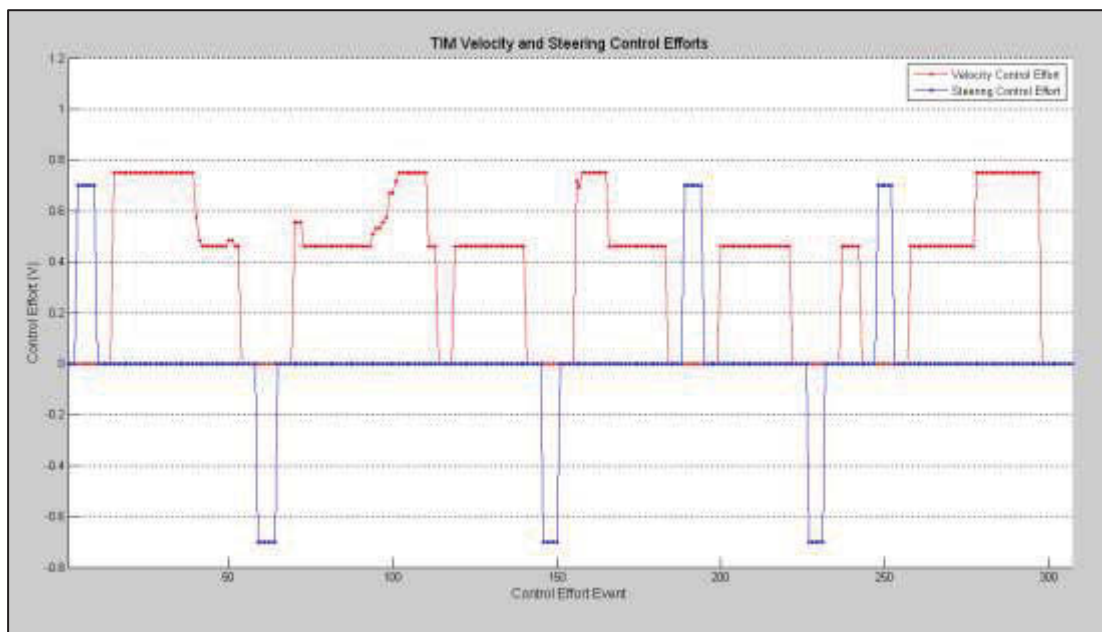
Figure 5-38: Participant 9 (Non-AB) Static Course using BCI Only Control Efforts
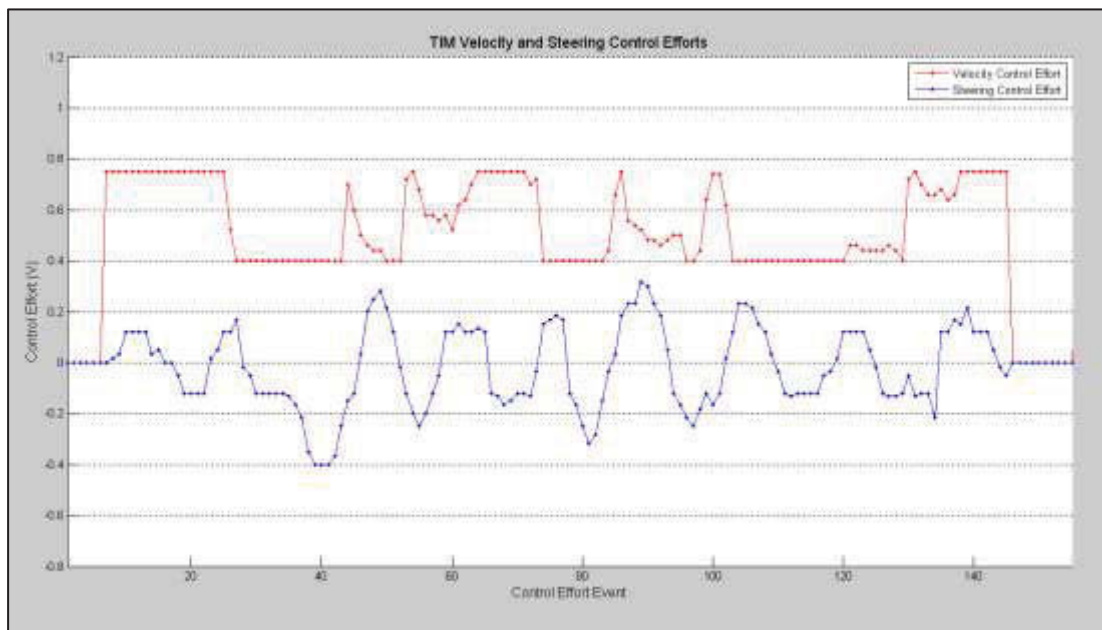
Figure 5-39: Participant 9 (Non-AB) Static Course using BCI+TIM Control Efforts

In both of these test examples, Participant 9 performed had a good level of control over the BCI hands-free control system. The BCI+TIM run was much smoother, evident in the differences between the control efforts graphs shown in Figure 5-38 and Figure 5-39, where the BCI Only run was attempted to be used safely with only forward or turning movements made independently and stops made in between each. The BCI Only Static Course run took

this participant 230.4 seconds to complete, whereas the BCI+TIM Static Course took considerably less time, at 69.8 seconds.

The average times taken for both participant groups (AB and Non-AB) between each check point in the Static Course using BCI Only and BCI+TIM controls, along with the control run of joystick only are all shown in Figure 5-40. The results were much more consistent between the participant groups during the presence of automated guidance assistance from TIM (BCI+TIM), where the average results were almost exactly the same for each check point between the groups.

Figure 5-40: Static Course using BCI Results – Check Point Time Averages by Participant Groups

As shown in Figure 5-41, the run from the Start Zone to the CP1 checkpoint was, similar to the HMC+TIM, on average performed fastest with BCI+TIM, again beating the Joystick Only control run for that leg. After this CP1 checkpoint obstacles and manoeuvres similarly create a challenge to both the BCI Only and BCI+TIM approaches. On average, however, the automated guidance assistance from TIM in the BCI+TIM control method provides consistently and considerably much faster performance between all checkpoints than the BCI Only control method.

Figure 5-41: Static Course using BCI Results – Check Point Time Averages

Overall 'Static Course' Results

Combining all this check point break-down data found from the Static Course tests using HMC Only, HMC+TIM, BCI Only, and BCI+TIM control approaches, the overall test times are displayed in Table 5-3. The mean completion times, standard deviation, with minimum and maximum error bar ranges, for each control mode are further displayed in Figure 5-42.

Participant	HMC Only	HMC+TIM	BCI Only	BCI+TIM
1	87.4	70.3	249.2	77.0
2	97.4	73.6		76.0
3	90.1	80.9		74.5
4	110.5	67.8		72.8
5	101.3	75.9		81.7
6	106.6	78.8		79.1
7	99.1	73.1		81.5
8	101.9	76.0		76.5
9	74.4	65.8	230.4	69.8
10		77.1		81.3
Mean	96.52	73.93	239.80	77.02
SD	10.38	4.56	9.40	3.77
Min	74.4	65.8	230.4	69.8
Max	110.5	80.9	249.2	81.7

Table 5-3: Static Course Overall Total Time Results (Seconds)
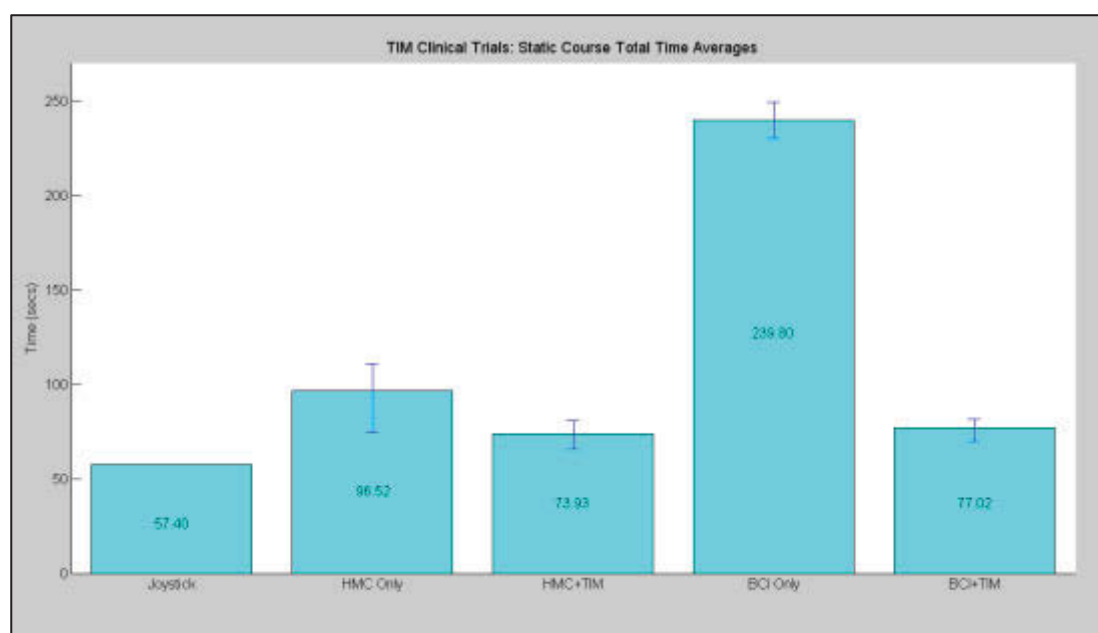
Figure 5-42: Static Course Total Time Averages for All Control Modes

The graph data displayed in Figure 5-42 shows that total average test times for control modes using the automated guidance of TIM (HMC+TIM and BCI+TIM) were very similar and featured low time variance between the two relevant control modes, as well as between the individual tests in each, evident in the small variation ranges of ±7.55 seconds and ±5.95 seconds, respectively. On average the BCI Only test was considerably slower and found to be more difficult than all other tests. The HMC Only test took on average 21.045±1.545 seconds longer than both of the TIM-assisted control mode tests, and also had a larger variation range of ±18.05 seconds.

Further results from the tests were found in the process of test facilitator interventions in the cases of impending collisions. No events requiring collision intervention occurred during the TIM-assisted control mode tests, however, two collision intervention events occurred over two separate HMC Only tests, and two collision intervention events occurred during one of the BCI Only tests.

5.6.2.2 'Dynamic Course' Test Results

Head-movement Controller (HMC) Hands-free Control System

The Dynamic Course was run in a similar sequence fashion to the Static Course. Example results for Participant 9 (Non-AB) are again displayed here. Control modes analysed are Joystick, HMC Only, HMC+TIM, and BCI+TIM. The BCI Only control mode was not safe enough for operation with people as obstacles so this was not conducted.
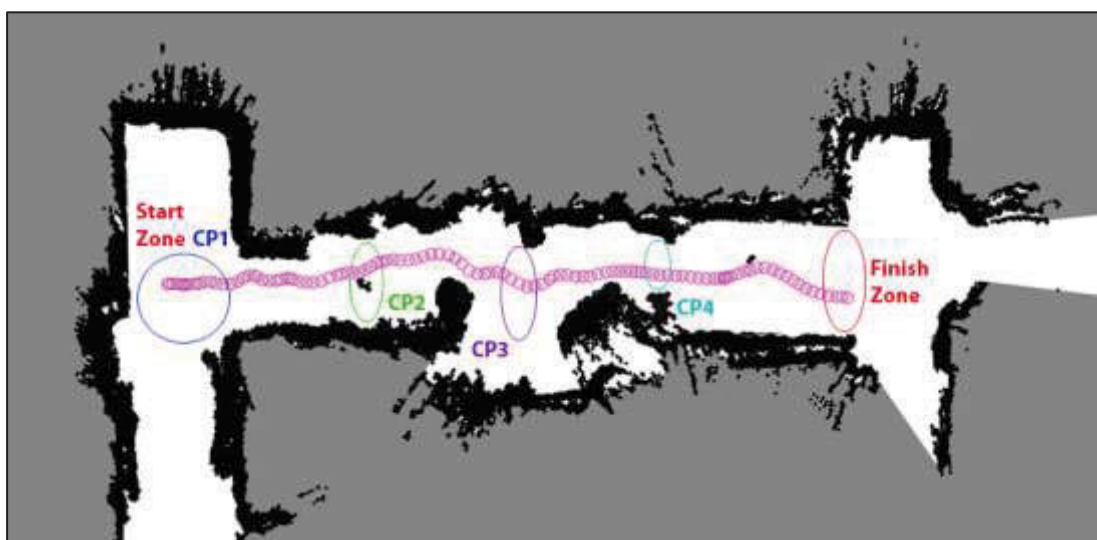
Figure 5-43: Participant 9 (Non-AB) Dynamic Course using HMC Only Map
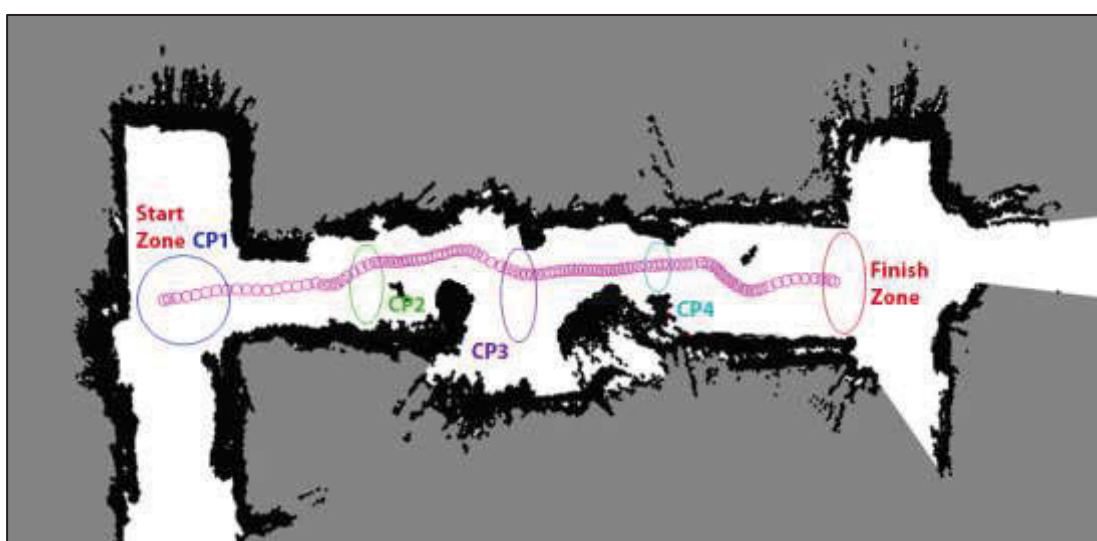
Figure 5-44: Participant 9 (Non-AB) Dynamic Course using HMC+TIM Map
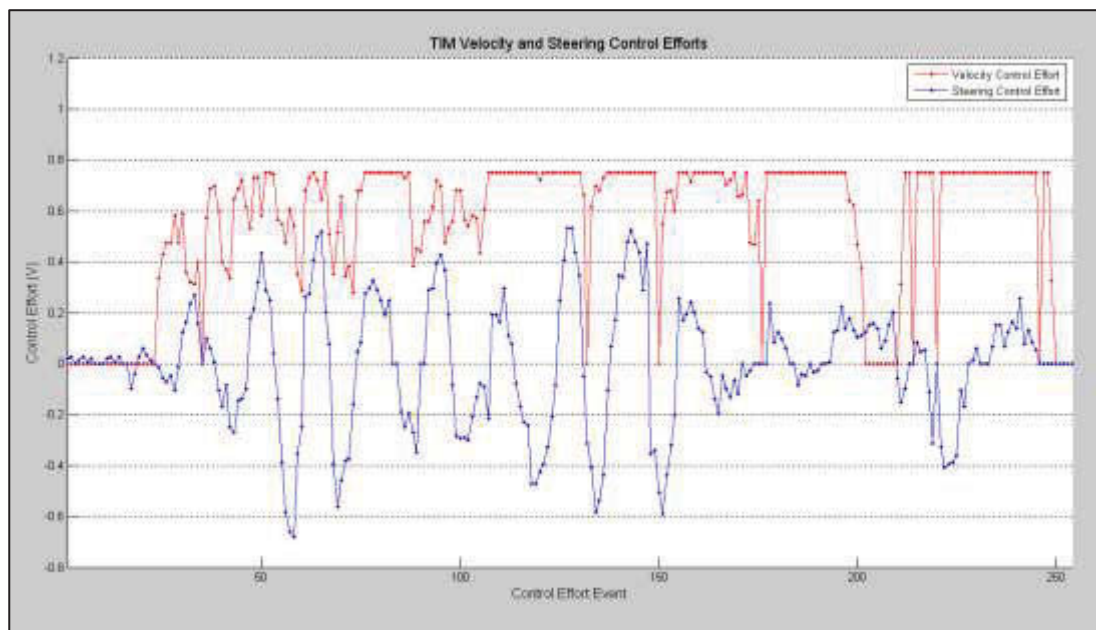
Figure 5-45: Participant 9 (Non-AB) Dynamic Course using HMC Only Control Efforts
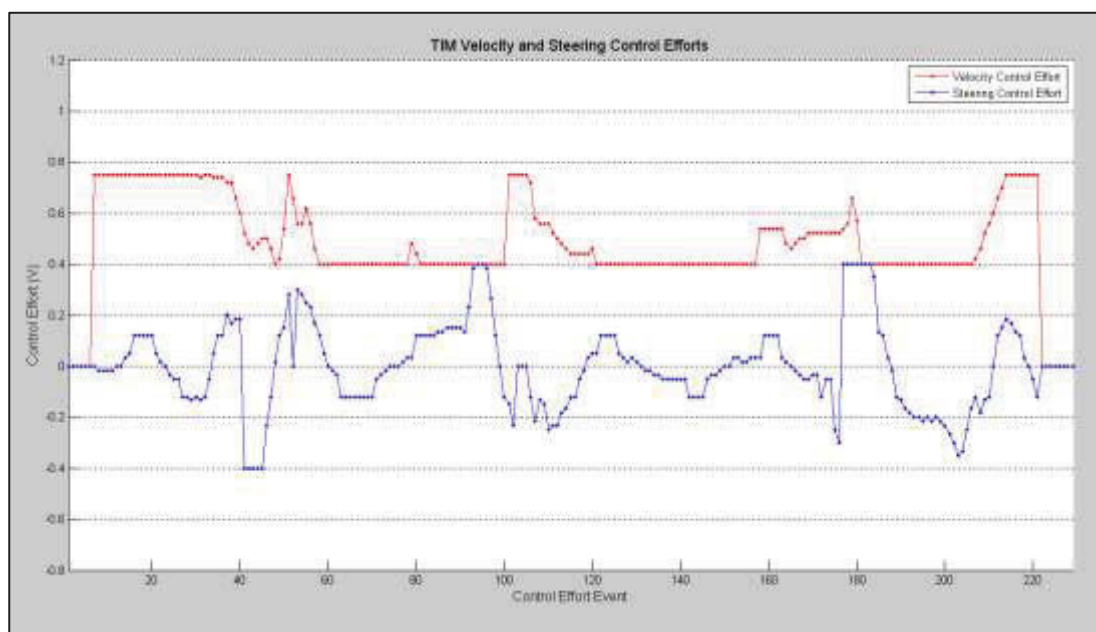
Figure 5-46: Participant 9 (Non-AB) Dynamic Course using HMC+TIM Control Efforts

Given the presence of dynamic moving people, both across the path of the wheelchair at CP2 and towards the wheelchair just after CP4 (which can be seen as the extra black dots on the produced maps in Figure 5-43 and Figure 5-44), this task was much more challenging for the participant when using HMC Only. The map in Figure 5-44 and the control efforts plots in Figure 5-46 can be seen to be much smoother with the assistance of TIM, where all the obstacles were avoided automatically and the participant did not need to issue any avoiding

commands. The HMC Only Static Course run took this participant 66.3 seconds to complete, whereas the HMC+TIM Static Course took 7.6 seconds less time, at 58.7 seconds.

The average times taken for both participant groups (AB and Non-AB) between each check point in the Dynamic Course using HMC Only and HMC+TIM controls, along with the control run of joystick only are all shown in Figure 5-47. The results were more consistent between the participant groups during the presence of automated guidance assistance from TIM. On average the Non-AB participant group, being wheelchair-users, were again able to complete most checkpoints in the course faster than the AB group when using the HMC Only control.
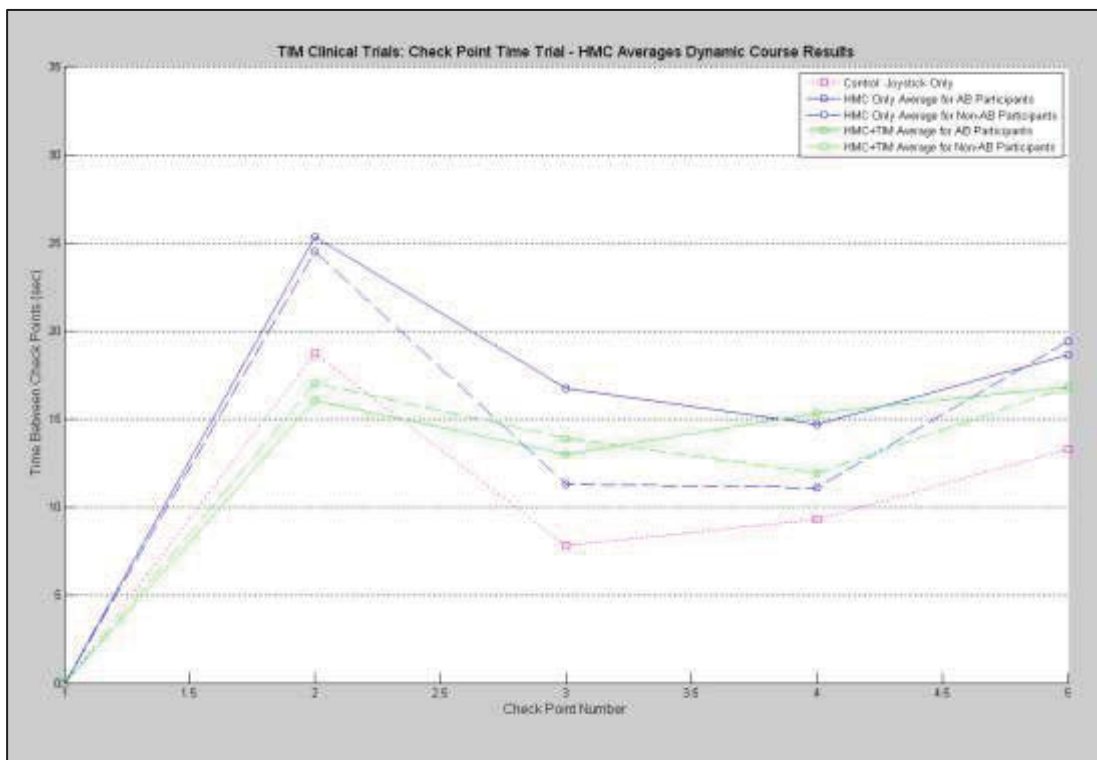
Figure 5-47: Dynamic Course using HMC Results – Check Point Time Averages by Participant Groups

As shown in Figure 5-48, the run from the Start Zone (CP1) to the CP2 checkpoint, on average, performed fastest with HMC+TIM. On average, the automated guidance assistance from TIM in the HMC+TIM control method provides faster performance between most checkpoints than the HMC Only control method, including the two areas where dynamic obstacles (people walking) were present.
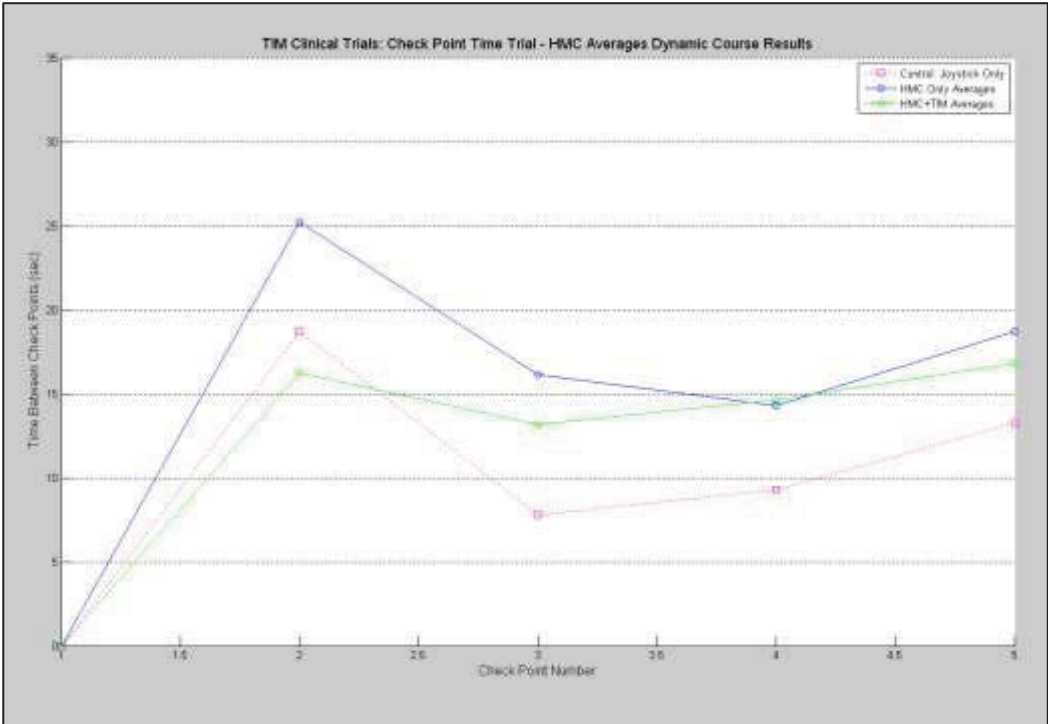
Figure 5-48: Dynamic Course using HMC Results – Check Point Time Averages

Brain-computer Interface (BCI) Hands-free Control System

The Dynamic Course was then run using the BCI system as the hands-free control method. Due to the fact people were walking in the path and the participants were unlikely to be able to manoeuvre the wheelchair quickly enough to avoid them when using BCI Only, this test was not conducted as it was not deemed safe enough, nor was it considered necessary.
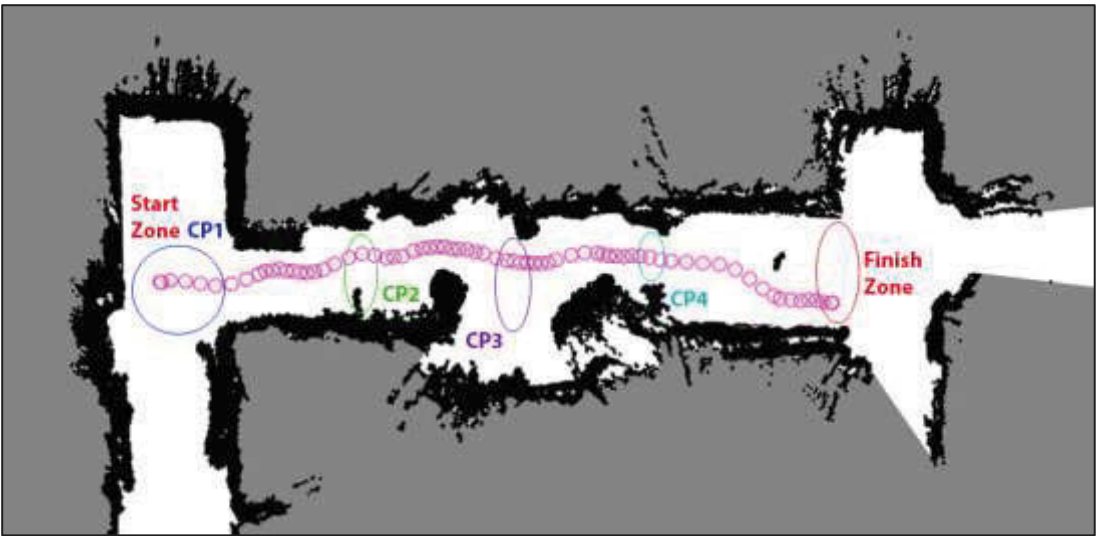
Figure 5-49: Participant 9 (Non-AB) Dynamic Course using BCI+TIM Map
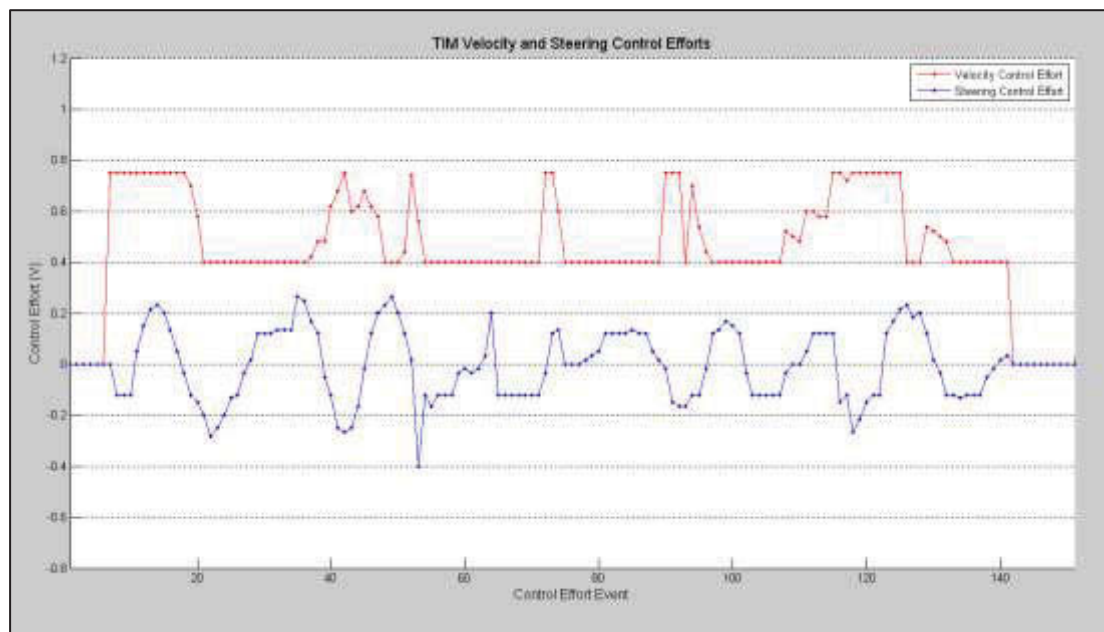
Figure 5-50: Participant 9 (Non-AB) Static Course using BCI+TIM Control Efforts

The BCI+TIM test for Participant 9 was a smooth run and only took 57.2 seconds. The average times taken for both participant groups (AB and Non-AB) between each check point in the Dynamic Course using BCI+TIM controls, along with the control run of joystick only are shown in Figure 5-51. The results were very consistent between the participant groups in the BCI+TIM tests, where the average results were again almost exactly the same for each check point between the groups.
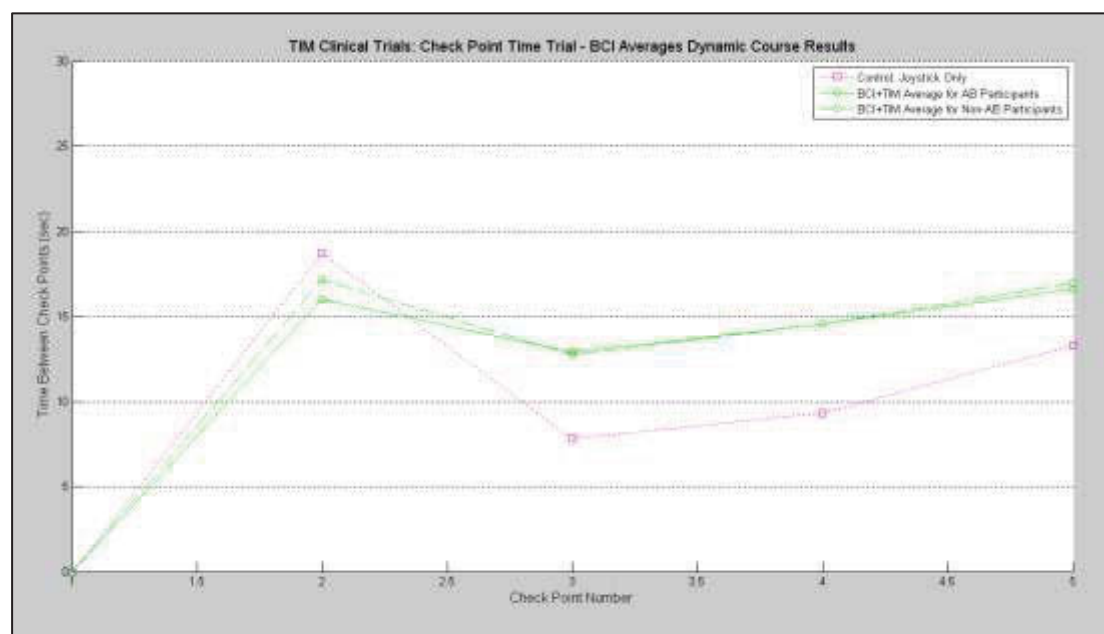
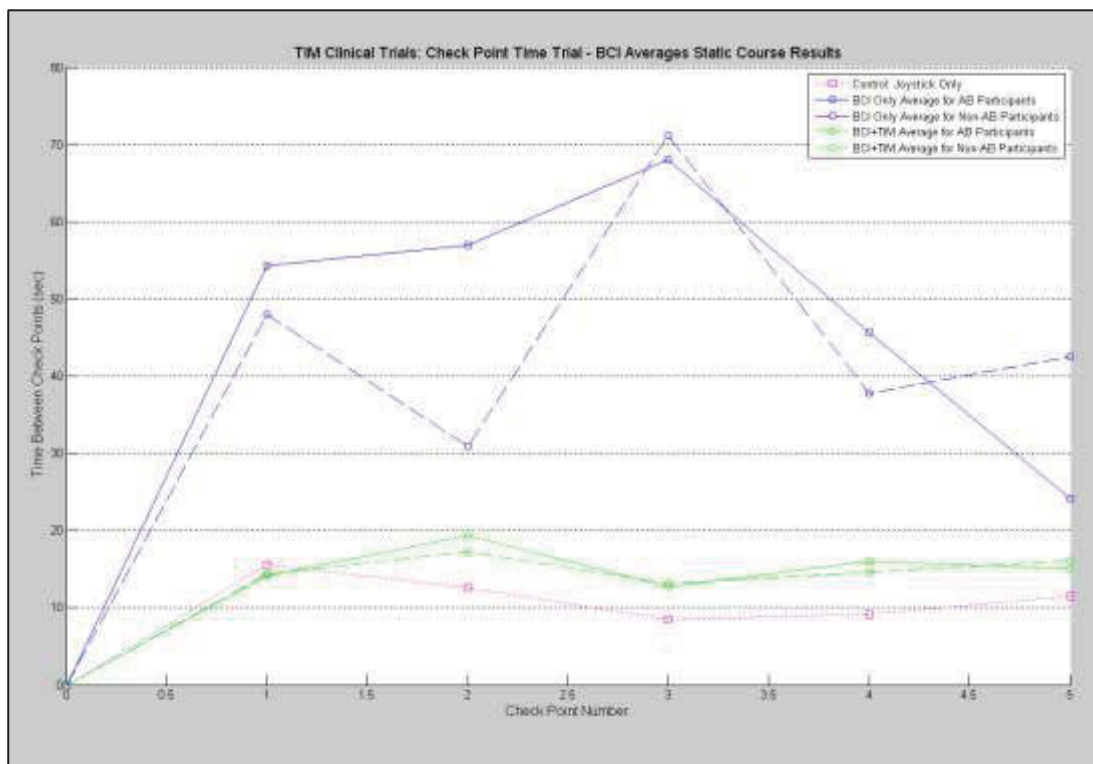Figure 5-51: Dynamic Course using BCI Results – Check Point Time Averages by Participant Groups

As shown in Figure 5-52, the run from the Start Zone (CP1) to the CP2 checkpoint was on average performed faster with BCI+TIM than the Joystick Only control run for that leg. After this CP2 checkpoint the BCI+TIM approach takes more time between checkpoints than the Joystick Only run, however, it still performs very well for using such hands-free controls.
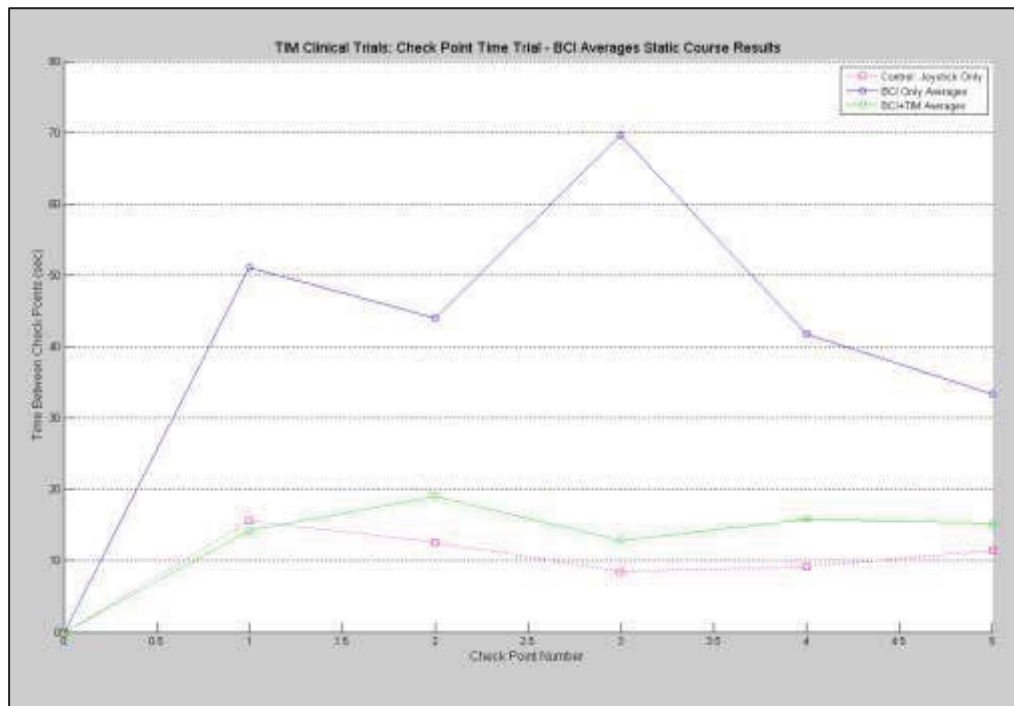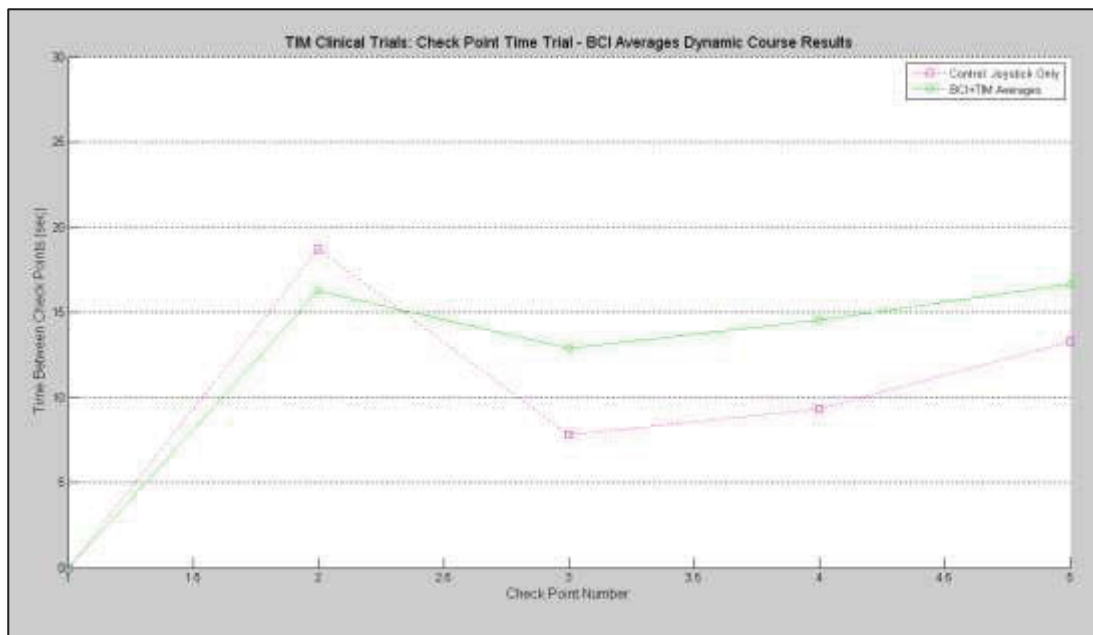

Figure 5-52: Dynamic Course using BCI Results – Check Point Time Averages

Overall 'Dynamic Course' Results

Combining the check point break-down data found from the Dynamic Course tests using HMC Only, HMC+TIM, and BCI+TIM control approaches, the overall test times are displayed in Table 5-4. Taking into consideration the fact that the BCI Only approach was not conducted for safety purposes, the TIM-assisted approaches (HMC+TIM and BCI+TIM) will both be compared against the HMC Only approach. This is adequate nevertheless, since in the „Static Course" tests the BCI Only runs took significantly longer than any of the other approaches and also produced more potential collisions that required facilitator intervention. The data in Table 5-4 is also graphed against the Joystick Only control run, as displayed in Figure 5-53.

Participant	HMC Only	HMC+TIM	BCI+TIM
1	61.3	57.1	65.2
2	88.1	54.4	56.0
3	73.5	60.3	56.2
4	85.6	61.6	60.2
5	84.4	65.1	54.8
6	68.2	65.2	65.4
7	69.4	60.2	62.0
8	72.5	65.7	60.8
9	66.3	58.7	57.2
10		60.5	65.6
Mean	74.37	60.88	60.34
SD	8.93	3.50	3.95
Min	61.3	54.4	54.8
Max	88.1	65.7	65.6

Table 5-4: Dynamic Course Overall Total Time Results (Seconds)
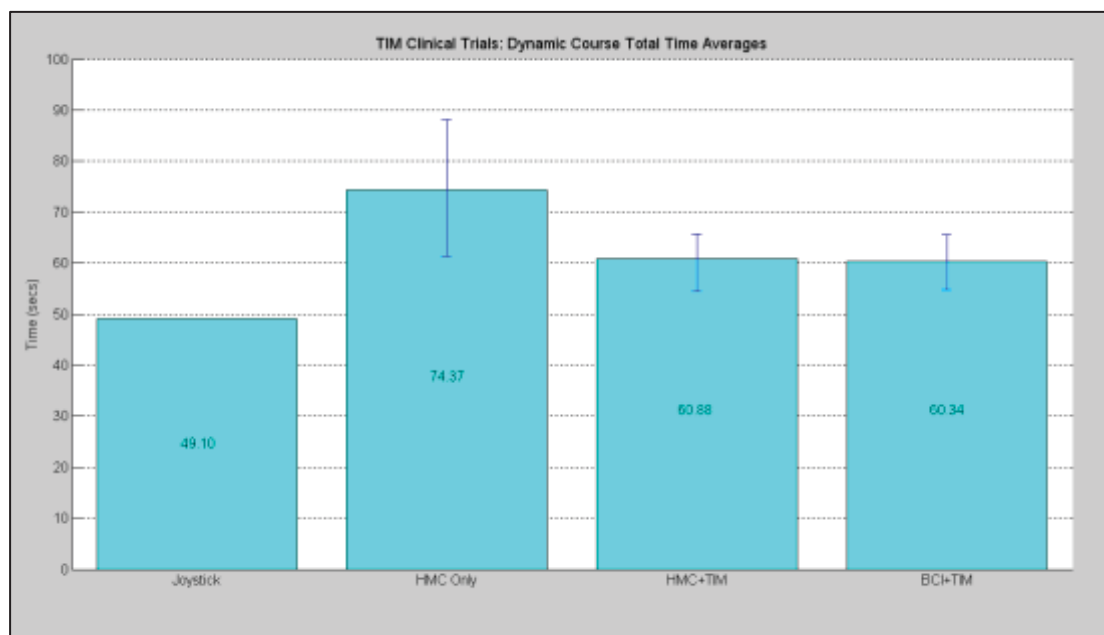
Figure 5-53: Dynamic Course Total Time Averages for All Control Modes

The graph data displayed in Figure 5-53 shows average Dynamic Course completion times, with minimum and maximum variation ranges, for each control mode. Again, the total average test times for control modes using the automated guidance of TIM were very similar and featured low time variance between the two relevant control modes, as well as between the individual tests in each, evident in the small variation ranges of ±5.65 seconds and ±5.40 seconds, respectively. The HMC Only test took on average 13.76±0.27 seconds longer than both of the TIM-assisted control mode tests, and also had a larger variation range of ±13.40 seconds. No collision interventions were necessary in any of the Dynamic Course tests.

5.6.2.3 Test Statement Review

The main test statements are:

- H1: "In the Static Course experiments, the assistance from TIM will allow both HMC and BCI control methods across all participants to be carried out in faster times than the HMC Only control".
- H2: "In the Dynamic Course experiments, the assistance from TIM will also allow both HMC and BCI control methods across all participants to be carried out in faster times than the HMC Only control".

Due to the fact that only a few BCI Only tests were conducted for the Static Test, these are not included in the analysis, despite the conclusions there being obvious based on the times taken to complete these tests. From Table 5-3, the HMC Only experiment runs in the Static Test produced a mean completion time of $\bar{x}_{S_1} = 96.53\ seconds$, with a standard deviation of $s_{S_1} = 10.38\ seconds$ across $n_1=9$ participants. Across $n_2=10$ participants with the assistance of TIM, the HMC+TIM runs produced a mean completion time of $\bar{x}_{S_2} = 73.93\ seconds$ with a standard deviation of $s_{S_2} = 4.56\ seconds$, and the BCI+TIM runs produced a mean completion time of $\bar{x}_{S_3} = 77.02\ seconds$ with a standard deviation of $s_{S_3} = 3.77\ seconds$. As the HMC+TIM results and the BCI+TIM results both used assistance from TIM, the data from these will be combined for this assessment testing and compared against the HMC Only experiment results. So the HMC+TIM/BCI+TIM data across $n_{2/3}=20$ participants produces a mean completion time of $\bar{x}_{S_{2/3}} = 75.48\ seconds$ with a standard deviation of $s_{S_{2/3}} = 4.46\ seconds$.

From Table 5-4, the HMC Only runs in the Dynamic Test produced a mean completion time of $\bar{x}_{D_1} = 74.37\ seconds$, with a standard deviation of $s_{D_1} = 8.93\ seconds$ across $n_1=9$ participants. Across $n_2=10$ participants with the assistance of TIM, the HMC+TIM experiment runs produced a mean completion time of $\bar{x}_{D_2} = 60.88\ seconds$ with a standard deviation of $s_{D_2} = 3.50\ seconds$, and the BCI+TIM runs produced a mean completion time of $\bar{x}_{D_3} = 60.34\ seconds$ with a standard deviation of $s_{D_3} = 3.95\ seconds$. Here, the HMC+TIM/BCI+TIM data across $n_{2/3}=20$ participants produces a mean completion time of $\bar{x}_{D_{2/3}} = 60.61\ seconds$ with a standard deviation of $s_{D_{2/3}} = 3.47\ seconds$.

These small sample tests will each be analysed using a t-distribution with a one-tailed test. For both these tests the significance level, α, is being allocated a critical value of $\alpha = 0.01$, meaning if a test statement is accepted it only has a less than 1% chance of being an accident. The degrees of freedom is found as $(n_1 - 1) + (n_{2/3} - 1) = (8 + 19) = 27$, giving a critical value of t, as found using a look-up table (McClave & Sincich 2009), as $t_\alpha = 2.473$.

Test Statement H1 Assessment:

The null statement for H1 is:

H1$_0$: $\left(\mu_{S_1} - \mu_{S_{2/3}}\right) = D_0 = 0$. The assistance of TIM has no significant reduction effect on completion times in the Static Course runs.

The alternative statement for H1 is:

H1$_1$: $\left(\mu_{S_1} - \mu_{S_{2/3}}\right) > (D_0 = 0)$. The assistance of TIM has a significant reduction effect on completion times in the Static Course runs.

Assuming H1$_0$:

A pooled sample estimator σ_S^2, denoted here as $s_{S_P}^2$, is found first:

$$s_{S_P}^2 = \frac{(n_1 - 1)s_{S_1}^2 + (n_{2/3} - 1)s_{S_{2/3}}^2}{(n_1 - 1) + (n_{2/3} - 1)} = \frac{(8)(10.38)^2 + (19)(4.46)^2}{(8) + (19)} = 45.9221 \qquad (5.13)$$

Test statistic:

$$t = \frac{\left(\bar{x}_{S_1} - \bar{x}_{S_{2/3}}\right) - D_0}{\sqrt{s_{S_P}^2\left(\frac{1}{n_1} + \frac{1}{n_{2/3}}\right)}} = \frac{(96.53 - 75.48) - 0}{\sqrt{(45.9221)\left(\frac{1}{9} + \frac{1}{20}\right)}} = 7.7389 \qquad (5.14)$$

$$\therefore t > t_\alpha$$

For this one-tailed test, the null statement H1$_0$ is rejected if $t > t_\alpha$. Since this is the case, there is statistical significance to accept the alternative test statement H1$_1$.

Test Statement H2 Assessment:

The null statement for H2 is:

H2$_0$: $\left(\mu_{S_1} - \mu_{S_{2/3}}\right) = D_0 = 0$. The assistance of TIM has no significant reduction effect on completion times in the Dynamic Course runs.

The alternative statement for H2 is:

H2$_1$: $\left(\mu_{S_1} - \mu_{S_{2/3}}\right) > (D_0 = 0)$. The assistance of TIM has a significant reduction effect on completion times in the Dynamic Course runs.

Assuming H1$_0$:

A pooled sample estimator σ_D^2, denoted here as $s_{D_P}^2$, is found:

$$s_{S_P}^2 = \frac{(n_1 - 1)s_{D_1}^2 + (n_{2/3} - 1)s_{D_{2/3}}^2}{(n_1 - 1) + (n_{2/3} - 1)} = \frac{(8)(8.93)^2 + (19)(3.47)^2}{(8) + (19)} = 32.1013 \qquad (5.15)$$

Test statistic:

$$t = \frac{\left(\bar{x}_{D_1} - \bar{x}_{D_{2/3}}\right) - D_0}{\sqrt{s_{D_P}^2 \left(\frac{1}{n_1} + \frac{1}{n_{2/3}}\right)}} = \frac{(74.37 - 60.61) - 0}{\sqrt{(32.1013)\left(\frac{1}{9} + \frac{1}{20}\right)}} = 6.0505 \qquad (5.16)$$

$$\therefore t > t_\alpha$$

For this one-tailed test, the null statement H2$_0$ is rejected if $t > t_\alpha$. Since this is also the case, there is statistical significance to accept the alternative statement H2$_1$.

Results

These tests have found that both the main test statements H1 and H2 have been accepted based on statistical significance using the t-tests detailed here. As specified, these statements have more than 99% probability of being correctly accepted.

5.6.2.4 Post-study Survey Results

Survey Details

The QUEST 2.0: Quebec User Evaluation of Satisfaction with Assistive Technology (Demers et al. 2002) survey consists of 12 questions, constructed of 8 „Device" questions and 4 „Service" questions. It was designed with the intention of use as a clinical and research instrument. Satisfaction is defined here as a person's critical evaluation of several aspects of a device. Furthermore, this evaluation is believed to be influences by a person's expectations, perceptions, attitudes, and personal values.

Due to these experimental studies only being a product prototype evaluation and not a service evaluation, only the 8 „Device" questions of the QUEST 2.0 survey were provided to the participants following the tests, for the purpose of collecting basic data about what they thought of the TIM smart wheelchair. In addition to these, they were also asked which of the hands-free control methods used (HMC or BCI) they preferred to use with TIM's automated guidance assistance.

1	2	3	4	5
not satisfied at all	not very satisfied	more or less satisfied	quite satisfied	very satisfied

ASSISTIVE DEVICE *How satisfied are you with,*					
1. the **dimensions** (size, height, length, width) of your assistive device? *Comments:*	1	2	3	4	5
2. the **weight** of your assistive device? *Comments:*	1	2	3	4	5
3. the **ease in adjusting** (fixing, fastening) the parts of your assistive device? Comments:	1	2	3	4	5

Table 5-5: Excerpts from the QUEST 2.0 Survey

A 5-point satisfaction scale, as shown in Table 5-5, is used to evaluate each question from 1 (not satisfied at all) to 5 (very satisfied). The 8 questions provided ask how satisfied the user is with the dimensions, weight, ease in adjusting, safety and security, durability, simplicity,

comfortability, and effectiveness of the TIM smart wheelchair. If the participant had any comments to add to any of the questions, these were also taken.

Survey Results

The results of the QUEST 2.0 „Device" survey were first reviewed by each question, as displayed in Table 5-6. Here, the mean score, standard deviation, and score range for each of the 8 questions are provided.

QUEST 2.0 'Device' Results by Question			
Question	Mean Score	Standard Deviation	Range (min-max)
1: Dimensions	4.400	0.490	4-5
2: Weight	4.400	0.663	3-5
3: Ease in Adjusting	3.900	0.539	3-5
4: Safety & Security	4.400	0.490	4-5
5: Durability	4.200	0.400	4-5
6: Simplicity	4.500	0.500	4-5
7: Comfortability	4.200	0.748	3-5
8: Effectiveness	4.600	0.490	4-5

Table 5-6: QUEST 2.0 „Device" Results by Question

No question was scored a negative (1 or 2) result. Question 3 (Ease in Adjusting) had the lowest mean score, at 3.900 ± 0.539 (Mean ± SD), which reflects the need to improve the adjusting of TIM wheelchair features. This was likely scored due to the lack of ease in adjusting footrest position and the fact that the position and orientation of the user screen and frame cannot be adjusted.

Question 5 (Durability) and Question (7) both had lower mean values than others, despite still scoring well at 4.200 ± 0.400 and 4.200 ± 0.748, respectively. Durability of the TIM smart wheelchair is strong, however, exposed components could potentially be damaged if knocked, so this will require improvement and protection in later developments. Comfortability is something to be also be improved, as this design does not include personalised cushions or custom sizing, meaning it may be fit for some users and not as comfortable for others. Future developments will see customisation options, as this is an important factor for wheelchair users.

Question 1 (Dimensions), Question 2 (Weight), and Question 4 (Safety and Security) all performed well with scores of 4.400 ± 0.490, 4.400 ± 0.663, and 4.200 ± 0.490, respectively. Dimensions and weight of the wheelchair are generally close to standard so should not produce many problems. The extra surrounding frame coverage, plus the wheelchair"s smooth ability to automatically avoid objects, meant that participants felt reasonably safe and secure when navigating during the tests.

Question 6 (Simplicity) had a high score of 4.500 ± 0.500, due to the fact that once shown the user interface and the functionality, participants mostly found the wheelchair quite easy to control. With the automated assistance of TIM carrying out the finer manouevres and obstacle avoidance, the simplicity factor is heightened, allowing minimal commands to get through complicated environments.

Question 8 (Effectiveness) attained the highest score of 4.600 ± 0.490, since the main goals of the TIM smart wheelchair are to effectively avoid both static and dynamic obstacles, be easily controlled, carry out the user"s actual intentions for travel, and do it all in a smooth manner. These were all achieved to a desirable extent, and hence this high score resulted. If the speed was increased, this field could gain an even higher score result.

QUEST 2.0 'Device' Examples of Comments		
Question	AB / Non-AB	Comments
1: Dimensions	Non-AB	Back sticks out too far; Frame near legs should be wider; Put headrest back in; Seatbelt
2: Weight	Non-AB	Pretty good because personally I prefer wheelchairs I'm steering to be heavier.
3: Ease in Adjusting	AB	Everything was pretty easy to manage, getting in and out was good.
4: Safety & Security	Non-AB	Awesome; Very stable and very easy to use and clever
5: Durability	AB	Seemed very sturdy
6: Simplicity	Non-AB	Didn't expect it to be so easy to use
7: Comfortability	Non-AB	People have special cushions so this is something to take into account.
8: Effectiveness	AB	Highly effective, no collisions.

Table 5-7: QUEST 2.0 „Device" Examples of Comments

Some examples of participant comments on the individual questions are shown in Table 5-7. These questions provide further assessment of the features that participants were satisfied with and where improvements can be made to suit a wider range of users in future developments.

The results of the QUEST 2.0 „Device" survey were then reviewed by the scores given by each participant, as displayed in Table 5-8. This allows the analysis of whether any significant

differences in overall satisfaction were determined between any of the participant groups, genders, or ages.

QUEST 2.0 'Device' Results by Participant				
Participant	Mean Score	Standard Deviation	Range (min-max)	Control Preference
1	3.875	0.599	3-5	HMC+TIM
2	4.375	0.484	4-5	BCI+TIM
3	4.250	0.433	4-5	HMC+TIM
4	3.750	0.433	3-4	HMC+TIM
5	4.875	0.331	4-5	(HMC/BCI)+TIM
6	4.625	0.484	4-5	HMC+TIM
7	4.750	0.433	4-5	HMC+TIM
8	4.250	0.433	4-5	HMC+TIM
9	4.500	0.707	3-5	BCI+TIM
10	4.000	0.000	4-4	BCI+TIM

Table 5-8: QUEST 2.0 „Device" Results by Participant

The lowest overall scores were provided from participants 1 and 4, being 3.875 ± 0.599 (Mean ± SD) and 3.750 ± 0.433, respectively. These were both able-bodied males, aged 24 and 34, meaning they were individual satisfaction results, and were different in scores provided from other males of varying ages.

The highest scorers, being Participants 5, 6, and 7, also did not provide any conclusive links between gender or age. So this means the able-bodied participants accounted for the lowest and the highest average score values, with neither gender nor age being a conclusively contributing factor to the scores seen. All participants, nevertheless, gave an overall positive response to the TIM smart wheelchair following experimental studies, and individual satisfaction scores would have been influenced by the personal expectations, perceptions, attitudes, and values.

The differences between the AB and Non-AB groups were also small, reflecting a reasonably consistent level of satisfaction across the two participant groups. The AB group had an overall mean ± SD score of 4.344 ± 0.374 and an average range of $3.750 - 4.875$, whilst the Non-AB group had an overall mean ± SD score of 4.250 ± 0.250 and a range of $4.000 - 4.500$.

Combining all participants produced an overall mean ± SD score of 4.325 ± 0.587. This meant that across all participants in this test, a positive response was received, on average being rated in between „quite satisfied" and „very satisfied".

The control preferences, also displayed in Table 5-8, showed that 75% of AB participants preferred the HMC+TIM over the BCI+TIM, being a more manual-style hands-free control system, with only one AB participant preferring BCI+TIM, and one AB having no preference between either HMC or BCI with TIM. In contrast to this, both Non-AB participants preferred the BCI+TIM. As observed from the tests, both of these participants found it more challenging to make movements of their head, given the slightly limited range of movement each expreienced. As a result, the BCI requiring no movement of the head was the preference for both, as they found it easy and simple to control and no difficult movements were required.

5.7 Discussion and Chapter Conclusion

This chapter has presented the final hardware and software implementations of the TIM smart wheelchair system, along with the biological inspiration of equine vision for the combined camera vision system. The overall system integration included the ability to work as a single functional system and integrate to hands-free control technologies, such as the head-movement system (HMC) and the brain-computer interface (BCI) proof-of-concept (POF) devices.

The biological inspiration of the equine vision system in the integration of both stereoscopic cameras and spherical cameras proved effective. This saw the stereoscopic cameras provide 66º of stereoscopic vision, to mimic the 65º binocular overlap inherent in a horse"s visual system, and the spherical cameras mimic the surrounding monocular vision of a horse, whilst removing the blind spots and providing 360º of monoscopic vision. The idea was taken to map static objects and detect dynamic objects ahead of the wheelchair using the stereoscopic cameras, and to also detect dynamic obstacles all around the wheelchair using the spherical cameras.

This led to the overall software architecture design of the TIM smart wheelchair, where all hardware components, including hands-free control devices, were integrated and all software modules were required to interact as a single real-time and operational system. This encompassed the ability to take control inputs from the user, camera data input from both camera systems, and wheel encoder data from the drive wheels, and then process all this data

to make effective decisions for safe navigation, which would then be automatically sent out via a digital-to-analog converter to control the drive wheels.

An advanced, real-time obstacle avoidance system was required for this application to allow the wheelchair to automatically avoid obstacles and make navigational decisions whilst carrying out the user‟s intentions for directions of travel. This incorporated concepts of Vector Field Histogram (VFH) methods, originally designed for smaller mobile robotic applications using sonar and ultrasonic sensors, and Vector Polar Histogram (VPH) methods, originally designed for adapting VFH type algorithms for use with laser rangefinders in similar applications.

The mixed concepts were extracted, improved, and adapted for use with the styles of mapping and obstacle detection using the camera systems in this TIM smart wheelchair design, with the produced algorithms being referred to as TIM-VPH. This method has the advantages of being able to take user commands at any instant during navigation and quickly adjust, to navigate in unknown environments, to change the style of navigational obstacle avoidance between open environments and cluttered environments, and to handle both static and dynamic obstacles in real-time. This is all achieved through a combination of importance being placed on 1) the direction the user commands TIM to travel towards, 2) the ability to commit to selected navigational paths and not deviate too far away from the current path being travelled if possible, and 3) to choose navigational paths with more free space, meaning in an open environment it will not need to pass obstacles too closely, whereas this may be necessary in smaller and more cluttered environments.

Experimental studies were conducted on the TIM smart wheelchair system, with a total of 10 participants, consisting of 8 able-bodied (AB) and 2 non-able-bodied (Non-AB) subjects. The main aims were to investigate the real-time performance of the wheelchair system when using hands-free control devices, such as the HMC and BCI, and to compare the operation with and without the automated assistance and obstacle avoidance from TIM. The experimental studies consisted of two obstacle course tests, being referred to as the „Static Course‟ and the „Dynamic Course‟. In the Static Course, participants were required to navigate down a corridor, make a turn, and travel down another corridor with a static obstacle course, consisting of lockers, tables, a bin, walls, doorways, and chairs. The Dynamic Course required the participants to travel down a slightly shorter version of the obstacle course, with

the addition of dynamic obstacles, being a person walking across the path of the wheelchair and another walking person later walking towards the wheelchair in the opposite direction.

In both course types the TIM-assisted approaches, HMC+TIM and BCI+TIM, proved reasonably consistent in timing variances for completion of the courses, and on average were performed significantly faster than the hands-free approaches operated without the assistance of TIM. The main statements H1 and H2 for these were also accepted based on statistical significance found using t-tests. These statements were as follows:

- H1: "In the Static Course experiments, the assistance from TIM will allow both HMC and BCI control methods across all participants to be carried out in faster times than the HMC Only control".

- H2: "In the Dynamic Course experiments, the assistance from TIM will also allow both HMC and BCI control methods across all participants to be carried out in faster times than the HMC Only control".

In addition to this, the TIM-assisted approaches performed almost as well as the conventional joystick control method for power wheelchairs. Both AB and Non-AB participants found TIM relatively easy to operate with the proof-of-concept hands-free control devices. These tests also proved the feasibility and effectiveness of the TIM smart wheelchair implementation in providing safe automated guidance assistance during navigation using hands-free control technologies.

Chapter 6

Conclusion and Future Work

"Governments throughout the world can no longer overlook the hundreds of millions of people with disabilities who are denied access to health, rehabilitation, support, education and employment, and never get the chance to shine." - Stephen Hawking

6.1 Discussions and Conclusion

The research conducted, designs and developments made, and performance results obtained from this project lead to the conclusion that the TIM smart wheelchair prototype has provided significant contributions toward providing new options, for independence in mobility, to many people in need. The methods and designs have a number of advantages over contemporary intelligent wheelchair designs found in research, and moreover, have formed a strong basis for further developments towards a commercially accessible product.

This research saw eye-opening statistics on disability provide significant motivation for undertaking the project. It was found that a great number of people, including families and caretakers of those suffering, could potentially benefit from new smart wheelchair technology, as about 5.8% of Australians, or approximately 1.3 million people, live with profound or severe disability which limits core activities in communication, mobility, and self-care (Australian Bureau of Statistics 2011). People with higher levels of physical disability, such as those with C-1 to C-3 tetraplegia and locked-in syndrome (LIS), are in serious need of new technologies for independence in mobility, as they currently have no available and adequate options.

Popular smart wheelchair designs found in research provided some good conceptual ideas for consideration, and downfalls to avoid or overcome. The ideas extracted from a small range of these were the inexpensive design concepts, the abilities to recognise certain changes in the environment during navigation, and the idea of potentially being a stand-alone system of components that could be attached and integrated into and power wheelchair system. The first disadvantage of many of these systems that was addressed in this project was the limitation in obstacle types that could be adequately recognised and avoided. Obstacles featuring parts that stuck out outside the range of laser rangefinder or ultrasonic sensor scan limits could potentially go unseen and cause accidents. Another downfall addressed was the inability of many to effectively handle dynamic obstacles moving in from any direction, which could cause problems in environments with crowds of people moving around.

Since cameras had not previously been efficiently utilised in smart wheelchairs designs, they were selected as the primary sensor type for the TIM smart wheelchair, based on them becoming increasingly accessible and inexpensive in recent years. Stereoscopic cameras are commonly used in smaller mobile robotic applications and were adapted for environmental mapping in this project. Spherical vision cameras are an extended application of monoscopic vision, which is not commonly used in such applications as smart wheelchairs, so these became an effective addition to the stereoscopic cameras here for real-time dynamic obstacle detection and user interface assistance, made possible due to its inherently large vision range.

The stereoscopic cameras were implemented into the wheelchair system through the design of a reliable method for constructing real-time 2-dimensional (2D) bird's eye view environment maps, which also utilised the installed wheel encoders. The conversion process from raw stereo images through to 2D environment maps involved raw image acquisition, pre-

processing steps to prepare the images, stereo processing to produce a disparity image, conversion into a 3-dimensional (3D) point map, removal of features that would not potentially cause collisions, and extraction of remaining object placement for mapping onto a 2D bird‟s eye view environment map. This then allowed the wheelchair to make intelligent navigational decisions based on the relative placement of mapped objects. Wheel encoder data and odometry change calculations also allowed maps to be „remembered‟ based on the wheelchair‟s relative movements, even when no longer inside the range of vision.

Optimisation for effective mapping involved the fact that the quality of mapping would vary between environments based on the stereo processing parameters, which could be tailored to suit individual environment types but would require adjustments when faced with different environments and lighting conditions. So the strategy designed and implemented required distinguishing environmental conditions into categories, and then allowing the stereo processing parameter selections to adapt in real-time, according to the environment classification at any given instant. All encountered environmental situations were separated into four categories, being 1) „General Illumination Contrast‟, 2) „Extreme Illumination Contrast‟, 3) „Consistent Dark‟, and 4) „Consistent Bright‟. Neural network classification, in real-time, of the environmental category was optimised to allow the TIM smart wheelchair to consistently produce reliable maps with minimal noise artifacts.

Given the limited 66º of horizontal stereoscopic vision range, spherical vision cameras were introduced to take into account highly likely encounters with common dynamic obstacles, such as people, moving all around the wheelchair. Strategies were designed and validated with the intention of being able to adequately detect obstacles in real-time surrounding the wheelchair, and hence optimise the vision range to provide 360º of obstacle detection in both static and dynamic environments.

Spherical vision provides the ability to display and process live panoramic video feeds, however, the inherent distortions in the panoramic representations make it difficult to effectively utilise common monocular vision image processing methods. For this reason, a new strategy was developed for instantaneously classifying panoramic segments into „Traffic Light‟ Zones. This involved the panoramic image being separated into five different segments and pre-processed, before neural network classification of the four main surrounding segments. These were grouped into horizontally-mirrored pairs (S1/S4 group and S2/S3 group), and classified in real-time into one of the following „Traffic Light‟ Zone categories,

being 1) Red: Stop, obstacles too close to move in that direction, 2) Yellow: Caution, obstacles near so move slowly if moving in that direction, or 3) Green: Go, no obstacles near so clear to move in that direction. With the addition of an effective overlayed edge-detection of objects method, the advanced version of this strategy produced high accuracies for real-time classification.

The challenge to then appropriately integrate the stereoscopic cameras and the spherical vision cameras into a coherent system was aided by looking into biological inspiration. It was found that the equine vision system was an effective basis for the integration, since horses inherently have a very wide vision range which incorporates both binocular and monocular vision traits. This is important to their survival due to the large amounts of time spent grazing with their heads lowered to the ground, during which their wide vision range helps them detect the movements of dynamic predation.

As such, the designed vision system of the TIM smart wheelchair saw the stereoscopic cameras provide 66º of stereoscopic vision, to mimic the 65º binocular overlap inherent in a horse's visual system, and the spherical cameras mimic the surrounding monocular vision of a horse, whilst removing the blind spots and providing 360º of monoscopic vision. This system allows mapping of static objects and detecting dynamic objects ahead of the wheelchair using the stereoscopic cameras, and to also detect surrounding dynamic obstacles using the spherical cameras.

Overall hardware and software system integration allowed the TIM smart wheelchair to take hands-free user input in real-time, including from proof-of-concept devices such as the head-movement controller (HMC) or the brain-computer interface (BCI). The panoramic video feed from the spherical vision camera system helped provide a simple and highly effective graphical user interface for commanding the wheelchair through these hands-free devices. It allowed the user to see everything going on around them without the requirement of head movement, and also allows them to select any direction for travel at any time. This is a step forward in the efforts to safely control the smart wheelchair with any type of control device, whether commercial or newly-developed.

To allow the hands-free control devices to be used with the TIM smart wheelchair's obstacle detection and mapping capabilities, an advanced, real-time obstacle avoidance system was also required. Concepts were extracted from Vector Field Histogram (VFH) methods and

Vector Polar Histogram (VPH) methods, combined, improved, and adapted to allow safe navigational decisions to be automatically made in real-time during operation. TIM-VPH, as the new obstacle avoidance strategy was called, deals with all the input commands from the user as well as all environment map information from the sensory input data, coming from the unique camera configuration of TIM and the wheel encoder data. It then has the ability to take user commands at any instant during navigation and quickly adjust, to navigate in unknown environments, to change the style of navigational obstacle avoidance between open environments and cluttered environments, and to handle both static and dynamic obstacles in real-time.

With the entire TIM smart wheelchair deployed as a functioning and finalised prototype system with the two separate options for hands-free control, the performance was then evaluated through experimental studies. A total of 10 participants, made up of 8 able-bodied (AB) and 2 non-able-bodied (Non-AB) subjects, completed the tests and provided feedback about the system. Through both the „Static Course" and „Dynamic Course" testing it was found that the TIM-assisted approaches, HMC+TIM and BCI+TIM, proved reasonably consistent in timing variances for completion of the courses across all participants, and on average were performed smoother, safer, and significantly faster than when the hands-free approaches were operated without the assistance of TIM. Through statistical significance found from t-tests on the data, the following test statements were accepted:

- H1: "In the Static Course experiments, the assistance from TIM will allow both HMC and BCI control methods across all participants to be carried out in faster times than the HMC Only control".
- H2: "In the Dynamic Course experiments, the assistance from TIM will also allow both HMC and BCI control methods across all participants to be carried out in faster times than the HMC Only control".

As a prototype design this TIM smart wheelchair has achieved desirable results and made significant contributions towards a product that will aim to improve the lives of many people who do not currently have access to technologies for mobility independence. For these reasons, and the fact that it has the ability to interface with brain-computer interfaces, the name TIM for this smart wheelchair was actually decided upon as an acronym, standing for „Thought-controlled Intelligent Machine". The factors taken into account in these designs which will be further translated into future implementations are cost, reliability, effectiveness, system autonomy and intelligence, ease-of-use, durability, comfort, adaptability, and

compatibility with many control methods, especially hands-free devices. The drawbacks of comfort, durability, and ease in adjusting parts will be taken into consideration, while the successes of the designs in this project will be taken forward and further improved upon in the next smart wheelchair designs, which will focus on becoming commercially available and accessible.

6.2 Future Work

The TIM smart wheelchair requires further development for both software and hardware to improve its performance, reliability, physical design, and ability to handle more situations and environments. It is intended that the wheelchair from here will be redesigned with an embedded system approach to computational processing, whereby a dedicated microchip processor will replace the tablet PC. Custom frames and covers will be designed to house the electronics and new hardware components, with an emphasis on it being a commercial-style design.

As discovered from the experimental studies, the ergonomics of the wheelchair will be an important issue, so collaborative work will be done with wheelchair manufacturers and custom designers, some of whom we are already in contact with. This will help us reach the target users the wheelchair is primarily designed for, as the current prototype does not have all the necessary extras for many of these people, such as custom pillows, adequate neck support and seatbelts.

The new designs will also need to take into account the ease in adjustments of all parts. The power wheelchairs themselves have many adjustable parts, but things like the user screen and the housing frames must all allow adjustments to be made to suit the user. A better way of swinging these or moving them out of the way, for easy access in and out of the wheelchair, will also be required.

Speed is an issue of importance to many wheelchair users. The current maximum speed and automated variations below this for the TIM smart wheelchair were set based on safety requirements for ethics approval. These speeds can be increased and still remain safe in operation, however, this is something that will need be further investigated to understand the

speed and safety relationships. Many wheelchair users like to travel faster when possible so this will aim to be improved whilst maintaining safe collision avoidance.

Some drawbacks of using cameras alone are mainly concerned with extreme lighting changes and with features that can sometimes be difficult for the system to adequately perceive. An example of this is clean windows when there are few reflections or marks on the surface, as the stereoscopic cameras and matching algorithms have trouble in the absence of image features to correlate. This is also sometimes the case for smooth and clean walls. For this reason the addition of ultrasonic sensors would be advisable. These could act as a strong complementing sensory system to the cameras due to the fact they can be used to help verify obstacle detections as well as detect clean walls and windows that the cameras may fail to detect.

Another situation ultrasonic sensors could help with is dangerous drops in the floor, such as stairs. Currently the TIM wheelchair has not taken a drop in stairs into account so has no way of detecting this danger. Ultrasonic sensors aimed downward towards the ground can be a potential and easy solution to this problem in detecting surface drops. This could later also be used for detecting gutters and potholes in designs for outdoor use. Furthermore, it could be very helpful to be able to determine uneven ground and differences in floor surface types, as the operations of the wheelchair may be required to vary based on such circumstances as the chance of slippage, bumpy navigational routes, or resistive surfaces requiring more torque when accelerating from a stationary position.

Outdoor use is the next issue since the current TIM smart wheelchair designs are aimed towards indoor use only so far. When the time comes to expand the applications of the intended smart wheelchair designs to outdoor use, there are many problems and dangers that will need to be accounted for. In general, there are many rules to obey on the streets and near roads in particular. Traffic, signs, lights, gutters, and road markings are some of the many outdoor features that must be able to be detected and understood for safe outdoor operation. This will be a great challenge for future expansions in the technology, and may even involve Global Positioning System (GPS) assistance for localisation and destination planning.

Once the ability to change locations has been accounted for, the smart wheelchair designs may also need to account for changes between known and unknown environments. This is necessary because automated guidance in unknown environments, as was implemented in this

project, can be different to the types of commands and travel abilities of the wheelchair in known environments. Known maps, landmarks, and destinations are all potential features of familiar and known environments, whereby the smart wheelchair may be commanded to go to a destination, such as a 'lounge room', and even if not in direct sight it will automatically know how to find its way there. Obstacles can also be dealt with and avoided as the turn up along the pre-planned paths. So the transition between known and unknown environments will require changes in operation ability and the style of commands the user can give.

Further common situations will be investigated, such as hospital, rehabilitation centres, and spaces in general that may have a number of smart wheelchairs. In these cases the wheelchairs may be able to be sent away to navigate automatically and park themselves out of the way in wheelchair ranks when not in use, and be called to return on demand. The ability for the smart wheelchairs to communicate in these situations would be beneficial, in that when moving from one location to another they could travel in similar fashions and not try to work together as opposed to treating each other like moving obstacles, possibly even taking swarm analysis algorithms into consideration in the designs. This would make for increased efficiency in these types of environments.

Lastly, the smart wheelchair designs will be designed further to help people with severe physical disability, but will also aim to be expanded for use by people with varying conditions, such as cerebral palsy. These types of conditions can have a wide range of effects on the individual, so it would be very beneficial to be able to provide more options for intelligent and safe control and operation of such devices as smart wheelchairs. These applications are not only limited to mobility, but are also intended to be expanded into the areas of assisting in communication, smart home control, and entertainment. If the user can effectively use the intelligent systems that will spawn from the TIM smart wheelchair research, we will hopefully be able to provide them many forms of independence to increase their quality of life. All efforts will move forward from here towards making these ideas for smart and assistive commercial products an accessible reality.

Bibliography

Acharya, T. & Ray, A. 2005, „Image Processing: Principles and Applications", *John Wiley and Sons, Inc.*, Canada.

An, D. & Wang, H. 2004, „VPH: a new laser radar based obstacle avoidance method for intelligent mobile robotics", *Fifth World Congress on Intelligent Control and Automation*, vol. 5, pp. 4681-4685.

Australian Bureau of Statistics, 2011, *One in five Australians with a disability*, viewed 19 October 2011, <http://www.abs.gov.au/ausstats/abs@.nsf/Latestproducts/4446.0Media% 20Release12009?opendocument&tabname=Summary&prodno=4446.0&issue=2009&num=& view>.

Aviator, 2012, *Aviator allows people to harness the freedom of their mind to overcome the limitations of their body*, viewed 5 June 2012, <uniquestportal.com/aviator/>.

Banks, J., Bennamoun, M. & Corke, P. 1997, „Non-parametric Techniques for Fast and Robust Stereo Matching", *IEEE Region 10 Annual Conference on Speech and Image Technologies for Computing and Telecommunications*, vol. 1, pp. 365-368.

Banner Engineering Corporation, 2006, *Ultrasonic Basics*, viewed 9 November 2011, < http://www.bannerengineering.com/training/faq.php?faqID=34&div=1>.

Bell, D., Levine, S., Koren, Y., Jaros, L. & Borenstein, J. 1994, „Design criteria for obstacle avoidance in a shared-control system", *Proceedings of the RESNA International Conference*, pp. 581-583.

Borenstein, J. & Feng, L. 1996, „Measurement and correction of systematic odometry errors in mobile robots", *IEEE Transactions on Robotics and Automation*, vol. 12, no. 6, pp. 869-880.

Borenstein, J & Koren, Y. 1989, „Real-time Obstacle Avoidance for Fast Mobile Robots", *IEEE International Conference on Systems, Man, Cybernetics*, vol. 19, no. 5, pp. 1179-1187.

Borenstein, J & Koren, Y. 1990, „Real-time Obstacle Avoidance for Fast Mobile Robots in Cluttered Environments", *IEEE International Conference on Robotics and Automation*, vol. 1, pp. 572-577.

Borenstein, J & Koren, Y. 1991, „The vector field histogram – Fast obstacle avoidance for mobile robots", *IEEE Transactions on Robotics and Automation*, vol. 7, pp. 278-288.

Brown, M.Z., Burschka, D. & Hagar, G.D. 2003, „Advances in Computational Stereo", *IEEE Transactions on Pattern Analysis and Machine Intelligence*, vol. 25, no. 8, pp. 993-1008.

Civera, J., Davison, A. & Martinez Montiel, J.M. 2008, „Inverse Depth Parametrization for Monocular SLAM", *IEEE Transactions on Robotics*, vol. 24, no. 5, pp. 932-945.

Cole, D.M. & Newman, P.M. 2006, „Using laser range data for 3D SLAM in outdoor environments", *IEEE International Conference on Robotics and Automation*, pp. 1556-1563.

Crispin, S.M., Matthews, A.G. & Parker, J. 1990, „The equine fundus – I: examination, embryology, structure and function", *Equine Veterinary Journal Supplement*, vol. 10, pp. 42-49.

Cristobal, G., Schelkens, P. & Thienpont, H. 2011, *Optical and Digital Image Processing – Fundamentals and Applications*, Wiley-VCH, Weinham.

Dario, P., Carrozza, M.C, Beccai, L., Laschi, C., Mazzolai, B., Menciassi, A. & Micera, S. 2005, „Design, fabrication and applications of biomimetic sensors in biorobotics", *Proceedings of the IEEE International Conference on Information Acquisition*, pp.263-266.

Demers, L., Weiss-Lambrou, R. & Ska, B. 2002, „The Quebec User Evaluation of Satisfaction with Assistive Technology (QUEST 2.0): An overview and recent progress", *Technology and Disability*, IOS Press, vol. 14, pp. 101-105.

Diamantas, S.C. & Crowder, R.M. 2009, „Localisation and Mapping Using a Laser Range Finder: A Goal-Seeking Approach", *Fifth International Conference on Autonomic and Autonomous Systems*, pp. 270-276.

Disabled World, 2011, *World Facts and Statistics on Disabled and Disability Issues*, viewed 19 October 2011 <http://www.disabled-world.com/disability/statistics/>.

Doble, J.E., Haig, A.J., Anderson, C. & Katz, R. 2003, „Impairment, activity, participation, life satisfaction, and survival in persons with locked-in syndrome for over a decade: follow-up on a previously reported cohort", *J Head Trauma Rehabilitation*, vol. 18, no. 5, pp. 435-444.

Faria, P.M., Braga, R.A.M., Valgode, E. & Reis, L.P. 2007, „Interface Framework to Drive an Intelligent Wheelchair Using Facial Expressions", *IEEE International Symposium on Industrial Electronics (ISIE 2007)*, pp. 1791-1796.

Fonseca, J., Martins, J. & Couto, C. 2001, „An Experimental Model For Sonar Sensors", *Proceedings of the 1st International Conference on Information Technology in Mechatronics*, Istanbul, Turkey.

Fotoohi, L. & Gaser, A. 2011, „Building a Safe Care-providing Robot", *IEEE International Conference on Rehabilitation Robotics*, Bremen, Germany, pp. 1-6.

Fox, D., Burgard, W. & Thrun, S. 1997, „The dynamic window approach to collision avoidance", *IEEE Robotics & Automation Magazine*, vol. 4, no. 1, pp. 23-33.

Gilando, C., Gonzalez, J. & Fernandez-Madrigal, J.A. 2006, „Control Architecture for Human-Robot Integration: Application to a Robotic Wheelchair", *IEEE Transactions on Systems, Man, and Cybernetics – Part B: Cybernetics*, vol. 36, no. 5, pp. 1053-1067.

Gill, P.E., Murray, W. & Wright, M.H. 1980, *Practical Optimization*, Academic Press Inc., New York.

Gong, J., Duan, Y., Man, Y. & Xiong, G. 2007, „VPH+: An Enhanced Vector Polar Histogram Method for Mobile Robot Obstacle Avoidance", *International Conference on Mechatronics and Automation*, pp. 2784-2788.

Gonzalez, J., Muaeoz, A.J., Gilando, C., Fernandez-Madrigal, J.A. & Blanco, J.L. 2006, „A Description of the SENA Robotic Wheelchair", *IEEE Mediterranean Electrotechnical Conference*, pp. 437-440.

Hagan, M.T. & Menhaj, M. 1994, „Training feed-forward networks with the Marquardt algorithm", *IEEE Transactions on Neural Networks*, vol. 5, no. 6, pp. 989-993.

Haig, A.J., Katz, R.T. & Sahgal, V. 1987, „Mortality and complications of the locked-in syndrome", *Arch Phys Medical Rehabilitation*, vol. 68, no. 1, pp. 24-27.

Harman, A.M., Moore, S., Hoskins, R. & Keller, P. 1999, „Horse vision and an explanation for the visual behaviour originally explained by the „ramp retina"", *Equine Veterinary Journal*, vol. 8, pp. 384-390.

Hartley, R. & Zisserman, A. 2000, *Multiple View Geometry in Computer Vision*, Cambridge University Press, Cambridge, UK.

Hobson, A.A. 2007, „Locked-in syndrome with no advance directives: an ethical analysis of the plan of care", *ProQuest Dissertations and Theses*, pp. 1-2.

Hu, H. & Brady, M. 1994, „A Bayesian approach to real-time obstacle avoidance for a mobile robot", *Autonomous Robots*, vol. 1, Kluwer Academic Publishers, Boston, pp. 69-92.

Hughes, A. 1977, „The Topography of Vision in Mammals of Contrasting Life Style: Comparative Optics and Retinal Organization", *Handbook of Sensory Physiology Volume VII/5: The Visual System in Vertebrates*, Springer, Germany, pp. 613-756.

Independent Living Centre NSW, 2009, *Invacare TDX A Powered Wheelchair*, viewed 9 February 2011, <http://www.ilcnsw.asn.au/item/7057#product_details>.

Jensfelt, P. & Christensen, H. 1998, „Laser Based Position Acquisition and Tracking in an Indoor Environment", *Proceedings of the IEEE International Symposium on Robotics and Automation*, vol. 1, pp. 331-338.

Joseph, T. & Nguyen, H. 1998, „Neural network control of wheelchairs using telemetric head movement", *Proceedings of the 20th Annual International Conference of the IEEE Engineering in Medicine and Biology Society*, vol. 5, pp. 2731-2733.

Kim, J. & Hasegawa, T. 2011, „A Simple Unevenness Detection System Using a Monocular Camera to Ensure Safety of a Handle Type Electric Wheelchair", *2011 IEEE 73rd Vehicular Technology Conference (VTC Spring)*, pp. 1-4.

Kodagoda, S. 2007, *Advanced Robotics Lecture Notes*, University of Technology, Sydney.

Lacey, N. 1998, *Image Representation: Key Concepts in Media Studies*, St. Martin"s Press, New York.

Lankenau, A., Meyer, O. & Krieg-Bruckner, B. 1998, „Safety in Robotics: the Bremen Autonomous Wheelchair", *5th International Workshop on Advanced Motion Control*, pp. 524-529.

Lankenau, A. & Rofer, T. 2001, „A versatile and safe mobility assistant", *IEEE Robotics & Automation Magazine*, vol. 8, no. 1, pp. 29-37.

Levine, S.P., Bell, D.A., Jaros, L.A., Simpson, R.C. & Koren, Y. 1999, „The Navchair Assistive Wheelchair Navigation System" *IEEE Transactions on Rehabilitation Engineering*, vol. 7, no. 4, pp. 443-451.

Li, S. 2006, „Monitoring Around a Vehicle by a Spherical Image Sensor", *IEEE Transactions on Intelligent Transportation Systems*, vol. 7, no. 4, pp. 541-550.

Li, S. & Isago, T. 2007, „Qualitative Localization by Full-View Spherical Image", *Proceedings of the 3rd Annual IEEE Conference on Automation Science and Engineering*, pp. 566-571.

Lim, P.A. & Tow, A.M. 2007, „Recovery and Regeneration after Spinal Cord Injury: A Review and Summary of Recent Literature", *Annals Academy of Medicine*, Singapore, vol. 36, no. 1, pp. 49-57.

Liverman, C.T. 2005, „Spinal Cord Injury Progress, Promise and Priorities", *National Academies Press*, Washington, DC, USA.

Lopez, A.C., Moita, F., Nunes, U. & Solea, R. 2007, „An Outdoor Guidpath Navigation System for AMRs Based on Robust Detection of Magnetic Markers", *2007 ETFA IEEE Conference on Emerging Technologies and Factory Automation*, pp. 989-996.

Lou, J.-G., Cai, H. & Li, J. 2005, „A real-time interactive multi-view video system", *Proceedings of the ACM International Conference on Multimedia*, Singapore, pp. 161-170.

Lu, J., Cai, H., Lou, J.-G. & Li, J. 2007, „An Epipolar Geometry-Based Fast Disparity Estimation Algorithm for Multiview Image and Video Coding", *IEEE Transactions on Circuits and Systems for Video Technology*, vol. 17, no. 6, pp.737-750.

McClave, J.T. & Sincich, T. 2009, *Statistics: Eleventh Edition*, Pearson Prentice Hall, USA.

McCulloch, W. S. and Pitts, W. H., 1943, *A logical calculus of the ideas immanent in nervous activity*, Bulletin of Mathematical Biophysics, pp. 115-133.

McGreevy, P. 2004, *Equine Behaviour: A Guide for Veterinarians and Equine Scientists*, Saunders, UK.

Microsoft Corporation, 2012, *Kinect Product Features*, viewed 16 September 2012, <http://www.microsoft.com/en-us/kinectforwindows/discover/features.aspx>.

MobilityBasics 2012, *Power Wheelchair Drive Controls*, viewed 20 July 2012, <http://mobilitybasics.com/drivecontrols.php>.

Moller, M.F. 1993, „A scaled conjugate gradient algorithm for fast supervised learning", *Neural Networks*, vol. 6, pp. 525-533.

Moravec, H. P. 1998, „Sensor fusion in certainty grids for mobile robots", *AI Magazine*, vol. 9, pp. 61-74.

Murphy, J., Hall, C. & Arkins, S. 2009, „What Horses and Human See: A Comparative Review", *Hindawi Corporation Internal Journal of Zoology*.

Murphy, R.R. 2000, „Introduction to AI robotics", *The Massachusetts Institute of Technology Press*, Cambridge, MA, USA.

Nguyen, H.T. 2012, „49275 Neural Networks and Fuzzy Logic", *University of Technology, Sydney*, Sydney, NSW, Australia.

Nguyen, S.T., Nguyen, H.T., Taylor, P.B. & Middleton, J. 2006, „Improved Head Direction Command Classification using an Optimised Bayesian Neural Network", *Proceedings of the 28th Annual International Conference of the IEEE Engineering in Medicine and Biology Society*, pp. 5679-5682.

Nishimori, M., Saitoh, T. & Konishi, R. 2007, „Voice Controlled Intelligent Wheelchair", *2007 SICE Annual Conference*, pp. 336-340.

Norton, L. 2010, „Spinal Cord Injury, Australia 2007-08", *Injury Research and Statistics Series – Number 52*, Australian Institute of Health and Welfare, Canberra.

Noto, N., Okuda, H., Tazaki, Y. & Suzuki, T. 2012, „Steering Assisting System for Obstacle Avoidance Based on Personalized Potential Field", *15th International IEEE Conference on Intelligent Transportation Systems*, Alaska, USA, pp. 1702-1707.

Panoramic Earth, 2012, *Panoramic Earth*, viewed 16 January 2012, <http://www.panoramicearth.com/>.

Pires, G., Araujo, R., Nunes, U. & de Almeida, A.T. 1998, „RobChair – A Powered Wheelchair Using a Behabiour-Based Navigation", *1998 5th International Workshop on Advanced Motion Control, 1998. AMC '98-Coimbra,* Portugal, pp. 536-541.

Point Grey Research Inc., 2003, *Triclops Stereo Vision Manual Version 3.1*, Vancouver, Canada.

Point Grey Research Inc., 2005, *Ladybug SDK User Manual and Ladybug2 Reference*, Vancouver, Canada.

Point Grey Research Inc., 2012, *The fully redesigned Flea 3 – Ultra-compact, versatile, cost-effective*, viewed 5 October 2012, <http://www.ptgrey.com/newsletters/june2006.html>.

Qiang, Z., Burdet, E., Rebsamen, B. & Chee Leong, T. 2007, „Evaluation of the Collaborative Wheelchair Assistant System", *2007 ICORR IEEE 10th International Conference on Rehabilitation Robotics*, pp. 601-608.

Qiang, Z., Rebsamen, B., Burdet, E. & Chee Leong, T. 2008, „A Collaborative Wheelchair System", *IEEE Transactions on Neural Systems and Rehabilitation Engineering*, vol. 8, no. 1.

Ripley, B.D. 1996, *Pattern Recognition and Neural Networks*, Cambridge, Cambridge University Press.

Roberts, S.M. 1992, „Equine vision and optics", *The Veterinary Clinics of North America. Equine Practice*, vol. 8, no. 3, pp. 451-457.

Rockey, C. 2012, *Laser Drivers*, viewed 18 August 2012, <http://www.isep.ipp.pt/roswiki/laser_drivers.html>.

Rofer, T. & Lankenau, A. 1999, „Ensuring safe obstacle avoidance in a shared-control system", *7th IEEE International Conference on Emerging Technologies and Factory Automation*, vol. 2, pp. 1405-1414.

Rosenblatt, F. 1958, „The Perceptron: A Probabilistic Model for Information Storage and Organization of the Brain", *Psychological Review*, vol. 65, no. 6, pp. 386-408.

Rubin, M. 2007, *Overview of Spinal Cord Disorders*, viewed 2 October 2012, <http://www.merckmanuals.com/home/brain_spinal_cord_and_nerve_disorders/spinal_cord_disorders/overview_of_spinal_cord_disorders.html>.

Rumelhart, D.E., Hinton, G.E. & Williams, R.J. 1986, „Learning internal representations by error propagation", *Parallel Distributed Processing: Exploration in the microstructure of cognition*, Cambridge, MA: MIT Press, vol. 1.

Samuelson, D.A. 1991, „Ophthalmic Embryology and Anatomy", *Veterinary Ophthalmology*, Lea & Febiger, Philadelphia, pp. 3-119.

Satoh, Y. & Sakaue, K. 2006, „Development of Omni-directional Stereo Vision-based Intelligent Electric Wheelchair", *The 18th International Conference on Pattern Recognition*, 799-804.

Schwartz, J.T., Scharir, M. & Hoperoft, J. 1987, *Planning, Geometry and Complexity of Robot Motion*, Ablex Publishing Corporation, Norwood, NJ.

SCI Research Advancement, 2007, *What is Spinal Cord Injury?*, viewed 11 July 2012, < http://www.scicure.org/whatis_SCI.htm>.

Sharp, 2011, *Data Sheet GP2D12 – Compact, High Sensitive Distance Measuring Sensor*, viewed 23 December 2011, <http://www.sharpsma.com/webfm_send/1203>.

Simpson, R.C. 2005, „Smart wheelchairs: A literature review", *Journal of Rehabilitation Research & Development*, vol. 42, no. 4, pp. 423-436.

Simpson, R.C. & Levine, S.P. 2002, „Voice Control of a Powered Wheelchair", *IEEE Transactions on Neural Systems and Rehabilitation Engineering*, vol. 10, no. 2, pp. 122-125.

Simpson, R.C., Poirot, D. & Baxter, F. 2002, „The Hephaestus Smart Wheelchair System", *IEEE Transactions on Neural Systems and Rehabilitation Engineering*, vol. 10, no. 2, pp. 118-122.

Skinner, B.T., Nguyen, H.T. & Liu D.K. 2007, „Classification of EEG Signals Using a Genetic-Based Machine Learning Classifier", *29th Annual International Conference of the IEEE Engineering in Medicine and Biology Society,* pp. 3120-3123.

Soderholm, S., Meinander, M. & Alaranta, H. 2001, „Augmentative and alternative communication methods in locked-in syndrome", *Journal of Rehabilitative Medicine*, vol. 33, no. 5, pp. 235-239.

Spinal Cord Injury Resource Centre, 2012, *Spinal Cord 101*, viewed 11 July 2012, <http://www.spinalinjury.net/index.html>.

Takahashi, O. & Schilling, R.J. 1989, „Motion planning in a plane using generalised Voronoi diagrams", *IEEE Transactions on Robotics and Automation*, vol. 5, no. 2, pp. 1573-1576.

Thomas, M. 2012, *Spinal Cord Responsibilities*, viewed 14 July 2012, <http://www.nature.com/scientificamericanmind/journal/v16/n3/box/scientificamericanmind1005-68_BX1.html>.

Thrun, S., Burgard, W. & Dieter, F. 2005, „Probabilitic Robotics", *The MIT Press*, England.

Ulrich, I. & Borenstein, J. 1998, „VFH+: Reliable Obstacle Avoidance for Fast Mobile Robots", *IEEE International Conference on Robotics and Automation*, vol. 2, pp. 1572-1577.

Ulrich, I. & Borenstein, J. 2000, „VFH*: Local Obstacle Avoidance with Look-Ahead Verification", *IEEE International Conference on Robotics and Automation*, vol. 3, pp. 2505-2511.

Umbaugh, S.E. 2011, *Digital Image Processing and Analysis – Human and Computer Vision Applications with CVIPtools, Second Edition*, CRC Press, Florida, USA.

Wahab, M.N.A., Sivadev, N. & Sundaraj, K. 2011, „Development of Monocular Vision System for Depth Estimation in Mobile Robot – Robot Soccer", *2011 IEEE Conference on Sustainable Utilization and Development in Engineering and Technology*, pp. 36-41.

Walsh, J., Dayton, A., Cuff. C. & Martin, P. 2005, „Long term care – actuarial analysis on long-term care for the catastrophically injured", *PriceWaterhouseCoopers*, Sydney.

Wang, C.M. 1988, „Location Estimation and Uncertainty Analysis for Mobile Robots", *IEEE International Conference on Robotics and Automation*, Michigan, pp. 1231-1235.
Wheelchair.ca, 2012, *Power Wheelchair Features and Resources*, viewed 4 June 2012, <http://wheelchair.ca/drives.php>.

Wickramasooriya, A., Hamilan, G., Jayawardena, S., Wijemanne, L. & Munasinghe, S. 2008, „Characteristics of Sonar Range Sensor SRF05", *4th International Conference on Information and Automation of Sustainability*, pp. 475-480.

WinterGreen Research, Inc, 2007, „Power Wheelchair Market Opportunities, Market Forecasts, and Market Strategies, 2007-2013", *Power Wheelchair Market Description, Market Analysis, Product Description, and Company Profiles*, WinterGreen Research, Inc, Lexington, Massachusetts.

World Health Organization, 2008, „The Global Burden of Disease – 2004 Update", *WHO Press, World Health Organization*, Geneva, Switzerland.

World Health Organization, 2011, „World Report on Disability 2011", *WHO Press, World Health Organization*, Geneva, Switzerland.

Yang, L., Zhao, D., Wu, X., Li, H. & Zhai, J. 2011, „An Improved Prewitt Algorithm for Edge Detection Based on Noised Image", *4th International Congree on Image and Signal Processing (CISP)*, vol. 3, pp. 1197-1200.

Yoda, I., Tanaka, J., Raytchev, B., Sakaue, K. & Inoue, T. 2006, „Stereo Camera Based Non-Contact Non-Constraining Head Gesture Interface for Electric Wheelchairs", *The 18th International Conference on Pattern Recognition (ICPR'06)*, 740-745.

Zitnick, C.L., Kang, S.B., Uyttendaele, M., Winder. S. & Szeliski, R. 2004, „High-quality video interpolation using a layered representation", *Proceedings of the ACM Conference on Computer Graphics*, pp. 600-608.

Zhan, Q., Huang, S. & Wu, J. 2008, „Automatic Navigation for a Mobile Robot with Monocular Vision", *2008 IEEE Conference on Robotics, Automation and Mechatronics*, pp. 1005-1010.

Zhang, B., Wang, J., Rossano, G. & Martinez, C. 2011, „Vision-guided Robotic Assembly Using Uncalibrated Vision, *Proceedings of the 2011 IEEE International Conference on Mechatronics and Automation*, pp 1384-1389.

Zhang, Z. 1998, „Determine the epipolar geometry and its uncertainty: A review", *International Journal of Computer Vision*, vol. 27, pp. 161-195.

Appendices

Appendix A

Publications

Nguyen, J.S. et al. 2012, 'Real-time performance of a hands-free semi-autonomous wheelchair system using a combination of stereoscopic and spherical vision', *34th Annual International Conference of the IEEE EMBS, San Diego, California USA, 28 Aug - 1 Sep 2012*, pp. 3069-3072. DOI: 10.1109/EMBC.2012.6346612

Note: Fulltext not include due to copyright restrictions.

Nguyen, J.S., Tran, Y., Su, S.W. & Nguyen, H.T. 2011, 'Semi-autonomous wheelchair developed using a unique camera system configuration biologically inspired by equine vision', *33rd Annual International Conference of the IEEE EMBS, Boston, Massachusetts USA, 30 Aug - 3 Sep 2011*, pp. 5762-5765 DOI: 10.1109/IEMBS.2011.6091426

Note: Fulltext not include due to copyright restrictions.

Kitoko, V. et al. 2011, 'Performance of dry electrode with bristle in recording EEG rhythms across brain state changes', *33rd Annual International Conference of the IEEE EMBS, Boston, Massachusetts USA, 30 Aug - 3 Sep 2011*, pp. 59-62.
DOI: 10.1109/IEMBS.2011.6089896

Note: Fulltext not include due to copyright restrictions.

Nguyen, J.S., Su, S.W. & Nguyen, H.T. 2010, 'Spherical vision cameras in a semi-autonomous wheelchair system', *32nd Annual International Conference of the IEEE EMBS, Buenos Aires, Argentina, 31 Aug - 4 Sep 2010*, pp. 4064-4067.
DOI: 10.1109/IEMBS.2010.5627614

Note: Fulltext not include due to copyright restrictions.

Nguyen, J.S., Nguyen, T.H. & Nguyen, H.T. 2009, 'Semi-autonomous wheelchair system using stereoscopic cameras', *31st Annual International Conference of the IEEE EMBS, Minneapolis, Minnesota USA, 2-6 Sep 2009*, pp. 5068-5071.
DOI: 10.1109/IEMBS.2009.5334266

Note: Fulltext not include due to copyright restrictions.

Nguyen, T.H., Nguyen, J.S. & Nguyen, H.T. 2008, 'Bayesian recursive algorithm for width estimation of freespace for a power wheelchair using stereoscopic cameras', *30th Annual International IEEE EMBS Conference, Vancouver, British Columbia Cananda, 20-24 Aug 2008*, pp. 4234-4237. DOI: 10.1109/IEMBS.2008.4650144

Note: Fulltext not include due to copyright restrictions.

Nguyen, T.H., Nguyen, J.S., Pham, D.M. & Nguyen, H.T. 2007, 'Real-time obstacle detection for an autonomous wheelchair using stereoscopic cameras', *Proceedings of the 29th Annual International Conference of the IEEE EMBS, Cité Internationale, Lyon France, 23-26 Aug 2007*, pp. 4775-4778. DOI: 10.1109/IEMBS.2007.4353407

Note: Fulltext not include due to copyright restrictions.

Appendix B

C++ Dynamic Link Library Code

```
//================================================================
// BumblebeeXB3 and Ladybug2 Image capture and processing for wheelchair "TIM"
// Written by Jordan Son Nguyen
// Last update: 21st November 2011
//================================================================


// MultiCamera DLL: stereoto3dpoints and greyscale image exports for use with LabVIEW
//
// Prior to running this program:
// Requires Triclops to be run first to correctly initialise the Bumblebee XB3
// then Flycapture to be run for the Ladybug2 and set the camera settings
// to Mode 0, Mono 8bit, 1024 x 3072, 40% bit rate, then press set Format7
//
// Once initialised, run the LabVIEW program that calls this DLL:
// Takes input from a Bumblebee and performs subpixel
// interpolation to create a 16-bit disparity image.
// The disparity data is then converted to 3-dimensional X/Y/Z
// coordinates which is exported as arrays.
// The Ladybug2 has images from 4 cameras captured at once and exported as
// an array of greyscale (8bit) pixels.
//
//================================================================


//================================================================
//        System Includes
//================================================================
#include "StdAfx.h"
#include <stdio.h>
#include <stdlib.h>



//================================================================
//        PGR Includes
//================================================================
#include "triclops.h"
```

```cpp
#include "pgrflycapture.h"
#include "pgrflycapturestereo.h"
#include "pnmutils.h"


// Ladybug
#include "pgrflycaptureplus.h"


//================================================================
//      Project Includes
//================================================================


//
// Macro to check, report on, and handle Triclops API error codes.
//

#define _HANDLE_TRICLOPS_ERROR( function, error ) \
{ \
   if( error != TriclopsErrorOk ) \
   { \
      printf( \
            "ERROR: %s reported %s.\n", \
            function, \
            triclopsErrorToString( error ) ); \
      exit( 1 ); \
   } \
} \


//
// Macro to check, report on, and handle Flycapture API error codes.
//
#define _HANDLE_FLYCAPTURE_ERROR( function, error ) \
{ \
   if( error != FLYCAPTURE_OK ) \
   { \
      printf( \
```

```
        "ERROR: %s reported %s.\n", \
        function, \
        flycaptureErrorToString( error ) ); \
    exit( 1 ); \
  } \
} \


// Maximum cameras on the bus. (Maximum devices allowed on a 1394 bus is 64).
#define _MAX_CAMERAS        10


// Number of buffers in memory per camera. Increasing this number may
// help performance on systems with slow disk writes.
#define _BUFFERS        10



//====================================================================
//      Small Functions
//====================================================================


inline float round2(float x) { return x > 0 ?  (float)((int)(x * 100 + 0.5)) / 100 : (float)((int)(x *
100 - 0.5)) / 100; }



//====================================================================
//      Global Variables
//====================================================================


  TriclopsContext             triclops;
  TriclopsError               te;



  FlyCaptureContext           flycapture[_MAX_CAMERAS];
  FlyCaptureImagePlus         flycaptureImagePlus[_MAX_CAMERAS];
  FlyCaptureImage             flycaptureImage[_MAX_CAMERAS];
  FlyCaptureInfoEx            pInfo[_MAX_CAMERAS];
```

```
FlyCapturePixelFormat        pixelFormat[_MAX_CAMERAS];
FlyCaptureError              fe;



TriclopsInput                stereoData;
TriclopsInput                colorData;
TriclopsImage16              depthImage16;
TriclopsImage                monoImage;
TriclopsColorImage           colorImage;


// Number of cameras
unsigned int                 NumCameras = _MAX_CAMERAS;


//==================================================================
//   FUNCTION: Initialise BumblebeeXB3 and Ladybug2 and start image transfer
//==================================================================


void __declspec(dllexport) CameraInit(int *settings, float *floatsettings)
//void CameraInit(void)
{

 // Local Function Variables CameraInit

  int iMaxCols = 0;
  int iMaxRows = 0;

  char* szCalFile;

  // Enumerate the bus
  fe = flycaptureBusEnumerateCamerasEx( pInfo, &NumCameras );
  _HANDLE_FLYCAPTURE_ERROR( "flycaptureBusEnumerateCamerasEx()", fe );

  // Open the camera
  fe = flycaptureCreateContext( &flycapture[0] );
  _HANDLE_FLYCAPTURE_ERROR( "flycaptureCreateContext()", fe );
```

```cpp
   fe = flycaptureCreateContext( &flycapture[1] );
 _HANDLE_FLYCAPTURE_ERROR( "flycaptureCreateContext()", fe );


 // Initialize the Flycapture context
 fe = flycaptureInitializePlus( flycapture[0], 0, _BUFFERS, NULL );
 _HANDLE_FLYCAPTURE_ERROR( "flycaptureInitializePlus()", fe );


 fe = flycaptureInitializePlus( flycapture[1], 1, _BUFFERS, NULL );
 _HANDLE_FLYCAPTURE_ERROR( "flycaptureInitializePlus()", fe );


 // Save the camera's calibration file, and return the path
 fe = flycaptureGetCalibrationFileFromCamera( flycapture[0], &szCalFile );
 _HANDLE_FLYCAPTURE_ERROR( "flycaptureGetCalibrationFileFromCamera()", fe );


 // Create a Triclops context from the cameras calibration file
 te = triclopsGetDefaultContextFromFile( &triclops, szCalFile );
 _HANDLE_TRICLOPS_ERROR( "triclopsGetDefaultContextFromFile()", te );


 pInfo[0].CameraMaxBusSpeed = FLYCAPTURE_S_FASTEST;


 pInfo[1].CameraMaxBusSpeed = FLYCAPTURE_S_FASTEST;


 // Start transferring images from the BumblebeeXB3 to the computer
 fe = flycaptureStart( flycapture[0], FLYCAPTURE_VIDEOMODE_ANY,
FLYCAPTURE_FRAMERATE_ANY );
 _HANDLE_FLYCAPTURE_ERROR( "flycaptureStart()", fe );


 // Start transferring Ladybug2 images, custom video mode used >> set first in Flycapture
 fe = flycaptureStart( flycapture[1], FLYCAPTURE_VIDEOMODE_CUSTOM,
FLYCAPTURE_FRAMERATE_ANY );
 _HANDLE_FLYCAPTURE_ERROR( "flycaptureStart()", fe );
```

```cpp
// Set up some stereo parameters:
// Set to output images 640x480 (RESET LATER IN EXPERIMENTS)
te = triclopsSetResolution( triclops, settings[6], settings[5]);//240, 320 );
_HANDLE_TRICLOPS_ERROR( "triclopsSetResolution()", te );


// Set disparity range
te = triclopsSetDisparity( triclops, settings[0], settings[1]); //0,115); or 0,63); //Custom
_HANDLE_TRICLOPS_ERROR( "triclopsSetDisparity()", te );


// Set Stereo and Edge Masks (Custom)
te = triclopsSetStereoMask( triclops, settings[2]); //11);
te = triclopsSetEdgeCorrelation( triclops, 1 );
te = triclopsSetEdgeMask( triclops, settings[3]); //11);


// Set Texture and Uniqueness validation (Custom)
//te = triclopsSetTextureValidation( triclops, 0 ); //Default
te = triclopsSetTextureValidation( triclops, 1 ); //Custom
_HANDLE_TRICLOPS_ERROR( "triclopsSetTextureValidation()", te );
te = triclopsSetTextureValidationThreshold( triclops, round2(floatsettings[0]));//0.22 );
//te = triclopsSetUniquenessValidation( triclops, 0 ); //Default
te = triclopsSetUniquenessValidation( triclops, 0 ); //Custom
_HANDLE_TRICLOPS_ERROR( "triclopsSetUniquenessValidation()", te );
//te = triclopsSetUniquenessValidationThreshold( triclops, 1.18); //Custom


// Turn on sub-pixel interpolation (Custom)
te = triclopsSetSubpixelInterpolation( triclops, 1 );
_HANDLE_TRICLOPS_ERROR( "triclopsSetSubpixelInterpolation()", te );


// Turn strict subpixel validation is on (Custom)
te = triclopsSetStrictSubpixelValidation( triclops, 1 );//1


// turn on surface validation (Custom)
te = triclopsSetSurfaceValidation( triclops, 1 );
te = triclopsSetSurfaceValidationSize( triclops, settings[4]); //285);//203 );
```

```cpp
te = triclopsSetSurfaceValidationDifference( triclops,
round2(floatsettings[1]));//1.00);//0.74 );

    // Set back forth to reduce noise in the readings
    te = triclopsSetBackForthValidation( triclops, 1 );


}



//====================================================================
//    FUNCTION: Acquire from BumblebeeXB3 and depth process, acquire from Ladybug2
//====================================================================


void __declspec(dllexport) CameraAcquire(int *xoutarray, int *zoutarray, float
*exportImage)
{

    // Local Function Variables

        float               x, y, z;
        int                 pixelinc ;
        int                 i, j, k;
        unsigned short*     row;
        unsigned short      disparity;

        int                 imageBufferSize; //for the ladybug image transfer
        int                 pixel;
        int                 cellNumber;

    // Grab the latest Bumblebee camera images and lock
    fe = flycaptureLockLatest( flycapture[0], &flycaptureImagePlus[0] );
    _HANDLE_FLYCAPTURE_ERROR( "flycaptureLockLatest()", fe );

    // Convert from flycaptureImagePlus into flycaptureImage structure for processing
    flycaptureImage[0] = flycaptureImagePlus[0].image;
```

```cpp
// Extract information from the FlycaptureImage
int imageCols = flycaptureImage[0].iCols;
int imageRows = flycaptureImage[0].iRows;
int imageRowInc = flycaptureImage[0].iRowInc;
int iSideBySideImages = flycaptureImage[0].iNumImages;
unsigned long timeStampSeconds = flycaptureImage[0].timeStamp.ulSeconds;
unsigned long timeStampMicroSeconds = flycaptureImage[0].timeStamp.ulMicroSeconds;


// Create buffers for holding the color and mono images
unsigned char* rowIntColor =
    new unsigned char[ imageCols * imageRows * iSideBySideImages * 4 ];
unsigned char* rowIntMono =
    new unsigned char[ imageCols * imageRows * iSideBySideImages ];


// Create a temporary FlyCaptureImage for preparing the stereo image
FlyCaptureImage tempColorImage;
FlyCaptureImage tempMonoImage;


tempColorImage.pData = rowIntColor;
tempMonoImage.pData = rowIntMono;


// Convert the pixel interleaved raw data to row interleaved format
fe = flycapturePrepareStereoImage(flycapture[0], flycaptureImage[0], &tempMonoImage,
&tempColorImage);
_HANDLE_FLYCAPTURE_ERROR( "flycapturePrepareStereoImage()", fe );


// Pointers to positions in the color buffer that correspond to the beginning
// of the red, green and blue sections
unsigned char* redColor = NULL;
unsigned char* greenColor = NULL;
unsigned char* blueColor = NULL;
```

```cpp
redColor = rowIntColor;
  if (flycaptureImage[0].iNumImages == 2)
  {
    greenColor = redColor + ( 4 * imageCols );
    blueColor = redColor + ( 4 * imageCols );
  }

 if (flycaptureImage[0].iNumImages == 3)
  {
    greenColor = redColor + ( 4 * imageCols );
    blueColor = redColor + ( 2 * 4 * imageCols );
  }

  // Pointers to positions in the mono buffer that correspond to the beginning
  // of the red, green and blue sections
  unsigned char* redMono = NULL;
  unsigned char* greenMono = NULL;
  unsigned char* blueMono = NULL;

  redMono = rowIntMono;
  if (flycaptureImage[0].iNumImages == 2)
  {
    greenMono = redMono + imageCols;
    blueMono = redMono + imageCols;
  }

  if (flycaptureImage[0].iNumImages == 3)
  {
    greenMono = redMono + imageCols;
    blueMono = redMono + ( 2 * imageCols );
  }
```

```
// Use the row interleaved images to build up a packed TriclopsInput.
  // A packed triclops input will contain a single image with 32 bpp.
  te = triclopsBuildPackedTriclopsInput(
    imageCols,
    imageRows,
    imageRowInc * 4,
    timeStampSeconds,
    timeStampMicroSeconds,
    redColor,
    &colorData );
  _HANDLE_TRICLOPS_ERROR( "triclopsBuildPackedTriclopsInput()", te );


  // Use the row interleaved images to build up an RGB TriclopsInput.
  // An RGB triclops input will contain the 3 raw images (1 from each camera).
  te = triclopsBuildRGBTriclopsInput(
    imageCols,
    imageRows,
    imageRowInc,
    timeStampSeconds,
    timeStampMicroSeconds,
    redMono,
    greenMono,
    blueMono,
    &stereoData);
  _HANDLE_TRICLOPS_ERROR( "triclopsBuildRGBTriclopsInput()", te );


  // Preprocessing the images
  te = triclopsRectify( triclops, &stereoData );
  _HANDLE_TRICLOPS_ERROR( "triclopsRectify()", te );


  // Stereo processing
  te = triclopsStereo( triclops ) ;
  _HANDLE_TRICLOPS_ERROR( "triclopsStereo()", te );
```

```cpp
// Retrieve the interpolated depth image from the context
te = triclopsGetImage16( triclops,
                         TriImg16_DISPARITY,
                         TriCam_REFERENCE,
                         &depthImage16 );
_HANDLE_TRICLOPS_ERROR( "triclopsGetImage16()", te );

// Rectify the color image if applicable
if ( pixelFormat[0] == FLYCAPTURE_RAW16 )
{
   te = triclopsRectifyColorImage( triclops,
        TriCam_REFERENCE,
        &colorData,
        &colorImage );
   _HANDLE_TRICLOPS_ERROR( "triclopsRectifyColorImage()", te );
}
else
{
   te = triclopsGetImage( triclops,
        TriImg_RECTIFIED,
        TriCam_REFERENCE,
        &monoImage );
   _HANDLE_TRICLOPS_ERROR( "triclopsGetImage()", te );
}

//declare linked arrays of x,y,z
int const ELEMENT_COUNT = 440;//depthImage16.ncols;

int *x_cur, *z_cur;
x_cur = new int[ELEMENT_COUNT];
z_cur = new int[ELEMENT_COUNT];
```

```cpp
//Set Backline of depth map to 9m for unmapped pixels
for ( i = 0; i < ELEMENT_COUNT; i++ )
{
      x_cur[i] = 900;
      z_cur[i] = 900;
}


// Initialise cellNumber for building exported array
cellNumber = 0;


// Determine the number of pixels spacing per row
pixelinc = depthImage16.rowinc/2;
for ( i = 0, k = 0; i < depthImage16.nrows; i++ )
{
  row     = depthImage16.data + i * pixelinc;
  for ( j = 0; j < depthImage16.ncols; j++, k++ )
  {
        disparity = row[j];

    // do not save invalid points
        if ( disparity < 0xFF00 )
        {
        // convert the 16 bit disparity value to floating point x,y,z
        triclopsRCD16ToXYZ( triclops, i, j, disparity, &x, &y, &z );

            // Look only at points within range
        if ((z<5.0)&&(z>0)&&(y<0.75)&&(y>-0.5)&&(x>-2.2)&&(x<2.2))
            {
                    cellNumber = int(100*((round2(x))+2.2));
            // save the closest points for each x value
          if ((z_cur[cellNumber]) > (round2(z))) //
              {
                z_cur[cellNumber] = int((100*(round2(z)))+200); //get to cm and add 2m
offset
                x_cur[cellNumber] = cellNumber;
```

```
                    }
                }
            }
        }
    }
}


// Reinitialise cellNumber for building export arrays
cellNumber = 0;


// Fill x and z arrays of the depth map to be exported to LV
for ( i = 0; i < ELEMENT_COUNT; i++ )
{
        // Only export filled data
        if ((x_cur[i] < 900) & (z_cur[i] < 900))
        {
                xoutarray[cellNumber] = x_cur[i];
                zoutarray[cellNumber] = z_cur[i];
                cellNumber++;
        }
}



// Done with Bumblebee Processing, Unlock image capture
fe = flycaptureUnlockAll( flycapture[0] );
_HANDLE_FLYCAPTURE_ERROR( "flycaptureUnlockAll()", fe );


// Delete the image buffer, it is not needed once the TriclopsInput
// has been built
delete rowIntColor;
redColor = NULL;
greenColor = NULL;
blueColor = NULL;

delete rowIntMono;
redMono = NULL;
```

```
  greenMono = NULL;
  blueMono = NULL;



  // Grab Ladybug Image and lock
  fe = flycaptureLockLatest( flycapture[1], &flycaptureImagePlus[1] );
  _HANDLE_FLYCAPTURE_ERROR( "flycaptureLockLatest()", fe );



  // Save image dimensions and Bayer info from first image of the ladybug (REVISE
AFTER)
  flycaptureImage[1] = flycaptureImagePlus[1].image;


  // Calculate each Ladybug image buffer size
  imageBufferSize = (flycaptureImage[1].iRows)*(flycaptureImage[1].iRowInc);


  // Fill export image array with Ladybug image data for exporting to LV
  for (pixel=0;pixel<imageBufferSize;pixel++)
  {
                  exportImage[pixel] = float(flycaptureImage[1].pData[pixel]);


  }


  // Done with Ladybug Processing, Unlock image capture
  fe = flycaptureUnlockAll( flycapture[1] );
  _HANDLE_FLYCAPTURE_ERROR( "flycaptureUnlockAll()", fe );


}
```

```cpp
//================================================================
//     FUNCTION: Close BumblebeeXB3 and Ladybug2 and destroy context
//================================================================


void CameraClose(void)
{

  // Close the camera
  fe = flycaptureStop( flycapture[0] );
  _HANDLE_FLYCAPTURE_ERROR( "flycaptureStop()", fe );


  fe = flycaptureStop( flycapture[1] );
  _HANDLE_FLYCAPTURE_ERROR( "flycaptureStop()", fe );


  // Destroy the Flycapture context
  fe = flycaptureDestroyContext( flycapture[0] );
  _HANDLE_FLYCAPTURE_ERROR( "flycaptureDestroyContext()", fe );
  fe = flycaptureDestroyContext( flycapture[1] );
  _HANDLE_FLYCAPTURE_ERROR( "flycaptureDestroyContext()", fe );


  // Destroy the Triclops context
  te = triclopsDestroyContext( triclops ) ;
  _HANDLE_TRICLOPS_ERROR( "triclopsDestroyContext()", te );


}
```
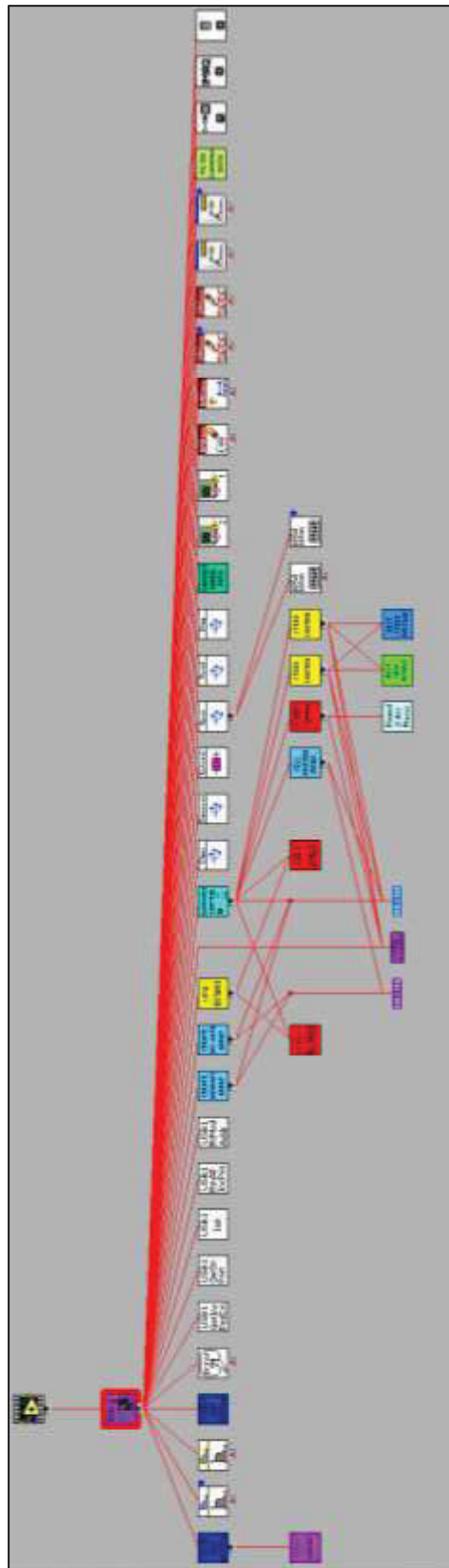
Appendix C

LabVIEW Main Program Code Excerpts

Figure C-1: Virtual Instuments (VI) Heirarchy in the Main Program
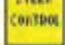
WC_AutomatedGuidanceForHMC_Continuous.vi
J:\PhD Work\2012 CLINICAL TRIAL PROGRAMS - TIM&EEG Program May2012\
WC_AutomatedGuidanceForHMC_Continuous.vi

SpeedVtoKPHConversion.vi
J:\PhD Work\2012 CLINICAL TRIAL PROGRAMS - TIM&EEG Program May2012\SpeedVtoKPHConversion.vi

ControlEffortSmoothing.vi
J:\PhD Work\2012 CLINICAL TRIAL PROGRAMS - TIM&EEG Program May2012\ControlEffortSmoothing.vi

Angle Compensator.vi
J:\PhD Work\2012 CLINICAL TRIAL PROGRAMS - TIM&EEG Program May2012\Angle Compensator.vi

weegClose.vi
J:\PhD Work\2012 CLINICAL TRIAL PROGRAMS - TIM&EEG Program May2012\weegClose.vi

weegStop.vi
J:\PhD Work\2012 CLINICAL TRIAL PROGRAMS - TIM&EEG Program May2012\weegStop.vi

exnSpectralBlock spectral measurements PSD WFM.vi
C:\Program Files\National Instruments\LabVIEW 8.6\vi.lib\express\express analysis\Spectral\Block\
exnSpectralBlock spectral measurements PSD WFM.vi

exnSpectralBlock spectral measurements PSD poly.vi
C:\Program Files\National Instruments\LabVIEW 8.6\vi.lib\express\express analysis\Spectral\Block\
exnSpectralBlock spectral measurements PSD poly.vi

NI_AALBase.lvlib:Butterworth Filter (DBL).vi
C:\Program Files\National Instruments\LabVIEW 8.6\vi.lib\Analysis\3filter.llb\Butterworth Filter (DBL).vi

NI_AALBase.lvlib:Butterworth Filter.vi
C:\Program Files\National Instruments\LabVIEW 8.6\vi.lib\Analysis\3filter.llb\Butterworth Filter.vi

weegExtractData.vi
J:\PhD Work\2012 CLINICAL TRIAL PROGRAMS - TIM&EEG Program May2012\weegExtractData.vi

weegRead.vi
J:\PhD Work\2012 CLINICAL TRIAL PROGRAMS - TIM&EEG Program May2012\weegRead.vi

weegConnect.vi
J:\PhD Work\2012 CLINICAL TRIAL PROGRAMS - TIM&EEG Program May2012\weegConnect.vi

weegOpen.vi
J:\PhD Work\2012 CLINICAL TRIAL PROGRAMS - TIM&EEG Program May2012\weegOpen.vi

VPHSteerControl_HMC_Continuous.vi
J:\PhD Work\2012 CLINICAL TRIAL PROGRAMS - TIM&EEG Program May2012\
VPHSteerControl_HMC_Continuous.vi

Degs to Rads.vi
J:\PhD Work\2012 CLINICAL TRIAL PROGRAMS - TIM&EEG Program May2012\Degs to Rads.vi

VPHSpeedControl.vi
J:\PhD Work\2012 CLINICAL TRIAL PROGRAMS - TIM&EEG Program May2012\VPHSpeedControl.vi

VPHSteerControl.vi
J:\PhD Work\2012 CLINICAL TRIAL PROGRAMS - TIM&EEG Program May2012\VPHSteerControl.vi

CellDistanceFromWC.vi
J:\PhD Work\2012 CLINICAL TRIAL PROGRAMS - TIM&EEG Program May2012\CellDistanceFromWC.vi

CellAngleFromWC.vi
J:\PhD Work\2012 CLINICAL TRIAL PROGRAMS - TIM&EEG Program May2012\CellAngleFromWC.vi

CellPositionRecalc.vi
J:\PhD Work\2012 CLINICAL TRIAL PROGRAMS - TIM&EEG Program May2012\CellPositionRecalc.vi

Figure C-2: List of Main SubVIs

Figure C-3: Main TIM Control Program Front Panel

Figure C-4: Main TIM Control Program Block Diagram

Figure C-5: TIM Automated Guidance Control Program Front Panel

Figure C-6: TIM Automated Guidance Control Program Block Diagram

Figure C-7: Steer Control Front Panel

Figure C-8: Steer Control Block Diagram

Appendix D

Experimental Study Results

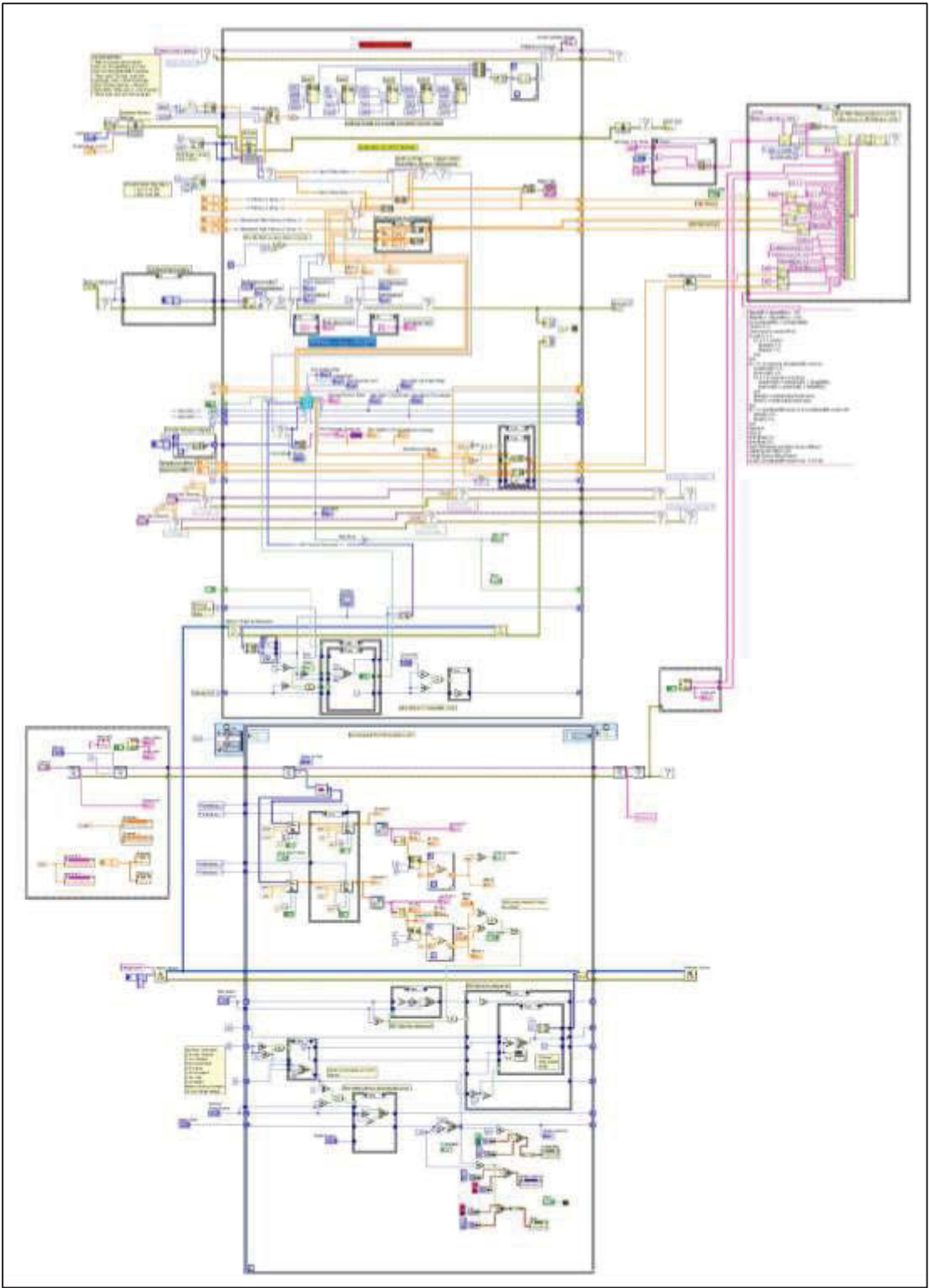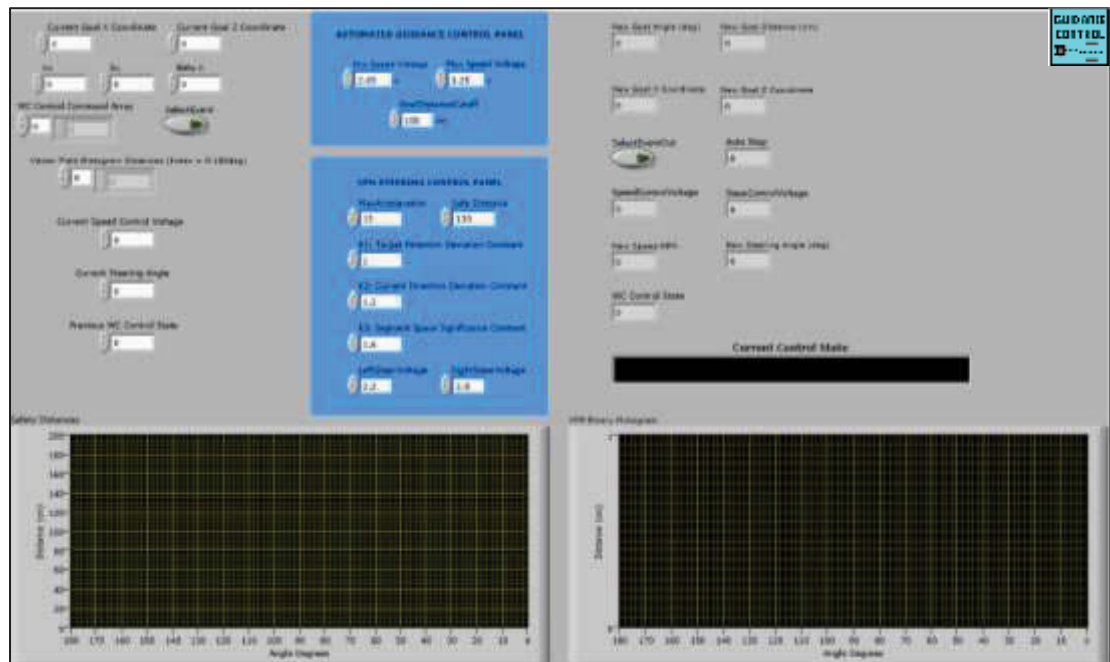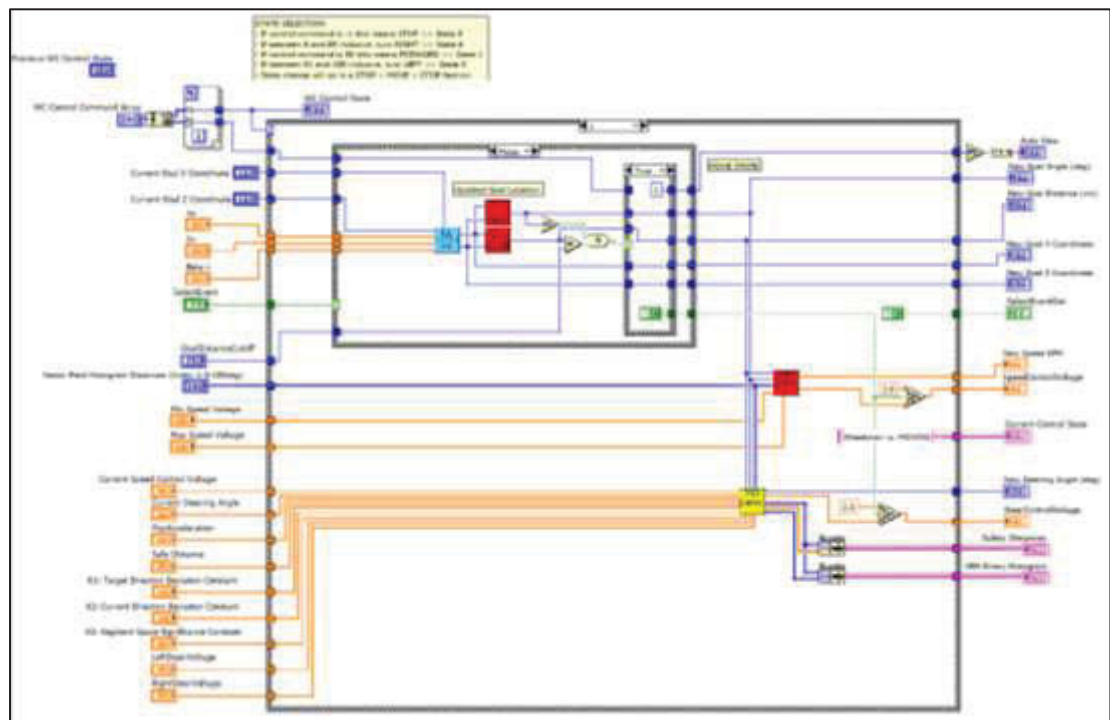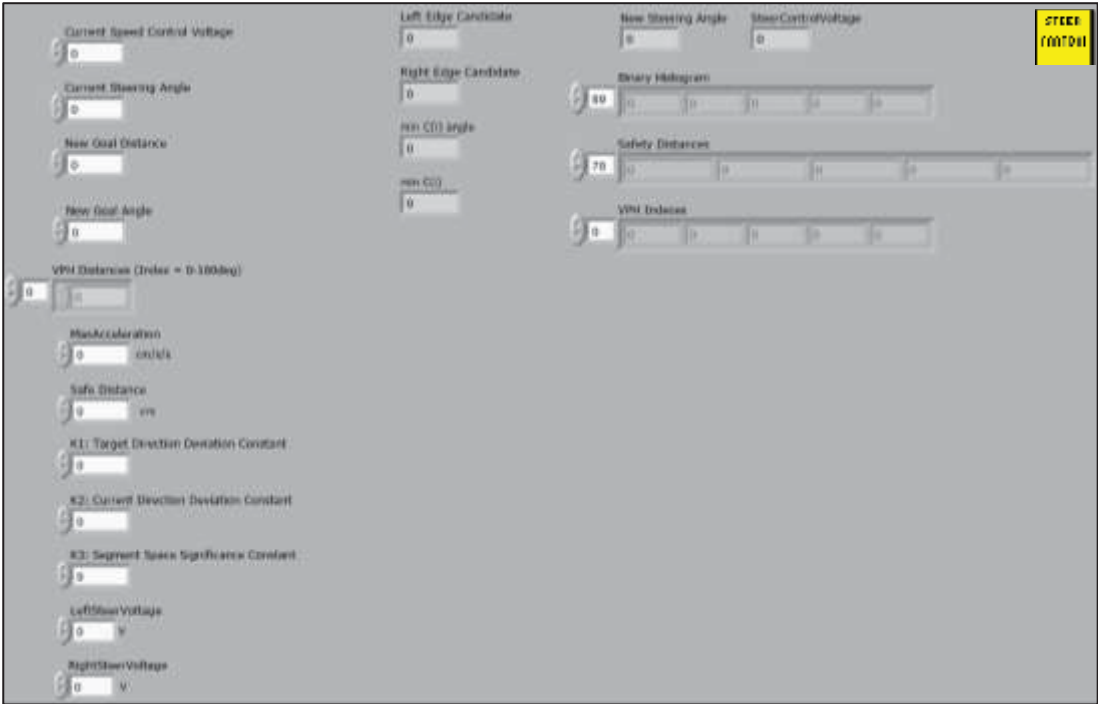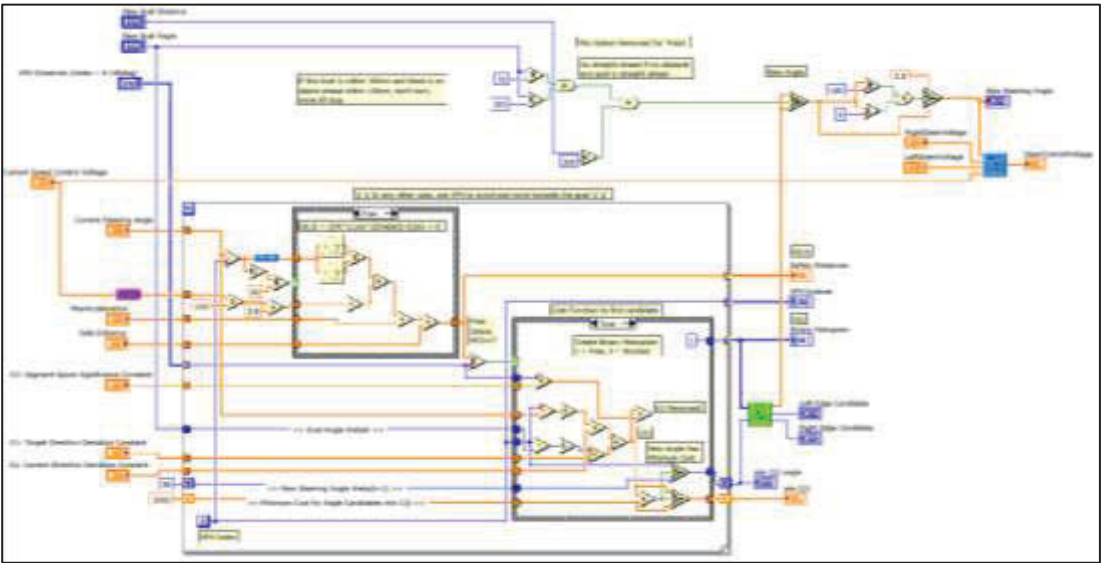| Participant Details										
Testing Date	12/06/2012	14/06/2012	15/06/2012	16/06/2012	18/06/2012	20/06/2012	21/06/2012	22/06/2012	24/06/2012	27/06/2012
Total Testing Time	4 hours	4 hours	4 hours	4 hours	4 hours	4 hours	4 hours	4 hours	4 hours	3 hours
Participant #	1	2	3	4	5	6	7	8	9	10
Gender	Male	Female	Male	Male	Female	Female	Male	Female	Male	Male
Age	24	23	45	34	23	56	21	24	20	33
Disability Level	AB	AB	AB	AB	AB	AB	AB	AB	C6-C7	C6-C7
Trial Course Status										
HMC Only Static Status	Done	Done	Done	Done	Done	Done	Done	Done	Done	N/A
HMC+TIM Static Status	Done	Done	Done	Done	Done	Done	Done	Done	Done	Done
HMC Only Dynamic Status	Done	Done	Done	Done	Done	Done	Done	Done	Done	N/A
HMC+TIM Dynamic Status	Done	Done	Done	Done	Done	Done	Done	Done	Done	Done
BCI Only Static Status	Done	N/A	N/A	N/A	N/A	N/A	N/A	N/A	Done	N/A
BCI+TIM Static Status	Done	Done	Done	Done	Done	Done	Done	Done	Done	Done
BCI Only Dynamic Status	Done	N/A	N/A	N/A	N/A	N/A	N/A	N/A	Done	N/A
BCI+TIM Dynamic Status	Done	Done	Done	Done	Done	Done	Done	Done	Done	Done
Individual HMC Course Time Results										
HMC Only Static Times:										
Start Zone to CP1	20.8	23.2	24.5	28.7	24.6	34.3	26.2	27.5	23.9	
CP1 to CP2	18.4	22.4	24.1	25.0	21.6	26.8	24.1	23.9	14.7	
CP2 to CP3	10.3	15.4	12.6	15.3	11.0	13.7	14.8	14.4	10.3	
CP3 to CP4	17.5	14.5	12.5	21.5	16.4	15.3	16.1	15.0	11.6	
CP4 to Finish	20.4	21.9	16.4	20.0	27.7	16.5	17.9	21.1	13.9	
Trial Run Time	87.4	97.4	90.1	110.5	101.3	106.6	99.1	101.9	74.4	
HMC+TIM Static Times:										
Start Zone to CP1	12.3	14.9	12.1	14.1	14.8	15.4	13.6	13.9	14.6	13.6
CP1 to CP2	21.5	18.3	21.4	16.9	20.6	22.0	21.2	24.9	14.0	21.2
CP2 to CP3	9.3	10.5	12.8	9.8	12.8	12.8	12.2	10.4	10.6	15.3
CP3 to CP4	13.4	13.8	17.4	15.8	15.5	16.3	14.1	13.2	12.3	15.6
CP4 to Finish	13.8	16.1	17.2	11.3	12.2	12.3	12.0	13.6	14.3	11.4
Trial Run Time	70.3	73.6	80.9	67.8	75.9	78.8	73.1	76.0	65.8	77.1
HMC Only Dynamic Times:										
Start Zone (CP1) to CP2	21.9	31.3	22.4	27.9	24.5	24.4	24.6	25.4	24.5	
CP2 to CP3	10.7	19.3	23.4	19.8	19.2	10.4	14.1	17.0	11.3	
CP3 to CP4	12.5	14.3	12.9	15.0	16.6	17.9	13.8	14.4	11.1	
CP4 to Finish	16.2	23.2	14.8	22.9	23.9	15.5	16.9	15.7	19.4	
Trial Run Time	61.3	88.1	73.5	85.6	84.4	68.2	69.4	72.5	66.3	
HMC+TIM Dynamic Times:										
Start Zone (CP1) to CP2	14.5	14.2	18.6	12.8	15.3	17.9	18.5	16.6	18.7	15.3
CP2 to CP3	11.6	11.7	12.2	12.7	15.8	13.2	11.8	14.9	12.9	14.9
CP3 to CP4	15.1	14.5	17.2	14.7	13.8	17.3	12.6	17.5	12.1	11.7
CP4 to Finish	15.9	14.0	12.3	21.4	20.2	16.8	17.3	16.7	15.0	18.6
Trial Run Time	57.1	54.4	60.3	61.6	65.1	65.2	60.2	65.7	58.7	60.5
Individual BCI Course Time Results										
BCI Only Static Times:										
Start Zone to CP1	54.3								48.0	
CP1 to CP2	57.0								30.9	
CP2 to CP3	68.1								71.2	
CP3 to CP4	45.7								37.8	
CP4 to Finish	24.1								42.5	
Trial Run Time	249.2								230.4	
BCI+TIM Static Times:										
Start Zone to CP1	13.6	12.3	12.4	14.8	14.4	14.1	15.7	16.1	13.8	15.0
CP1 to CP2	22.0	18.0	18.1	15.5	24.7	17.3	20.7	19.0	13.7	20.8
CP2 to CP3	11.6	14.1	13.2	10.0	12.6	14.6	14.1	11.4	11.6	14.8
CP3 to CP4	16.3	16.4	16.5	16.4	15.8	18.4	14.6	14.3	14.5	14.6
CP4 to Finish	13.5	15.2	14.3	16.1	14.2	14.7	16.4	15.7	16.2	16.1
Trial Run Time	77.0	76.0	74.5	72.8	81.7	79.1	81.5	76.5	69.8	81.3
BCI+TIM Dynamic Times:										
Start Zone (CP1) to CP2	17.6	17.9	14.0	15.3	15.8	15.4	16.7	15.5	15.6	18.7
CP2 to CP3	12.8	9.8	12.3	11.4	12.9	15.5	14.8	13.8	12.2	13.3
CP3 to CP4	18.0	10.3	16.9	14.3	12.8	14.9	14.8	14.2	13.5	15.6
CP4 to Finish	16.8	18.0	13.0	19.2	13.3	19.6	15.7	17.3	15.9	18.0
Trial Run Time	65.2	56.0	56.2	60.2	54.8	65.4	62.0	60.8	57.2	65.6
QUEST Survey Results - TIM Wheelchair (1: Not Satisfied at all -> 5: Very Satisfied)										
1. Dimension Satisfaction	4	5	4	4	5	5	5	4	4	4
2. Weight	4	4	4	3	5	5	5	5	5	4
3. Ease In Adjusting Parts	3	4	4	3	5	4	4	4	4	4
4. Safe and Secure	4	4	4	4	5	5	5	4	5	4
5. Durability	5	4	4	4	4	4	4	4	5	4
6. Simplicity	4	4	5	4	5	5	5	4	5	4
7. Comfort	3	5	4	4	5	4	5	5	3	4
8. Effectiveness	4	5	5	4	5	5	5	4	5	4

Table D-1: Experimental Study Results

Appendix E

Human Research Ethics Application Documents

APPLICATION FOR APPROVAL
UTS HUMAN RESEARCH ETHICS COMMITTEE

PROJECT TITLE: A Smart Wheelchair System using a Combination of Stereoscopic and Spherical Vision Cameras

Chief Investigator/Supervisor: Prof. Hung T. Nguyen AM	
Faculty/School: FEIT	Address: CB10.03.573
Email: Hung.Nguyen@uts.edu.au	Phone No: 9514-4441
Qualifications: B.E. (First Class Honours, University Medal), Newcastle University, 1976 M.E. Newcastle University, 1977 Ph.D. Newcastle University, 1980	
Experience relevant to this application: Leading researcher in health technology, including assistive devices for the disabled.	
Co-investigator/Co-supervisor: Dr. Steven W. Su	
Faculty/School: FEIT	Address: CB01.24.10B
Email: Steven.Su@uts.edu.au	Phone No: 9514-7603
Qualifications: B.E., Harbin Institute of Technology, 1990 M.E., Harbin Institute of Technology, 1993 Ph.D. Australian National University, 2003	
Experience relevant to this application: More than 7 years experience working in this field of engineering.	

Student (name): Jordan Son Nguyen	UTS student number: 10050781
Faculty/School: FEIT	Address: CB01.18.1107
Email: Jordan.S.Nguyen@eng.uts.edu.au	Phone No: 9514-7532
Qualifications: B.E. (First Class Honours), University of Technology, Sydney, 2008	
Degree being undertaken (attach letter of candidature): Doctor of Philosophy	
Has doctoral/masters assessment been obtained? Yes	
Experience relevant to this application: 5 years experience in biomedical health technology design, including assistive devices for the disabled.	

CONSULTATION:

Have you undertaken any consultation in preparing this application (e.g., supervisor, Research Ethics Officer/Manager, HREC member, Jumbunna, etc). Give details:
Consulted chief investigator Prof. Hung Nguyen (most appropriate in this case), supervisor Dr. Steven Su, Susanna Gorman – UTS Research Ethics Manager (Human), and Racheal Laugery – UTS Research Ethics Officer.

FUNDING:

(a)   Have you applied for funding in relation to this research? If yes, list the source of funding (e.g. funding body/type) and attach a copy of the funding approval, budget page and any contract or agreement from the funding application.
Not relevant. Candidature is supported by an Australian Postgraduate Award Scholarship

(b)   Total amount of funding (including in-kind contribution) sought or obtained (please indicate which is applicable)
n/a

(c)   What is your relationship to the funding source (e.g. grant recipient, industry partner, contractor, employee, office bearer, personal, other)?
n/a

(d)   Is there any potential conflict of interest for you as a researcher because of the funding or commercial arrangements? If yes, provide details.
No

(e)   Are there any constraints on the research as a result of the funding arrangements, e.g. to intellectual property, publication, etc? If yes, provide details.
No

(f)   If you have not applied for funding, do you intend to do so in future? If yes, provide details.
n/a

PROPOSED COMMENCEMENT DATE: *(of data collection – HREC cannot give retrospective approval)*	July 2011

| ANTICIPATED COMPLETION DATE:
(of this research study – note that ethics approval includes the collection, analysis, publication and storage of data) | July 2013 |

SECTION I – METHODOLOGY AND RESEARCH DESIGN

1.   DESCRIPTION OF YOUR RESEARCH

(a)   What is your research about? Please include a brief description using plain English of what your research is about.

This smart wheelchair system utilises the innovative and unique combination of stereoscopic camera system, for depth-mapping vision ahead of the wheelchair, and spherical vision camera system, for detecting potential obstructions all around the wheelchair. These serve the purposes of obstacle detection and collision avoidance during autonomous navigation of the wheelchair in unknown environments, which can assist both commercialised and new hands-free wheelchair control technologies. Advanced shared control strategies will allow the user to command and the wheelchair to assist in navigation. This will provide ease and safety to people with severe disability when operating their power wheelchair using hands-free technologies. . Commercialisation of this product will involve creating cheaper camera units and an embedded processing system

(b)   What do you hope the outcome of this research will be?

This system will contribute to advances in biomedical technology, and the aim is to first directly market to people with severe disabilities before moving into other innovative biomedical applications. Commercialisation of this product will involve creating cheaper camera units and an embedded processing system, minimising expenses for the target market. The aim of creating intelligent vision and automated guidance systems into the wheelchair is to accompany any hands-free control technology on the market, as well as new control technologies being developed, such as head-movement systems and brain-computer interfaces. This will provide severely disabled people with some navigational mobility independence.

*(*c)   Who do you think will benefit from this research?

Today about 680,000 people require power wheelchairs resulting from spinal chord injury alone. Direct communication with people who work with the disabled has given me insight into how difficult it can be for patients to use commercialised hands-free control technologies such as the "Chin Stick" (Catalyst, 2010) and "Sip-N-Puff" (Axistive, 2010). Many people with severe disability cannot adequately use any of the limited commercialised control technologies. So this research is to fill the gap and mainly benefit the many people who do not have any independence in mobility, namely high level tetraplegics.

(d)   Please provide details of the research design (approximately 350 words) including details of your aims/hypotheses or research questions and the significance of your research.

A prototype has been constructed consisting of a power wheelchair with frames attached to support the stereoscopic cameras at the front and the spherical vision cameras above the back of the wheelchair, as well as a tablet PC processing unit placed in front of the user to simultaneously conduct all processing and provide an easily-accessible graphical user interface. Methods have been researched and improved for the stereoscopic vision cameras to be able to determine depth of objects and map out the local environment ahead of the wheelchair. To complement this, new methods for spherical vision (due to the lack of results from research) were created and optimised to allow obstructions and their placements all around the wheelchair to be classified (with Neural Networks), and taken into account when the wheelchair is navigating semi-autonomously under the user's instructions.

All designs for these have been created in a way that allows easy interfacing with any hands-free control technology through the shared control between user and wheelchair guidance system. This shared control allows the user to be in control and the wheelchair to help guide and carry out the user's intentions for navigation.

(e)   Is this a clinical trial?
No

2.   LITERATURE REVIEW AND REFERENCE LIST

(a)   Please give a brief literature review of no more than 500 words. The aim is to explain how your research fits into the context of other research in the area.

Power wheelchairs provide assistance in mobility for severely disabled people. In many cases, however, the assistance provided by power wheelchairs is not sufficient for independent use without a caregiver, depending on the level of user's disability. To address these issues many wheelchairs have been upgraded with equipment and capabilities usually seen in robotics applications, such as sensors and autonomous navigation assistance, moving these types into the category of „smart wheelchairs" [1].

There is obviously a trade-off presented between manual independent control and autonomous control over a wheelchair. Users tend to prefer systems as close to the manual side of the scale as possible, but the level of manual control depends on the level of disability [1]. This project focuses on semi-autonomous control of the wheelchair, whereby a directional command is provided to the wheelchair from the user, through hands-free control technology, and it then has to use this to assist with navigation and obstacle-avoidance in an unknown environment.

„Smart wheelchair" commercial systems that assist the user with guidance have included the NavChair Assistive Wheelchair Navigation System which utilizes ultrasonic sensors [2], the Hephaestus Smart Wheelchair System [3], and the Bremen Autonomous Wheelchair which both use ultrasonic sensors [4]. Current developments in intelligent wheelchairs often use laser range finders which can be very expensive. The most common laser sensors used provide fast and accurate distances to objects, but normally only on a 2D plane [1]. Other sensors usually accompany these for localization in known environments.

The wheelchair development of this project navigates semi-autonomously using camera systems for depth mapping ahead of the wheelchair, and for vision and obstacle detection all around the wheelchair, which is more suitable for the target market of severely disabled people. Machine vision is increasingly becoming a more attractive choice as camera uses rise and prices fall. They are compact, accurate, can be used to provide useful information about an environment, and are a sensor users can easily relate to given that vision is the primary sense used by humans and animals to perceive and navigate though their environment [5].

An intelligent electric wheelchair recently developed [6] utilizes a stereo omni-directional camera system, being able to see all around the wheelchair with any part of the environment in the range of vision being seen from two cameras. This allows disparity images of the entire scene to be produced allowing for depth mapping of the entire environment. This omni-directional camera system, however, comprises of a total of 36 CCD cameras [6].

So the main advantages the wheelchair in this project has over others are:
- Reduced costs
- Simplicity
- Efficiency
- Safety
- Increased vision directly to the user from the cameras on the graphical user interface.
- Real-time operation
- Adaptable to assist any hands-free control systems
- Navigation in unknown environments

(b)   Please attach a list only *of references used in the literature review and cited in your application.*

[1]   R. C. Simpson, "Smart Wheelchairs: A Literature Review", Journal of Rehabilitation Research & Development, vol. 42, pp. 423–436, 2005.
[2]   S. P. Levine, D. A. Bell, A. J. Lincoln, R . C. Simpson, Y. Koren, J. Borenstein, "The NavChair Assistive Wheelchair Navigation System", IEEE Transactions on Rehabilitation Engineering, vol. 7, no. 4, 1999.
[3]   R. C. Simpson, D. Poirot, F. Baxter, "The Hephaestus Smart Wheelchair System", IEEE Transactions on Neural Systems and Rehabilitation Engineering, vol. 10, no. 2, 2002.
[4]   U. Frese, P. Larsson, T. Duckett, "A Multigrid Algorithm for Simultaneous Localization and Mapping", IEEE Transactions on Robotics, vol. 21, no.2, pp. 1–12, 2005
[5]   A. J. Davidson, I. D. Reid, N. D. Molton, O. Stasse, "MonoSLAM: Real-Time Single Camera SLAM", IEEE Transactions on Pattern Analysis and Machine Intelligence, vol. 29, 2007.
[6]   Y. Satoh and K. Sakaue, "Development of Omni-directional Stereo Vision-based Intelligent Electric Wheelchair", The 18th IEEE International Conference on Pattern Recognition, 2006.

SECTION II – RESEARCH PARTICIPANTS

In line with the National Statement, the definition of participants includes not only those humans who are the primary focus of the research but also those who will be affected by the research. The Committee regards the principle of respect for persons as of paramount importance.

3.   Recruitment of research participants/subjects

(a)   How do you propose to initially select and contact your participants/subjects (outline how you will obtain their contact details)?

☐   letter
☐   advertisement/flyer
☒   telephone
☐   e-mail
☐   internet
☐   organisation
☒   personal contact
☒   other (give details)

Personal contacts working at the Royal Rehabilitation Centre Sydney (RRCS) in Ryde are helping recruit participants as they have direct contact with potential participants as well as relevant contacts who can help recruit. Details of the trials are forward over the phone by myself or my personal contacts at the RRCS, being Prof. Ashley Craig and Dr. Yvonne Tran.

(b)   How many participants/subjects do you intend to recruit

Between 15 to 20 able-bodied subjects (depending on timing and availability of all involved), up to 5 paraplegic subjects, around 2 tetraplegic subjects. All subjects will be adults (18+ in age).

(c)   Explain how and why you have chosen this number.

The able-bodied subjects have been chosen for the first trials because it will be easier to run these trials with reduced setup time. They will also be used to provide feedback about the running of the autonomous aspects of the system, and through the subject numbers and amount of feedback, this will provide enough data for statistical analysis. The numbers will be easy to find and will increase statistical analysis in a number of aspects of the system (ease of use, efficiency, ergonomics, etc).

The paraplegic subjects will then trial the system. They will need assistance moving in and out of the wheelchair but the subjects chosen have use of their arms so will not require complete assistance. The volunteers chosen, despite not having the utmost need for such a system, will be able to appreciate the assistance from the wheelchair and provide feedback from the perspective of wheelchair users. This number of subjects will add to the statistical analysis.

The tetraplegic subjects will be last to trial the system. The level of disability here is no use of limbs, but vocal communication is desired for documenting feedback. These

trials will be more time consuming and will require experienced and trained staff with appropriate equipment such as hoists in the RRCS to assist moving in and out of the wheelchair. Only one or two patients will be used here to prove this system can be used by the people this system has been designed to target, and to gain their unique feedback that no others will be able to provide.

The differences between groups of users will then also be able to be documented, providing a wealth of information such as learning times, operational abilities, ergonomics feedback, desired improvements, etc.

(d)   Explain your selection and exclusion criteria for participants.
Selection criteria from able-bodied will involve those who are interested in the research. Selection criteria for the paraplegic subjects will be those who have at least some use of their arms and use wheelchairs (either power wheelchairs or manual). Selection criteria for the tetraplegic subjects will exclude those who have any use of limbs (lower level tetraplegics, falling into the paraplegic category for the purposes of these trials), and will include those who have communication abilities and are whilling to be moved into our wheelchair for the trial purposes.

4.   HOW WILL research participants/subjects BE AFFECTED?

In order to consider your research, the Committee will need to know what it will involve for your participants.

(a)   What procedures will participation in this research involve for your participants/subjects?
A brain-computer interface (BCI) will be used for the input of commands, and the wheelchair will do the rest, navigating and avoiding all collisions in the environment it has already been tested in at the RRCS.

Data collection:
This will be done prior to the physical trial. Conductive gel will be applied to keep the impedance level low and for better electrical contact. Non-invasive 2-channel wireless electroencephalogram (EEG) electrodes will be placed on the subject‟s head for acquisition of their brain-waves. Participants need to perform mental tasks including mental arithmetic, figure rotation, letter composing, visual counting and eyes close/open tasks. The able-bodied subjects will be using a generic adaptive BCI whereas an individual personalised system will be created for each of the paraplegic and tetraplegic subjects. For this reason, able-bodied subjects will move immediately onto the physical trial whereas the data collection process will be done at least a day in advance to the physical trial for all paraplegic and tetraplegic subjects, to allow the personalisation of the user interfaces.

Physical Trial:
Each subject will trial the BCI simulation control program and become familiar with the operation of the system and their set tasks. Following this the subject will be placed in the wheelchair (assisted) with a tablet PC graphical user interface mounted

in front of them, containing the same program as the simulation. They will be required to communicate a „forward" command to the wheelchair which will take them down a small corridor, then they will need to communicate „stop", „rotate left 90degree", and „forward" commands to select a different (longer) corridor path in which the wheelchair will navigate and avoid obstacles along the way. At the end of the trial the subject will be assisted out of the wheelchair (and back into their own if required).

Feedback will then be collected from the subject in survey form, based on the trial, about a range of aspects relating to the system and its usability.

(b)   What time commitment will the research involve for your participants/subjects?
The data collection process will require about 30minutes to 40minutes total. The physical trial will require between 30minutes to 75minutes. Trial feedback will take around 15minutes. This means a total of 75minutes to 130minutes total.

(c)   In what location will the research/data collection take place (*public area, office, café etc)*?
As the data collection process is easy to setup and equipment is very portably, these will be conducted at locations convenient to the subjects, and I will personally drive to any required locations. The Royal Rehabilitation Centre in Ryde will be used for all physical trials.

(d)   What travel, if any, does the research involve for your participants/subjects?
All transport will be organised for the individual subjects. Paraplegic and tetraplegic subjects will likely already be located in the RRCS and if not special transport will be organized. Able-bodied patients will be reimbursed for their travel expenses to and from the trials.

5.   RISK/HARM

Risk or harm could be described as damage or hurt to the wellbeing, interests or welfare of an individual, institution or group. Harm could range from physical hurt or damage such as illness or injury, to psychological or emotional hurt or damage, such as embarrassment or distress. Please note that as a researcher, you are not necessarily immune from risk yourself and should give careful consideration to this question.

(a)   Describe any risk or harm that research participants and related groups might experience while participating in the research, including the likelihood of such risk/harm occurring.
* Physical injury from collision: If for some unlikely circumstance the wheelchair has a collision, physical injury could result. The likelihood for this is very low as many precautions are being put in place to prevent these events from occurring, such as slow wheelchair speeds, multiple safety kill switches, and extensive collision avoidance testing prior to trials.
* Physical injury from moving in or out of the wheelchair: This is a potential risk, mostly relating to the paraplegic and tetraplegic subjects. The likelihood of this

occurring is very low as there will be trained and experienced staff present when necessary, as well as assistive hoisting equipment where needed.

* Annoyance if the wheelchair does not respond as required: If the wheelchair does not correctly pick up on the participant"s intended commands this may become irritating. The likelihood of this is reasonably low as optimised and personalised hands-free controls (BCI) suited to the subject should allow intended controls to be properly acquired by the system.

* There is the potential for participants (in particular the tetraplegic subjects) to experience disappointment after the study when they return to their own wheelchairs or other mobility equipment. However this study will provide valuable feedback which will be taken into consideration for further developments and contribute toward future commercialization, which may see the technology become available to these participants in the future.

(b)   Is there any possibility of risk or harm to participants and related groups resulting from the research at any time in the future? If yes, please describe.
No

(c)   Describe how you propose to minimise <u>any</u> risk for participants/subjects and related groups.
* Extensive optimisation and testing of the system prior to any trials, making sure that the wheelchair can navigate the intended environment and not have any collisions at any time, no matter what user command has been provided to it.
* Slow wheelchair speeds also minimise the risk and reaction time for collision avoidance.
* Multiple safety kill switches to the wheelchair to stop it immediately if any unforeseen problems occur.
* Trained and experienced staff will be employed to assist when necessary.
* Assistive hoisting equipment will be used where necessary.
* Careful attention to every aspect of the trials will be adhered to at all times from all involved.

(d)   Describe any risk or harm the researchers might encounter in the research, including the likelihood of such risk/harm occurring.
* Emotional impact is a possibility as working with physically disabled people may be emotionally confronting. The likelihood of this is low due to the fact that all researchers involved have had experience communicating directly with people who have similar physical disabilities to the target participants.
* Physical injury is also a risk if an accident occurs with the wheelchair or when moving the subject between wheelchairs. Again, likelihood will be low based on the amount of amount of safety preparations put in place and the experienced staff assisting where necessary.

(e)   Describe how you propose to minimise <u>any</u> risk for researchers.
* Checks for all researchers involved will be made regularly throughout the trials for any emotional discomfort or concern.

* The extensive testing and practice involving the experienced staff will minimise the risk of physical injury to all involved.

6. BENEFITS/PAYMENT

Researchers sometimes acknowledge the value of the input of participants by offering them rewards or benefits. Such benefits must not constitute an undue or improper inducement. Benefits will be made in the form of cinema gift cards and retail gift cards, book vouchers, chocolates, sharing the findings, or recompense for out-of-pocket expenses are all acceptable, whereas linking participation to assessment for students would not be acceptable.
Describe and justify any benefit, payment or compensation the participants will receive.
Retail gift cards will be provided to non-able bodied subjects involved to essentially provide a form of payment for their time and extremely important assistance.

Able-bodied subjects will be provided with cinema gift cards.

7. DECEPTION

Whenever possible, research should be free of any deception of participants. If you believe that deception is necessary for the integrity of your research, please present a sound rationale.
(a) Does this research involve any deception of participants? If yes, please describe. If not, go to the next question (8).
No

(b) If yes, why is such deception necessary?

(c) How and when do you intend to debrief the participants if deception has been used?

8. PRE-EXISTING RELATIONSHIP TO RESEARCH PARTICIPANTS/SUBJECTS

Researchers sometimes assume that it will be easier to conduct research with participants they know, such as in the workplace, with family or friends. In fact, the reverse can be true and unexpected problems arise precisely because of the pre-existing relationship. For example, it is harder for participants to refuse or to withdraw from research when they know the researcher, which means that the research could be unintentionally coercive.

(a) Do you have an existing relationship to the research participants/subjects (e.g. employer/employee, colleague, friend, relation, *student/teacher, etc)? If yes, please describe your relationship. If no, go to question 9.

Yes, only able-bodied subjects. Able-bodied subjects will be selected amongst volunteering friends.

(b)   Could student assessment, employee security, etc., be affected by participation in this research? Please give details.
No

(c)   How might this relationship influence their decision to participate or create potential ethical conflict? Please describe your strategy for dealing with this.
It will not. There are no obligations and this will be made clear to all volunteers, only those who are interested and whilling to assist will be selected. Withdrawals from the research can be made at any time, and checks at regular intervals will be made throughout the trials to check whether there are any uncertainties or concerns, for which the trial will be stopped for that subject if there are.

(d)   How might this relationship be affected by the proposed research or create potential ethical conflict? Please describe your strategy for dealing with this.
It will not be affected. Only people with no relationship to the project nor any foreseeable ethical conflict to the research will be selected.

APPLICATION FOR AMENDMENT TO EXISTING ETHICS APPLICATION
UTS HUMAN RESEARCH ETHICS COMMITTEE

PROJECT TITLE: A Smart Wheelchair System using a Combination of
Stereoscopic and Spherical Vision Cameras

Approval Number: 2011-245A

Chief Investigator/Supervisor: Prof. Hung T. Nguyen AM	
Faculty/School: FEIT	Address: CB10.03.573
Email: Hung.Nguyen@uts.edu.au	Phone No: 9514-4441

Co-investigator/Co-supervisor: Dr. Steven W. Su	
Faculty/School: FEIT	Address: CB01.24.10B
Email: Steven.Su@uts.edu.au	Phone No: 9514-7603

Student: Jordan Son Nguyen	
Faculty/School: FEIT	Address: CB01.18.1107
Student ID: 10050781	Phone No: 9514-7532
Email: Jordan.Nguyen@uts.edu.au	
Has doctoral/masters assessment been obtained since your original approval? If not, when will it be sought? Already obtained before original approval	

SUMMARY OF PROJECT DETAILS

Please provide a brief summary of your research proposal, based on your original
ethics application.

This smart wheelchair system utilises the innovative and unique combination of
stereoscopic camera system, for depth-mapping vision ahead of the wheelchair, and
spherical vision camera system, for detecting potential obstructions all around the
wheelchair. These serve the purposes of obstacle detection and collision avoidance
during autonomous navigation of the wheelchair in unknown environments, which
can assist both commercialised and new hands-free wheelchair control technologies.
Advanced shared control strategies will allow the user to command and the
wheelchair to assist in navigation. This will provide ease and safety to people with
severe disability when operating their power wheelchair using hands-free
technologies.

CHANGES TO PROJECT DETAILS

To cross the check boxes, double click on the check box and tick checked (under default value)

Change to completion date	Change to personnel	Change to research instruments/ participant material	Change to research methodology	Change to recruitment of participants
☐ Yes ☒ No	☐ Yes ☒ No	☒ Yes ☐ No	☒ Yes ☐ No	☒ Yes ☐ No

What changes to your original ethics application are you proposing?
Change of location for experiments from Ryde Rehabilitation Centre, Sydney (RRCS) to Building 2 Level 3 of UTS. As such, no approval is required from RRCS, since their facilities are no longer required.
Change of participant numbers (reduced), and no longer requiring high level tetraplegic participants.
Changes to allow some personal data to be collected, and photos/videos to be recorded during trials. These will only be used for research/media purposes if allowed by the participants, which they confirm in the amended consent form.

RATIONALE FOR PROPOSED CHANGES

Why do you wish to make these changes?
The Rehabilitation Studies Unit of RRCS was demolished in the second half of 2011 for reconstruction of facilities. This, unfortunately, meant relocation of the experimental trials, which were then decided to be conducted at UTS.

Based on the lack of adequate facilities at UTS for moving high level tetraplegic subjects into the wheelchair, only able-bodied and paraplegic subjects will participate in the trials, due to the relative ease in moving into the smart wheelchair.

Presentations and applications for further funding, investment, etc. will require proof to be displayed about the trials. For this reason the extra data gathering process is necessary.

IMPACT OF AMENDMENT ON RESEARCH PARTICIPANTS

This section requires you to consider the ways in which your proposed amendments may impact upon the ethical issues raised on your original application. Specifically, we ask you to outline the effects (if any) of your amendments on the following areas, and how you intend to deal with them. Does your amendment affect any of the following:

(a)   Outcome of your research?   No

(b)   Current or future applications for funding?   Yes
Photos/videos being taken may assist in acquiring funding in the future for further developments and trials.

(c)   Recruitment of participants (quantity, methods)   Yes
Less participants are now recruited, being around 8 able-bodied and 2 C-6/C-7 tetraplegic participants

(d)   Anticipated risk or harm to participants and/or researchers? (Please explain how do you propose to minimise these risks) Yes
Less risks associated than previous application due to the nature of participant disability levels.

(e)   Relationships (if any) between researchers and participants?   No

(f)   Consent from Participants? (Please attach revised consent form and information sheet if applicable)   Yes
Revised consent form is attached.

(g)   Data collection, interpretation, storage and/or disposal? (Please attach changes to surveys/questionnaires/interview questions if applicable) Yes
Data collection now consists of name, age, disability level (if applicable), photos and videos. Confirmation of all of data are included in the consent form and must be approved by the participant.
These will be collected through the surveys and cameras. The data will be stored in a dedicated secure location (external hard-disk drive) and only allowed to be accessed, analysed, and presented by the authors specified in this application.

(h)   Privacy and confidentiality of participants?   Yes
No identifying data will be used if the participant does not give approval. However, if they do approve to release the data, they may be put into publications and presentations resulting from these trials.